The character and genesis of pedogenic calcrete in southern Australia

Paul Grevenitz
University of Wollongong

The Character and Genesis of Pedogenic Calcrete in Southern Australia

**A thesis submitted in fulfilment of the requirements for the award of the degree*

DOCTOR OF PHILOSOPHY

from

UNIVERSITY OF WOLLONGONG

by

Paul Grevenitz BSc (Hons)

School of Earth and Environmental Sciences

March 2006

Certification

I, Paul Grevenitz, declare that this thesis, submitted in fulfilment of the requirements for the award of Doctor of Philosophy, in the School of Earth and Environmental Sciences, University of Wollongong, is wholly my own work except where otherwise acknowledged. The document has not been submitted for qualifications at any other academic institution.

Paul Grevenitz
March 2006

Abstract

Pedogenic calcrete profiles from temperate, semi-arid and arid regions of southern Australia show a diversity of forms, both in large-scale structure and texture determined in the field, and microstructures as determined by thin-section and scanning electron microscopy. Accumulations of microcrystalline calcite with varying degrees of cementation are typical of the majority of samples regardless of texture or form. Calcified filaments are prevalent at a micro-scale in the upper sections of most profiles, occurring as laminated coatings and channel infillings in hardpan calcrete, pisoliths and nodules. Organic matter occurring as filamentous and dendritic masses is commonly found associated with the calcified filaments and the formation and growth of the filaments are considered to cause the brecciated and pisolitic textures common in mature pedogenic calcrete.

Rhizogenic calcrete occurs in various host materials as taproot fragments with either dense grey micritic cement and microspar crystals which are larger adjacent to enclosed quartz grains, mottled dense micritic and microsparitic calcrete or alveolar-like fabrics. Root-formed channels are also prevalent in many indurated nodular and hardpan samples. Discrete and incipient calcrete nodules containing alveolar fabrics and microcodium grains and platy pedogenic calcrete containing fenestral microfabric were also observed. Needle-fibre calcite is present as the dominant component in some profiles, occurring as discontinuous semi-indurated channel fillings and sheets. The morphology of their occurrence suggests rhizogenic influence in their formation.

The collected samples are analysed for stable carbon and oxygen isotopic composition in order to determine if there are detectable differences across regions of different climate and host material. Many samples show within-sample variability with biogenic or rhizogenic features co-existing with micritic overgrowths and cements. In order to examine the relationship between pedogenic calcrete type and method of formation, carbon and oxygen isotopic measurements were taken from numerous sub samples within each sample to determine the extent of variation in isotopic composition within individual samples. The total spread of values is -1.0 to -12.5% and 2.0 to -10% (standard delta notation versus PDB) for carbon and oxygen isotopic composition, respectively, for all samples with large sample variation and positive co-

variation as displayed by multiple sample aliquots commonly observed. The results suggest within-sample variation caused by different and coexisting cement types, with contribution of heavy carbon by calcified filaments and carbonate precipitated through carbon dioxide degassing, and light carbon contributed by rhizogenic influences. The positive co-variation in carbon and oxygen is not depth related and indicates a simple mixing line between two end-members with differing isotopic compositions, possibly due to concomitant evaporative enrichment and carbon dioxide degassing in different carbonate cement phases. Soil organic matter carbon analysed for isotopic composition shows relative little variation across the climatic zones and no correlation with coexisting carbonate carbon isotopic composition.

Selected pedogenic calcrete samples developed in soils overlying radiogenic basement rocks from sites in arid and semi-arid western South Australia and Western Australia are analysed for 87Sr/86Sr in order to evaluate the contribution of calcium derived from silicate weathering to pedogenic calcrete. Fresh parent materials collected at the sites show 87Sr/86Sr ratios ranging from 0.7100 to 0.7993 and pedogenic calcrete 87Sr/86Sr ratios ranging from 0.7106 to 0.7198. Samples from sites in coastal and inland South Australia have 87Sr/86Sr ratios close to marine values (0.8093) indicating low calcium contribution from bedrock. Samples from Western Australia have variable and higher 87Sr/86Sr ratios indicating considerable calcium input for parent material and bedrock.

Whole rock pedogenic calcrete and host material sampled in profiles were analysed by X-ray diffraction to determine mineralogical composition and then determine relative changes in carbonate composition within the profile. Samples were further analysed by instrumental neutron activation analysis for a suite of major and trace elements and subjected to a variety of statistical tests to determine the phase relationships of the elements to each other and, in particular, calcium within the pedogenic calcrete profile. Most elements are found to be associated with residual phases such as clay, feldspar and iron oxide correlation to calcium, in some samples, and therefore are of possible interest in geochemical exploration as pathfinder elements in the search for buried ore deposits.

Acknowledgements

Certain scientific and technical aspects of this thesis would not have been possible without the expertise of the following people at the School of Earth and Environmental Sciences, University of Wollongong, Australia. As such, I wish to thank the following people for t heir assistance in developing my skills and helping me to accomplish the work that is this thesis.

David Carrie for his help and guidance in preparing samples for thin section and scanning electron microscope analysis. David Wheeler for his assistance with the stable carbon and oxygen isotopic analyses. Richard Miller for his help with drafting the diagrams and Stephen Barry for helping me learn and understand computer programming and also for assisting in other computer problems that I have so regularly experienced through the course of this thesis. Also I would like to thank Professor Allan R. Chivas for his academic guidance and for giving me direction in my research.

Outside of the University of Wollongong several people have assisted scientifically and technically. Graham Mortimer at the Australian National University spent significant effort to show me how to prepare samples and run the ICP-MS for strontium isotopic analysis and Ravi Anand from CSIRO, Kensington, Western Australia, spent time in the field showing the location of many interesting sites in the Western Australian goldfields region. An Australian Postgraduate Award, two AINSE grants and two Society of Economic Geologists Student Grants kindly granted funding for the research.

Most of all I would like to thank my long suffering partner Angela Reeves for her patience and understanding though the course of this degree.

Table of Contents

Table of Contents

List of Figures

List of Tables

List of Plates

Table of Contents

Table of Contents

Chapter 1

Introduction

1.1 Project Objectives

The formation of pedogenic (soil-formed) calcrete has long been of interest to earth scientists owing to the possible stratigraphic and palaeo-environmental information such deposits can yield. As such, a substantial volume of literature exists on this topic from the fields of sedimentary geology and soil science. Yet in many respects our understanding of pedogenic calcrete formation remains rudimentary and further descriptive and experimental work is needed to understand the links between the processes responsible for formation and the physical and chemical properties of pedogenic calcrete. The need for research into the origins of calcrete is enhanced by the fact that anomalously high concentrations of Au occur within pedogenic calcrete where bedrock mineralisation of Au occurs at depths of up to 50 m (Lintern and Butt, 1993; Hill *et al.*, 1998; Chen *et al.*, 2002), making pedogenic calcrete a useful geochemical sample medium for Au exploration in favourable bedrock terranes.

Significant research on the origins of pedogenic calcrete in southern Australia is sparse when compared to other calcrete-forming areas such as Spain and the southwest United States. Contributions on mineralogy and major-element geochemistry (Hutton and Dixon, 1981; Milnes and Hutton, 1983) and stable isotopes (Quade *et al.*, 1995) are concentrated on the coastal and sub-humid regions of South Australia. The current study aims to extend the geographical

extent of these previous studies to the semi-arid and arid interior regions of South Australia and Western Australia, focusing on the following aspects:

- The effect of climate and vegetation on the carbonate mineralogy, stable carbon isotopic composition of carbonate and organic matter, stable oxygen isotopic composition, and the morphology and microstructure of pedogenic calcrete.
- Determining the source of calcium (host material/bedrock vs. atmospheric/dust) using strontium isotopes.
- Examining the host mineral phases and mobility of trace elements within pedogenic calcrete sampled on a variety of host materials.

The general aim of the project is to provide a review and further evidence for the mechanisms of formation, in particular the effect of biological influences on pedogenic calcrete formation in the southern Australian continent.

1.2 Location and Climate/Vegetation Summary

Southern Australia contains temperate climatic zones with a latitudinal gradation from warm-arid with sporadic rainfall in central inland regions to cool semi-arid Mediterranean type climates on the southern coast (Figure 1.1). The location and names of the major of sample sites and the place names used in the text are given in Figure 1.2. Yearly mean maximum temperatures range from 21°C to 27°C, with summer temperatures commonly exceeding 40°C. Winter temperatures are mild and the average annual precipitation occurs predominantly during the winter months of April to September. Evaporation rates vary from less than 100mm per month in winter to 250-350mm per month in summer i.e. greatly exceeding precipitation. Winds throughout the region reflect the westerly system and strong southerly and westerly components dominate every season.

The pre-settlement vegetation in the southern subhumid/semi-arid margin of southwestern New South Wales, northwestern Victoria, southern South Australia and southwestern Western Australia typically occurs as open mallee *Eucalypt* scrubland (e.g. *E. oleosa, E. dumosa*), a small multi-trunked tree 3 to 6 m in height, which dominates the solonised soils of plains and ridges throughout the region. Scattered stands of Belah (*Casuarina spp.*), Sugarwood (*Myoporum spp.*) and Native Pine (*Callitris spp*.) occur in alliance with mallee species. The understorey generally consists of low chenopod shrubs (*Atriplex spp., Chenopodium spp. and Maireana spp.*), Spinifex (*Triodia spp.)* or a variety of seasonal herbs and woody plants. In the arid inland plains of New South Wales, South Australia and the Nullarbor region of Western Australia a saltbush-bluebush steppe or low chenopod shrubland (*Atriplex spp., Chenopodium spp. and Maireana spp.*) is typical on grey-brown and red calcareous soils. Stands of Salmon Gum (*E. salmonophloia)* and Gimlet Gum (*E. salubris*) woodland with chenopod understorey dominate semi-arid regions in Western Australia. Mulga shrubs (*Acacia sp*.) are the dominant vegetation in the arid regions in the western interior of the continent.

Hattersley (1983) recorded a marked shift in the abundance of C3 grasses in coastal regions, to C4 grasses in semi-arid regions and arid-inland areas, reflecting the transition from temperate coastal to arid interior climates. The nomenclature C3 and C4 refers to differences in the photosynthetic pathways used by plants to reduce carbon dioxide to organic carbon. All plants do not assimilate carbon equally and C3 plants discriminate against heavy carbon (^{13}C) to a greater extent than do C4 plants. The different photochemical mechanisms used by C4 plants enable them to capture carbon dioxide with minimal water loss (with a subsequent reduction in productivity) and as a result C4 plants are better adapted to higher temperatures and drier conditions than C3 species. A third type of photosynthetic pathway, known as CAM (Crassulean Acid Metabolism) is not present in plant species of southern Australia. Typically C4 plants are grasses whereas C3 plants are trees and/or grasses.

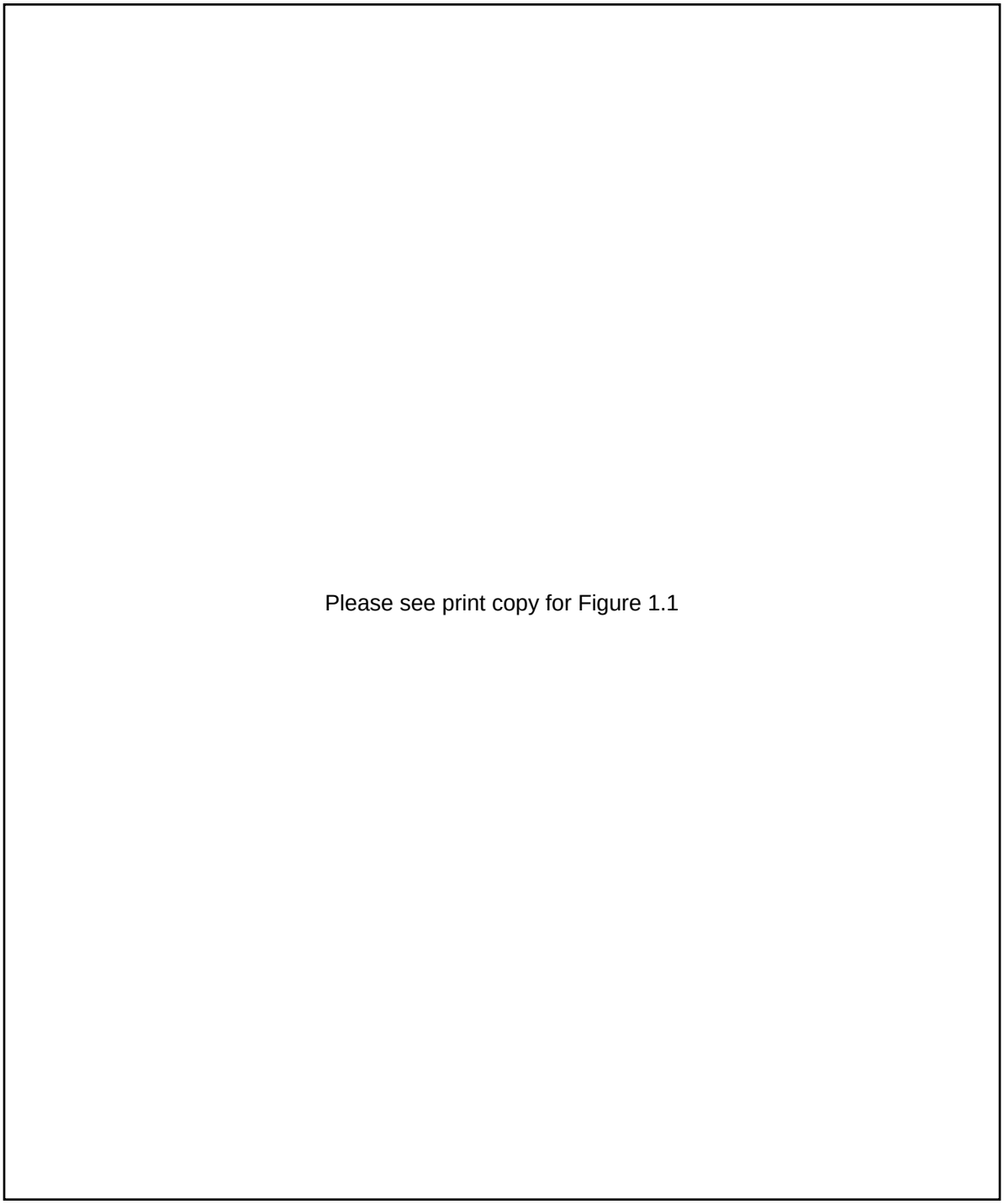

Figure 1.1. Average annual rainfall on the Australian continent (top). Quarterly Rainfall analysis for 2003/2004. A: January to March. B: April to June. C: July to September. D: October to December (Commonwealth Bureau of Meteorology).

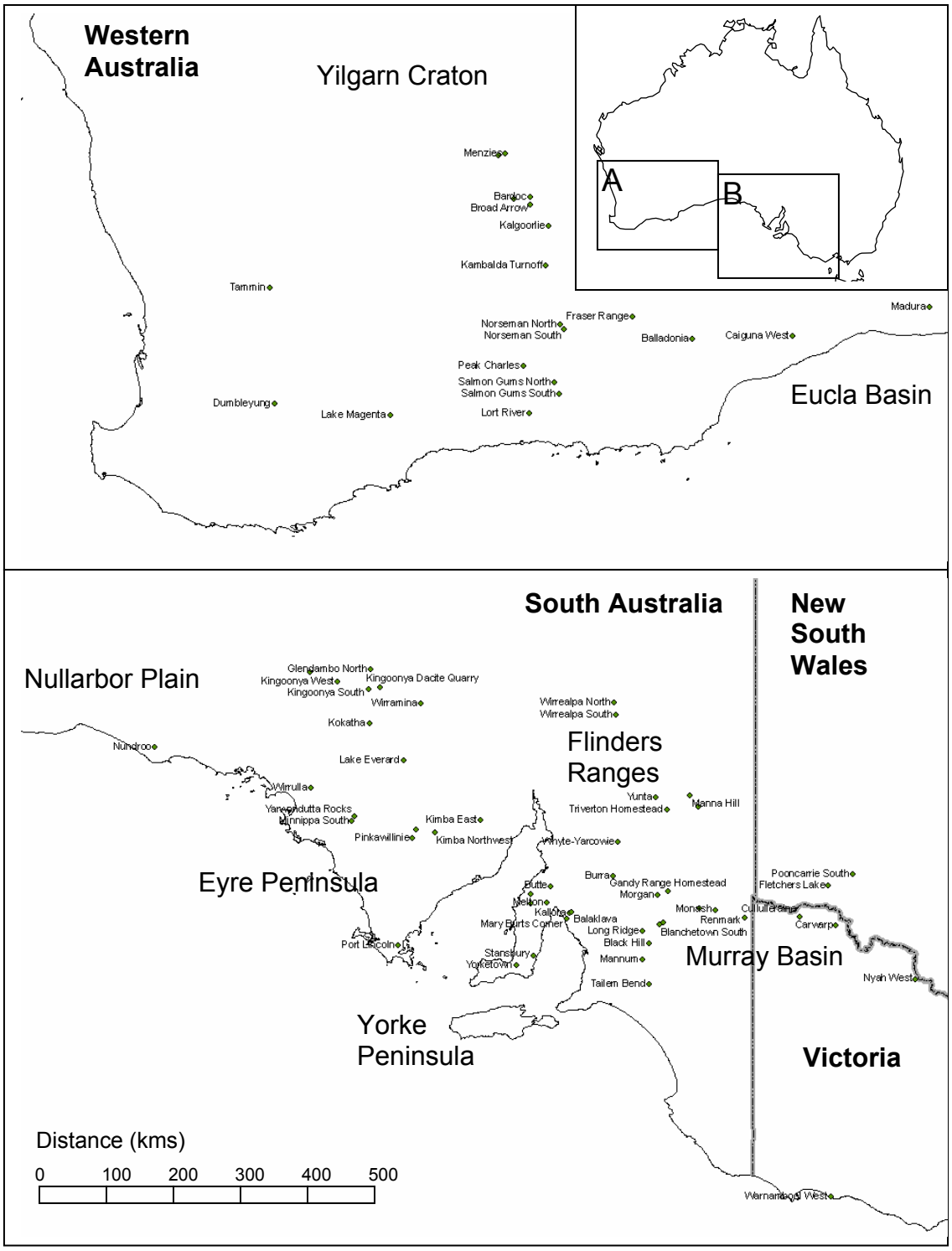

Figure 1.2. Location diagram

1.3 Geologic Summary

The simplified geology of the study areas in southern Western Australia and southern South Australia is shown Figure 1.3.

The Yilgarn Craton dominates the bedrock geology of southwestern Australia. This is a planated, deeply weathered and regolith-dominated terrain underlain by Archaean granitoids and north-northwest trending greenstone belts (mafic and ultramafic volcanic and sedimentary rocks). The landscape is generally low relief consisting of sandplains, plateaux, breakaways, colluvial and alluvial plains and minor bedrock exposures as isolated domes or inselbergs and north-northwest striking ridges (Anand and Paine, 2002). Extensive palaeo-drainage systems, now buried and clogged with sediment and containing large playas and dunes, occur along broad valleys (Gregory, 1914; van de Graaf *et al.*, 1977). Ollier *et al.* (1988) and Clarke (1994) considered that the incision of an extensive palaeo-drainage system into weathered Archaean bedrock occurred in the Jurassic period, prior to the break-up of Gondwana. The variety of regolith types (such as calcretes, laterites, silcretes, red-brown hardpan, young and old soils) that occur on the Yilgarn Craton are considered to be the product of the interaction between a long period of tectonic stability and a variety of climatic regimes (Ollier, 1978; Ollier et al., 1988).

The Gawler Craton, a Proterozoic granitic and volcanic province, dominates the bedrock geology of Eyre Peninsula and surrounding regions. With respect to the regolith geology, the landscape of the Gawler Craton is generally low relief consisting of sandplains and alluvial plains punctuated by low ranges.

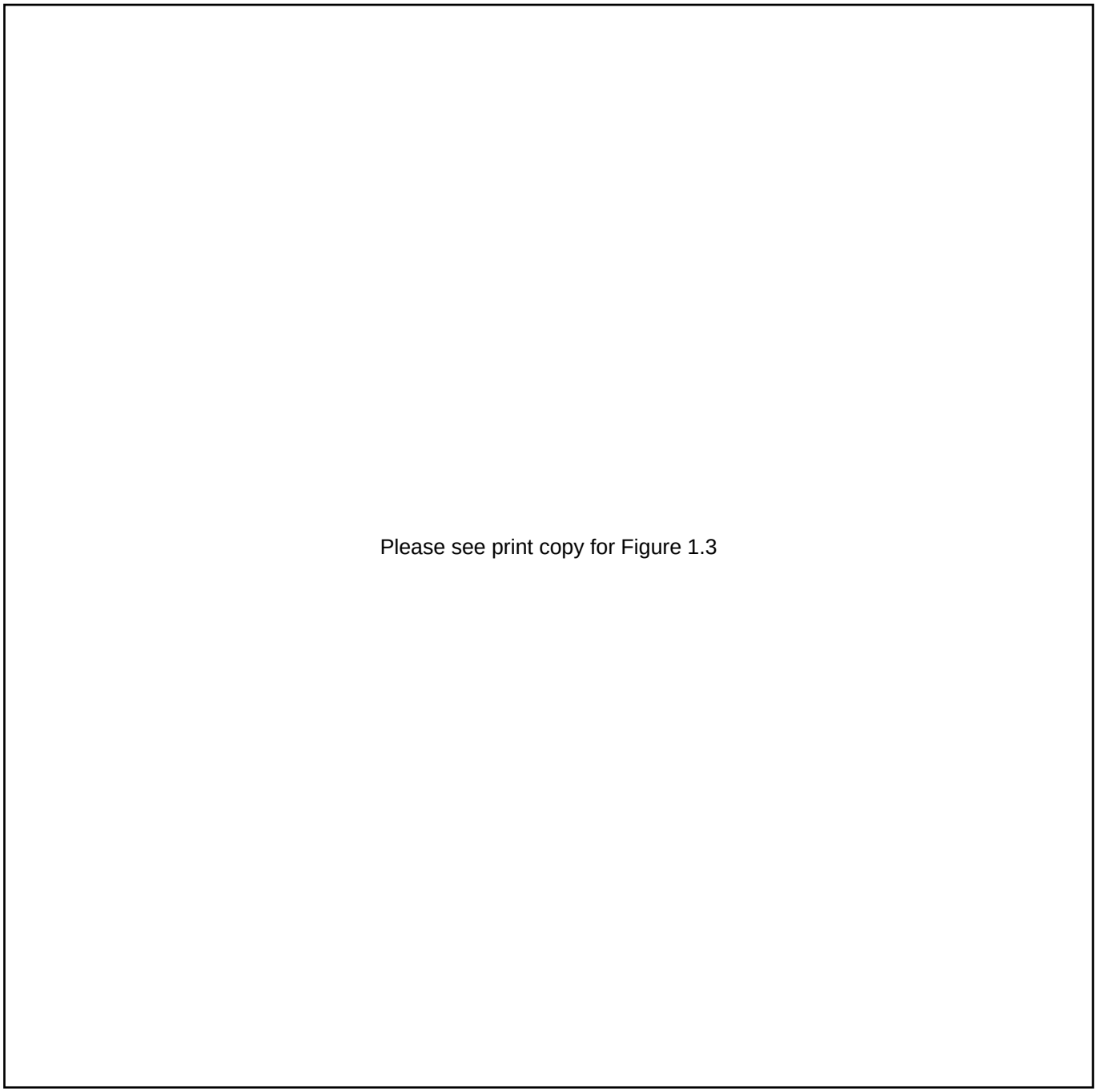
Please see print copy for Figure 1.3

Further west, the Eucla Basin forms a large southern marginal basin in South Australia and Western Australia. Extensive dense grey crystalline limestone of Eocene to Early Miocene age forms the plateaux of the Nullarbor Plain and is covered by a thin capping of calcrete. Widespread uplift and subsequent coastal erosion during the Pleistocene has removed the marine limestone from the coastal Roe Plain where a sandy marine coquina deposited on this shoreline is also calcretised.

The highland regions of folded and uplifted Adelaidian (Proterozoic) sediments are flanked by thick depositional sequences composed of clastic sediments commonly containing pedogenic calcrete. These alluvial fan aprons merge down-slope into piedmont slopes and basin plains where chronological control is limited. These deposits are commonly referred to as the Late Pleistocene Pooraka Formation (Williams, 1973). Williams and Polach (1971) and Williams (1973) describe three separate periods of soil formation characterised by calcrete accumulation within alluvial and aeolian deposits in the Lake Torrens piedmont plain. Radiocarbon dates for carbonised detrital wood in which the oldest palaeosol was developed indicate that deposition commenced more than 38 ka ago and continued until about 30 ka. Two subsequent periods of soil formation occurred between 16 ka to 12 ka, and 6 ka to 1.5 ka.

The surficial regolith in which pedogenic calcrete occurs throughout much of the semi-arid and arid regions of southern Australia is typically desert aeolian in origin. Saline playas consisting of gypsiferous clay and associated kopi (powdery gypsum) dunes also are common features of the present landscape. However, geological evidence indicates that aridity is a relatively recent feature of the landscape, and that, overprinted on the fluctuating cool-arid glacial and warm-moist interglacial

climatic phases is a progressive drying of the continent during the Neogene (Bowler, 1976; Williams *et al.*, 1998, p.176). That aridity was more widespread during glacial phases is evident by the considerable volumes of dust and loess that were deposited on land and adjacent oceans during these periods (Hesse, 1994). These aeolian dust deposits (red-brown sandy clays) mantle large areas of southern Australia, covering many geological and structural entities. The most recent period of aeolian activity occurred between 25 ka and 15 ka as indicated by radiocarbon age measurements on pedogenic calcrete from younger members of the aeolian Woorinen Formation in the Murray Basin (Bowler and Polach, 1971); the dunes are thought to have stabilized between 12 ka and 6 ka (Bowler, 1976). Successive horizons within the dune-field represent arid climatic regimes spanning the major climatic oscillations of the Quaternary period (Bowler, 1976; Lawrence, 1966).

Preceding the present and Late Pleistocene arid phase(s) within the Murray Basin, the Bungunnia Limestone and Blanchetown Clay were deposited in a large freshwater body known as Lake Bungunnia during the Late Pliocene and Early Pleistocene (2.5-3.5 Ma to ~0.7 Ma, An *et al.*, 1986). Blanchetown Clay sediments are up to 20m thick and comprise greenish grey sandy clay, dolomitic limestone and red-brown and green mottled clays. Climatic fluctuations caused shoreline migrations in the shallow lake resulting in inter-fingering of the Blanchetown Clay and fluvial Chowilla Sands near the lake margin (An *et al.*, 1986). The draining of Lake Bungunnia, probably caused by fluvial erosion and down-cutting that resulted in a breach in coastal or tectonic barriers approximately 600 ka ago fragmented the lake into separate smaller clastic-starved basins in which the thinly-bedded micritic lacustrine carbonate of the Bungunnia Limestone was deposited (Firman, 1967a,b).

The exposed coastline of southern Australia, buffeted by high-energy swells and prevailing onshore southwesterly winds, is dominated by Pleistocene and Holocene

bioclastic beach-, barrier- and transgressive dune sediments, (stacked aeolianite sequences commonly capped by calcrete) known as the Bridgewater Formation (Boutakoff, 1963). This sequence is considered to be time-transgressive, spanning much of the Pleistocene. The Murray Basin and Bridgewater Formation contain both mafic and silicic inliers, erosional remnants of crystalline basement projecting through younger sediments.

J.B. Firman, proposed a calcrete (palaeosol) stratigraphy for southeastern South Australia, referring to palaeosols as the Loveday Soil (Firman, 1966), Bakara Soil (Firman, 1963, 1964) and the Ripon Calcrete (Firman, 1967a,b). Subsequent researchers, however, have found this calcrete stratigraphy unworkable, citing the difficulty in distinguishing the specific calcretes and the cyclic repetition of calcrete formation in coastal sequences throughout the Quaternary as problematic (Phillips and Milnes, 1988). The thick hardpan profiles common throughout much of the mapped area are composite, their formation spanning much of the Quaternary.

1.4 Terminology

The term calcrete, coined by Lamplugh (1902) to describe carbonate-cemented gravels (parallel to the terms silcrete and ferricrete for materials cemented by silica and iron-oxide, respectively), has come to be used in later literature to cover a wide range of authigenic carbonates. The term is virtually synonymous with caliche, kunkar, calcareous crust and other terms used by overseas researchers. Wright and Tucker (1991), after Goudie (1973), and Watts (1980) defined calcretes as:

'A near surface, terrestrial, accumulation of predominantly calcium carbonate, which occurs in a variety of forms from powdery to nodular to highly indurated. It results from the cementation and displacive and replacive introduction of calcium carbonate

into soil profiles, bedrock and sediments, in areas where vadose and shallow phreatic groundwaters become saturated with respect to calcium carbonate. …Calcretes are not restricted to soil profiles (pedogenic calcretes) but can also occur, for example, below the zone of soil formation but within the vadose zone, or at the capillary fringe and below the water table to form groundwater calcrete'.

Though this very general definition is preferred, there is debate as to whether many simple types, such as fine, loose powdery calcretes and calcified soils containing 10-50% carbonate as grain coatings and patches of powdery carbonate should be included as calcrete (Goudie 1983). However, to set an exact minimum value for carbonate content, or the degree of induration of the calcrete is impractical (Chen *et al.*, 2002) reflecting the fact that many calcretes form a gradational lithification sequence through stages of development from primary sediment through powder or semi-indurated to cemented forms. Debate as to whether dolomitic and ankeritic carbonate accumulations should be included within the definition of calcrete also remains unresolved (see discussion by Hill *et al.*, 1998 and reply by Anand *et al.*, 1998). In order to avoid ambiguity and confusion, Milnes and Hutton (1983) recommended using the term calcrete only in its broadest sense for carbonate accumulations, and more specific adjectival terms (for example pisolitic carbonate, laminated carbonate, massive concretionary hardpan or calcareous fine earth) for the descriptions of the various forms. Hill *et al.* (1998) used the alternative term 'regolith carbonates' to incorporate all secondary carbonate minerals within the regolith, thereby including dolomite-dominant types (and presumably magnesite, aragonite and any other carbonate minerals?), sediment layers with few scattered nodules, bedrock voids containing carbonate and calcified soils in the definition. Anand et al. (1998) considered the use of the term (pedogenic) calcrete exclusively for soils containing calcite as impractical and failing to recognise the compositional gradation that occurs in the field. Furthermore, the existence of two terms meaning the same, but slightly different things makes communication confusing and may

leave the reader uncertain about the context of the terms and whether they are interchangeable. This thesis deals with carbonate formed in the soil moisture zone and will use the terminology of Goudie (1983) when describing individual calcrete samples. In accordance with Milnes and Hutton (1983) the term pedogenic calcrete is used in this thesis to refer to any accumulation of calcite, dolomite or ankerite that exhibits features typical of vadose or pedogenic origins.

1.5 Calcrete Origins and Distribution

Pedogenic calcretes are widespread in climatic zones where a seasonal rainfall deficit occurs allowing $CaCO_3$ to accumulate (Goudie, 1983). The processes considered responsible for the precipitation of carbonate within soil profiles are:

1. Evaporation and evapo-transpiration of calcium- and magnesium-charged soil water.
2. Carbon dioxide degassing of soil waters.
3. Biogenic processes.

Pedogenic calcrete characterises large tracts of land, with an estimated 20 million km^2, or 13% of the Earth's terrestrial surface (Yaalon, 1988). Up to 21% of the Australian continent (Chen *et al.*, 2002) is covered by soils containing authigenic carbonate. The control of climate on calcrete formation is evident by the abundance of pedogenic calcrete in southern Australia (Figure 1.4), occurring in a broad region bounded by the temperate regions of southwest and southeast Australia where conditions of continual moisture excess dissolve and remove carbonate from the landscape and, the northern arid regions of inland central and western Australia were the climate is arid - with less than 200mm mean annual rainfall and potential evaporation of 3000mm per year.

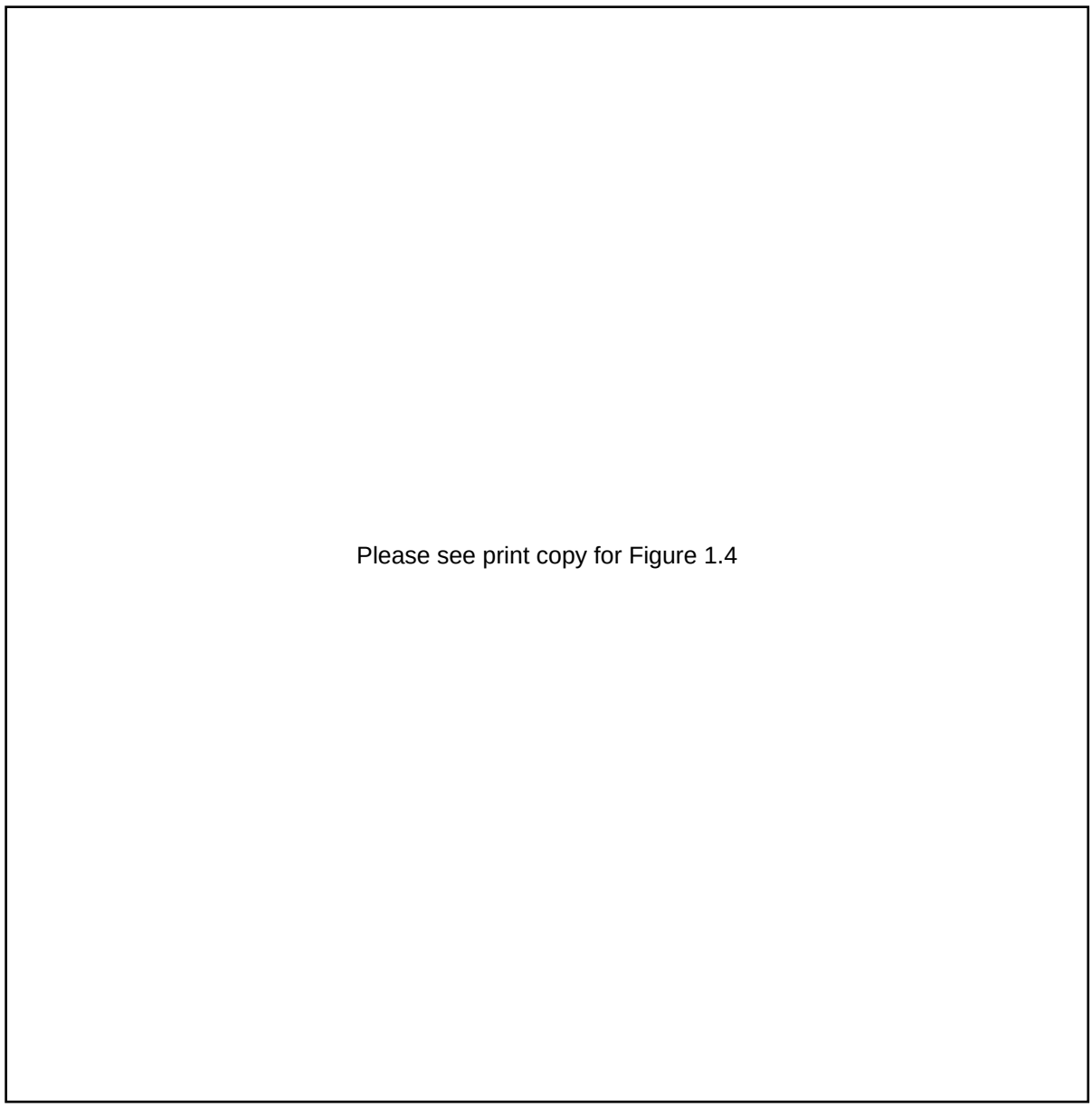

Figure 1.4. Divisions of calcrete landscapes: $I_{(1-3)}$= hardpan calcrete along ancient drainage valleys (western, central and eastern subdivisions); II= nodular calcrete of the southern Yilgarn Plateau; III- calcrete of the mallee soil zones; IV= tubular and hardpan calcrete of coastal dunes; V= nodular regolith carbonates in aeolian dust deposits; VI= boulder/nodular/pisolitic calcrete of the Nullarbor Plain; VII= regolith carbonate nodules in clayey soils on Ca-rich parent material in semi-arid to sub-humid zones; VIII= nodular regolith carbonate in aeolian sands in central Australia;

IX= crustal calcrete overlying limestone of the western coastal plain; X= humid regions with very rare regolith carbonates. (from Chen *et al.*, 2002).

At latitudes less than approximately 30°S, thick groundwater or valley calcrete occurs in trunk drainage systems or broad fossil valleys that are remnants of ancient drainage systems formed during the Tertiary or earlier (van de Graaf *et al.*, 1977). In Western Australia, the boundary between the groundwater calcrete in the north and the pedogenic calcrete in the south is termed the Menzies Line (Butt *et al.*, 1977) and divides the summer-rain dominant areas in the north from the winter-rain dominant areas in the south. The preferential occurrences of pedogenic calcrete in the winter rainfall regions reflects a difference in climatic and hydrologic conditions where, in the north, summer storms infiltrate quickly or runoff and evaporate rapidly from landscape depressions, leaving little opportunity for the precipitation of carbonate in the soil moisture zone. In contrast, the southern winter rainfall dominated regions retain soil moisture for longer, resulting in a greater build up of salts (including carbonate) in the soil and longer seasonal plant growth causing greater root respiration and soil CO_2 (Butt *et al.*, 1977; Carlisle *et al.*, 1978). The source of calcium (and magnesium) is ultimately derived from either bedrock through surface weathering and dissolution by soil or groundwater, or atmospheric sources in the form of aeolian dust and rainwater. Calcareous dusts and connate salts in rainfall were found to be more abundant in the south (Hingston and Gailitis, 1976), possibly reflecting a stronger coastal influence in winter rainfall from the south (Hutton, 1982; Keywood *et al.*, 1997).

Calcretised aeolian sandy clays and clayey sands account for a significant proportion of the landscape on Eyre Peninsula, Yorke Peninsula and the Murray Basin, disconformably overlying Pleistocene or older sediments and crystalline bedrock (Milnes and Hutton, 1983). Crocker (1946) described these calcretes as massive

travertine or lime rubble of the solonised brown ('mallee') soil zone, regarding them as an illuvial B-horizon and suggesting that the 'calcium carbonate was initially derived as fine material winnowed from the calcareous beach and backshore dune-complexes of the coastal regions during the Pleistocene, and carried in as loess under south-western and western components of the prevailing wind regime, possibly supplemented by additions of cyclic (atmospheric) calcium salts'. Many subsequent researchers have concurred with Crocker's ideas on the formation of calcrete (Crawford, 1965; Milnes and Hutton 1983). Firman (1967a) considered that the process of formation involved 'development of soil carbonate horizons from a thin but extensive blanket of loess on the landscape, followed by repeated cementation and brecciation of carbonate horizons with concomitant in-mixing of clastic material'.

Chapter 2

Calcrete Sedimentology

2.1 Literature Review

2.1.1 Genetic and Morphological Classification

Pedogenic calcrete occurs within soil or regolith, typically within the B-horizon of the standard soil terminology (i.e. A, B, C horizons). Where calcareous, the B-horizon is referred to as a Bca horizon. Pedogenic calcrete ranges in thickness from tens of centimetres to several metres and typically forms two or more sub-profiles with distinctive morphologies. Numerous models have been suggested for the formation and classification of calcrete; most are rudimentary, reflecting our limited understanding of calcrete formation. Perhaps the most important model with respect to the genesis of calcrete is that compiled by Carlisle (1980), which classified calcrete on the basis of hydrological setting (Figure 2.1). There are however, conceptual and practical difficulties classifying these genetic types, such as differentiating the soil moisture zone from the gravitational water zone and changes in hydrological setting and morphological characteristics common to both pedogenic and groundwater types (Chen *et al*., 2002). In practice, only pedogenic and groundwater calcrete are readily distinguishable. The occurrence of groundwater calcrete is commonly related to drainage axes and playas in arid regions (i.e. Carlisle, 1983; Arakel, 1986; Nash and McLaren, 2003). Such calcrete tends to be massive, not forming profiles typical of pedogenic calcrete with evidence of biological activity, clotted micrite, pisolitic or powdery forms (Wright and Tucker, 1991; Khadkikar *et al*., 2000). Exceptions occur where phreatophytic plants form laminar and rhizoconcretionary calcrete at the capillary fringe zone in dunes (Semeniuk and Meagher, 1981).

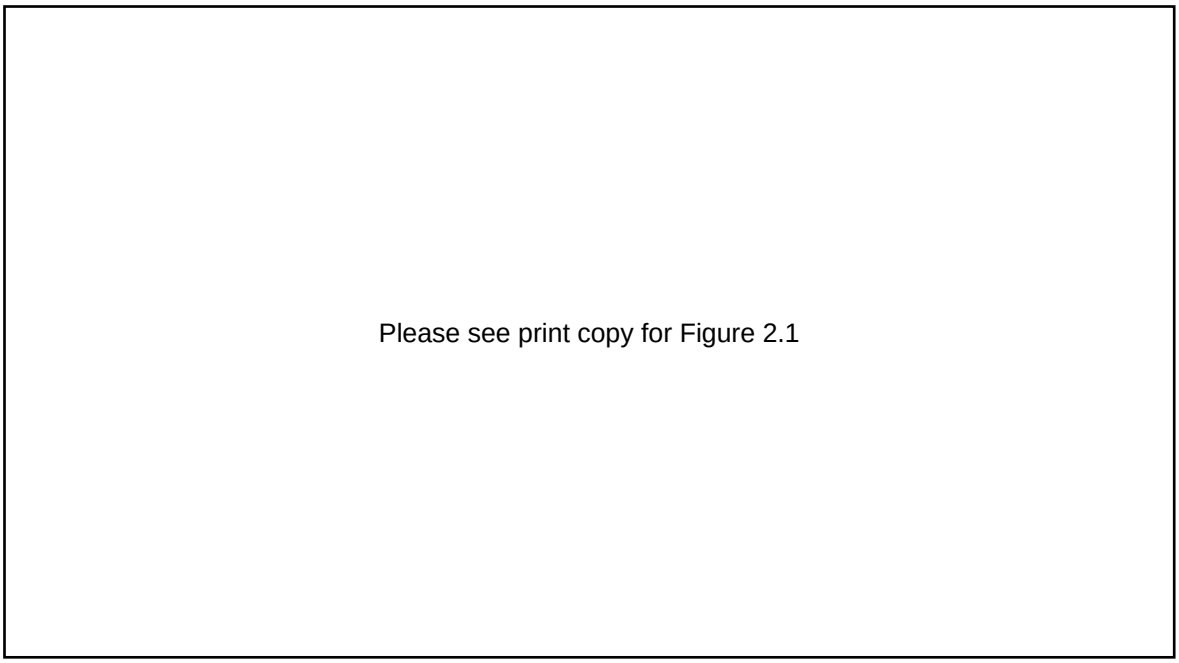

Figure 2.1. Classification of calcretes based on hydrological setting (from Carlisle, 1983).

The most comprehensive and widely used morphological classification system (Table 2.1) is that of Netterberg (1980) and Goudie (1983) modified by Wright and Tucker (1991) and Chen *et al*. (2002). The structure of calcrete relates to stages of development of profiles, for example, nodular calcretes coalesce to form hardpan and later weather to form boulder calcretes. The possible use of pedogenic calcrete for stratigraphic interpretation was first described by Gile *et al*. (1966) who introduced the concept that carbonate morphology in soils changes with time and can be described by a sequence of morphological stages. Among various maturity-related models (Netterberg, 1980; Wieder and Yaalon, 1982; Arakel, 1982), that of Gile *et al*. (1966), modified by Machette (1985), is the most comprehensive (Table 2.2 and Figure 2.2) and has been used to estimate accretion rates in alluvial systems. The model classifies the whole calcrete profile on the basis of specific diagnostic features and makes the distinction between calcretes developed on gravel-rich substrates and gravel-poor substrates because profiles tend to develop more rapidly in gravel-rich substrates. The stage of development is determined by residence time as well as calcium supply and sediment accretion rate, i.e. if sediment accretion rates are low, mature calcrete develops as hardpan.

Table 2.1 Morphological classification system based on Netterberg (1967, 1980), Goudie (1983) and Wright and Tucker (1991).

Morphological Type	**Description**
Calcareous soil	Very weakly cemented or uncemented soil with small carbonate accumulations as grain coatings, patches of powdery carbonate including needle fibre calcite, carbonate filled fractures and small nodules.
Calcified soil	Firmly cemented soil, just friable; few nodules, 10-50% carbonate.
Powder calcrete	Fine, loose powder of calcium carbonate as a continuous body with little or no nodule development.
Rhizomorphic calcrete	Secondary carbonate forming encrustations around roots or filling roots or other tubes.
Nodular calcrete	Discrete soft to very hard concretions of carbonate-cemented and/or replaced soil. Nodule shape is commonly irregular but not significantly extended in one or two dimensions and may contain laminated coatings.
Pisolitic calcrete	Highly indurated round concretions with well-developed internal concentric structures and core of massive carbonate and/or detrital grains. May be loose or cemented within hardpan profiles.
Hardpan calcrete	An indurated horizon, sheet-like or with a complex internal fabric. Commonly contains coalesced nodules, pisoliths, brecciated calcrete fragments and floating clasts of host material. Thickness ranges from several centimetres to tens of metres with a sharp upper surface and gradational lower surface.
Laminar calcrete	Indurated sheets of carbonate, typically undulose. Usually developed over hardpans or indurated rock substrates.
Boulder calcrete	Disrupted or brecciated hardpans. Due to fracturing, dissolution and rhizobrecciation (including tree heave). Clasts are rounded due to dissolution.

Table 2.2. Classification of pedogenic calcrete based on stages of development (from Machette, 1985). High gravel content refers to >50% gravel. Low is < 20% gravel. The $CaCO_3$ content refers to < 2mm fraction. (*K* is a carbonate soil horizon;

Please see print copy for Table 2.2

m refers to induration).

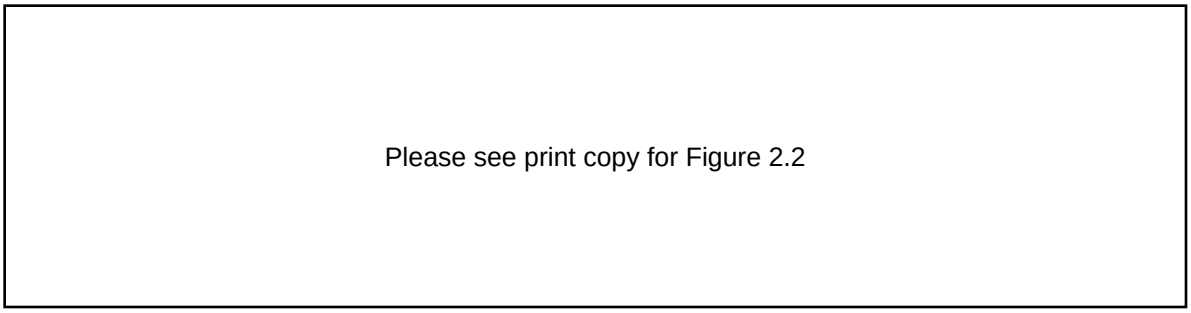

Figure 2.2 Stages in calcrete development in fine-grained sediment corresponding to Table 2.2 (diagrams from Wright, 1990).

Estimates for the formation of a mature (stage 4) profile range from 3 ka to over 1 Ma (Wright, 1990), possibly due to differences in climatic and hydrological regimes, landscape position and host lithology. For example, the local abundance of limestone strongly influences the availability of calcium for calcrete formation. This model also corresponds only to some of the morphological types described and assumes simple conditions such as steady landscape, climatic and hydrological regimes. Variations in profile form and thickness have also been considered by calcrete researchers in terms of the landscape position and erosion/deposition or reworking within the profile and it is possible that some nodular calcretes may be fragments of hardpan calcretes transported mechanically by fluvial or colluvial processes to form detrital calcretes (Figure 2.3). Degradation through erosion and physical break up by plant roots and dissolution by percolating waters can also be responsible for variations in morphology (Milnes, 1992). Lateral variations in profile thickness, from thin calcretes on hills and slopes to thickening on depositional plains, is indicative of lateral migration of carbonate due to infiltration and runoff in the catena (Ruellan, 1971). The down-slope increase in abundance of soil carbonate may also be a function of porosity and friability of the host material rather than of lateral dispersion (Anand and Paine, 2002).

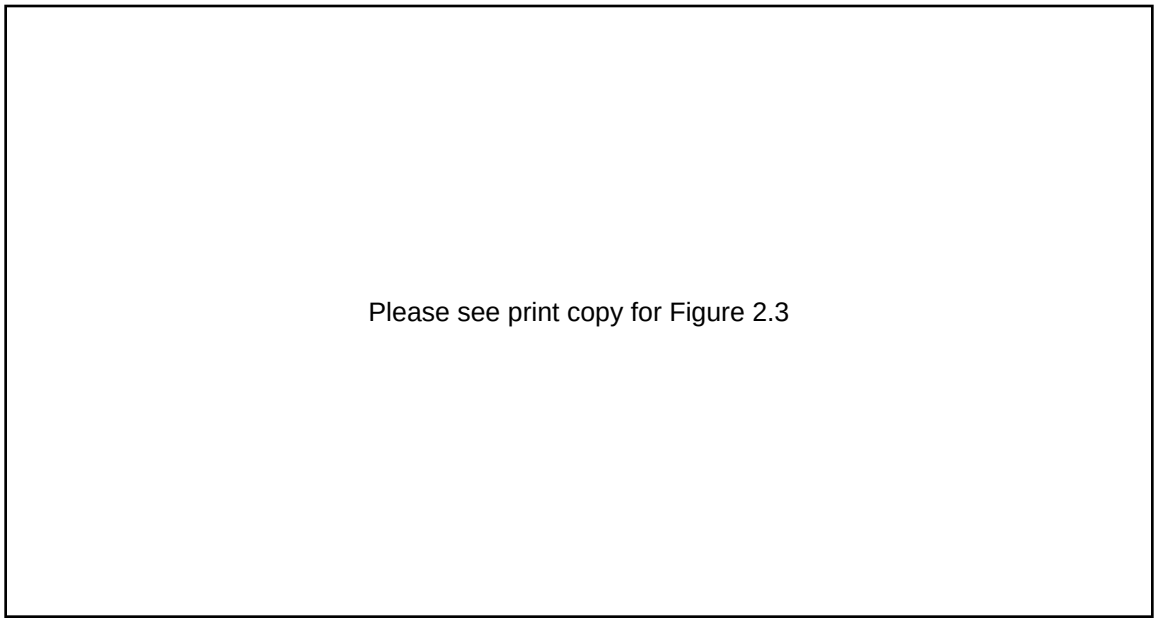

Figure 2.3. Model of detrital calcrete formation (from Carlisle *et al.*, 1978).

Many authors have documented the importance of micro-organisms in calcrete formation (Section 2.1.3). Wright and Tucker (1991) advocated a simple two end-member micro-fabric classification; biogenic (beta) types exhibiting macro- and micro-scale features attributed to the existence and activities of micro-organisms; and inorganic (alpha) types lacking any evidence of biological input. The addition of calcified remains of micro-organisms in pores spaces within the host sediment increases the $CaCO_3$ content of the host soil, particularly in upper parts of the profile, and may contribute significantly to case hardening in pedogenic calcrete (Loisy *et al.*, 1999; Phillips and Self, 1987; Phillips *et al.*, 1987).

2.1.2 Calcrete Micromorphology and Formation

The carbonate component of pedogenic calcrete, most commonly low-Mg calcite but also dolomite and ankerite, occurs in a variety of forms and is considered to form due to rapid CO_2 degassing and evaporative processes. Three size grades of calcite crystals are recognised; micrite (1-5 μm); microspar (~ 5-15μm) and spar (>15μm).

Host material composition (texture, grainsize and pore space) is regarded as an important control on calcite micro-morphology (Weider and Yaalon, 1974, 1982). In host materials with coarse texture, sparry fabrics are typical in primary pore space. Micrite forms thin envelopes on constituent grains (bridge, meniscus or gravity cements) on the unconsolidated substrate within the lower part of the soil moisture zone (Knox, 1977). Their formation is attributed to the fluctuations in volume and salinity of a film of attached water left on grains after gravitational water has drained from the pores. Loss of water from the attached film and meniscus water through evapo-transpiration and concurrent changes in ρCO_2 levels of the pores causes micrite to precipitate in a structure reminiscent of that of the distribution of pore waters held by surface tension (Reeves, 1976; Netterberg, 1980). With continued carbonate precipitation, primary pore spaces are filled and permeability is reduced, eventually resulting in a massive diagenetic packstone (Gile *et* al., 1966; Machette, 1985). At this stage of formation, porosity is reduced and cementation occurs at the top of the profile to form massive or brecciated hardpan calcrete. In mature calcrete profiles the degree of cementation decreases downward with friable calcareous soils and mottled powder occurring in the lower part of the profile beyond the reach of dissolution/re-precipitation effects of percolating rainwater.

The formation of nodules is typical in medium- to fine-textured soils (Wieder and Yaalon, 1982; Machette, 1985). Wieder and Yaalon (1974) noted that clay minerals control the crystal size of pedogenic calcite, influencing the stability of fine-grained carbonate; 'micro-calcite crystallites (within nodules) are uniformly distributed and strongly integrated with the clay minerals……in such a fabric the degree of integration of the non-carbonate clay and fine carbonates is so high that the birefringence of the clay minerals cannot be distinguished'. Massive fabrics within nodules consist of dense accumulations of cryptocrystalline calcite showing various

degrees of transmittance in thin section. This 'variate' texture reflects variations in crystal size and the amount of clay and iron oxides present and has been variously termed 'clotted' (Tandon and Friend, 1989) or 'mottled' (Wright and Tucker, 1991) texture. Hay and Wiggins (1980) refer to a flocculent structure similar to that produced by coalescing globules as 'clotted texture'.

The origins of pedogenic calcrete nodules are poorly understood. Wright and Tucker (1991) considered that the 'diffusion of carbonate to certain sites is a critical factor, followed by precipitation and displacive growth, for most nodules contain little of the original host material'. Voids formed around the nodule during desiccation may promote precipitation around the nodule margin during wetting and drying events (Chadwick *et al.*, 1987). The aggregation of carbonate and the displacement of silicate grains can be attributed to the affinity of ionic calcite bonds and the inability of carbonate to form bonds with non-carbonate grains (Chadwick and Nettleton, 1990). Colluvial processes and bioturbation (in particular tree-heave) resulting in mechanical movement and brecciation may also be involved in the formation of nodular calcrete (Carlisle *et al.*, 1978; Semeniuk and Meagher, 1981).

Grain coatings are a common feature in mature pedogenic calcretes. Coatings of concentrically laminated calcrete occur on pedogenic calcrete nodules forming by accretion, either in void space or displacing adjacent sediment. Sand and silt are usually excluded by undulose laminations several millimetres in thickness. Nodules that are not moved within the profile develop asymmetric coatings with preferential growth on either upper or lower (pendant cements) surfaces (Hay and Reeder, 1978). Coated grains typically form above an impermeable horizon, possibly in the thin temporarily perched water table after rains. Where grains are moved (rotated)

down-slope by gravity they become evenly coated forming round pisolites (Read, 1974; Arakel, 1982).

Small peloids or ooids commonly form in fracture fillings and other cavities (Siesser, 1973). The downward percolation of fresh water dissolves some of the more soluble carbonate, which is subsequently precipitated as concentric rings of carbonate mud around suitable nuclei, locally pushing grains apart (Hay and Wiggins, 1980; Seisser, 1973).

Carbonate coatings appear to have two main origins; some consist of simple micrite coatings with admixtures of non-carbonate material (Hay and Wiggins, 1980; Seisser, 1973); whereas others are biogenic (Section 2.1.3) consisting of microbial tubules or needle-fibres (Knox, 1977; Calvet, 1982; Calvet and Julia, 1983; Wright, 1986; Beier, 1987). Laminations in calcareous concretions are thinner over edges and corners of angular nuclei, thus increasing the sphericity of the particle. As yet no satisfactory explanation has been given for this phenomenon but the effect of surface tension due to coatings of sepiolite clay and opal gels (Hay and Wiggins, 1980) has been suggested.

Laminar calcrete commonly consists of a finely laminated, dense micritic horizon at the top of the profile at the interface between rock and air or beneath a thin cover of soil. The precipitation of calcite from carbonate-laden soil water ponded above an impermeable layer is the generally held explanation for the formation of laminar calcretes (Gile *et* al., 1966; Read, 1974; Semenuik and Meagher 1981; Arakel, 1982). Esteban and Klappa (1983) noted concomitant micro-stalactitic features composed of calcite spar in laminar textures.

Microbial and rhizogenic precipitation may also contribute to the formation of laminar calcrete. Termed terrestrial stromatolites by Krumbein and Giele (1979) and Wright (1989), laminated surficial calcretes with distinct bright and dark laminae are produced by calcification induced by cyanobacteria or lichens. Laminar calcrete with spar-filled tubular fenestrae (tubiform pores with concentric and convolute laminated micrite lining) is considered to represent 'densely interwoven rootlet horizons which were calcified, possibly while the rootlets were alive, by micritic and microspar calcite' (Wright *et al*., 1988).

2.1.3 Microbiological fabrics

Soil microflora are thought to be responsible for inducing calcite precipitation in many pedogenic calcretes (Kahle, 1977; Knox, 1977; Klappa, 1978, 1979a,b, 1980; Calvet, 1982; Calvet and Julia, 1983; Callot *et al*., 1985; Wright, 1986). Calcite precipitation by terrestrial bacteria and fungi has been demonstrated in culture experiments using soils from Israel (Krumbein, 1968) and New Mexico (Monger *et al*., 1991). Boquet *et al*., (1973) found many bacterial organisms were capable of producing calcite crystals in calcium-rich solid media and concluded that crystal formation by bacteria is almost purely a function of the medium used. Filamentous microstructural features are commonly well preserved in pedogenic calcrete and are undoubtedly the result of calcification of, or by, micro-organisms. In many cases, however, there is uncertainty about the organism responsible for the structure and whether calcification occurs during the life of the organism (*in vivo*) or through post-mortem replacment. Bacteria, algae, fungi and lichens have filamentous structures and are possible precursors to micro-rods and calcified filaments (Phillips *et al*., 1987).

Many authors have attributed bacteria as being responsible for the formation of submicron sized fibres, termed micro-rods (Phillips and Self, 1987; Chafetz and Buczynski, 1992; Verrecchia and Verrecchia, 1994). Loisy *et al*. (1999) identified two types of rod-shaped organisms, bacilliform and threadlike bacteria, as being responsible for the formation of micro-rods.

Calcified filaments, tubiform microstructures (2-10 μm in diameter) with a central hollow, have been attributed to calcification associated with the root hairs of vascular plants (Klappa, 1979b). Phillips *et al*. (1987), however, noted their branching nature and an association with calcified spheres, thought to resemble the fruiting bodies of fungi, and attributed their formation to calcification by fungal hyphae.

Needle-fibre calcite, elongate crystal rods of low-Mg calcite typically up to 10μm wide and 50 to 100μm long, occurs in pedogenic calcrete either randomly stacked, tangential around particles or as arcuate bridging cements precipitated in void space. The origin of needle-fibre calcite has been debated for years with many calcrete researchers attributing their growth to physico-chemical precipitation, citing rapid crystal growth during high degrees of supersaturation (James, 1972; Sehgal and Stoops, 1972; Harrison, 1977; Durand, 1980; Given and Wilkinson, 1985; Solomon and Walkden, 1985) and/or the inhibition of lateral crystal growth by absorbed ions (Mg^{2+}, Na^{+}, SO_4^{2-} or organic matter; James, 1972; Folk, 1974; Knox, 1977, Braithewaite, 1983). Other workers have suggested a biogenic origin (Ward, 1975; Esteban and Klappa 1983; Calvet and Julia, 1983; Wright 1984, 1986) noting their close association with roots and root hairs or with fungi. Verrecchia and Verrecchia (1994) suggested that a 'purely physico-chemical origin by precipitation in pores would result in different sizes related to different phases of growth, but

needles occupying pores already appear to be mature; the smaller crystals are broken or dissolved pieces of longer ones and not young crystals in the process of growing'. Callot *et al*. (1985) and Phillips and Self (1987) demonstrated the formation of needle-fibre calcite within fungal mycelial strands and release by lysis (decomposition).

2.1.4 The Influence of Plants

The influence of higher plants, in particular their root systems, is important in many aspects of calcrete formation (Kahle, 1977; Klappa, 1978; Semeniuk and Meagher, 1981), however relatively little is known about their role in the structural and genetic development of calcrete profiles. The presence of up to 20 percent calcium and magnesium in the ash of vegetation and litter (Lintern, 1998) suggests that plants contribute significantly to the chemical budget of pedogenic calcrete. Listed below are the effects plants have that may lead to calcite precipitation:

- Chemical effects on soil water: evapo-transpiration, respiration and acid reactions to procure vital elements effect the concentrations of dissolved salts, CO_2 partial pressure and the pH of soil water, important factors for the dissolution and precipitation of carbonate. Certain ions important in carbonate equilibria (Ca^{2+}, HCO_3^- and CO_3^{2-}) may be preferentially excluded during fluid uptake by plants (Thompson, 1975).
- Physical action by roots: roots provide channels and penetrate joints causing mechanical disaggregation and they control water percolation. Tree heave may also affect profile development causing brecciation (Semeniuk and Meagher, 1981).

- Root structures: carbonate is commonly found precipitated around living or decayed plant roots in the form of vertical hollow or filled cylindrical concretions and some laminar calcretes (Wright, 1989). Organo-sedimentary accumulations formed by cementation and/or replacement around and within higher plant roots are variously termed rhizomorphs, rhizoconcretions, pedotubules, rhizocretions or rhizoliths (Klappa, 1980 and references therein).
- Petrifaction or impregnation of root cells by calcite is also common and many micro-features within calcretes are attributed to the former presence of plant roots and associated micro-organisms. Microcodium and alveolar texture is attributed to the preservation of root material (Esteban, 1974; Esteban and Klappa 1983; Klappa, 1978). Calcium oxalate can be found precipitated within the cell vacuole of some plant cells. Vacuoles are membrane-bound regions within plant cells that contain liquid (cell sap) composed of water and other components such as salts, sugars and proteins. When concentrations of calcium are sufficiently great in the cell sap, calcium oxalate crystals precipitate, assuming several different forms including needle fibres and spherical druses (Raven *et al.*, 1980 p. 25).
- Associated micro-organisms: Concentrations of micro-organisms occur on and within plant root tissue, commonly in symbiotic relationships. Mycorrhizal fungi are especially important in the absorption and transfer of nutrients in soils of low fertility. The hyphal network of mycorrhizal fungi extends several centimetres from plant roots, exploiting large volumes of soil (Raven *et al.*, 1986 p. 526).

2.1.5 Diagenic Processes

The volume of carbonate in calcrete typically exceeds that required for the filling of original pore space (passive cement precipitation). The processes involved in the 'growth' of calcrete, particularly mature calcrete, in terms of replacive or displacive crystallisation are still poorly understood (Watts, 1978; Wright and Tucker, 1991) and have received relatively little attention in the literature. Isolated or floating grains of quartz are a microscopic feature of most calcretes and debate has centred on whether replacement or displacement of the original host material is responsible for this texture (Watts, 1978). Watts (1978) considered displacement an important process in the formation of floating grains and brecciated features in grain-supported sediment, as indicated by the displaced brecciated fragments being able to fit together, the slight etching of detrital quartz, and spar-filled cracks with 'growth patterns' visible under cathodoluminescence. The ability of a growing crystal to exert a linear force on its surroundings is well documented in both laboratory and field studies (Weider and Yaalon, 1974; Buczynski and Chafetz, 1987), the force of crystallisation being strong enough to cause quartz grain breakages and separation by the growth of carbonate cement.

Replacement is also an important process in calcrete formation, particularly on unstable host lithologies (for example, Hay and Reeder, 1978). Using cathodoluminescence, Tandon and Friend (1989) were able to show growth patterns demonstrating peripheral growth of spar towards a quartz grain, interpreting this as evidence for calcite replacement of quartz. Surface etching of detrital minerals may also provide evidence for replacive growth but is rarely described in the literature.Microfabrics exhibiting 'mottled' or irregular crystal mosaics, where crystal size ranges from micrite to spar in patches with diffuse margins, are thought by

many authors to be the result of the replacement of finer crystals by coarser ones (Tandon and Narayan, 1981; Wieder and Yaalon, 1982; Tandon and Friend, 1989). Textures visible with cathodoluminescence provide evidence that dissolution and reprecipitation can occur repeatedly during subaerial vadose diagenesis. Growth patterns in spar-filled cracks and voids and spar-replaced micrite indicate recurrent dissolution and progressive replacement of earlier micrite fabrics (Solomon and Walkden, 1985; Tandon and Friend, 1989). Alonzo-Zarsa *et al*. (1998) suggest that microspar crystals with sharp irregular boundaries and dissolution features may not only be the product of recrystallisation processes, but may also be due to multiple phases of growth and dissolution, or to processes of displacive and non-uniform growth.

2.2 Southern Australian Pedogenic Calcrete Profiles

For this thesis research, pedogenic calcrete profiles were sampled from exposed sites at locations throughout southern Australia (Figure 2.4). Site localities where chosen on the basis of quality and depth of exposure, with the aim of examining pedogenic calcrete developed on a variety of host materials and climatic regions. Profiles were logged and the sample locations within the profile sprayed with paint before being photographed and sampled. Sample intervals down profile were at 10-20 cm spacing, depending on vertical changes in morphology, down to bedrock or host material where possible. Diagrammatic logs of sampled profiles are given in Appendix I with a description of the location, vegetation and micro-morphology. Calcrete with poor outcrop were collected as grab samples and are listed in Appendix I. The forms of calcrete within a profile are given in the legend accompanying the logs.

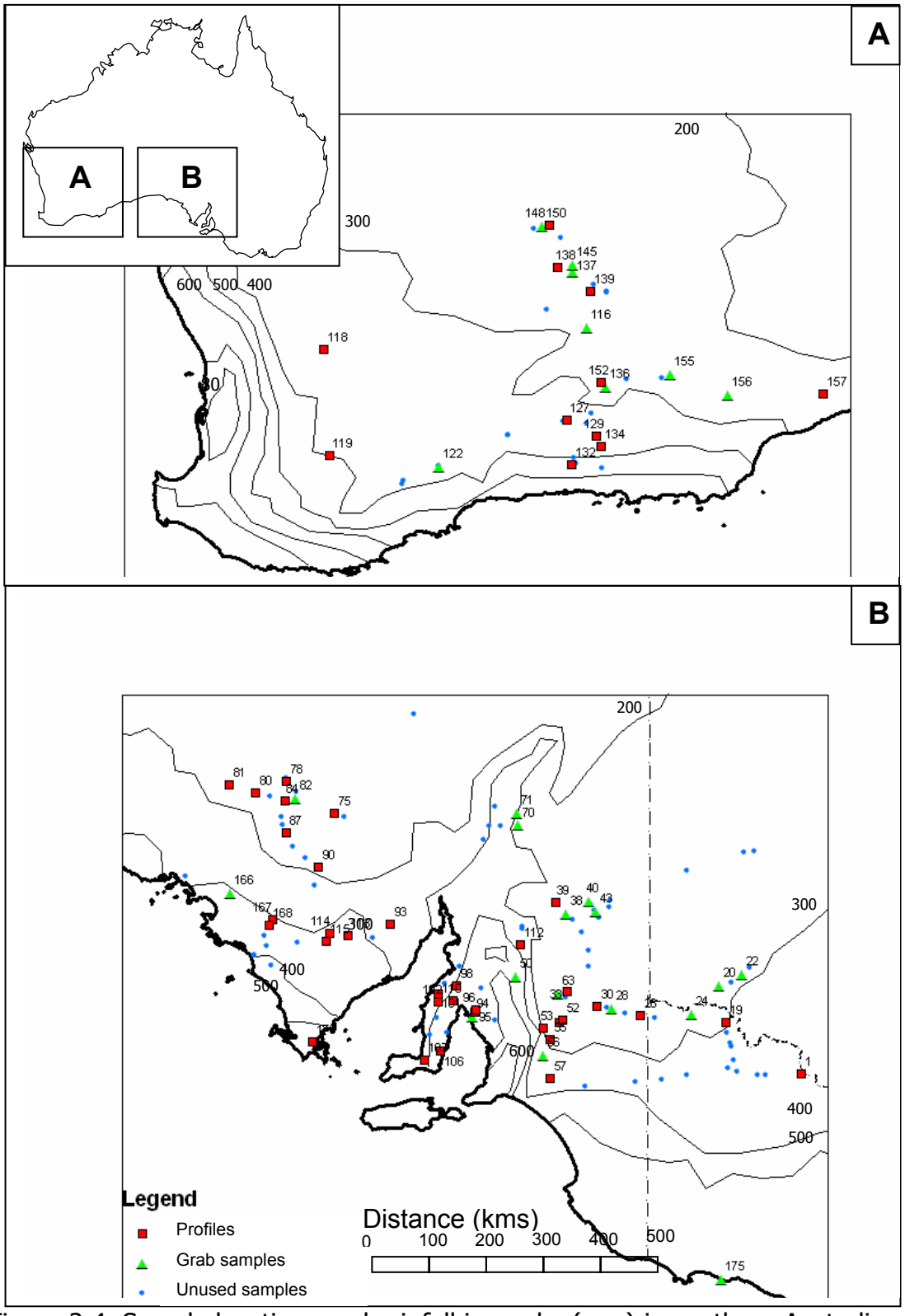

Figure 2.4. Sample locations and rainfall isopachs (mm) in southern Australia.

On **unconsolidated substrates** pedogenic calcrete typically occurs with or without a thin (0 to 0.3m) surficial non-calcareous or nodular A horizon; an indurated Bca-horizon; grading downward to a friable massive or mottled calcareous C-horizon occurring at the base of profile. The Bca-horizon is characteristically indurated to moderately cemented containing nodular, hardpan and boulder morphologies. Powdery or semi-indurated calcified soils occur either below indurated horizons (as C horizon) or as independent massive or mottled forms in youthful calcrete (as Bca-horizon). The morphology of powdery or semi-indurated calcrete as C-horizon is typically massive, in some cases occurring as mottles or stringers (sub-horizontal veins). In several profiles pedogenic calcrete occurs as incipient nodules, small newly formed concretions occurring isolated within the host sediment.

Platy or sheet-like morphologies and infiltration veins following fractures into host material develop in **lithified substrates**. Crudely laminar features are typical of platy samples; these can be distinguished from the dense finely surficial laminar calcrete developed from precipitation of carbonate from soil water ponded over an impermeable surface.

2.3 Micro-morphological Analysis and Description

One hundred and forty oriented samples were cut and impregnated with epoxy resin before mounting on 2 x 10cm glass slides and grinding down to produce a thin section. Half of the thin section was etched with 10% HCl for 10 seconds, then stained with combined potassium ferricyanide and Alizarin red solution according to Dixon's method (Dixon, 1965). The staining and etching allows better optical recognition of microstructures and the distribution of detrital minerals, and detection of calcite (red) and dolomite (purple) on the basis of stain colour. Considerable difficulty in thin section preparation was encountered, with many samples cracking the glass slide when heated or when excess sample was cut off. The cause of this is considered to be stress within the section dueto the expansion/contraction of

swelling clays within the sample when heated/cooled. Success rates with thin section preparation were moderately improved when a lower temperature was used to set the epoxy resin. Seventy-five broken fragments of selected samples were mounted on aluminium stubs and heavily sputter-coated with gold prior to viewing with a scanning electron microscope. Whereas most data regarding the distribution and relationships of the constituents are obtained optically from thin section using a petrographic microscope, SEM allows much higher magnifications and visualisation of the three dimensional form of the constituents.

Texture and fabric are terms used by geologists and pedologists to describe aspects of the size, shape and arrangement of the constituents of rocks and soils at high magnification. Traditionally, scientific enquiry into the formation and origins of pedogenic calcrete has used geological terminology to describe observed microfeatures. While this nomenclature is preferred in the current thesis some soil fabric terminology from Brewer and Sleeman (1988) is utilised were no geological term exists to adequately describe the observed micro-feature. The following sections describe the micromorphology of the sampled pedogenic calcrete. Sample names are given in the form of a site name (a nearby locality) and a site number with a suffix denoting the depth of the sample (in metres).

2.3.1 Calcified soils

Calcified soils occur as powdery and friable to semi-indurated massive or mottled horizons in the lower parts of mature profiles and as 'younger' calcretes developed on recent dune sands. The major constituents in coarsely textured soils are typically a grain-supported skeleton of coarser particles (quartz grains) with aggregates of microcrystalline carbonate and sparse calcified filaments in intergranular spaces. The massive semi-indurated dolomitic soils and mottled calcrete sampled from the lower sections of profiles typically consist of microcrystalline fine powdery carbonate. Porosity in these 'softer' samples tends to be intergranular and vughy, however

plucking of samples during thin section preparation commonly leads to false porosity observations.

2.3.2 Dense Micritic fabrics

Dense accumulations of microcrystalline calcite with floating grains of quartz are typical of many indurated nodular and hardpan samples as well as epigenetic (infiltration) veins cementing lithified host material aggregates. This fabric is massive and shows varying degrees of transmittance in thin section due to the presence of clays and void-filling microspar and spar calcite, and commonly contains pellets, ooids and spar-filled fractures. Texture and the amount and type of porosity in micritic fabrics is highly variable and irregular even over small distances. The majority of porosity is observed as being vughy or channel type porosity. This fabric has been reported worldwide and is generally considered to form through the inorganic precipitation of crystallites through carbon dioxide degassing or evaporation and subsequent supersaturation of meteoric waters i.e. secondary crystic fabric of Brewer and Sleeman (1988) or the alpha fabric of Wright and Tucker (1991).

2.3.3 Fabrics composed of laminated rinds

Features such as coatings, channels and recemented or loose pisoliths typically occur in the upper section of profiles suggesting that dissolution and re-cementation processes occur when percolating rainwater interacts with the carbonate. Laminar rinds in nodular and hardpan calcrete occur both internally and externally and are commonly truncated by dissolution features and in-filled channels (Figure 2.4). Clasts of diverse size and shape including indurated (re-cemented) calcrete and soil, ferruginous nodules, host rock fragments and black pebbles form nuclei for the precipitation of laminar rinds. Under magnification, the lamination in these rinds is crude and discontinuous. Many laminated rinds and in-filled channels are not

accretionary layers of calcite successively deposited from calcium-charged waters, rather they are composed of calcified filaments. These occur as sinuous tubular microstructures composed of a calcite sheath (4 to 7μm, rarely up to 10μm external diameter) with radial crystallinity and a central pore (1 to 2μm). They may be well preserved or overgrown with micritic cement so that only their (filamentous) porosity is preserved. Thin sections stained with Alizarin red / K-ferricyanide solution (that is Dixon's stain without the mild hydrochloric acid etching) are particularly useful in outlining their form (Plate 2.1). Calcified filaments are commonly the dominant component in nodular and hardpan calcrete. Their growth appears to be displacive, as indicated by floating quartz grains and the displacement of residual minerals in laminated coatings. Organic matter is commonly associated with the calcified filaments, being visible in thin section as dark amorphous filaments or dendritic accumulations in laminations, voids or micro pore-space (Plates 2.2, 2.3c, 2.4c).

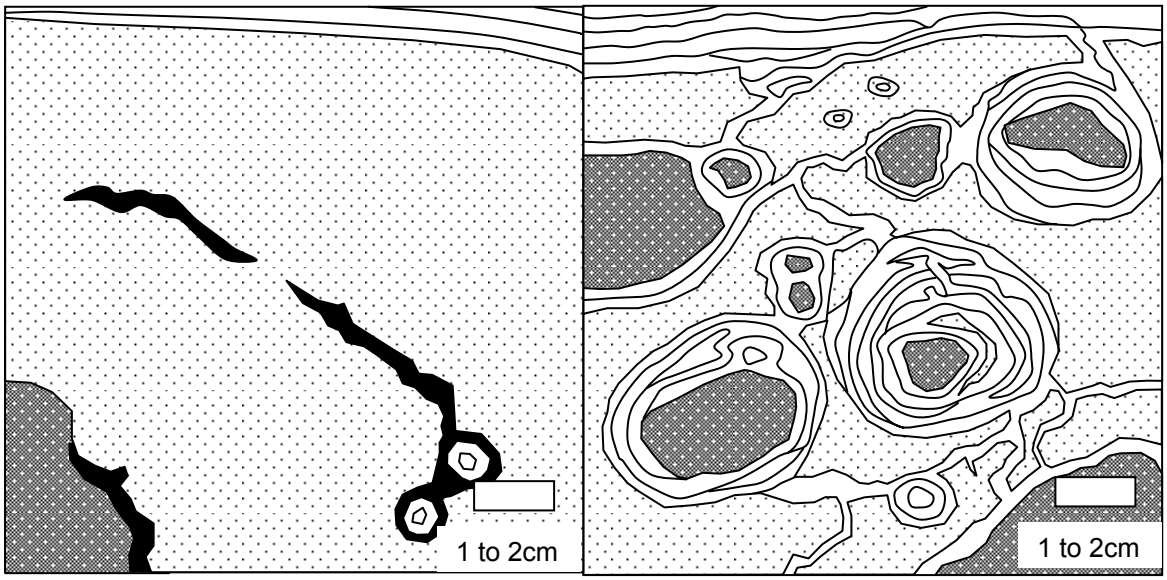

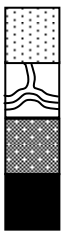

Dense micritic fabric

Laminated coatings and channels

Reworked clasts

Void space

Figure 2.4. Common massive (left) and coated grain or pisolitic (right) structure in indurated calcrete.

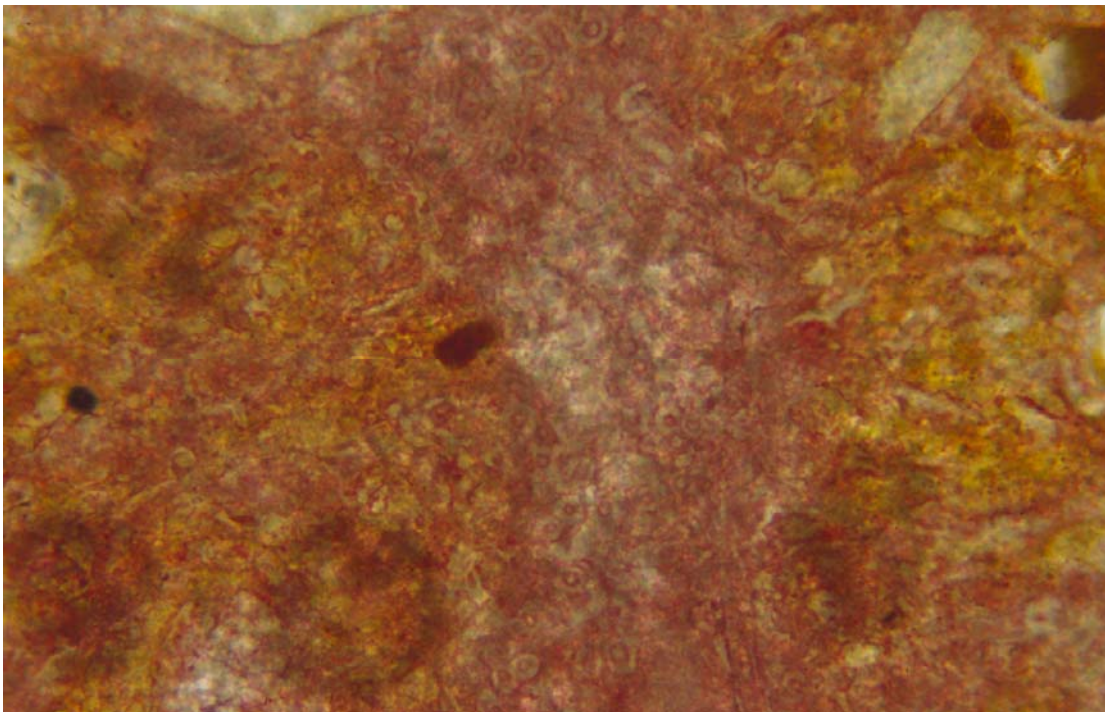

Plate 2.1. Thin section photomicrograph of laminar rind in pisolith sample 26A-0.2 from Renmark showing abundant calcified filaments. Sample stained with Alizarin red / K-ferricyanide. Field of view is 0.30mm

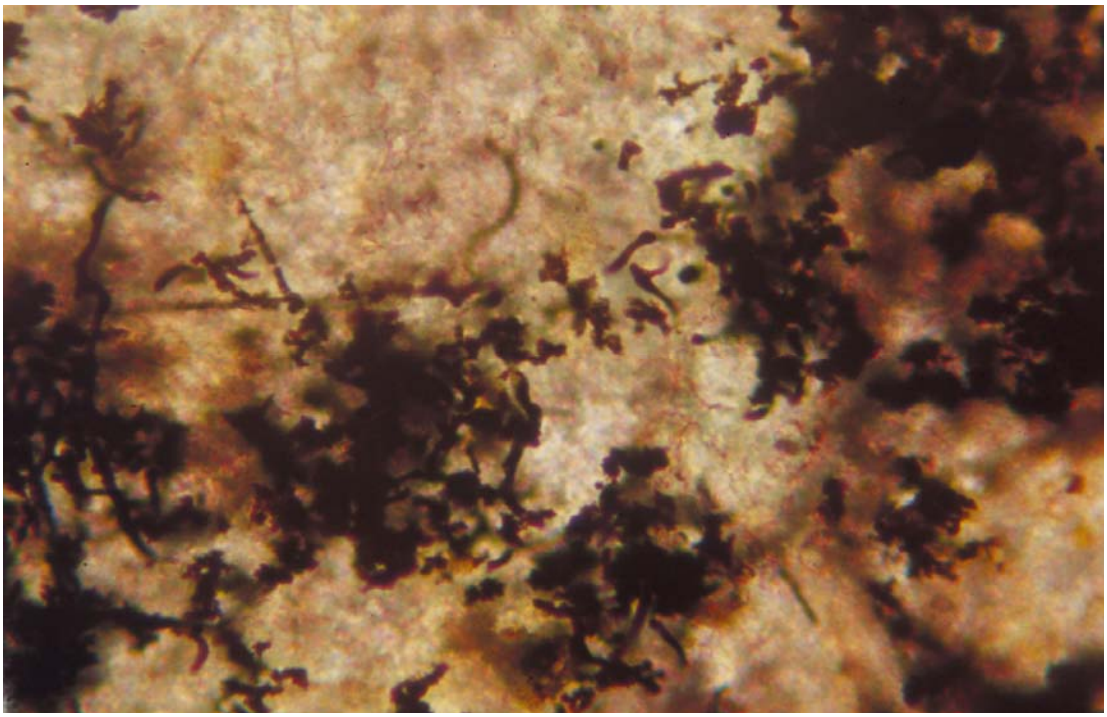

Plate 2.2. Thin section photomicrograph of laminar rind in hardpan sample 163A-0.2 from Nundroo showing abundant filamentous organic matter. Field of view is 0.30mm

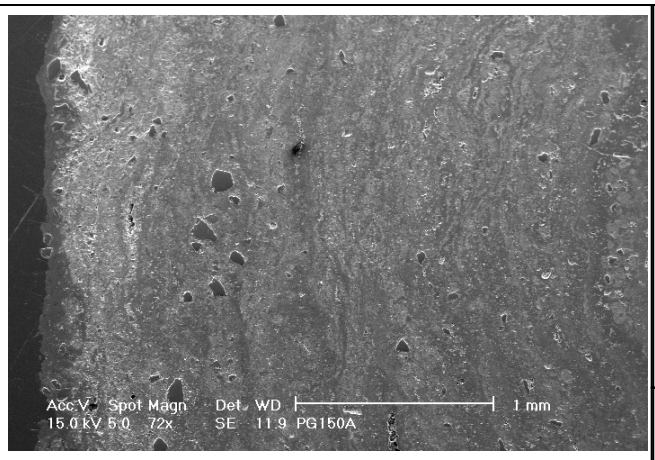

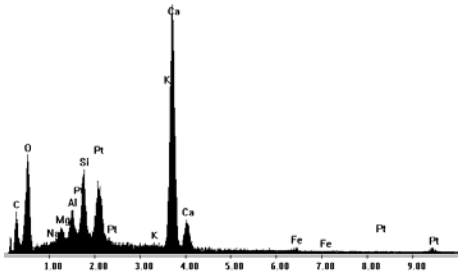

A. Broad spectrum of concentric coating on pisolith contained within hardpan.

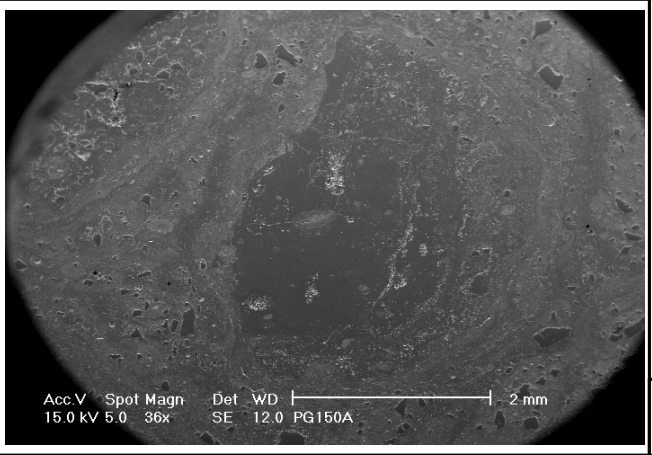

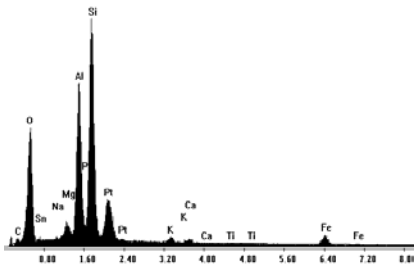

B. Clay clast in centre of pisolith.

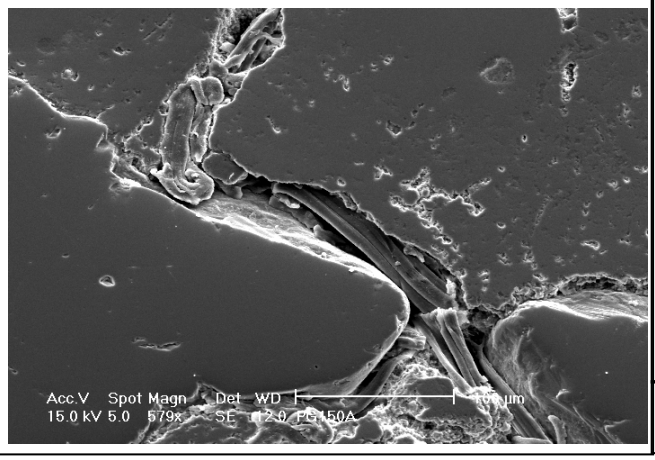

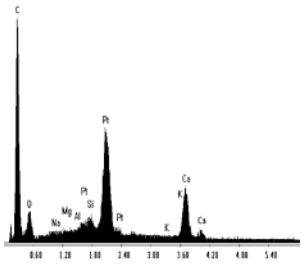

C. Filamentous organic matter contained within concentric coating.

Plate 2.3. Scanning electron images and results from EDAX spot analysis of Pt-coated polished section from calcrete hardpan sample from Riverina (150A-0.4).

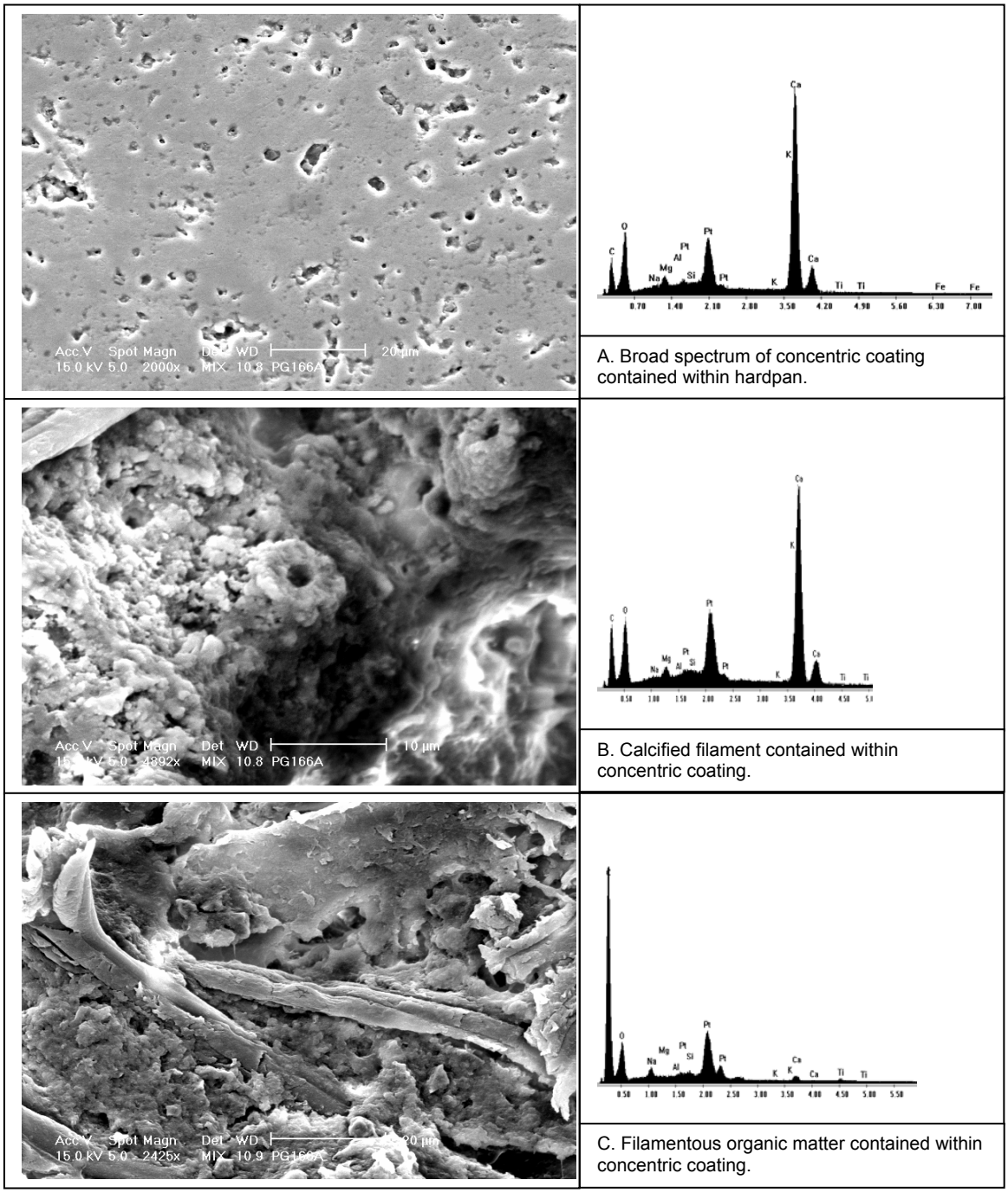

Plate 2.4. Scanning electron images and corresponding results from EDAX spot analysis of Pt-coated polished section of internal coating from calcrete hardpan sample from Wirrulla (166A-0.2).

2.3.4 Other Biological and Rhizogenic Fabrics

Relatively few examples of needle-fibre calcite were observed in the collected samples. Their occurrences are generally restricted to pore-filling bundles or bridging cements within channels in host material, calcified soils and nodules. The resultant fabric produced by the preferential orientation of the needle-fibres into convoluted networks is termed alveolar septal structure (Esteban and Klappa, 1983; Verrechia and Verrechia, 1994). Examples of this distinctive structure are found in channels within platy hardpan calcrete sampled from Wirramina (75C-0.6; Figure 2.8A). Needle fibre calcite is the dominant carbonate form in the profile sampled from Dumbleyung (119C-0.5) in the temperate southern wheat belt region of Western Australia. The profile is composed of macroscopic friable sub-horizontal "sheets" in soil overlying weathered ultramafic bedrock. The needle fibres are typically overgrown forming a random mesh fabric (Plate 2.5 A and B). The occurrence of needle fibres in channels and sheets suggests a rhizogenic influence on their formation. Microrods with a filamentous micro-morphology (Plate 2.5 C to E) occur in semi-indurated calcrete sampled from Kingoonya West (80A-0.1) and contain organic matter resembling conidiospores (Plate 2.5F). These are characteristic asexual fungal spores of ascetomycetes fungi (Raven *et al.*, 1986 p. 205). Sample 138A-0.3, collected from an exposed pit at Ora Banda in the Western Australian Goldfields region is composed of massive nodules with birds-nest structures, root moulds and p-type poly-crystals visible at high magnification (Plate 2.6). The channelled structures within the sample (Plate 2.6 A and B) suggest the influence of plant roots, however the morphology of the poly-crystals and birds-nest structure is possibly of microbial origin.

Many morphological features of calcrete such as platy structures, vertically elongate nodules, tubular rhizoliths and channel structures can be attributed to the presence of roots of higher plants (Klappa, 1980). Channels that are tubular and elongate with a cross-section approximating a circle are common in many southern Australian

nodular and hardpan calcretes. The cause of these channels is considered to be the action of plant roots displacing host material on a centimetre to sub-millimetre scale. Subsequent infilling and cementation of the channel by calcified filaments, needle-fibre calcite or convoluted micritic or sparry layers occurs without the incorporation of detrital minerals.

Micromorphological evidence for the preservation and direct replacement of plant tissue structures by calcite (Plate 2.7A sample 148C-0.6) occurs in incipient calcrete nodules sampled from Menzies in Western Australia. The degraded amorphous and vughy microtexture in the sample is clearly seen using scanning electron microscopy (Plate 2.7B-D). Vertically oriented cylindrical rhizoliths sampled from Wamberra Road South (21-0.1) in the Murray Basin and a massive cemented river gravel (38-0.4) sampled from Triverton Homestead contain dense grey cements composed of uniform microspar crystals and grey micritic cement with recognisable microspar crystals which are larger adjacent to enclosed grains (commonly quartz) and arranged so that the longest axis of each individual is arranged approximately normal to the boundary between the matrix and enclosed grains (Plate 2.8B) (termed normalic fabric in soil terminology of Brewer and Sleeman, 1988). The presence of quartz and the peculiar arrangement of calcite in this fabric suggest post-mortem introduction and calcification of wet carbonate mud in space formerly occupied by plant roots. One unusual rhizolith profile sampled from Tammin (118B-0.65 to 118E-1.7) in the Western Australian wheat belt contains vertically stacked dolomitic nodules with a fabric resembling alveolar septal structure (Plate 2.8C) but composed of dense euhedral to anhedral dolomitic micrite. Indurated samples with a platy morphology, taken from below massive indurated limestone at Melton (samples 110A-0.55 to 110C-1.05) or within thick tabular hardpan sampled from Kadina (sample 101C-0.9) are composed of contorted layers of dense microcrystalline calcite with fenestral pores and little or no detrital quartz and clay. These are interpreted as being horizontal calcretized root conduits after Wright et al. (1988). Microcodium-like structures (Plate 2.8E sample 134B-0.3) and the preservation of plant tissue structures occur in incipient calcrete nodules sampled from Salmon Gums South.

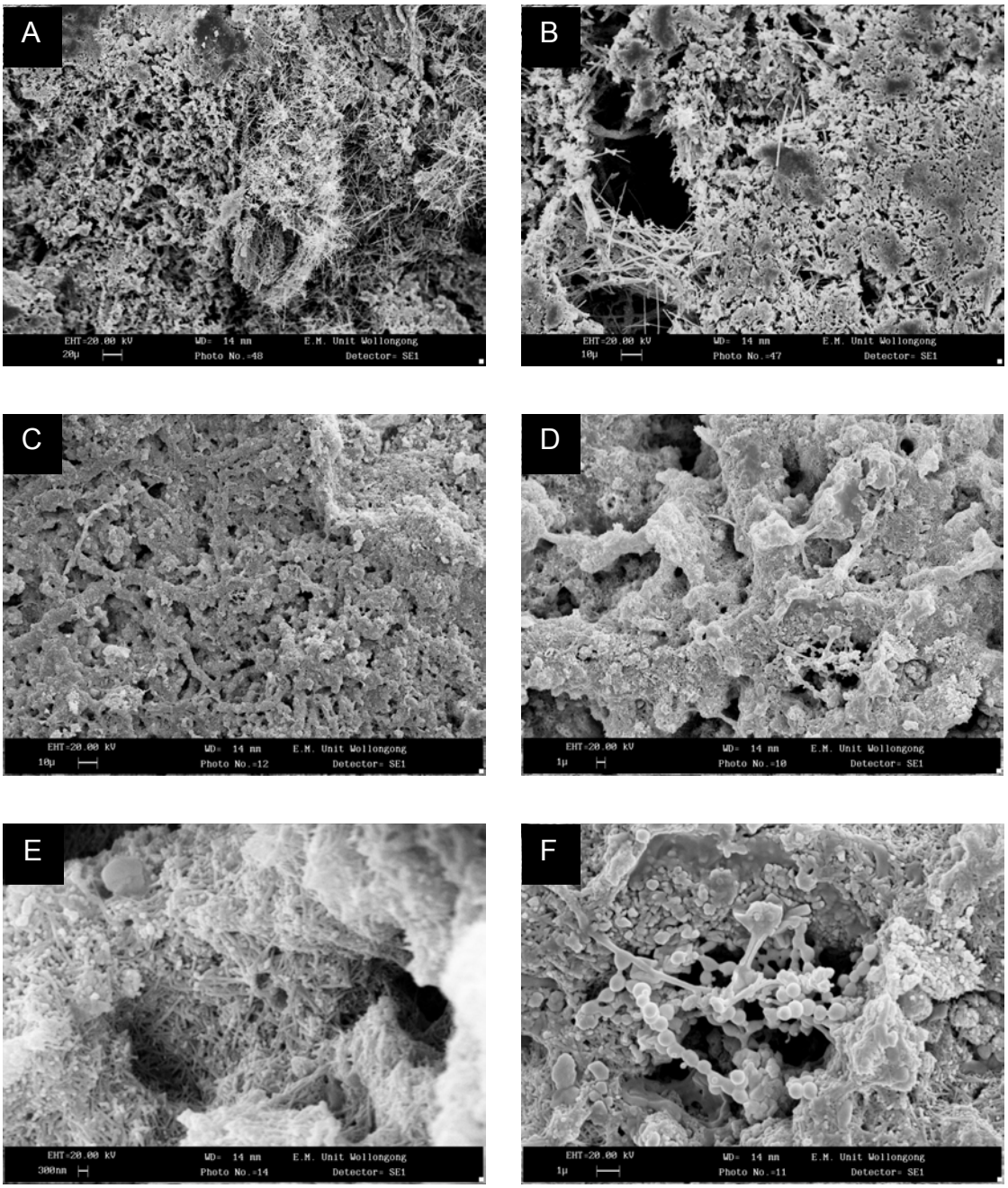

Plate 2.5. Scanning electron photomicrographs of microbial calcrete.

A and B – needle-fibre calcite from Dumbleyung (119C-0.5). C to F – microrods with filamentous structure and organic matter (conidiospores – characteristic of ascetomycetes fungi) from massive calcrete from Kingoonya West (80A-0.1).

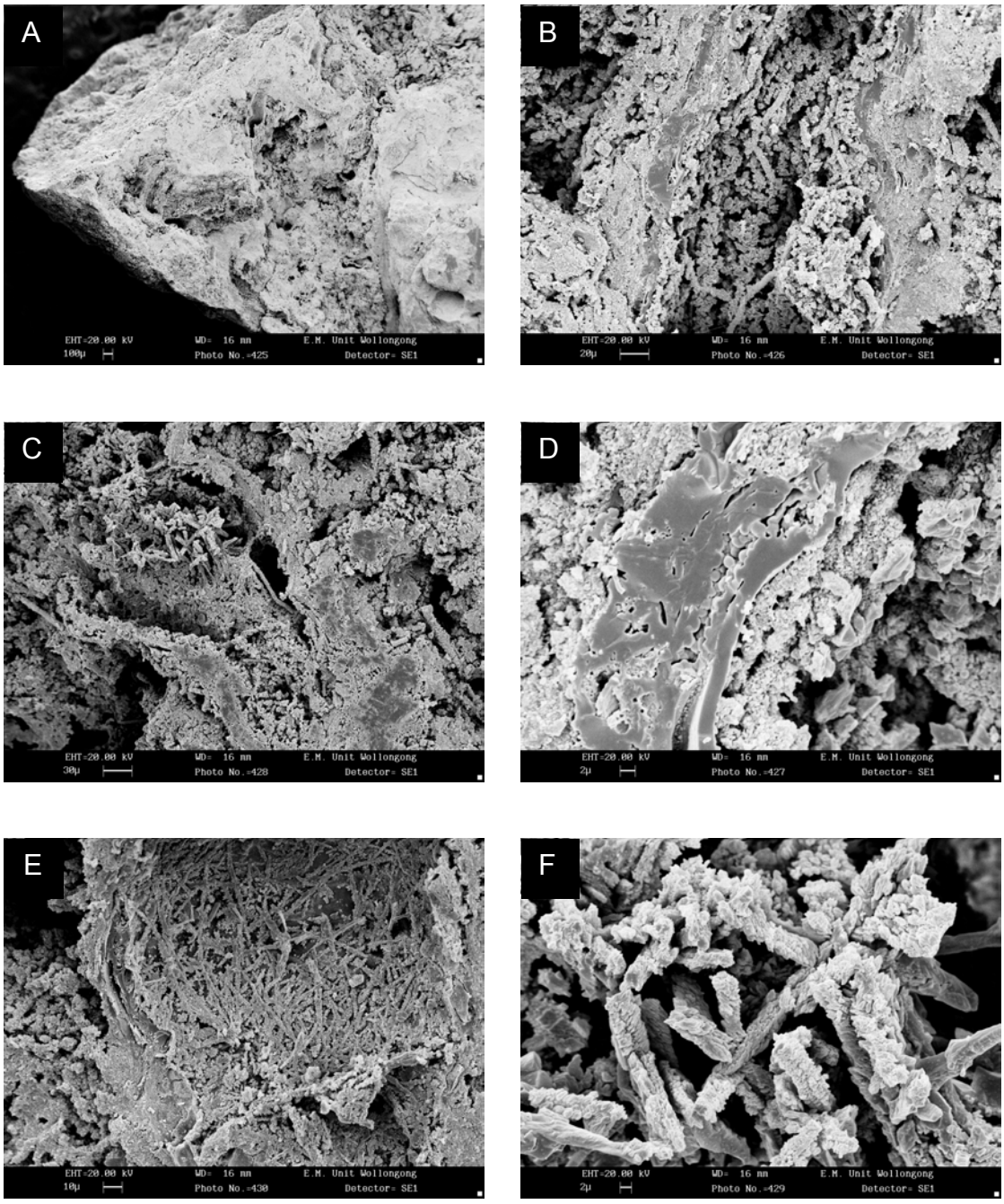

Plate 2.6. Scanning electron photomicrographs of massive nodule from Ora Banda (138A-0.3). A - Low magnification view of nodule showing channelled structure. B to D - High magnification view of root mould structures. E - Birds nest structure. F - High magnification view of P-type poly-crystals.

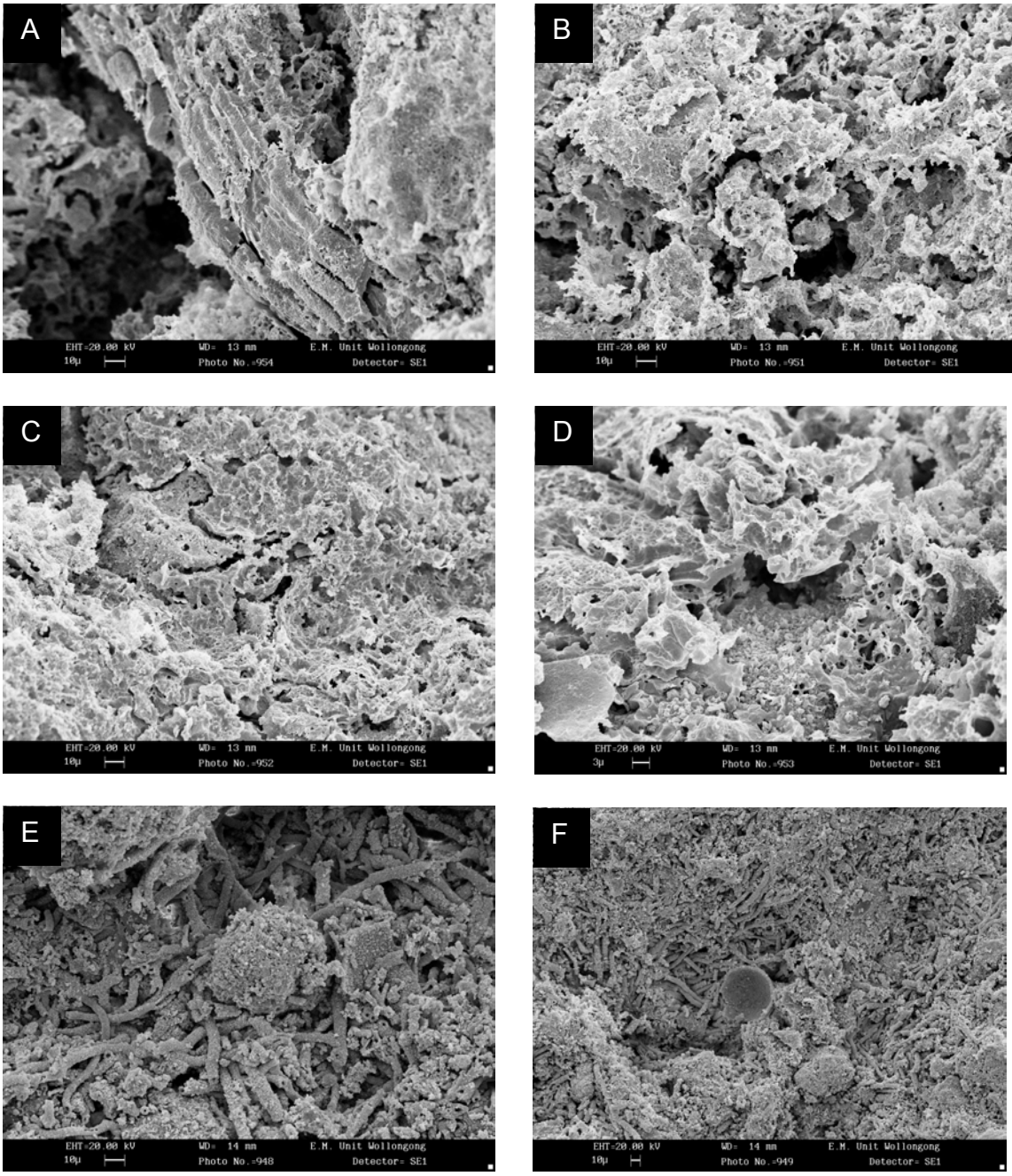

Plate 2.7. Scanning electron photomicrographs of rhizogenic calcrete microtextures and calcified filaments from Menzies (148C-0.6). A to D – sample shows direct replacement of plant root tissue and degraded amorphous calcite with vughy texture in an incipient nodule. E and F – the same sample showing calcified filaments and sphere (centre image F).

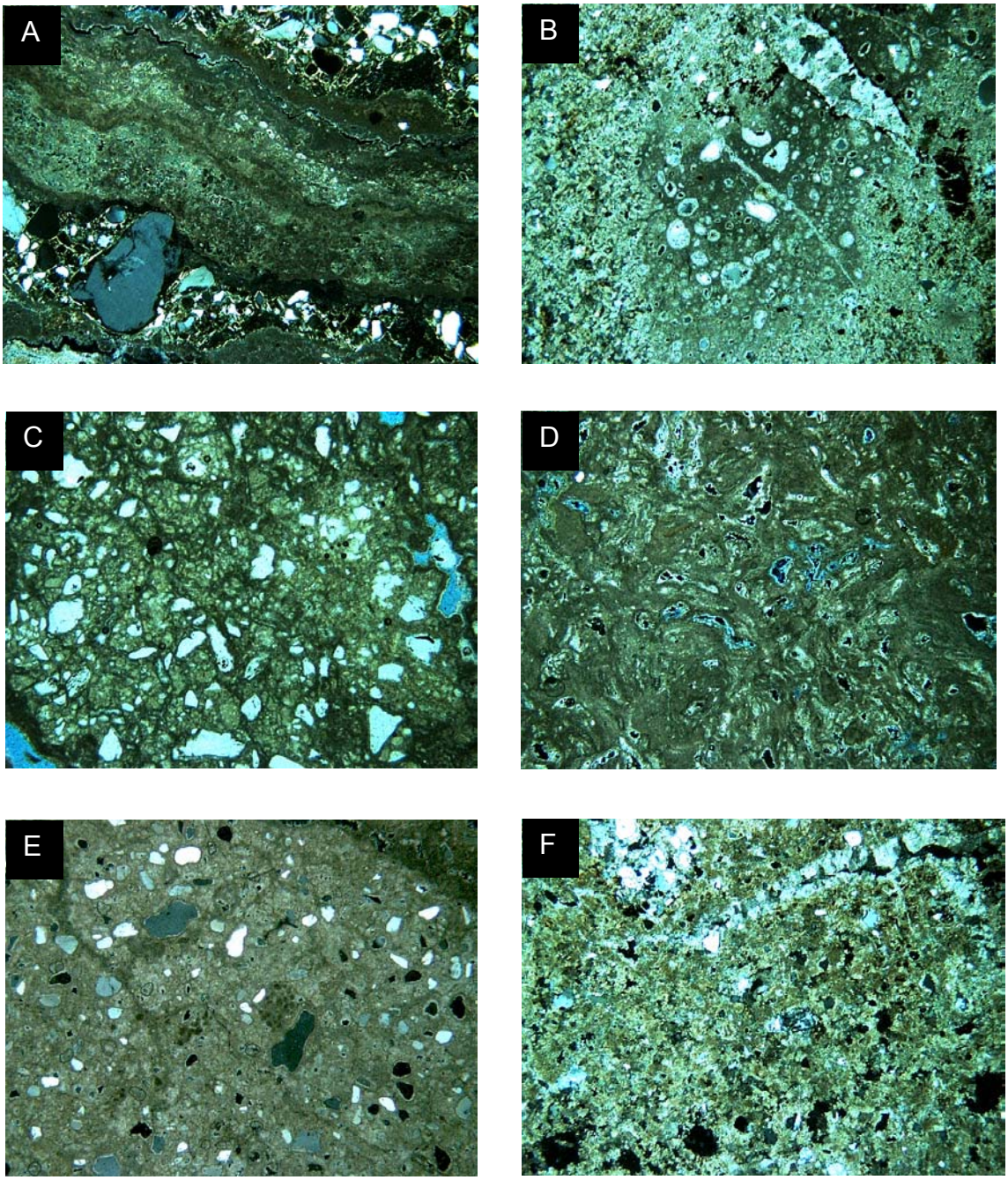

Plate 2.8. Thin section photomicrographs. A. Wirraminna (75C-0.6) horizontal channel composed of needle fibre calcite. B. Triverton Homestead (38B-0.7) showing normalic and granular fabric. C. Tammin (118C-0.9) showing alveolar-like fabric resembling replaced cells. D. Thick (approx 5 to 10cm channel) from Kadina (101B-0.7) showing fenestral fabric. E. Salmon Gums South (134B-0.45) showing alveolar-like fabric and microcodium-like grain (centre right). F. Burra (50-0.7) showing coarse granular fabric. Field of view is 48mm in all photomicrographs.

2.3.5 Phreatic Calcrete

Two grab samples from Burra and Triverton Homestead (50-0.7 and 38-0.7, respectively), collected from valleys in the uplands of the Adelaide Fold Belt, were originally considered to be massive pedogenic calcrete. In thin section, these samples are dominated by coarse granular fabric that consists of calcite spar as prismatic crystals (15 to 25 μm) that lack any preferred orientation and are in contact over all of their surfaces (Plate 2.8B and F) and lacking visible voids apart from large vughs. Conditions required for the formation of large calcite crystals with such fabric are considered to be prolonged periods of saturation. Thus these deposits are not typical of pedogenic calcrete and are tentatively interpreted as being valley or phreatic calcrete, however further detailed sampling and mapping is required.

2.4 Cathodoluminescence Petrography of Murray Basin Samples

In order to further investigate the petrographic properties of pedogenic calcrete eleven indurated samples from the upper sections of profiles sampled from the Murray Basin region of South Australia were prepared as polished sections mounted on 2 x 5 cm glass slides for examination using cathodoluminescence (CL). The process known as CL occurs when energetic electrons bombard the surface of minerals causing excitation of electrons within the mineral. After a short delay these electron return to their former energy state and may emit radiation in the form of visible light and other forms of radiation. The wavelength (colour) and intensity of the emission characterise certain impurities within the sample. In the case of carbonates, minute amounts of manganese (approximately 10–20ppm) within the crystal lattice are considered to produce visually detectable luminescence that appears as a bright orange–red glow. Other elements occurring as impurities, in particular rare earth elements, are also known to activate CL, whereas high

concentrations of iron are known to quench CL (Miller, 1988). The colour and intensity of the emitted radiation is dependent on several variables including beam voltage, current and current density (beam focus) and the nature and composition of the sample (Miller, 1988).

At present there are many difficulties in quantifying CL intensity and interpretation using CL petrography is subjective, its use being restricted to revealing fabrics rather than providing direct geochemical information. The importance of CL for interpreting diagenetic history of pedogenic carbonate comes from its potential to reveal textural details of cement stratigraphy, growth zonation and possibly relict structures not visible with a petrographic microscope.

Of the eleven samples prepared only three showed visible CL. These samples are used to provide a reconnaissance study into the cathodoluminescence petrography of the common mature forms of pedogenic calcrete found in the semi-arid zone of South Australia. The sample from Mannum (56A-0.1) is a semi-indurated nodule with grain-supported quartz and ferruginous grains with massive interstitial micrite cement. CL within the sample varies in intensity from intense pink luminescence (Plate 3.9 A and B) of a recemented round calcrete clast within the nodule, to less intense violet colour (Plate 2.9C and D) or poorly luminescent cements (Plate 2.9E and F) succeeding the recemented clast. The sample from Gandy Range Homestead (33A-0.1) is an indurated nodule containing dense massive and laminar cements. The sample contains numerous dissolution channels, caused by plant roots, which are clearly visible under transmitted light. CL in this sample is pink or violet in colour and highlights textures visible with transmitted light, in particular the dissolution channels, which are infilled with late-stage luminescent cements (Plate 2.10). The sample from Black Hill (55A-0.1) (Plate 2.11) is taken from hardpan composed of coalesced pisoliths; the concentric coatings are composed of calcified filaments. CL in this sample is orange-red coloured and highlights precipitation features associated with the density of calcite in the coatings and clotted micrite cements.

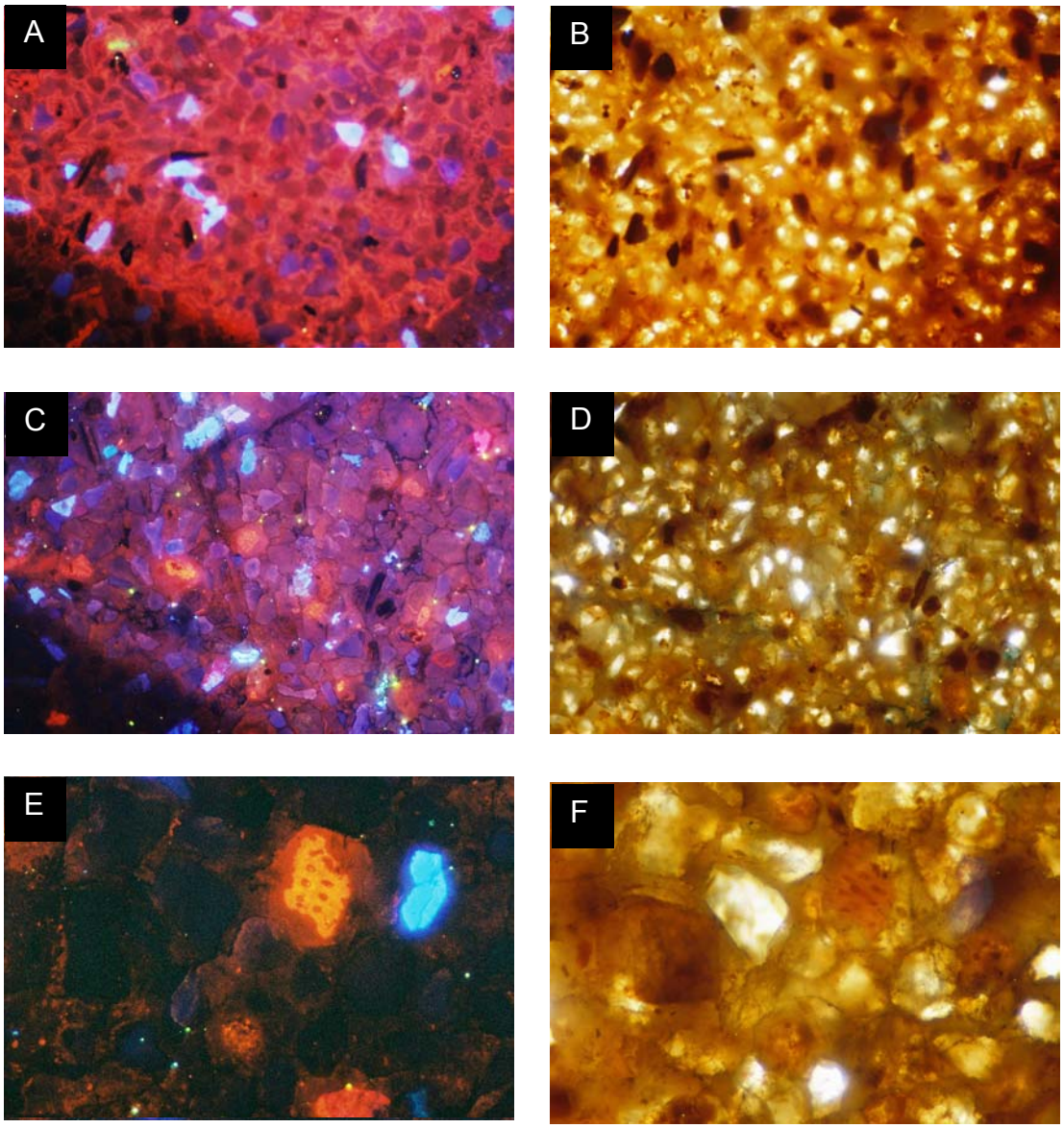

Plate 2.9 Cathodoluminescence (left column) and equivalent transmitted-light photomicrographs (right column) of Mannum sample (56A-0.1). A and B. Luminescent calcrete clast. Note bottom right corner is edge of clast and late stage non-luminescent cement. Field of view 29mm. C and D. Luminescent calcrete clast. Field of View 29mm. E and F. Late stage non-luminescent cement and luminescent residual minerals. Field of View 17mm. Note that bottom left hand corner of luminescence photomicrographs shows beam shadow.

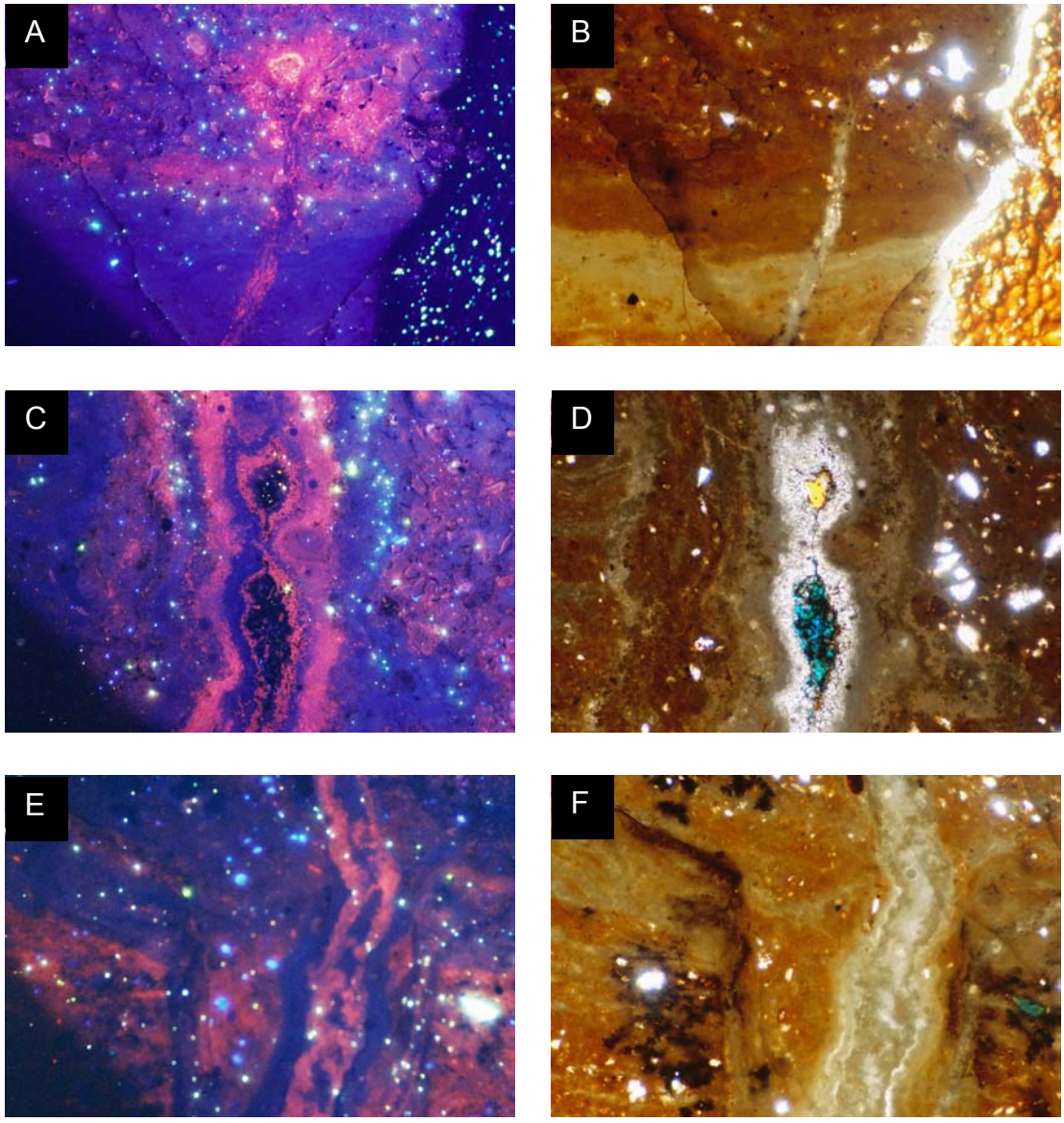

Plate 2.10 Cathodoluminescence (left column) and equivalent transmitted-light photomicrographs (right column) of Gandy Range Homestead sample (33A-0.1). A and B. Luminescent dense micritic laminar (bottom) and massive (top) cement and calcified root channel. Field of view 29mm. C and D. Luminescent channel infill. Field of View 17mm. E and F. Dissolution feature associated with calcified root and luminescent residual minerals. Field of View 17mm. Note that bottom left hand corner of luminescence photomicrographs shows beam shadow.

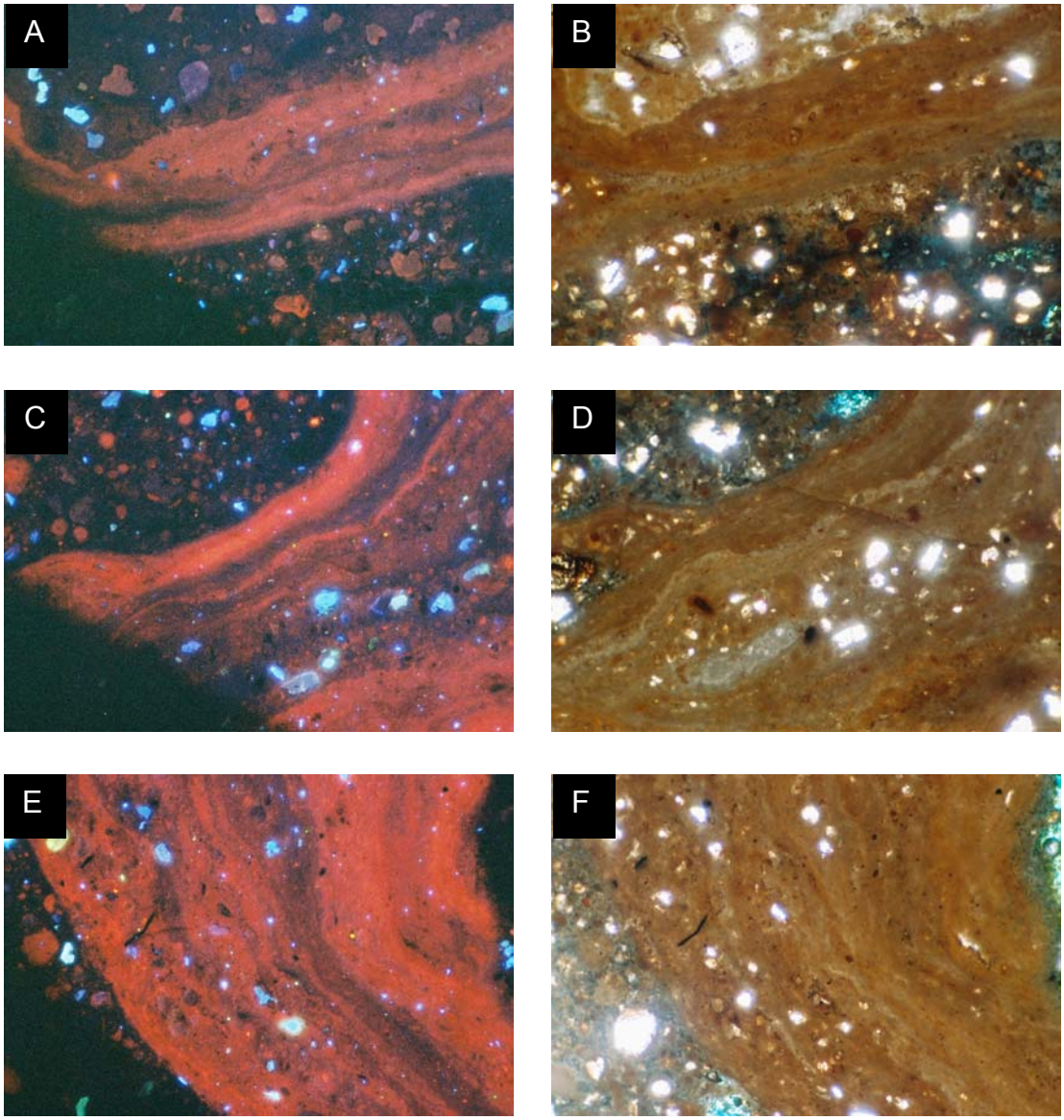

Plate 2.11 Cathodoluminescence (left column) and equivalent transmitted-light photomicrographs (right column) of Black Hill sample (55A-0.1). A and B. Luminescent coatings. Field of view 29mm. C and D. Luminescent coatings. Field of View 29mm. E and F. Luminescent coatings. Field of View 29mm. Note that bottom left hand corner of luminescence photomicrographs shows beam shadow.

2.5 Organic Matter

Microscopic examination of pedogenic calcrete shows that organic matter is commonly preserved in pedogenic calcrete as dark amorphous masses in channels and voids or as filamentous or dendritic accumulations associated with calcified filaments (Plates 2.2, 2.3 and 2.4). The viability of such organic matter were investigated using sixty-four different samples with high organic matter contents cultured on solid media using the technique of Boquet *et al*. (1973). Freshly broken calcrete samples were ground with sterilised water to a slurry and introduced to agar media enriched with calcium and glucose. Abundant bacterial and fungal colonies along with patches of microcrystalline calcite (tested for effervescence using mild HCl) covered all plates after incubation for one week at 30°C. While care was taken in regard to sterile conditions, the hyper abundance of organisms on the plates is regarded to be the result of weedy opportunistic organisms, possibly not indigenous to the soil, colonising the media. Further experimentation by biologists is needed to isolate and identify the organisms responsible for calcite precipitation in soils. Suggestions as to further research include varying the dilution and types of calcium compounds and nutrients in the culture media, examining variations with respect to light and mimicking the soil conditions under which the organisms formed using a Winogradsky-type technique (B.D. Dyer, pers. comm., 2005).

2.6 Discussion

That microbial and rhizogenic mechanisms contribute to carbonate precipitation is well documented and evident in many petrographically examined samples in this study. By far the most common microbiological components are calcified filaments

whose excellent states of preservation and common association with organic matter indicates that they are precipitating continuously and currently in mature pedogenic calcrete. While the calcified filaments occur in abundance in the coatings and channels that are common in most mature pedogenic calcretes, they are not restricted to such textural features and do also occur in massive nodules and hardpan. The occurrence of other micro-features such as alveolar-septal structures and needle-fibre calcite in channels and sheets, microcodium-like fabric in incipient nodules, fenestral fabrics in laminar or platy layers and in-filled channels caused by the action of plant roots are easily recognisable in thin-sectioned samples, indicating rhizogenic processes contributed to pedogenic calcrete formation. The occurrence of the various morphologies is problematic and as yet there are no clear answers as to what extent biogenic and rhizogenic features found in pedogenic calcrete are contributors to calcification or whether they are only accessory occurrences. Table 2.4 is constructed to simplify and clarify the terminology with respect to the following chapters and to summarise the results of this petrographic study.

Fabrics produced by the precipitation of vadose carbonate cements show considerable variation in terms of induration and density, porosity, granularity and the size, shape and distribution of residual minerals even within individual samples. Furthermore, vadose carbonate commonly occurs integrated with finely dispersed clay minerals, and cement distribution within samples can be massive or contain various biogenic microstructures. Vughs that are wholly or partly filled primary and secondary pore space are common as would be expected if carbonate precipitation proceeded as a cavity filling cement. The typical floating textures observed in many samples also show displacement of residual grains along with intense precipitation of dense carbonate. Discussion on the cause of this grain displacement has centred

Table 2.4. Summary table of pedogenic calcrete types found in this petrographic study.

Morphology	Occurrence	Description and Possible Origin
Laminar	Topmost horizon	The term laminar is restricted to the uppermost laminar horizon (<10 cm thick), thin continuous micritic laminations, considered to form by ponding and evaporation of surface water above an impermeable horizon.
Coatings and channels	Brecciated hardpan Nodules Pisoliths	Discontinuous laminations and infilling cements composed of calcified filaments.
Massive indurated to semi-indurated	Hardpan Nodules Solutional veins	Massive micritic cement and clay with floating grains of quartz and iron oxides. Possibly formed by intense evaporation or carbon dioxide degassing.
Massive friable	Calcified soil at the base of hardpan or nodular calcrete	Pore filling micrite and clay with grain-supported quartz and iron oxides. Possibly formed by carbon dioxide degassing.
Rhizogenic calcrete	Nodules	Alveolar (lung-like) microtexture.
	Taproot fragments	Normalic or massive microtexture.
	Platy/sheetlike	Needle-fibre calcite or fenestral microtexture.
Recent powder calcrete	Mottles	Formed as recent calcrete in dune sands, possibly by evapo-transpiration.

on the processes of partial or total replacement of minerals unstable at atmospheric temperature and pressure, and displacive or expansive carbonate crystallisation from supersaturated vadose solutions (Watts, 1978; Klappa, 1979). There is no evidence to suggest 'atom by atom' replacement of host minerals with vadose carbonate and replacive textures observed are considered by this author to be the result of apparent displacement whereby minerals dissolved in the vadose zone are passively replaced by void-filling carbonate cements.

The current study includes a number of examples of pedogenic calcrete developed in ferruginous duricrust host material in the interior arid regions of South and Western Australia. The detrital ferruginous grains or clasts contained within the dense to relatively porous micritic carbonate are typically well-rounded granules and pebbles. The abrasion evident on the clasts is a result of weathering and disaggregation of host material caused by dissolution and reprecipitation processes (and movement caused by displacive crystallisation and desiccation), and expansion of the host material through repeated mechanical penetration and displacement by organisms, in particular the root networks of higher plants. The same processes presumably operate on host materials composed of more resistant minerals such as quartz without the abrasion of grains being visually obvious in thin section. In addition, cathodoluminescence petrography reveals no evidence of fabrics and textures replaced by carbonate cements suggesting that precipitation of pedogenic calcrete proceeds by dissolution and re-precipitation reactions resulting in the destruction of previous fabric. The presence of fine quartz grains at depths of up to one metre in pedogenic calcrete developed on mafic and ultramafic host material (sites at Dumbleyung; site 119, and Norseman North; site 152) indicates that significant

mixing occurs within the profile between overlying aeolian soil contributions and underlying lithologies. The cause of this mixing is considered to be a result of the gravitational filling of primary and secondary channels and voids caused largely by plant root displacement and the result of many phases of carbonate dissolution and re-precipitation. The affect of burrowing organisms, in particular insects such as ants, may also contribute to mixing of the pre-existing soil with vadose carbonate cements, however evidence for this was not noted in the examined samples.

The influence of higher plants on the development and fabric of pedogenic calcrete is not necessarily restricted to the rhizogenic features described previously. For example, the cathodoluminescence images in Plates 2.10A and B shows an in-filled root channel penetrating dense micrite, the root dividing into smaller rootlets on entering the clotted micrite. The brightly luminescent cement filling the root channel and the zone where the root contacts the clotted micrite is suggestive of water and nutrient extraction by the plant and concomitant micrite precipitation. Wright *et al.* (1988) considered certain peloids to be associated with root-mat horizons. The same association was found in the present study at the Melton site (110A-0.55 to 110C-0.105) and the Kadina site (101C-0.9), which consists of alternating layers of fenestral and peloidal micrite. However, peloidal micrite is also typical of alpha or non-biogenic clotted cements thus creating uncertainty about its origin.

Chapter 3

The Mineralogy of Pedogenic Calcrete

3.1 Background

3.1.1 Authigenic carbonate

By definition, calcrete is dominantly composed of calcite. However, as discussed in Section 1.4, debate exists as to whether dolomitic carbonate accumulations within the regolith should be included as calcrete. Part of this problem arises from the fact that, within a pedogenic calcrete profile the calcite/dolomite ratio commonly decreases with depth and dolomite commonly occurs as the dominant component at the base of a profile. This makes a nomenclature based on dolomite content (such as proposed by Netterberg, 1980) somewhat impractical for categorizing pedogenic calcrete.

Calcium and magnesium carbonate constitute a compositional or substitution series forming a group of minerals with different compositions. In addition iron can substitute for the cations in the crystal lattice of dolomite to give ferroan dolomite (>2 mole % $FeCO_3$) and ankerite (up to 25 mole % $FeCO_3$). Calcite is an ionic solid with a hexagonal (rhombohedral) crystal system and an aqueous solubility product of $10^{-8.4}$ at 25°C and atmospheric CO_2 pressure (Langmuir, 1968). The mineral dolomite has the ideal stoichiometric composition $(Ca,Mg)CO_3$, with equal proportions of calcium and magnesium in alternating layers or lattice planes separated by layers of CO_3. The 'ordering' of the carbonate crystal lattice has effect

on the thermodynamic stability and crystallization of dolomite. Significant problems in dealing with the kinetics of the dolomite reaction exist and it has been impossible to synthesize ordered stoichiometric dolomite at atmospheric temperature and pressure without biological and chemical mediation (the so-called dolomite problem, for reviews see Warren, 2000, and Tribble *et al.*, 1995).

At temperatures less than 100°C dolomite formed tends to be Ca-rich and lacking order and over time these dolomite-like phases are considered to alter to ordered stoichiometric dolomite. The exact mechanism of dolomite formation in the sedimentary environment is not known and while dolomite is common in the sedimentary record there are few modern analogues for dolomite precipitation, such as in sabkhas or saline lagoons like the Coorong region of South Australia (Alderman and Skinner, 1957). The dissolution of dolomite is slower than calcite in acidic solutions and comparison of free energy values for calcite and dolomite indicate that dolomite is slightly more stable than calcite (Robie *et al.*, 1978). The solubility product of dolomite is hard to define with estimates based on dissolution experiments by numerous researchers as summarized by Lippman (1973), cluster at around 10^{-17}, significantly lower than that needed to precipitate dolomite directly from seawater at the concentrations in which it occurs. Lippman (1973) further suggested that the electrostatic strength of bonding of the small magnesium ion to dipole water molecules inhibits entry into the anhydrous crystal structure of dolomite. Many researchers (i.e. Warren, 2000; Kelleher and Redfern, 2002; Schmidt *et al.*, 2005) have observed the formation of hydrous and amorphous CaMg-carbonate during laboratory synthesis of dolomite and have termed this as protodolomite (Graf and Goldsmith, 1956), considering that it is an intermediate or

precursor compound through which ordered dolomite is formed in low temperature environments.

Whole-rock XRD data can give information on the Mg content of calcite and the Ca/Mg excess of dolomite. The Mg ion being smaller than the Ca ion results in a decrease in the d_{104} lattice spacing and consequent shift in the position of the d_{104} XRD peak, the precise position of which is determined using quartz as an internal standard or reference point (Hardy and Tucker, 1988). The regression line (equation) can apparently be projected from calcite through dolomite giving only slight errors (Goldsmith *et al.*, 1961). Ferroan dolomite however poses a problem in that the slightly larger size of the Fe ion relative to the Mg ion causes a noticeable increase in the lattice spacing of the d_{104} XRD peak (Goldsmith and Graf, 1958). Thus note has to be taken when analyzing iron-rich carbonates. Quantification of mixtures of carbonate can also be determined using the peak height (Cu K_∞ intensity) of the d_{104} peak of calcite (2θ 29.43°) and dolomite (2θ 30.98°) in the following linear relationship (Goldsmith and Graf 1958):

dolomite/(dolomite + calcite) = 0.01 wt% dolomite – 0.023

Information regarding the ordering of dolomite crystals is also obtained using whole rock XRD. The segregation of cations into separate sheets within the dolomite causes a set of superstructure reflections corresponding to the d_{105}, d_{021} and d_{101} lattice spacings (Hardy and Tucker, 1988). The relative intensity or peak height of these ordering peaks when compared to non-affected diffraction peaks can be used to give a measure of the degree of ordering of the dolomite crystal. Typically the

ratio of the height of the ordering peak 015 (35° 2θ) to diffraction peak 110 (37° 2θ) is used i.e. the lower the ratio, the higher the degree of disorder.

3.1.2 Detrital minerals

It is important to recognize that pedogenic calcrete is a mixture of authigenic carbonate minerals containing pre-existing phases of the parent material. The bulk of the residual mineral content is composed of the resistant phases quartz, feldspars, iron oxides and various forms of the residual clays illite, kaolinite and montmorillonite. In arid areas calcrete commonly forms distinctive intergrade crusts with indurated ferruginous duricrusts and red-brown hardpans where carbonate has penetrated as veins and layers into these previously formed regolith materials (Anand and Paine, 2002).

3.1.3 Authigenic clays and calcium oxalate

The neoformed magnesian clays palygorskite [$(Mg,Al)_2Si_4O_{10}(OH).4H_2O$] and sepiolite [$Mg_4Si_6O_{15}(OH)_2.6H_2O$] are commonly associated with pedogenic calcrete. It seems that vadose conditions leading to calcrete development are favorable for in-situ palygorskite and sepiolite formation. According to Watts (1980) the neoformation of these minerals is explained as a result of the release of magnesium by high-Mg to low-Mg calcite transformations and either subsequent alteration of precursor clay minerals or concomitant precipitation from solution.

Calcium oxalate is a common biomineral with a widespread occurrence among plants, algae, fungi and lichens. It appears to be related to various possible

functions including tissue calcium regulation, protection from herbivory and metal detoxification (Nakata, 2003). The solubility of calcium oxalate is low and precipitation takes place readily when oxalate (as oxalic acid: $H_2C_2O_4$) is present; this is commonly derived from higher plants and fungal processes in sediments and soils. Calcium oxalate occurs as crystals in a variety of shapes and as monohydrated and dihydrated forms (whewellite: $CaC_2O_4.H_2O$ and wedellite: $CaC_2O_4.2H_2O$, respectively) and its presence indicate currently forming rhizogenic calcrete (Cailleau *et al.*, 2005).

3.2 Methods

XRD analyses on finely powdered samples whole-rock pedogenic calcrete samples from profiles were performed using a Philips 1150PW Bragg-Brentano diffractometer with Cu K_∞ radiation, and a graphite monochrometer. Identification and quantification of the X-ray diffractograms were performed using μPDSM and siroquant software. XRD traces are given as .cpi files in the Appendix CD and the identified minerals and calcite:dolomite ratios are listed on the logs in Appendix I.

Accurate determination of clay mineralogy is difficult using only whole rock diffractograms and analysis of the acid insoluble <2μm fraction and heating or glycolation experiments are needed to conclusively quantify the clay fraction. Considering the number of samples, the usefulness of whole rock data in determining the Mg content and lattice ordering of carbonates, and the search for calcium oxalates that are destroyed by acid reaction (the importance of calcium oxalate derives from its origin as a direct biological product of plants and fungi), only whole-rock XRD data were obtained in the present study.

3.3 Results and Discussion

A gradation in mineralogy from calcitic calcrete in upper samples, grading to dolomitic calcrete at the base of the profile, is typical of many pedogenic calcretes sampled from sub-humid to semi-arid regions on all bedrock types. In contrast, pedogenic calcrete profiles sampled from arid regions in the vicinity of Tarcoola and Kingoonya in South Australia and Menzies in Western Australia are calcitic with no gradation to dolomite at the base of the profiles. This suggests influence from either climate or rainfall composition on the occurrence of dolomite in the deeper horizons of pedogenic calcrete profiles. Samples from the Tammin profile (site 118) are peculiar in that they are indurated and dolomitic with rhizogenic macro- and micro morphology. Such pedogenic calcrete has not been reported previously in the literature. The calcite present in the samples is invariably low-magnesium calcite as is typical of pedogenic calcrete. Dolomite in the samples is typically calcian dolomite with up to 10% but commonly less than 5% calcium excess. These results are, however, affected by iron (ankerite) content of the carbonate giving results that may be excessively calcian. The ratio of the height of the ordering peak 015 (35° 2θ) to diffraction peak 110 (37° 2θ), for powdered samples with dolomite as the dominant component, is given in the Appendix CD as file xrdcounts.xls. Dolomitic samples had d_{015} peaks and ordering ratios ranging from 0.3 to 1.4 with many profiles showing steady values or apparently random results through the profile. A general downward decrease in ordering ratio is observed for a number of profiles where dolomite occurs close to the surface (within the top 0.2m) with semi-indurated and powdery samples lower in the profile having relatively lower ordering ratios than dolomite occurring close to the surface. This downward decrease in the degree of order is possibly a function of temperature and/or moisture availability.

Calcite/dolomite ratios are not related specifically to morphological or host material type, rather, dolomite occurs at the base of the profile were the calcrete morphology is semi-indurated or powdery and commonly mottled. The composition of these morphological types can also be calcitic. Pedogenic calcrete samples collected in the South Australian Murray Basin and Adelaide Fold Belt regions are typically developed on dolomitic host materials such as Blanchetown Clay, Bungunia Limestone, Eocene-Miocene marine limestone and dolomitic Adelaidean siltstone. The source of dolomite (and possibly calcite) in these cases is presumably the host material with the pedogenic calcrete forming through vadose dissolution and reprecipitation of the dolomite component within the profile. Discrete dolomitic clasts are commonly incorporated into the calcitic upper nodular and hardpan sections of the profile such as in sites at Renmark (PG26), Tailem Bend (PG57) and Salmon Gums North (PG129) where the pisoliths, nodules and hardpan contain cores of fragmented dolomite with (micro) fractures penetrated by sparry and microcrystalline calcite. The Mg-content of calcite and dolomite also remains relatively constant down-profile indicating that two discrete phases exist rather than a gradational transition from calcitic to dolomitic carbonate.

Samples collected on non-calcareous host materials such as aeolian dunes and alluvial/fluvial red-brown sandy clays, colluvial deposits, basic intrusive rocks, as well as thick pedogenic calcrete profiles where the host material is undetermined, also show basal dolomite concentration to greater or lesser extents. Based on major-element geochemical data from pedogenic calcrete profiles in southeastern South Australia, Hutton and Dixon (1981) considered the regularity of the decrease in Ca/Mg ratio with depth to indicate leaching that caused *in situ* modification of pedogenic calcrete profiles. The mechanism of this vertical differentiation is

proposed to involve the precipitation of calcite in upper parts of the profile by a saturated soil solution that subsequently dissolves and retains magnesium as soluble hydrated magnesium carbonate (nesquehonite - $MgCO_3.3H_2O$) as it percolates down the profile. The precipitation of dolomite at the base of the profile is considered to involve meteoric water penetration down to depths of up to 2m and higher precipitation rates during Pleistocene times are proposed as the cause of the change in chemistry/mineralogy with depth. The fact that pedogenic calcrete sampled from arid inland climatic settings are calcitic with no gradation to dolomite at the base of the profile supports this hypothesis. However, because of the difficulties in synthesising dolomite at low temperatures in the lab, the solubility product and hence calcium, magnesium concentrations and pCO_2 required to precipitate dolomite are not known. Thus models explaining vertical Ca/Mg differentiation are conjectural and consideration should also be given to the influence of biologically produced calcite, in particular the abundance of calcified filaments in the upper sections of many hardpan profiles, or perhaps the effect of mixing shallow magnesium-rich ground waters with percolating meteoric waters.

Hutton and Dixon (1981) discounted the calcareous loess hypothesis of Crocker (1946) on the basis that carbonates deposited from such a source would be uniform in chemical composition and accessory minerals over wide areas, whereas the pedogenic calcrete sampled from southeast South Australia show considerable variation in carbonate and clay mineral composition and appear to reflect the composition of the underlying rock. This conclusion, however, seems contradictory to the leaching and reprecipitation hypothesis explaining the concentration of dolomite in the lower sections of a calcrete profile. A blanket of loess derived from wind-blown deposits during arid phases associated with sea-level lowstands and

glacial periods would presumably initially cover the land surface unevenly in dune-like formations and be reworked into low-lying areas of the landscape. This deposit would be subject to the same dissolution and reprecipitation processes as envisaged by Hutton and Dixon (1981) to cause the leaching of dolomite to the lower sections of a pedogenic calcrete profile; the resulting carbonate deposit being mixed with pre-existing regolith material. The profile at Yorketown (site 107) is a calcareous dune sampled from a coastal region from the southern Yorke Peninsula with incipient calcrete development occurring as massive semi-indurated micritic nodules throughout the 2m profile. The lack of calcrete development indicates a recent (Pleistocene) origin for this deposit and the proximity of the site to the coast suggests that the dolomitic composition of this deposit is characteristic of aeolian loess derived from the exposed continental shelf during sea-level lowstands.

Determination of clay mineralogy in the current study is rudimentary due to the whole-rock analysis performed. The common phases identified are illite and palygorskite whereas sepiolite, kaolinite and montmorillonite occurrences are typically subordinate. Quartz is generally the dominant residual component occurring in all profiles including those developed on mafic and ultramafic rocks were quartz is not present in the host material. Feldspar is typically a minor mineral in most profiles, varieties identified by both thin section and XRD ranging from orthoclase and microcline to anorthite and albite, the later being the most common. Apart from being derived directly from granitic, gneissic and mafic parent materials, minor amounts occur in profiles developed on aeolian and fluvial parent materials indicating transported material as a source. Calcium oxalate was not identified on any of the X-ray diffraction traces.

Chapter 4

Carbon and Oxygen Stable Isotopes and Calcrete Formation

4.1 Background

The use of carbon and oxygen isotopic compositions of pedogenic carbonate as proxies for palaeo-climatic and palaeo-ecological conditions at the time of formation has been formulated through numerical models by Cerling (1984), Amundson *et al*. (1988), Quade *et al*. (1989), Cerling *et al*. (1989) and others. The basis of these models is the condition that carbonate is precipitated from a soil solution in an open system where equilibrium is maintained between dissolved carbonate and bicarbonate ions (HCO_3^- and CO_3^{2-}) in the soil solution and gaseous CO_2 during carbonate precipitation (Emrich *et al*., 1970; Margaritz and Amiel, 1980). In other words, any carbon gained from the dissolution of pre-existing carbonate (the carbon isotopic composition of marine carbonates averaging 0 ± 3 ‰) is overwhelmed by carbon from gaseous CO_2 within the soil, which is derived from plant respiration, the decay of organic matter and atmospheric carbon dioxide (all examples and results are reported in the conventional delta (δ) notation with respect to the Vienna Pee Dee Belemnite (PDB) standard for both carbon and oxygen). The relationship between atmospheric $^{13}CO_2$ ($\delta^{13}C$ = -6 ‰ PDB, pre-industrial value) and biological sources is demonstrated in diffusion mixing models where soil CO_2 partial pressure is higher than atmospheric CO_2 partial pressure; the flux of CO_2 from the soil environment to the atmosphere varies seasonally and regionally depending on elevation, temperature, precipitation and depth of water penetration (Cerling, 1984; Amundson *et al*., 1989; Quade *et al*., 1989) and diffusional inmixing of atmospheric CO_2 is considered to contribute to the $\delta^{13}C$ of pedogenic carbonate only in arid soils with very low respiration rates and in the upper tens of centimetres in profiles in

temperate regions. The carbon isotopic composition of pedogenic carbonate is, therefore, directly dependent on soil CO_2 gas plus the sum of the fractionation factors for the reactions 1 – 4 (totalling +10.2 ‰, Emrich et al., 1970; Margaritz and Amiel, 1980) as shown:

$$CO_{2\,(g)} \Leftrightarrow CO_{2\,(aq)} \quad (1)$$

$$CO_{2\,(aq)} + 2H_2O \Leftrightarrow H_3O^+ + HCO_3^- \quad (2)$$

$$HCO_3^- + H_2O \Leftrightarrow H_3O^+ + CO_3^{2-} \quad (3)$$

$$CO_3^{2-} + Ca^{2+} \Leftrightarrow CaCO_{3\,(s)} \quad (4)$$

Plants and other soil organisms can produce relatively large amounts of CO_2 as they respire and decay. The isotopic composition of plants using the C3 or C4 photosynthetic pathway have $\delta^{13}C$ values averaging –27 and –13 ‰, respectively, and calculations indicate that pedogenic carbonate should have $\delta^{13}C$ values approximating –12 and +2 ‰ for samples derived from pure C3 and C4 vegetation, respectively. Cerling *et al*. (1989) found that the isotopic composition of soil carbonate is systematically higher than coexisting organic matter by 14 (25° C) to 17 (0° C) ‰ in modern soils in samples from North America and elsewhere and considered the data to confirm the previous theoretical calculations. These conditions are observed only for modern soils with moderate to high respiration rates and generally at depths greater than 0.5 metres.

Dissolution and reprecipitation of carbonate occurs readily in the soil environment. Using stable isotopes and radiocarbon dating on recent pedogenic calcrete profiles with well-constrained ages in southwest USA, Pendall *et al*., (1994) found that fine-grained carbonates below 0.9m underwent little or no dissolution and reprecipitation, whereas carbonate rinds precipitated above 0.4m undergo continual dissolution and reprecipitation. Between 0.9m and 0.4m carbonate accumulates as rinds that do not redissolve subsequently. These results may, however, be area

specific depending on soil and calcrete porosity, climatic factors and possibly the position of the groundwater table.

The oxygen isotopic composition of pedogenic carbonate is considered to be related to the isotopic composition of local meteoric waters with enrichment from evaporative effects and addition of atmospheric water through the carbonate reaction as shown above.

4.2 Objectives and Methodology

The current isotope research is aimed at examining the factors inducing pedogenic carbonate precipitation and their possible affect on the stable carbon and oxygen isotopic composition of the pedogenic calcrete profiles sampled. Many of the previous studies on the use of pedogenic calcrete as a palaeo-climatic indicator are based on relatively few samples and have not been related to calcrete micromorphology. The current work focuses on examining within-profile and textural variations and their effect on isotopic values of the sampled pedogenic calcrete.

Whole-rock samples were chipped into fractions weighing up to 1.5 mg and analysed using a PRISM III mass spectrometer at the University of Wollongong. This sampling technique was utilised rather than grinding and splitting samples because it allows analysis of different fractions within a particular sample. Moreover, where ground and split samples give average values and 'neater results', samples analysed in such manner give no information about the variation in isotopic composition within individual samples. This matter is important in the analysis of pedogenic calcrete samples for two main reasons. Firstly, cementation by carbonate in pedogenic calcrete is progressive and may occur slowly over many thousands of years, possibly leading to gradual variations in the isotopic composition of the

cement. Secondly, many samples contain carbonate with a variety of micro-morphologies, for example, a massive nodule may contain minute channels containing calcified filaments, thin micritic coatings on residual quartz grains and pore-filling microspar cements on a scale visible only under high magnification with a petrographic or scanning electron microscope. Ideally, minute sampling of these individual fractions would yield detailed isotopic information allowing conclusions to be made about their cause and formation.

With the previous chapter showing the micro-morphological evidence for various types of biological carbonate precipitation and the presence of co-existing organic matter, found to be abundant in many profiles, it is postulated that soil organic matter $\delta^{13}C$ could show a direct relationship with carbonate $\delta^{13}C$ where biologically precipitated carbonate is abundant and coeval with pedogenic calcrete. Organic matter observed in thin section and under scanning electron microscopy, typically as relatively abundant filamentous or dendritic growths, is closely associated with calcified filaments and considered to be fungal in origin. Other possible contributors to the organic matter fraction include the remains of dead and living plant roots as well as other soil organisms not responsible for carbonate precipitation. Where observed, these were avoided during sampling and grinding. To determine the $\delta^{13}C$ values for soil organic matter (SOM), gravimetric carbonate analyses were made on ground samples treated with enough dilute (1M) HCl for the reaction to go to completion (overnight) then centrifuged and rinsed four times and dried at 60°C. Elemental carbon content and organic matter $\delta^{13}C$ were measured using a Carlo Erbo 1500 elemental analyser. Samples containing dolomite were excluded from these analyses for the reason that organically formed carbonate is typically low-Mg calcite. Furthermore, possible un-reacted dolomite within treated samples could affect elemental carbon weight and organic matter $\delta^{13}C$.

4.3 Results and Discussion

The results for stable carbon and oxygen isotopic analyses plotted against depth for the sampled pedogenic calcrete profiles are given on the logs in Appendix I. Raw isotope data are given Appendix III. A total of 631 samples from 73 sites were analysed for $\delta^{13}C$ and $\delta^{18}O$. Figure 4.1 shows the frequency histograms of carbon and oxygen isotopic composition for all samples analysed. The total spread in carbon isotopic values for pedogenic calcrete samples in South Australia and Western Australia ranges from –1.0 to –12.5 ‰ with the highest frequency falling between –6 and –4 ‰. Carbon isotopic values for terrestrial limestone analysed in the present study typically range from –1 to 3 ‰. Oxygen isotopic values for the pedogenic calcrete range from 2 to –10 ‰ with the highest frequency falling between -2 and -4 ‰. Oxygen isotopic values for marine and terrestrial limestone analysed in the present study typically range from 3 to 6 ‰.

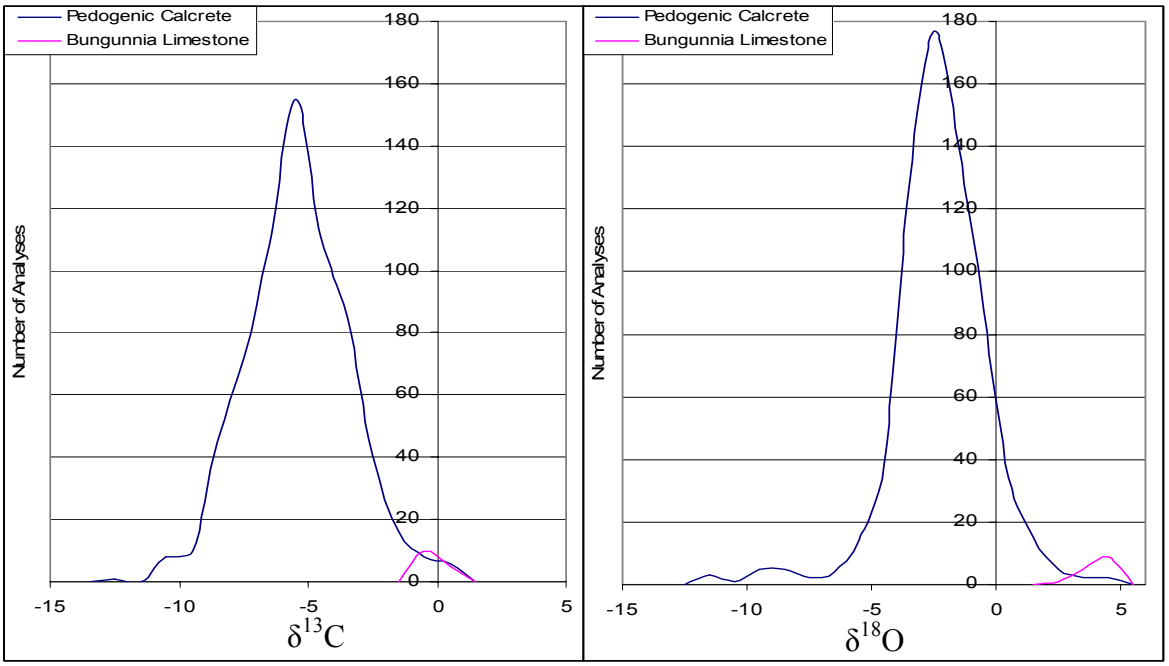

Figure 4.1. Frequency histograms of carbon and oxygen isotopic composition for all carbonate samples analysed.

The isotopic composition of soil organic matter in the sampled pedogenic calcrete shows a range between –20.5 and –25.2 ‰ and SOM concentrations vary from 0.1 to 0.9 % of the acid insoluble residue. Within-profile isotope results can be variable and commonly show an up-profile increase of up to 2 ‰. Carbonate $\delta^{13}C$ plotted against coexisting soil organic matter $\delta^{13}C$ for samples taken between 0.3 and 1.2m depth (all samples plotted are labels with and asterix in appendix 3 and classified according to table 2.4) show recent calcrete has considerably greater than the 14 to 17 per mil difference found in recent North American pedogenic calcrete by Cerling *et al*. (1989). This suggests different climatic conditions during the time of formation (last glacial period) of these calcretes. The graph also shows clearly that rhizogenic forms of calcrete typically have lower $\delta^{13}C$ values than do other morphological types of pedogenic calcrete.

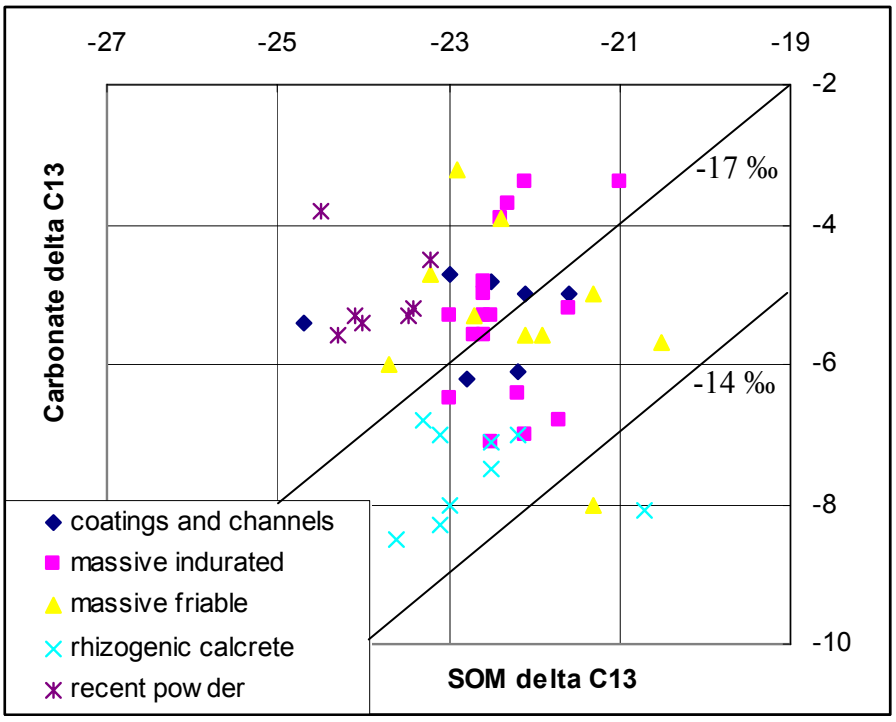

Figure 4.2. Average carbonate $\delta^{13}C$ plotted against corresponding soil organic matter $\delta^{13}C$ values for analysed individual pedogenic calcrete sample fractions.

Within-sample and within-profile variation of $\delta^{13}C$ and $\delta^{18}O$ in the sampled pedogenic calcrete is commonly large and is assessed by plotting values of $\delta^{13}C$ versus $\delta^{18}O$ within single profiles (Figure 4.3). That pedogenic calcrete is composed of mixtures of cement or carbonate types is obvious in the variation in $\delta^{13}C$ and $\delta^{18}O$ shown in many samples and profiles. Some samples show a linear trend and positive co-variation between $\delta^{13}C$ and $\delta^{18}O$ within the profile. The range in both $\delta^{13}C$ and $\delta^{18}O$ values suggests a mixing line between two end-members with different isotopic compositions. That the variation is not depth-related is obvious from the fact that within-sample variation can be greater than whole profile variation and that samples do not plot sequentially with depth along the trendlines.

The profile sampled at Melton (site 110) in the north of Yorke Peninsula, South Australia, is a platy hardpan composed purely of calcite with no detrital impurities and is developed as a thick calcrete layer within massive limestone host material. Two fabric types are recognised in thin section, fenestral and peloidal. These are individually composed of micritic walls or peloids with sparry void-filling cements on a micro-scale. Carbonate $\delta^{13}C$ and $\delta^{18}O$ values vary by over 6 and 7 ‰, respectively (Figure 4.3A). The cause of this large co-variation is considered to be an effect caused by non-contemporeignity of precipitated carbonate in the pedogenic calcrete. Whether or not the micromorphology of the different carbonate fractions effects the carbonate $\delta^{13}C$ and $\delta^{18}O$ values is unclear from the present study.

The Salmon Gums profile (site 129), composed of massive nodules, boulders and hardpan overlying calcified soil as undifferentiated calcrete plain, shows a 6.5 ‰ range in $\delta^{13}C$ and over 12 ‰ variation in $\delta^{18}O$ (Figure 4.3B). Microscopically the samples are composed of massive cryptocrystalline cements with sparse calcified

filaments as coatings and channels penetrating massive dolomitic carbonate. Both carbonate species co-exist in samples on a small scale within the profile and this is reflected in the covarying isotopic ratios of samples with the same morphology. The variation suggests either integration of cements throughout the profile under different climatic/vegetation regimes. The Lort Piver profile (site 132), composed of incipient nodules in calcified soil formed on mottled green-brown clay saprolite, is similar (Figure 4.3C). Both samples come from the southern Western Australian mallee zone and the variation in carbon isotopic values is in accordance with the likelihood that coastal areas are more likely to experience dramatic climatic changes than continental areas. However, the strongly linear co-variation in both carbon and oxygen values suggest differences in the mode of formation of carbonate cements on a micro-scale, thus it is uncertain whether such isotopic differences are climatically dependent.

Significant variation in $\delta^{18}O$ values is common within most samples and profiles and is considered to be due to progressive carbonate precipitation from variably evaporated solutions, not necessarily induced by changing climatic conditions. The profiles sampled from Broad Arrow and Bardoc (sites 137 and 145), from the Western Australian goldfields region, are composed of thick micritic veins and platy hardpan calcrete penetrating ferruginous duricrust and show only small variations in $\delta^{13}C$ (approximately 2 ‰) whereas the $\delta^{18}O$ range is up to 5 ‰ within the profile (Figures 4.3D and 4.3E). While the occurrence of pedogenic calcrete overprinted on contrasting and previously formed regolith is indicative of the changing climatic conditions during the Neogene or Pleistocene from moist temperate conditions to the current semi-arid climatic regime, the narrow range in $\delta^{13}C$ values for these profiles suggests their formation under a single vegetation type.

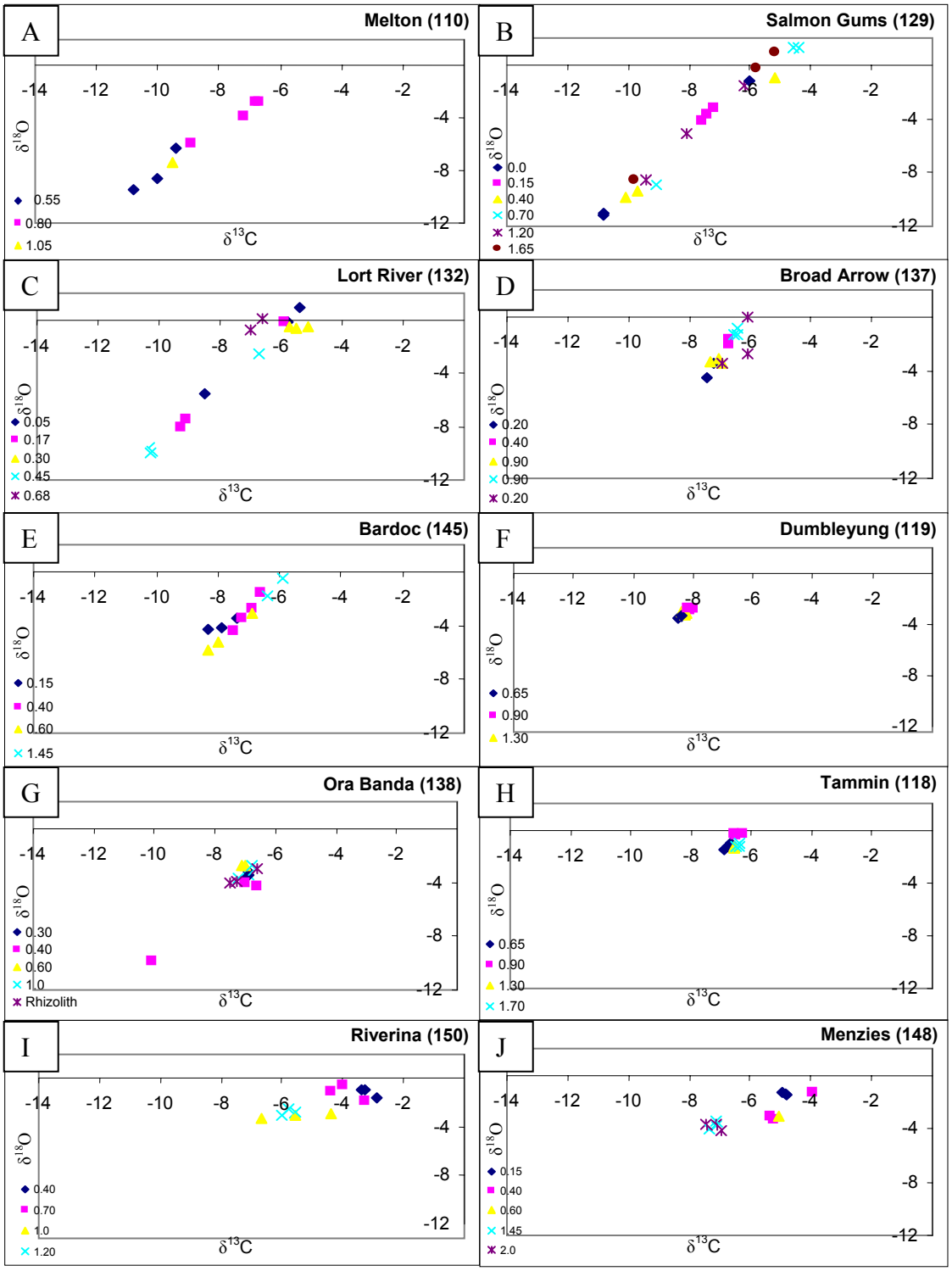

Figure 4.3. $\delta^{13}C$ vs. $\delta^{18}O$ plots for individual pedogenic calcrete profiles. Sample depths are shown on bottom right corner of graph.

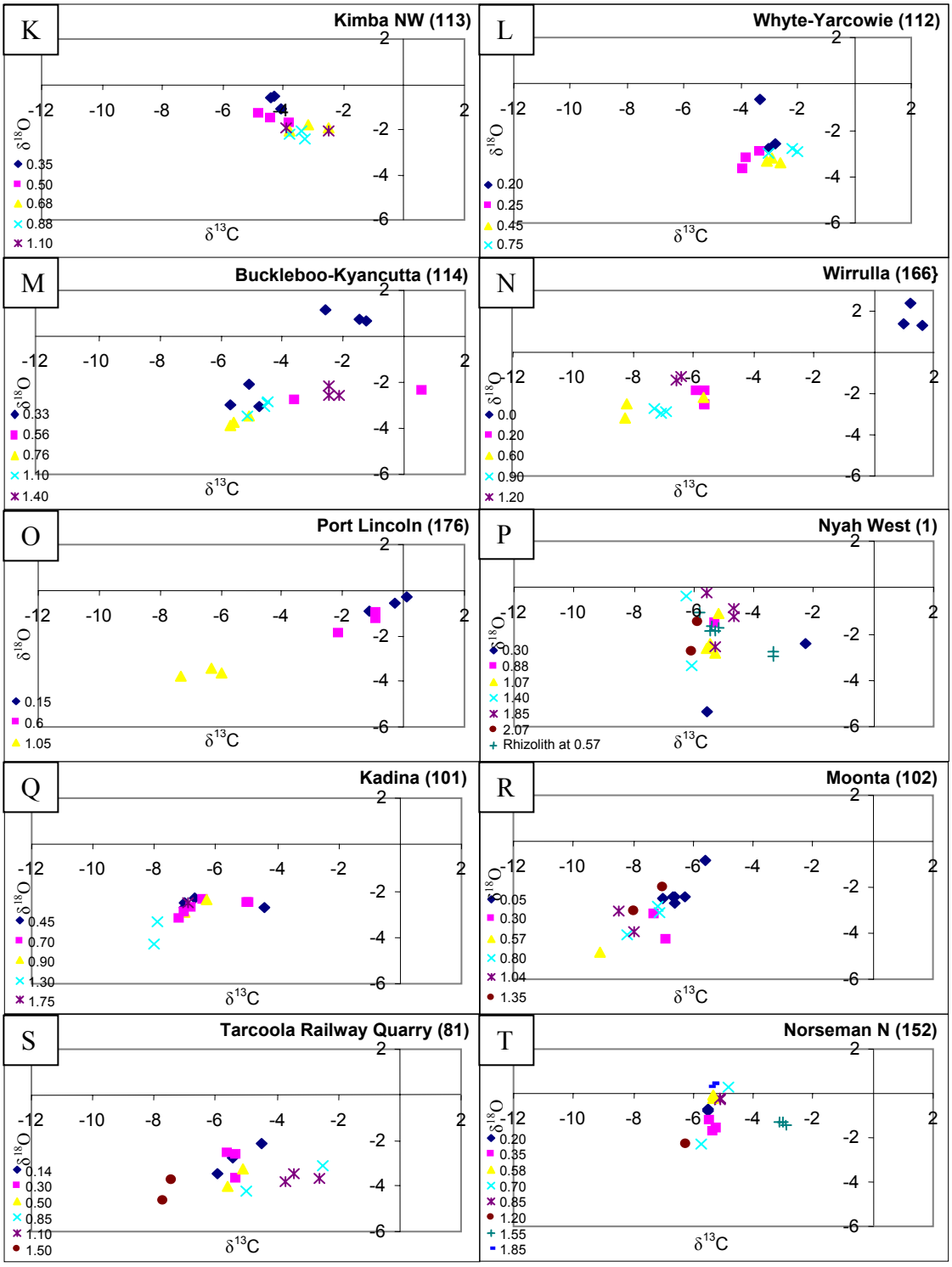

Figure 4.3 (cont.)

Many pedogenic calcrete profiles sampled in Western Australia show obvious rhizogenic characteristics in accord with their having low $\delta^{13}C$ values. The profile sampled at Dumbleyung in the subhumid wheat-belt zone of southwest Western Australia (site 119) is composed of powdery calcite with platy and sheet-like structure developed on weathered ultramafic host material. The calcrete sub-samples showing co-variation with less than one per mil range in $\delta^{13}C$ and $\delta^{18}O$ (Figure 4.3F). Needle-fibre calcite and micritic overgrowths are the only cement types recognised in thin section and SEM studies of this profile suggest that this is a recent profile with little diagenetic cementation or isotopic overprinting. The profile sampled from Ora Banda (site 138) is a boulder and nodular calcrete overlying sub-horizontal powdery sheets and rhizoliths at 0.5 m, developed on weathered and disaggregated ferruginous duricrust in the Western Australian Goldfields region. Carbonate in the nodules was found to be biogenic and composed of birds-nest structures, p-type poly-crystals and root-moulds. Lower in the profile the carbonate occurs as massive taproot fragments and rhizogenic sheets with a strange 'crazed' microspar fabric. The carbon isotope values within this profile range from –6.0 to –7.3 ‰ (Figure 4.3G). Sampled in the eastern wheatbelt region of Western Australia, the Tammin profile (site 118) is composed of vertically stacked dolomitic nodules with an alveolar-like micro-fabric; the narrow range in $\delta^{13}C$ and $\delta^{18}O$ values within this profile occurs from -6.3 to -6.9 and from -0.3 to -1.5 ‰, respectively (Figure 4.3H).

Some pedogenic calcrete profiles sampled from the Western Australian Goldfields region have brecciated and pisolitic morphologies as characteristic horizons composed of calcified filaments and micritic cements. The profile sampled at Riverina (site 150) is a nodular and pisolithic hardpan calcrete overlying semi-

indurated carbonate stringers in red-brown hardpan, sampled west of Menzies; the profile being the most northerly of samples collected in the present study. The Menzies profile (site 148) was collected in the same vicinity and is composed of packed nodules overlying incipient nodules and powdery mottles developed in red-brown alluvial clayey loam. Stable carbon and oxygen isotope values within these profiles show a definite contrast between the upper pisolithic, nodular and hardpan samples containing calcified filaments and micritic cements with higher carbonate $\delta^{13}C$ and $\delta^{18}O$ values and the lower mottled powders and incipient nodules (Figures 4.3I and 4.3J).

With few exceptions, petrographically examined samples from southeast South Australia are of the typical nodular and hardpan 'calcified filaments with micrite cement' type of pedogenic calcrete. This is particularly true where pedogenic calcrete forms extensive plains such as in the sub-humid southeastern and peninsular regions of South Australia and in the Murray Basin region in the eastern rain-shadow of the ranges. Many of these profiles sampled show a clustering of $\delta^{13}C$ values between -3 and -5 ‰ with random variation through the profile (Figures 4.3K, 4.3L and 4.3M). The profile sampled at Whyte-Yarcowie (site 112) is a hardpan calcrete overlying powder calcrete at 0.5 m developed on alluvial piedmont slopes of the Mt Lofty Ranges, South Australia. The profiles sampled at Kimba, Buckleboo-Kyancutta and Wirrulla (sites 113, 114 and 166) are hardpan profiles developed in undifferentiated alluvial/fluvial or aeolian red-brown clayey sand in the northern semi-arid regions of the Eyre Peninsula. The carbonate in these profiles is the typical calcified filaments and dense micritic cement grading down-profile to calcified soil. Some of these, such as at Buckleboo-Kyancutta and Wirrulla, sampled in aeolian dunes, demonstrate random scatter within the profile

with no apparent or predictable variation with depth except higher oxygen and carbon isotopic values in surficial soil or external coatings in the A-horizon (Figures 4.3M and 4.3N). This is also seen in the profile sampled at Port Lincoln (site 176), sampled from southernmost Eyre Peninsula, South Australia, and developed on Proterozoic gneiss. This is a massive hardpan composed of porous micrite grading down to powder calcrete at approximately 0.7 m. Again there is a large contrast in both $\delta^{13}C$ and $\delta^{18}O$ values between the cemented upper section with high $\delta^{13}C$ and $\delta^{18}O$ values and the lower powdery section within this profile (Figure 4.3O). Perhaps the cause of this incongruence in isotopic values is a result of in-mixing and subsequent cementation of aeolian-derived marine carbonate at the top of the profile, which is derived as windblown dust possibly sourced during sea-level low stands during arid glacial periods (in accordance with Crocker's 1946 hypothesis), and the pedogenic carbonate precipitated at the base of the profile.

Several profiles sampled from recent aeolian dunes of the Woorinen Formation in northwest Victoria show multiple developments of calcareous soils. For example, the profile at Nyah West (site 1) is composed of three layers of massive semi-indurated to friable micritic carbonate cemented loamy sands located at the railway cutting at Nyah West. These "young" pedogenic calcrete layers have been dated at between 15000 to 25000 years before present using radiocarbon methods by Bowler and Polach (1971), thus their formation spans much of the Last Glacial Maximum. The stable carbon compositions of the layers show no significant differences other than within-sample variability, suggesting that they formed under a variable, typically arid, climate. Inter-layered between the calcareous soils are rhizoliths (taproot fragments) and mottled powders with similar or slightly lower stable carbon and oxygen isotope values (Figure 4.3P). Other recent dunes with young (Machette

stage 2) pedogenic calcrete development, sampled from Yorke Peninsula (PG95 and PG107), have average (approx. –6 ‰) or high $\delta^{13}C$ values suggesting that they formed during an arid climate.

Petrological evidence for rhizogenic calcrete occurs in the temperate climatic regions of southeastern South Australia. Pedogenic calcrete sampled from Yorke Peninsula at Kadina and Moonta (site 101 and 102) is up to 2m thick with a 0.5m to 1m thick hardpan. Layers of fenestral fabric are contained within the hardpan similar to the previously discussed rhizogenic cement in the Melton profile (site 110) and have $\delta^{13}C$ as low as –9.5 ‰ (Figure 4.3Q and 4.3R). The typical coatings and channels composed of calcified filaments, and micrite carbonate cement types in these and other profiles from this region commonly have $\delta^{13}C$ values lower than –6 ‰.

Scarce petrologic evidence for rhizogenic pedogenic calcrete was found in central arid South Australia (with the exception of the Wirramina profile, site 75). Typically the samples from this region are alpha or non-biogenic type calcrete and are have $\delta^{13}C$ values greater than –6 ‰, commonly as high as –4 ‰ and up to –2 ‰ in surficial laminar calcrete. Purely non-biogenic pedogenic calcrete was, however, scarce in the sampled profiles and many samples contain at least minor amounts of recognisable calcified filaments. The profiles sampled at Tarcoola Railway Quarry (site 81) sampled from central South Australia and Norseman North (site 152) from the Western Australian goldfields, developed in indurated and slightly weathered quartz metasediment and basalt respectively, are morphologically similar, being composed of infiltration veins with dense alpha or non-biogenic micritic cement penetrating highly indurated host material. Both $\delta^{13}C$ and $\delta^{18}O$ values are variable with the Norseman North samples having distinctly higher $\delta^{18}O$ value. The unusual

feature of these profiles is that both have high $\delta^{13}C$ values at depths of between 1m and 1.5m (Figures 4.3 T and 4.3S). Considering that C4 vegetation can be deep-rooted, this phenomenon is considered to represent the influence of C4 vegetation at this site.

4.4 Regional Synthesis

The pedogenic calcrete samples analysed in this study show considerable $\delta^{13}C$ and $\delta^{18}O$ variation as displayed by multiple samples of carbonate in individual soil profiles. A positive co-variation of $\delta^{13}C$ and $\delta^{18}O$ is common but not universal. These variations are explained in terms of either climatically induced (glacial/interglacial) changes in vegetation and evaporation, or the presence of varying cement types with different modes of origin and isotopic composition. At this stage the significant features can be summarised as:

- Pedogenic calcrete samples showing rhizogenic features typically have low $\delta^{13}C$ values indicating the dominant influence of C3 vegetation in these samples regardless of climate. Carbonate $\delta^{13}C$ values significantly less than –7 per mil are recorded for pedogenic calcrete with fenestral fabrics, sheet-like pedogenic calcrete with obvious rhizogenic structures or needle-fibre calcite, incipient nodules with microcodium. Taproot fragments, however, typically have $\delta^{13}C$ values similar to non-rhizogenic calcrete found in the same profile suggesting that this type of calcrete formation is caused by carbonate cements filling pore-spaces left by decayed roots.

- Indurated pedogenic calcrete samples dominated by calcified filaments and micritic cement types tend to have carbonate $\delta^{13}C$ values greater than – 6 ‰ in arid and semi-arid regions. However, in temperate climatic regions samples composed predominantly of calcified filaments typically have $\delta^{13}C$ values close to –6 ‰ suggesting that biogenic calcite and micritic cements are effected by the process of carbon dioxide degassing.

- The stable oxygen isotopic values of the pedogenic calcrete sampled show no apparent regional variation or trend.

Within-profile variation in both $\delta^{13}C$ and $\delta^{18}O$ values commonly show a slight trend toward higher isotopic values toward the surface in many profiles. In the case of oxygen this trend is expected due to evaporative enrichment of near surface soil waters. Likewise, in the case of carbon a similar trend is expected if ^{12}C has preferentially diffused out of the profile through the process of carbon dioxide degassing, and through in-mixing of atmospheric CO_2 occurring down into the profile in cases where $\delta^{13}C$ is higher than –6 ‰. Explanations as to the cause of this phenomenon also be related to the preferential effect of C4 vegetation close to the surface as root systems of annual herbs and grasses are typically shallow and fibrous in nature, or possibly caused by the contribution of aeolian carbonate in the form of marine-derived dust from coastal regions. The isotopic composition of calcified filaments has yet to be precisely determined in a micro-morphological scale, however, their abundance toward the top of many profiles suggests that they contribute to $\delta^{13}C$ values.

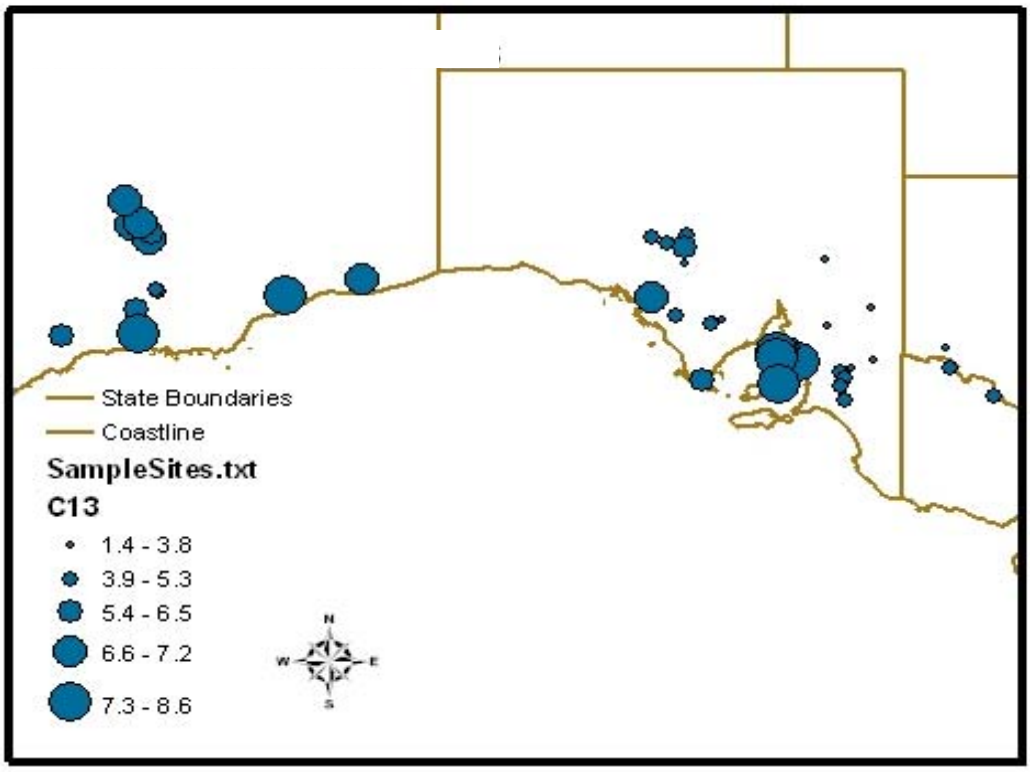

Figure 4.4. Proportional symbol map constructed using the average $\delta^{13}C$ values for pedogenic calcrete samples

Figure 4.4 is a proportional symbol map constructed using the average $\delta^{13}C$ values for samples in Appendix III, note that the sizes of the graduations in the diagram are in reverse order to the magnitude of $\delta^{13}C$. The temperate coastal zone is reflected in the isotopic results with low carbonate $\delta^{13}C$ in pedogenic calcrete of Yorke Peninsula and coastal Western Australia. The interior regions of South Australia show a valid climatic response with distinctly higher $\delta^{13}C$ values in samples to the east of the ranges and in the central regions of the Gawler Craton. In contrast, pedogenic calcrete sampled from inland regions of the Western Australian Yilgarn Craton have relatively low $\delta^{13}C$ values. The cause of this is unclear and is possibly the result of vegetation and climatic change during the Quaternary period.

Rhizogenic morphologies were commonly present within profiles and petrographically examined samples from Western Australia, this is indicative of formation during a more temperate climatic regime than the one currently operating. This region currently receives slightly higher rainfall than inland regions of South Australia, and this, combined with strong winter seasonality of the rainfall may be enough to affect regional soil carbonate $\delta^{13}C$ values. Detailed dating studies on selected sites might resolve this issue.

Chapter 5

Strontium Isotopic Tracers

5.1 Background and Methods

The ultimate source of the calcium in pedogenic carbonate derives from either an external origin (typically dust or marine aerosol), or through local or in situ weathering of calcium-bearing minerals. The extent of calcium contribution from these two sources can be quantified by the strontium isotope method provided the $^{87}Sr/^{86}Sr$ ratio between them differs significantly. Strontium is a divalent alkaline earth element with similar chemical properties (charge, ionic radius and electron configuration) to calcium and substitutes for calcium in carbonate minerals. The four naturally occurring strontium isotopes and their relative abundances are:

^{84}Sr – 0.56%

^{86}Sr – 9.87%

^{87}Sr – 7.04%

^{88}Sr – 82.53%

Strontium can be used as a proxy for calcium and for a mixture with two end members the mass fraction of strontium within carbonate derived from atmospheric and weathered bedrock sources is calculated from the following two-component mixing equation.

$$\frac{M^{Sr}_1}{M^{Sr}_1 + M^{Sr}_2} = \frac{(^{87}Sr/^{86}Sr_{carbonate} - {}^{87}Sr/^{86}Sr_{bedrock})}{(^{87}Sr/^{86}Sr_{atmosphere} - {}^{87}Sr/^{86}Sr_{bedrock})}$$

The fraction of ^{87}Sr varies in nature due to input by radioactive ß-decay of ^{87}Rb whereas the amounts of ^{84}Sr, ^{86}Sr and ^{88}Sr remain constant. Rubidium occurs in high abundance in potassium-bearing minerals such as alkali feldspars, micas and clays, hence also in rocks bearing these minerals (Table 5.1). Over time, the amount of ^{87}Sr increases as radioactive ^{87}Rb (half-life 48.8 billion years) decays (Stewart *et al.*, 1998). Therefore, minerals in crustal areas that have been accumulating ^{87}Sr for long periods of time are expected to have a high $^{87}Sr/^{86}Sr$ ratio. Regions such as the Archaean Yilgarn Craton, Western Australia, and Gawler Craton, South Australian, should thus provide large isotopic contrasts between atmospheric and bedrock strontium values. The atmospheric input (dust/rainfall/marine-aerosol) of strontium was not determined in the present study and the assumption is made that the $^{87}Sr/^{86}Sr$ ratio of the combined atmospheric input approximates that of modern seawater (0.70928).

Table 5.1. Some average elemental Sr, Ca, Rb and K concentrations in crustal rocks (from Capo *et al.*, 1998).

Please see print copy for Table 5.1

The common occurrence of pedogenic calcrete on non-calcareous parent materials in many parts of the world is considered to require an input of calcium from external sources through aeolian transport and recycling mechanisms such as dust and rainfall as indicated by the strontium isotopic ratios of pedogenic calcrete being close to dust and marine values (Quade *et al.*, 1995, coastal South Australia; Chiquet *et al.*, 1999, central Spain; Capo and Chadwick, 1999, southwest USA; Naiman *et al.*, 2000, southwest USA; Hamidi *et al.*, 2001, Morrocco). This was recognised even by early workers such as Crocker (1946) who considered the extensive pedogenic calcrete mantle of southeastern South Australia as a dust-derived or loessal addition sourced from coastal areas. Crocker (1946) supposed that the quantity of calcium-bearing dust is greater during glacial or sea level low-stand periods on account that the continental shelf exposed at these times would provide an abundant source of marine calcium in the form of calcareous tests from perished marine organisms. The dust formed during exposure, desiccation and erosion of these former seabeds would be redeposited in the direction of prevailing westerly winds. If so, the rates of calcium and strontium addition to the continent would vary significantly from modern rates.

The results from strontium isotopic measurements of pedogenic calcrete samples and respective host material from South Australia and western Victoria (Quade *et al.*, 1995) indicate that the ocean is the principal source of calcium to profiles developed on aeolianite, basalt, granite, red-brown sandy clays and laterites in coastal sites (carbonate $^{87}Sr/^{86}Sr$ between 0.7094 and 0.7098). Further inland the strontium isotopic ratios of pedogenic calcrete typically increases to between 0.7100 and 0.7150, with the highest value (0.7183) from a pedogenic calcrete developed on Precambrian metasediment of the Adelaide Fold Belt. The host-rock strontium

isotopic ratios, particularly granites, are considerably higher than the corresponding pedogenic calcrete samples and dust sourced upwind from areas in central and western Australia are proposed as the source of calcium. These dusts are likely to have relatively high $^{87}Sr/^{86}Sr$ ratios due to the presence of Archaean bedrock in these regions. Results in the Quade *et al*., (1995) dataset from pedogenic calcrete developed on basaltic regolith in the Lake Bolac region show higher $^{87}Sr/^{86}Sr$ ratios (0.7102 to 0.7115) than corresponding bedrock samples (0.7047). This indicates an external input, other than marine calcium, as the source of some of the calcium in these samples.

Regolith maps of areas in the northern Yilgarn Craton, WA, compiled by Anand *et al*. (1997) show a close relationship between pedogenic calcrete and outcropping greenstones. Greenstones are rich in calcium-bearing minerals such as plagioclase, tremolite and hornblende. Pedogenic calcrete development was found to be less prevalent in granitic terrains and the authors suggest that local weathering of rocks is a major source of calcium in the pedogenic calcrete. The present study aims to examine the role of substrate on the calcium budget of pedogenic calcrete in the arid inland regions of South and Western Australia. Samples were selected from a variety of substrates including mafic and ultramafic rocks, granite, duricrusts and argillaceous sediments. Almost all pedogenic calcrete samples were sampled from profiles developed directly on bedrock, pre-existing duricrusts or alluvium/colluvium locally derived from bedrock. Samples from aeolian sand sheets were avoided for strontium isotopic analysis because of the obvious transported source of these deposits.

The strontium isotopic composition of selected pedogenic calcrete and host material samples from the Yilgarn and Gawler Cratons was determined using a Finnigan MAT Neptune Inductively-Coupled Plasma Mass Spectrometer (ICP-MS) with faraday cup collectors at the Australian National University, Canberra. Approximately 0.1g of powdered carbonate sample was dissolved with HNO_3 and silicate bedrock samples dissolved in HNO_3 + HF, and the strontium separated using standard strontium selective ion-exchange column chemistry. Instrument precision for $^{87}Sr/^{86}Sr$ ratios is to 0.00001.

5.2 Results and Interpretations

The $^{87}Sr/^{86}Sr$ ratios of the analysed samples are given in Table 5.2 along with calculated proportional bedrock contributions. Pedogenic calcrete sampled from locations proximal to the southern coastline show $^{87}Sr/^{86}Sr$ ratios typically close to marine values. The $^{87}Sr/^{86}Sr$ ratios of pedogenic calcrete from the profile at Yarwondutta Rocks (site 167), Eyre Peninsula, South Australia, are between 0.7106 and 0.7109. The corresponding granite on which the hardpan calcrete is developed has a contrastingly high $^{87}Sr/^{86}Sr$ ratio of 0.7809 indicating that the contribution from locally weathered bedrock is negligible (<1 %).

Pedogenic calcrete sampled from the inland region of central South Australia, near the locality of Kingoonya (sites 82 and 80), have $^{87}Sr/^{86}Sr$ ratios between 0.7114 and 0.7117, with the host materials on which these samples developed have values of 0.7993 and 0.7512 for the Yardea Dacite and Meta-granite of the Archaean Mulgathing Complex, respectively. This indicates that the bedrock Ca contribution to the overlying calcrete is minimal in both cases (<6% and 2.5%, respectively). The

Table 5.2. $^{87}Sr/^{86}Sr$ ratios and calculated proportional bedrock calcium contributions to the analysed samples.

Site Name and Number	Sample No., Depth (m) and Description * host material	$^{87}Sr/^{86}Sr$	Bedrock Ca Contribution (%)
Kingoonya West (site 80)	B – 0.5 powder calcrete	0.7117	5.73
	C – 1.1 powder calcrete	0.7118	5.97
	D – 2.0 * meta-granite	0.7512	
Tarcoola Railway Quarry (site 81)	A – 0.1 platy hardpan calcrete	0.7116	
	C – 0.5 solutional calcrete veins	0.7120	
	E – 1.1 solutional calcrete veins	0.7129	
	G – 2.0* metasediment	Below det.	
Kingoonya Quarry (site 82)	A – 0.1 semi-indurated platy calcrete	0.7114	2.33
	B – 3.0* dacite	0.7993	
Kambalda Turnoff (site 116)	B – 0.2 nodular calcrete	0.7157	11.19
	C – 0.5 semi-indurated massive calcrete	0.7174	14.16
	D – 0.0* greenstone sediment	0.7665	
Dumble-yung (site 119)	B – 0.3 semi-indurated sheet-like calcrete	0.7162	50.74
	C – 0.55 semi-indurated sheet-like calcrete	0.7162	50.74
	D – 0.85 powdery calcrete stringers	0.7158	47.79
	G – 1.55* ultramafic igneous rock	0.7229	
Peak Charles (site 127)	B – 0.25 nodular calcrete	0.7180	32.22
	C – 0.5 nodular calcrete	0.7178	31.48
	D – 0.7 nodular calcrete	0.7177	31.11
	E – 1.0 nodular calcrete	0.7175	30.37
	G – 1.6* colluvial sandy clay	0.7363	
Salmon Gums North (site 129)	A – 0.1 nodular calcrete	0.7142	
	B – 0.2 nodular calcrete	0.7147	
	D – 0.7 massive semi-indurated calcrete	0.7150	
	F – 1.7 massive semi-indurated calcrete	0.7148	
Lort River (site 132)	B – 0.2 nodular calcrete	0.7122	34.34
	C – 0.3 nodular calcrete	0.7122	34.34
	D – 0.5 nodular calcrete	0.7121	31.53
	E – 0.7 nodular calcrete	0.7120	28.72
	F – 0.9* mottled green-brown clay	0.7187	

Table 5.2. cont.

Site Number	Sample No., Depth (m) and Description * host material	$^{87}Sr/^{86}Sr$	Bedrock Ca Contribution (%)
Broad Arrow (site 137)	B – 0.4 indurated solutional calcrete vein	0.7161	
Ora Banda (site 138)	B – 0.4 hardpan calcrete D – 0.8 semi-indurated calcrete stringers	0.7196 0.7198	
Yilgarn Craton	Archaean gabbro (from Broad Arrow) Archaean granite (from Peak Charles)	0.7066 0.8059	
Kalgoorlie (site 139)	B – 0.4 nodular calcrete D – 0.95 nodular calcrete F – 1.7* red clay and colluvial clasts G – 2.2 powdery dolomitic calcrete	0.7168 0.7155 0.7245 0.7159	49.34 40.79 43.43
Menzies (site 148)	A – 0.15 nodular calcrete B – 0.4 nodular calcrete C – 0.6 nodular calcrete D – 1.45 mottled powdery calcrete E – 2.0* red-brown clay	0.7139 0.7139 0.7140 0.7140 0.7163	65.71 67.14
Riverina (site 150)	A – 0.4 nodular calcrete B – 0.7 nodular calcrete C – 1.0 semi-indurated calcrete stringers D – 1.0* red-brown hardpan	0.7159 0.7153 0.7160 0.7240	44.90 40.82 45.58
Norseman North (site 152)	B – 0.2 nodular calcrete D – 0.6 nodular calcrete I – 1.85 indurated solutional calcrete veins J – 2.2* Basalt	0.7135 0.7148 0.7150 0.7179	48.48 63.95 66.28
Fraser Range (site 155)	B – 0.1 hardpan calcrete C – 0.2 hardpan calcrete D – 0.3* feldspathic gneiss	0.7152 0.7156 0.7100	
Yarwondutta Rocks (site 167)	B – 0.25 hardpan calcrete C – 0.45 hardpan calcrete D – 0.6 hardpan calcrete F – 1.6* Granite	0.7106 0.7106 0.7109 0.7809	1.82 2.23

$^{87}Sr/^{86}Sr$ ratios from platy hardpan and solutional veins in siliceous metasediment in the profile at Tarcoola Railway Quarry (site 81), central South Australia, have values of 0.7116 to 0.7129 increasing down profile. Both calcium and strontium concentration in the host material (a siliceous metasediment) was below detection indicating that the bedrock contribution of Ca to the overlying calcrete is negligible.

Western Australian nodular calcrete samples from the profile at Lort River (site 132), approximately 50 km north of Esperance near the southern Australian coast have $^{87}Sr/^{86}Sr$ ratios between 0.7120 and 0.7122. The host material at this site consists of mottled green-brown clay with an $^{87}Sr/^{86}Sr$ ratio of 0.7187. The bedrock at undetermined depth is Archaean granite with an assumed $^{87}Sr/^{86}Sr$ ratio of approximately 0.8000; the different $^{87}Sr/^{86}Sr$ ratios suggesting that calcium from dust or marine aerosols are influencing the pedogenic calcrete and the sedimentary clays. Similar nodular calcrete was sampled farther north (approximately 130km from the coast) in the vicinity of Peak Charles (site 127). The bedrock in this region is granite and the host material for the calcrete is colluvial brown sandy clay with $^{87}Sr/^{86}Sr$ ratios of 0.8059 and 0.7363 respectively. The $^{87}Sr/^{86}Sr$ ratios of the calcrete are between 0.7180 and 0.7175, considerably greater than the coastal samples. A possible explanation for this phenomenon is the decreasing influence of coastal aerosols.

Further inland, in the vicinity of the Fraser Range (site 155), adjacent to the western Nullarbor Plain, a sampled hardpan calcrete directly overlying weathered feldspathic gneiss returned $^{87}Sr/^{86}Sr$ ratios between 0.7152 and 0.7156 whereas the $^{87}Sr/^{86}Sr$ ratio of the gneiss is 0.7100. Given these values, there is clear evidence that dust with $^{87}Sr/^{86}Sr$ ratio higher than 0.7156 has deposited calcium at this site. Sampled

at the locality of Salmon Gums, approximately 100km north of Esperance, is a thick profile (>1.7m, site 129) composed of hardpan calcrete grading down to semi-indurated dolomitic calcrete, similar in appearance and thickness to the hardpan calcrete that mantles much of southern South Australia. The host material was below the depth of exposure but the thickness and the apparent absence of any calcareous source for such a large calcrete accumulation suggests that this is a valley-fill deposit with dust being a likely source of calcium. The $^{87}Sr/^{86}Sr$ ratio of this calcrete sample ranges between 0.7142 and 0.7150, tending to increase with depth.

Pedogenic calcrete samples collected on Archaean greenstone host material have $^{87}Sr/^{86}Sr$ ratios that are seemingly consistent with a significant bedrock input. Results of analysed calcrete samples collected near Dumbleyung, Western Australia (site 119), in the temperate southwest wheat belt region, show $^{87}Sr/^{86}Sr$ ratios of between 0.7158 and 0.7162. The host material at this site, ultramafic igneous rock composed of augite, albite, phlogopite and various weathering products such as maghemite and montmorillonite, has a calcium concentration of 6.0 weight percent and an $^{87}Sr/^{86}Sr$ ratio of 0.7229. Assuming that the external source of strontium has a marine $^{87}Sr/^{86}Sr$ ratio then the approximate bedrock contribution of Ca to the overlying calcrete is up to 50%. A nodular pedogenic calcrete with dolomitic solutional veins penetrating into mafic host rock composed of riebeckite, magnesiohornblende, pyrophyllite, albite and weathering products such as hematite and goethite, was collected from a railway cutting at Norseman North, Western Australia. The host material has a calcium concentration of 5.5 weight percent and an $^{87}Sr/^{86}Sr$ ratio of 0.7179. Carbonate $^{87}Sr/^{86}Sr$ ratios range from 0.7135 to 0.7150 increasing down profile. The apparent bedrock contribution, assuming the external

source of strontium has a marine $^{87}Sr/^{86}Sr$ ratio, is between 48 and 67%, and is strongly controlled by down profile depth demonstrating the competing influence of atmospheric source and bedrock weathering within the one profile.

Analysed samples from the site at Kambalda turnoff (site 116), south of Kambalda in the Western Australian Goldfields region, provide contradicting evidence for greenstone bedrock contributions to pedogenic calcrete. The host material at this site is steeply dipping volcaniclastic sandstone with the sediment presumably being greenstone derived. The calcium concentration and $^{87}Sr/^{86}Sr$ ratio of the host material are 6.3% and 0.7665, respectively, whereas the $^{87}Sr/^{86}Sr$ ratios of the pedogenic calcrete samples are 0.7157 and 0.7174 increasing with depth. Assuming a marine value for external calcium input, this would indicate an 11.2 to 14.2% bedrock contribution. The $^{87}Sr/^{86}Sr$ ratios of greenstone parent materials show a range of values whereas only minor variation occurs in the $^{87}Sr/^{86}Sr$ ratios of the respective pedogenic calcrete sampled. This suggests overestimations of the bedrock contribution due to the higher $^{87}Sr/^{86}Sr$ ratios of atmospheric dust and the low $^{87}Sr/^{86}Sr$ ratios of the greenstone parent materials.

Other pedogenic calcrete samples collected in the Kalgoorlie region have variably high $^{87}Sr/^{86}Sr$ ratios. Samples from profiles at Broad Arrow and Ora Banda (sites 137 and 138) developed in ferruginous duricrust return values of 0.7161 and 0.7197, respectively. The host material was not analysed for $^{87}Sr/^{86}Sr$ because its calcium concentration is negligible. A bedrock gabbro sample from unknown depth in the vicinity of site at Broad Arrow (site 137) was analysed for $^{87}Sr/^{86}Sr$ returning a value of 0.7066. This result suggests that calcium input from the weathering of greenstones may be significant on a local level. Samples from the site at Kalgoorlie

(site 139) are composed of incipient nodular calcrete with dolomitic stringers down to 2.2m developed in red clay with abundant sedimentary colluvial clasts. The samples returned carbonate $^{87}Sr/^{86}Sr$ ratios between 0.7155 and 0.7168. Dissolving the carbonate from a basal sample with mild acetic acid and analysing the residue for silicate $^{87}Sr/^{86}Sr$ obtained a host material ratio of 0.7245. The bedrock contribution assuming marine $^{87}Sr/^{86}Sr$ ratio for atmospheric input is between 40 and 50% for these samples.

The northernmost locations that pedogenic calcrete were collected was in the vicinity of Menzies, Western Australia. The Menzies profile (site 148) was developed on alluvial red-brown clay whereas the Riverina profile (site 150) was developed on red-brown hardpan host material. In both cases the bedrock at depth is granitic. Carbonate $^{87}Sr/^{86}Sr$ ratios are 0.7140 for the Menzies profile and between 0.7153 and 0.7160 for the Riverina profile. Host material (silicate) $^{87}Sr/^{86}Sr$ ratios are 0.7163 and 0.7240 respectively, and bedrock contributions (assuming marine $^{87}Sr/^{86}Sr$ ratios) approximately 65% and 45%, respectively. Considering the proximity of the samples to one another (approximately 10km) and the co-variation in $^{87}Sr/^{86}Sr$ ratio of the carbonate samples and host material, these results suggest the influence of host material on the strontium isotopic composition.

In order to examine the $^{87}Sr/^{86}Sr$ data on a regional level, the ratios are plotted against latitude (Figure 5.1). If bedrock were to make no contribution to the strontium composition of pedogenic carbonate there should be a relatively smooth increase in $^{87}Sr/^{86}Sr$ ratios of pedogenic calcrete with distance from the coastline due to the competing influences of marine aerosol and terrestrial dust (Quade *et al.*, 1995). In the western Australian samples the coastal influence of marine aerosols

on $^{87}Sr/^{86}Sr$ ratios wanes quickly with distance from the coast. Considerable scatter in the $^{87}Sr/^{86}Sr$ ratios occurs in the Western Australian samples indicating that local bedrock has a strong influence on the strontium isotopic composition and hence the calcium budget of pedogenic calcrete. In contrast, the South Australian pedogenic calcrete samples show a strong marine influence even in pedogenic calcrete sampled at a considerable distance from the coast. $^{87}Sr/^{86}Sr$ ratios of the Nullarbor limestone have been measured as 0.7092 and 0.7096 by Lintern *et al.* (submitted) and the cause of the low $^{87}Sr/^{86}Sr$ ratios in pedogenic calcrete of the Gawler Craton is interpreted as being a result of the predominant westerly winds depositing calcium-rich dust derived downwind from limestone of the Nullarbor karst region and the calcareous aeolianite that occurs abundantly in coastal South Australia.

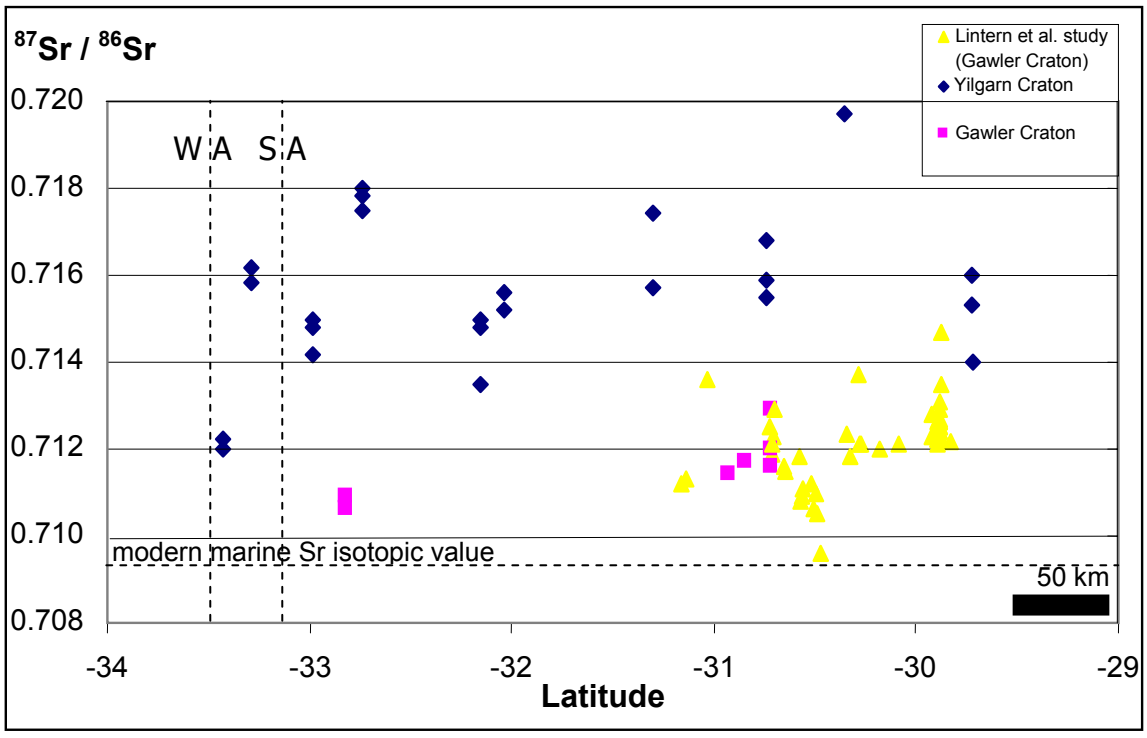

Figure 5.1. The $^{87}Sr/^{86}Sr$ ratio of pedogenic calcrete from Eyre Peninsula, South Australia, and the Yilgarn Craton, Western Australia, versus latitude. The vertical dotted lines represent the approximate locations of respective coastlines.

Chapter 6

Trace Element Geochemistry

6.1 Background

Trace element geochemical data for pedogenic calcrete is potentially very useful not only in the search for buried or blind ore deposits, but also for examining the process of chemical weathering and the precipitation of calcite in the vadose zone. Published data on the trace element concentrations of pedogenic calcrete are however very scarce and investigations into their use as a geochemical sample medium for gold and base metal exploration are often confidential and retained by exploration and mining companies. Furthermore, the significance of pedogenic calcrete in regard to gold exploration was not fully realised until the 1990s and it was not used systematically in the search for buried or blind ore deposits until recently.

Being a secondary accumulation or overprint on existing regolith, pedogenic calcrete was initially considered as a geochemical diluent with respect to economically important or pathfinder trace elements (Mazzuchelli, 1972) and efforts were made to enhance trace element content through carbonate dissolution and analysis of the residue (Garnett, 1982). Research by CSIRO and later CRC LEME during the late 1980s and 1990s has demonstrated that gold could be highly concentrated in pedogenic calcrete overlying auriferous deposits in the Yilgarn Craton, Western Australia. The discovery of the Challenger gold deposit in the Gawler Craton, South Australia, by a Dominion Mining Ltd and Resolute Resources Ltd joint venture in 1995 being hailed as confirmation of the usefulness of pedogenic calcrete sampling

as an exploration technique. Lintern (2002) has comprehensively described the CRC LEME and other published case studies to date and the methodology used in implementing and interpreting geochemical surveys using pedogenic calcrete as a sampling medium. The following discussion is a brief synthesis of the above-mentioned developments.

The results of various ore deposit case studies show that gold and calcium are correlated vertically within the soil profile. There is also a relative accumulation of gold (derived from either the host material or buried mineralisation) within the pedogenic calcrete in cases where the weathering profile is complete or partially truncated, even over significant thicknesses of Au-poor saprolite. Furthermore, lateral dispersion of the gold serves to form broad epigenetic anomalies thus assisting exploration by providing a larger target anomaly. Geochemical data from ore deposit case studies of pedogenic calcrete developed on thick transported overburden overlying mineralisation (typically palaeo-channels containing significant Au mineralisation in basal gravels - known as deep leads) however are equivocal, with calcrete showing either a weak or no response with respect to the surface expression of buried mineralisation.

The cause of the pedogenic calcrete-gold association is yet uncertain. Lintern (2002) considered a process whereby organic ligands (produced by soil flora and fauna) complex colloidal and chemical Au dispersed from host material. During rainfall events this relatively mobile/soluble Au is slowly redistributed towards the surface by the processes of meteoric infiltration and evaporation and/or evapo-transpiration. Similar meteoric processes presumably govern calcium distribution and after numerous rainfall events gold and calcium will become congruently distributed. Redistribution of gold to the surface through absorption by plants may also be a significant process and is confirmed by the presence of Au in plant tissues

(Lintern, 1989). Another factor that is potentially very important in controlling the distribution of gold and other trace elements within the regolith is the pH contrast that commonly exists between pedogenic calcrete and underlying regolith materials. Pedogenic calcrete is alkaline; the high pH can reduce the chemical mobility of many elements derived/dissolved from underlying neutral to acid regolith causing their precipitation in the lower section of the calcrete horizon.

Two forms of gold (micron-sized <10μm) have been found associated with pedogenic calcrete, crystalline and amorphous. Amorphous gold 'appears to have undergone a transformation to a chemical species that allows it to become concentrated within, rather than diluted by the calcrete', whereas crystalline gold presumably has 'become physically incorporated into the calcrete, either as a discrete grain or incorporated within a host (e.g. a ferruginous granule)' (Lintern, 2002). In cases were anomalous gold occurs in pedogenic calcrete developed in transported overburden, causes other than vertical (hydromorphic) remobilisation and re-precipitation of Au are implicated by Lintern (2002). In particular, lateral (mechanical and chemical) dispersion from upslope residual soils lying on the same mineralised trend is suggested as the cause of these surficial gold-calcrete anomalies.

6.2 Objectives and Methodology

Exploration geochemistry requires a sound knowledge of the geochemical behaviour of elements caused by weathering, soil formation and sedimentary redistribution during surface geological processes. The current study examines the concentrations of trace elements in the sampled pedogenic calcrete profiles with the aim of determining what geochemical changes occur in the zone of calcium accumulation with respect to substrate. In simple terms, does the minor and trace element

composition of pedogenic calcrete reflect the detrital components (parent material residue or windblown aeolian input) such as quartz, clays and lithic fragments diluted only by carbonate; or are certain trace elements associated with calcium in the pedogenic calcrete profile? The results of these investigations will provide information as to the effective baseline concentrations of these elements on various parent materials and determining what type of geochemical anomalies (hydromorphic/chemical or residual) occur in pedogenic calcrete with respect to the various trace elements.

Whole-rock trace element composition of 315 samples of pedogenic calcrete from 55 profiles was determined by instrumental neutron activation analysis (INAA) at Becquerel Laboratories, Lucas Heights, Sydney. The suite of 30 elements analysed include rare earth elements La, Ce, Sm, Eu, Tb, Yb and Lu; transition metals Ag, Cr, Co, Au, Fe, Hf, Mo, Sc, Ta, W, Zn and Zr; metalloids Sb, As and Te; alkali metals Na, K, Cs and Rb; alkaline earth metals Ba and Ca; and the actinides U and Th. W and Ta were excluded from the data set due to possible contamination from the tungsten-carbide ring-mill used for crushing samples. Ag (1 ppm), Mo (5 ppm), Ir (5 ppb), Te (2 ppm) and Se (1 ppm) were below detection levels in all samples. Gold was below detection levels in many samples. Raw data are given in the Appendix CD folder labelled INAA data.

The geochemical data were treated on a profile-by-profile basis with graphs of every element constructed using a program developed in windows excel using VBA (Visual Basic for Applications). The files containing these graphs (INAA_graphs.xls) along with the file containing the calculated Pearson's correlation coefficients (pearson.xls) and the programs used to cluster the INAA data (cluster.xls) are given as files in the appendix CD folder labelled "INAA Data".

Selected sample aliquots (approximately 100 g of ground whole-rock sample) were each leached with excess mild acetic acid (10%), mild hydrochloric acid (5%) or strong aqua-regia solution (75:25 HCl and HNO_3) for 15 hours then rinsed once with the respective acid solution and three times with distilled water. The acid-insoluble residues were analysed by INAA in order to examine the partitioning of the trace elements within the pedogenic calcrete. Histograms showing the elemental content, given in weight % retained in residue, calculated from the elemental concentration and mass of sample before and after leaching (acid_digest.xls) is given in the appendix CD folder labelled INAA Data. The proportion (weight %) retained in residue is calculated using the following equation:

weight % = [conc.* mass (residue)] / [conc.* mass (whole rock)] * 100%

The first step in statistical treatment of the data was to draw scatter-plots of the elements (continuous variables) within each profile to check for linearity and co-varying trends within samples from the same profile. Pearson's correlation coefficients (r) were calculated for every combination of elements within each profile using SPSS (Statistical Package for the Social Sciences) version 10.0 software. The value of Pearson's correlation coefficient for continuous data ranges from +1 to –1. Positive correlation indicates that either variables increase or decrease together, whereas negative correlation indicates that as one variable increases, so the other decreases. The nearer the scatter of the points is to a straight line, the higher the strength of association of the two variables and the closer r is to + 1 or – 1. The purpose of identifying co-varying trends between elements is to match correlated elements; two elements with positive co-variation are likely to be associated with the same residual mineral phase. Elements with negative co-variation with respect to calcium suggest dilution associated with displacive (or replacive) calcrete growth.

Further statistical analysis using ratios calculated from all the possible combinations of elements was carried out on each profile. The use of element ratios to standardise the data in this manner alleviates problems associated with variation in concentration of samples within profiles and parent material. A coefficient of variation is used to determine which ratios remain constant within individual profiles, a constant ratio indicating two elements associated within a particular mineral phase. This coefficient is calculated by dividing the standard deviation by the mean of the samples within each profile (including parent material), thus providing a normalised measure of variation of the element ratios through the profile. No statistical test suitable for clustering data of this type (associated pairs of elements) could be found; therefore a computational method was devised in order to determine which combinations of elements group together. The logic for this method ranks the coefficient of variation for the element ratios within each profile then groups them according to every element, i.e. within each profile every element is ranked according to the corresponding element in order of the coefficient of variation. If an element shows interrelation by ranking highly with a corresponding element, and the corresponding element also ranks highly with the initial element the two are considered to correlate. This process favours element ratios having a coefficient of variation that ranks highly for both elements and was necessary because the both-way variation of the ratio (i.e. the X/Y and Y/X) is variable. If either element is found to cluster with another element then the correlated element is added to the cluster. Note that this calculation is statistical rather than purely mathematical and the resulting clusters should be treated as probable rather than definite correlations.

The file and program written to calculate the results are given in the Appendix data CD and labelled cluster.xls. To activate the macro click "enable macros" when opening the file. To view the code, open the visual basic editor using the tools

dropdown menu and clicking the macro button then click on the button labelled visual basic editor, alternatively press the Alt and F11 keys simultaneously. To run the macro click on the button labelled ► and select the macro labelled process_each_site. The macro takes approximately 100 minutes to run to completion. Pressing the Ctrl and Pause/Break buttons simultaneously stops the macro. Changing the number in the last line of code changes the number of cells the macro counts down when correlating ranked elements i.e. loop until counter = 6, correlates elements ranked to sixth according to the coefficient of variation.

6.3 Results

Considerable difficulty is encountered in the acid-leach experiments involving the selected pedogenic calcrete samples. The results of these experiments and their graphed relationships, provided as Figure 6.1 and as enrichment-depletion diagrams in the file labelled acid_digest.xls in the appendix CD, show that elemental concentrations are broadly similar for each of the three different acid digests within the same sample. However, between-sample results were equivocal and variable with many elements showing partial leaching by the acid solution (i.e. no elements were concentrated wholly in the acid insoluble residue and many were retained between 60 to 80 % in the residue). This could suggest that either significant amounts of the relevant trace element are weakly adsorbed onto clay minerals, or that the acid solution leaches significant amounts from residual minerals thus making the separation between carbonate and residual phases difficult. The solubility of many of the minerals encountered in pedogenic calcrete is poorly known and there are likely to be appreciable differences in the leachability of trace elements from different minerals. Furthermore, considerable error is introduced into the expression of proportion in residue as three sources of analytical error (precision and accuracy) are multiplied; the whole rock analysis, collection and analysis of the

residue and the gravimetric determination of carbonate proportion. Thus the acid-leach experiments are considered as inconclusive with respect to determining proportions of trace elements contained within the carbonate fraction. Further chemical experimentation with attention to the leachate concentration, leaching time, temperature, grainsize and the type of leachate used in the extraction experiment are needed along with analysis of the acid leachate by wet chemical techniques such as ICP-MS to adequately resolve these issues. Moreover, the acids used for the digest experiments are strong acids and perhaps digests with weak acids are better for extracting the acid soluble carbonate element fraction.

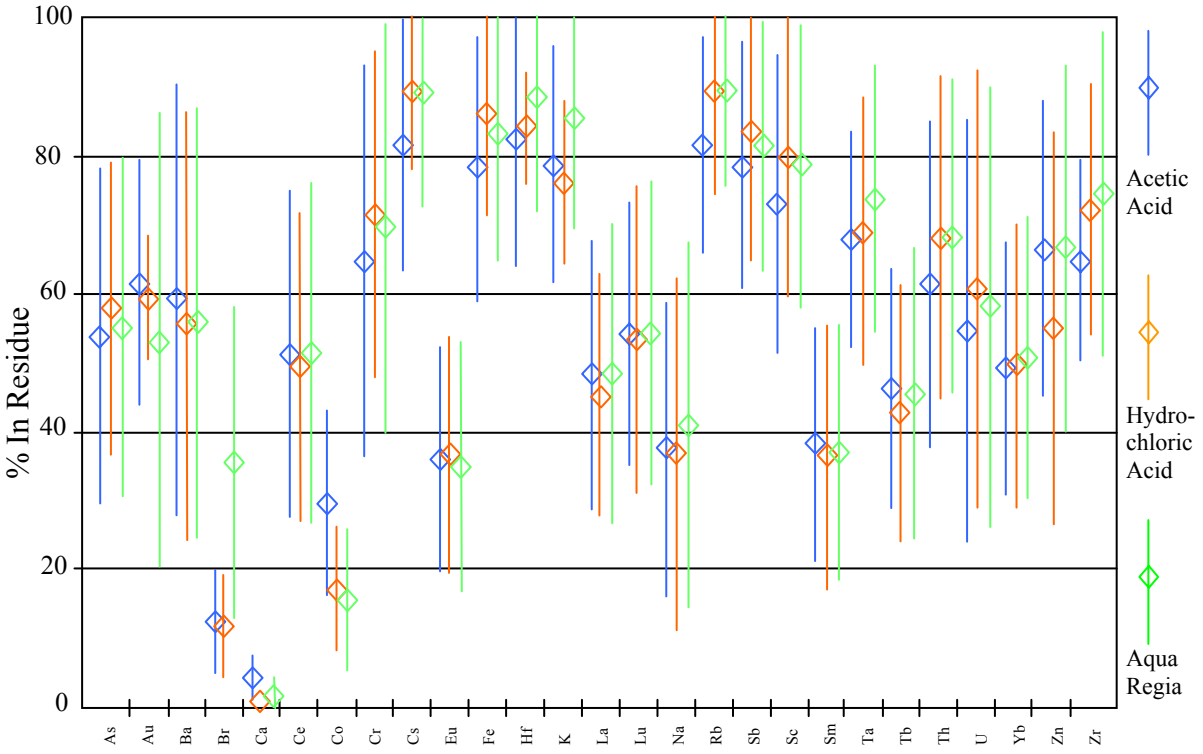

Figure 6.1. Mean and one standard deviation bar graphs of trace element amount (as a percent of total trace element in untreated calcrete samples) retained in the acid-insoluble residue.

Table 6.1 summarises the number of times the Pearson's correlation coefficient is above the 0.05 and 0.01 % level of significance (close to 1 or – 1) for each combination of elements in the 55 profiles sampled. Table 6.2 summarises the average (bold) and standard deviation of all the Pearson's correlation coefficients for each combination of elements. The results of these data are summarised in Section 6.4. The element clusters calculated by ranking corresponding elements on the basis of their coefficient of variation calculated on the within-profile element ratios are given in Table 6.3. Elements are correlated to the sixth rank. Also detailed in the table is the calcrete-gold association as determined by vertical distribution with the pedogenic calcrete profile and the parent material.

Table 6.1. Number of statistically significant Pearson's correlation coefficients for each combination of elements in the 55 profiles analysed. Top right is 0.05 % confidence level; bottom left is 0.01% confidence level.

	As	*Ba*	*Br*	*Ca*	*Ce*	*Cr*	*Cs*	*Fe*	*Hf*	*K*	*La*	*Na*	*Rb*	*Sb*	*Sc*	*Sm*	*Th*	*U*	*Yb*	*Zn*	*Zr*
As		4	4	5	13	9	5	12	7	4	4	3	6	9	9	4	7	5	3	5	5
Ba	2		8	7	6	6	8	3	5	10	10	11	8	5	6	11	6	8	12	7	6
Br	1	3		20	11	10	9	10	13	12	9	15	14	7	14	7	10	8	10	6	8
Ca	3	1	9		11	18	17	20	26	19	8	12	20	8	21	9	14	8	9	11	15
Ce	2	3	5	4		23	18	23	26	21	42	5	18	6	31	37	41	8	36	10	17
Cr	4	1	5	13	9		23	37	24	23	15	9	26	12	35	15	25	6	18	17	13
Cs	3	2	2	7	10	13		31	23	26	14	10	34	10	34	11	25	7	17	13	13
Fe	7	2	5	14	15	27	19		27	23	16	11	30	17	46	13	29	6	17	18	15
Hf	3	1	4	12	15	12	13	16		24	18	3	21	9	30	23	33	7	23	12	30
K	1	4	6	5	7	12	13	16	10		13	12	34	9	27	15	24	9	16	13	11
La	1	1	2	4	32	8	6	9	10	5		10	14	3	23	52	30	8	44	8	15
Na	2	3	8	5	2	12	3	6	2	5	5		13	6	14	10	8	8	9	9	8
Rb	4	5	5	11	11	17	19	25	15	20	6	5		10	32	13	29	9	18	15	15
Sb	6	1	4	5	5	7	6	10	4	4	2	5	7		12	3	11	9	5	8	7
Sc	4	3	7	15	16	29	19	40	14	14	11	7	22	6		20	35	7	25	17	18
Sm	1	4	3	4	32	7	5	9	9	5	42	3	6	2	10		26	5	47	7	13
Th	5	2	2	10	32	19	14	22	19	12	20	2	18	7	24	20		11	29	9	23
U	1	2	2	2	4	1	3	2	5	2	2	2	1	1	1	1	5		8	5	5
Yb	0	1	2	5	24	7	7	10	15	6	35	4	8	3	10	35	22	3		8	16
Zn	1	2	2	4	3	8	8	10	3	6	2	5	9	4	10	3	4	2	4		7
Zr	1	1	4	5	7	5	5	7	19	1	5	2	3	1	10	3	10	2	8	1	

Table 6.2. Mean (bold) and standard deviation of Pearson's correlation coefficients for all combinations of elements.

	Zr	*Zn*	*Yb*	*U*	*Th*	*S*	*Sc*	*Sb*	*Rb*	*Na*	*La*	*K*	*Hf*	*Fe*	*Cs*	*Cr*	*Ce*	*Ca*	*Br*	*Ba*
As	**0.08** 0.57	**0.04** 0.71	**0.20** 0.52	**0.23** 0.57	**0.26** 0.61	**0.15** 0.54	**0.31** 0.58	**0.49** 0.51	**0.14** 0.61	**0.05** 0.56	**0.13** 0.55	**0.12** 0.53	**0.16** 0.61	**0.39** 0.60	**0.21** 0.51	**0.32** 0.58	**0.22** 0.57	**-0.04** 0.6	**0.0** 0.61	**0.02** 0.58
Ba	**0.26** 0.48	**0.24** 0.56	**0.33** 0.52	**0.13** 0.58	**0.32** 0.54	**0.33** 0.50	**0.26** 0.47	**0.03** 0.55	**0.34** 0.51	**0.0** 0.61	**0.36** 0.50	**0.34** 0.50	**0.19** 0.51	**0.28** 0.46	**0.31** 0.46	**0.15** 0.54	**0.30** 0.53	**-0.11** 0.56	**-0.17** 0.56	
Br	**-0.11** 0.58	**-0.23** 0.53	**-0.13** 0.58	**-0.17** 0.53	**-0.24** 0.57	**-0.14** 0.59	**-0.34** 0.54	**-0.17** 0.51	**-0.29** 0.53	**0.15** 0.66	**-0.19** 0.57	**-0.31** 0.48	**-0.19** 0.61	**-0.28** 0.54	**-0.24** 0.52	**-0.25** 0.54	**-0.19** 0.59	**0.42** 0.53		
Ca	**-0.32** 0.57	**-0.43** 0.58	**-0.19** 0.54	**-0.17** 0.57	**-0.39** 0.51	**-0.17** 0.56	**-0.51** 0.49	**-0.24** 0.55	**-0.54** 0.46	**-0.28** 0.57	**-0.23** 0.54	**-0.44** 0.52	**-0.49** 0.53	**-0.53** 0.47	**-0.39** 0.54	**-0.44** 0.51	**-0.31** 0.51			
Ce	**0.55** 0.42	**0.45** 0.52	**0.76** 0.39	**0.06** 0.63	**0.89** 0.16	**0.77** 0.39	**0.70** 0.37	**0.30** 0.46	**0.60** 0.44	**0.11** 0.53	**0.82** 0.33	**0.57** 0.45	**0.65** 0.42	**0.60** 0.41	**0.63** 0.38	**0.52** 0.52				
Cr	**0.43** 0.50	**0.62** 0.51	**0.39** 0.55	**-0.06** 0.61	**0.53** 0.53	**0.36** 0.56	**0.74** 0.40	**0.38** 0.54	**0.49** 0.57	**0.14** 0.56	**0.40** 0.55	**0.51** 0.50	**0.57** 0.51	**0.72** 0.42	**0.51** 0.52					
Cs	**0.43** 0.52	**0.56** 0.43	**0.43** 0.49	**0.07** 0.60	**0.67** 0.38	**0.43** 0.46	**0.74** 0.37	**0.31** 0.54	**0.78** 0.32	**0.21** 0.55	**0.50** 0.45	**0.72** 0.32	**0.58** 0.41	**0.71** 0.37						
Fe	**0.42** 0.53	**0.64** 0.40	**0.43** 0.52	**0.06** 0.58	**0.65** 0.42	**0.44** 0.47	**0.88** 0.24	**0.50** 0.51	**0.70** 0.39	**0.15** 0.57	**0.48** 0.45	**0.64** 0.41	**0.66** 0.42							
Hf	**0.69** 0.45	**0.48** 0.51	**0.43** 0.59	**-0.06** 0.59	**0.71** 0.42	**0.37** 0.62	**0.65** 0.44	**0.36** 0.51	**0.60** 0.48	**0.02** 0.55	**0.43** 0.59	**0.54** 0.46								
K	**0.43** 0.52	**0.63** 0.34	**0.33** 0.55	**0.01** 0.60	**0.58** 0.49	**0.37** 0.51	**0.63** 0.42	**0.26** 0.50	**0.79** 0.32	**0.20** 0.59	**0.46** 0.48									
La	**0.40** 0.53	**0.43** 0.51	**0.85** 0.32	**0.10** 0.64	**0.70** 0.43	**0.95** 0.14	**0.61** 0.41	**0.26** 0.43	**0.48** 0.50	**0.12** 0.55										
Na	**0.10** 0.52	**0.31** 0.56	**0.08** 0.56	**0.23** 0.56	**0.06** 0.58	**0.16** 0.54	**0.24** 0.57	**0.05** 0.52	**0.21** 0.60											
Rb	**0.38** 0.55	**0.60** 0.43	**0.37** 0.60	**0.0** 0.58	**0.64** 0.48	**0.40** 0.52	**0.68** 0.41	**0.32** 0.51												
Sb	**0.14** 0.56	**0.29** 0.61	**0.24** 0.47	**0.18** 0.54	**0.34** 0.53	**0.26** 0.45	**0.42** 0.51													
Sc	**0.45** 0.55	**0.69** 0.41	**0.56** 0.47	**0.08** 0.57	**0.70** 0.43	**0.58** 0.44														
Sm	**0.34** 0.55	**0.41** 0.53	**0.88** 0.30	**0.12** 0.61	**0.63** 0.47															
Th	**0.59** 0.44	**0.43** 0.57	**0.69** 0.40	**0.11** 0.64																
U	**0.17** 0.54	**-0.03** 0.54	**0.12** 0.61																	
Yb	**0.40** 0.53	**0.38** 0.56																		
Zn	**0.38** 0.52																			

Table 6.3. Calcrete-gold concentrations and element clusters calculated by ranking corresponding element ratios on the basis of their coefficient of variation. * Sites have bedrock/parent material analysed, n = number of samples.

Site	Element clusters	Calcrete-gold association	Parent Material
Carwarp Site 19; *n = 9	Ce-Fe-K-Rb-Sc-Th-Zn Eu-La-Sm-Yb Hf-Zr	2.6 ppb Au in calcified soil at 0.8m, others below detection	Sandy aeolian dune
Renmark Site 26; *n = 7	As-Br-Cs-K-Sb Ce-Hf-La-Th-Zr Fe-Sc Eu-Sm-Yb	3.1 ppb in hardpan, 2.5 ppm in lacustrine, else below detection	Dolomitic Blanchetown Clay
Waikerie Site 30; *n = 6	Cr-Cs-Fe-Rb-Sc Br-Na-U Ce-Th-Yb Eu-La-Sm As-Zn	Variable within hardpan up to 3.8 ppb Au, host up to 6.8 ppm	Dolomitic Blanchetown Clay
Gandy Range Site 33; *n = 4	Cs-Fe-K-Rb-Sc As-Cr-Hf-Sb-Zn Ce-Sm-Th-Yb	Max. 7.8 ppb Au in hardpan, host below detection	Dolomitic Blanchetown Clay
Yunta Site 39; *n = 7	Cs-K-Rb-Zn As-Cr-Hf-Sb-Zr Sc-Th-Yb Ce-Eu-La-Sm-Ta	Nodules up to 5.0 ppb Au, host below detection	Proterozoic dolomitic marine mudstone
Dlorah Downs Site 43; *n = 5	Rb-U Hf-K-Zr Cr-Na-Ta-Th Ce-Eu-La-Sm-Tb-Yb Br-Ca		Weathered granitic terrain
Blanchetown S. Site 51; *n = 7	Fe-Sc Hf-Na Rb-Zr Eu-La-Sm-Yb	Hardpan 2.5 ppb Au, host below detection	Weathered Neogene marine limestone
Blanchetown E. Site 52; *n = 7	Cs-Fe-Sc Ce-Cr-Th Br-Hf-Sb Ca-Zr Eu-La-Tb-Sm-Yb As-U	Hardpan up to 5.9 ppb Au, host below detection	Dolomitic Blanchetown Clay
Long Ridge Site 53; *n = 3	Cs-Fe-Zn Cr-Eu-La-Sm-Tb Ta-Na Ce-Th-Yb As-Br-Ca Hf-Zr Rb-K	Hardpan up to 5.6 ppb Au, host below detection	Weathered granitic terrain
Long Ridge Site 54; *n = 6	Cr-Fe-K-Rb Sc-Cs-Zn Ta-Na Hf-Zr Ce-Eu-La-Sm-Tb-Th-Yb As-Br-Ca	Nodules up to 7.4 ppb Au, host below detection	Weathered granitic terrain
Black Hill Site 55; *n = 7	Fe-Sc Cs-Rb Ba-Ce-Cr-Na-Sm-Ta-Tb-U-Zn-Zr	Hardpan and calcified soil up to 7.1 ppb Au, host below detection	Weathered Black Hill Norite
Mannum Site 56; *n = 7	Fe-K-Sc Cs-Rb-Zn Br-Ca-Na-U Ce-La-Th-Sm-Yb	Below detection	Loose yellow carbonate soil
Tailem Bend Site 57; *n = 8	Cs-Fe-K-Rb-Sc Ce-La Sm-Th-Yb As-Br-Na-U	Below detection	Loose yellow carbonate soil
Wirramina Site 75; *n = 6	Fe-Sc As-Cr-Cs-Yb Hf-Ta-Th Eu-Na-Rb-Sb-Sm Br-Ca	Hardpan and calcified soil up to 6.7 ppb, host below detection	Lithified red-brown sandstone
Glendambo N. Site 78 *n = 5	Ce-Cr-Fe-K-Sc-Th Ba-Sb As-Eu-Sm-U-Yb-Zn Br-Ca Hf-Zr	Calcified soil up to 7.7 ppb Au, host below detection	Lithified red-brown sandstone
Kingoonya W. Site 80; *n = 4	K-Rb Cr-Yb-Zn Sc-Tb Ta-Th-Zr Ce-La-Na-Cs Sm-Eu Br-Ca Fe-U	Laminar calcrete and calcified soil to 11.4 ppb, host below detection	Unweathered metagranite
Tarcoola R.Q. Site 81; *n = 7	Fe-Hf-Sc K-Rb Ce-Rb-Ta-Th Na-Sb Eu-La-Sm-Tb-Yb Br-Ca	Platy calcrete/infiltration veins to 19.7 ppb, host below detection	Siliceous metasediment
Kingoonya S. Site 84; n = 3	Cr-Fe Sc-Th As-Br-Ca-Na-U Ce-Hf-La-Ta-Tb-Zn Eu-Sm-Yb	Surficial nodules concentrated up to 5.9 ppb Au	Colluvium composed of angular dacite clasts
Kokatha Site 87; n = 4	As-Rb Ce-Fe-Sc-Th La-Yb Br-Na Sm-Eu Hf-Zr	2.6 ppb Au in surficial laminar calcrete, else below detection	Sandy aeolian dune

Table 6.3 (cont.)

Site	Element clusters	Calcrete-gold association	Parent Material
Lake Everard Site 90; *n = 5	As-Br-Fe-Sc-Zn Rb-Th-Yb Hf-Zr Ce-Eu-Sm-Tb-U Ba-Cs-K	Below detection	Undifferentiated red-brown sandy clay
Kimba E. Site 93; n = 5	Fe-Sb-Zn As-Ce-Cr-Sc Br-Na-Rb-K Eu-La-Sm-Tb Ca-Cs-Ta-Th-U Hf-Zr	Low concentrations up to 3.1 ppb Au in hardpan and nodules	Undifferentiated red-brown sandy clay
Mary-Burts C. Site 94; n = 3	Ce-Cr-Fe-Hf-Sc-Th La-Sm-Yb Cs-Rb As-Ca-K-U Ba-Eu-Na-Tb	Low concentrations up to 2.5 ppb Au in hardpan	Undifferentiated calcrete plain
Kallora Site 95; *n = 6	Cr-Fe-Sc Rb-Th-Zr Hf-Ta Ba-La-Tb-Yb Eu-Sm Br-Ca	Below detection	Sandy aeolian dune
Balaklava Site 96; n = 3	Cr-Fe-Hf-Sc K-Ta-Zr As-Eu-La-Sm-Tb-Yb Br-Ca	Low concentrations up to 2.7 ppb Au in (basal) calcified soil	Undifferentiated calcrete plain
Bute Site 98; n = 4	As-Fe-Hf-Sc-Th Cr-Eu Ce-La-Sm Ba-Sb Ta-Yb Cs-Rb Na-U	Low concentrations up to 3.4 ppb Au in (basal) calcified soil	Undifferentiated calcrete plain
Kadina Site 101; n = 5	Ba-Ce-Cr-Th-U-Yb Fe-Sc-Th Ba-Eu-Sm Ca- Br	Below detection except 2.7 ppb Au in (upper) hardpan	Undifferentiated calcrete plain
Moonta Site 102; n = 5	Ce-Fe-Hf-La-Sc As-Ba-Ca-Sb-U-Zr Cr-Sm-Th-Yb Cs-Eu-K-Rb Br-Na	Below detection except 2.5 ppb Au in (basal) calcified soil	Undifferentiated calcrete plain
Stansbury Site 106; n = 5	Cr-Cs-Fe-Sc Ba-Ca-Na-Sb-Zr As-Hf-Th Ce-Yb Eu-La-Sm	Variable within profile with concentrations to 3.0 ppm Au	Undifferentiated calcrete plain
Yorketown Site 107; n = 5	Cr-Fe-Sc Br-Na Cs-Zn Eu-Sm-Th-Yb Ce-La	Variable within profile with concentrations up to 3.4 ppb Au	Loose yellow carbonate dune (recent)
Whyte-Yarcowie Site 112; n = 4	Fe-Rb Cr-Sc-Th Sb-U-Zr Yb-Cs Eu-La-Sm-Tb Br-Ca	Low concentration with hardpan enriched up to 3.6 ppb Au	Undifferentiated red-brown sandy clay
Kimba NW. Site 113; *n = 6	Cr-Fe-Hf-K-Rb-Sc-Ta-Tb Eu-Yb Ce-La-Sm-Th-Zn Ba-Br-Ca	Hardpan concentrations up to 7.6 ppb Au, host below detection	Sandy aeolian dune
Buckleboo-Kyan Site 114; *n = 6	Cr-Cs-Fe-Sc La-Sm-Tb-Yb-Eu-Sm As-Sb Br-Na	Hardpan concentration up to 3.9 ppb Au, host below detection	Undifferentiated red-brown sandy clay
Pinkawillinie Site 115; n = 4	Cr-Sm-Yb Ce-Fe-La-Sc-Th As-Ca Br-Na Hf-Zr	Below detection	Undifferentiated red-brown sandy clay
Kambalda T.O. Site 116; *n = 4	Ba-Br-Sb-U Rb-Ta As-Fe Th-Hf-Zr Cr-Eu-Hf-Th-Yb La-Sc Ce-Sm Ca-Na	Nodule concentration up to 19.8 ppb Au, host 7.8 ppb Au	Weathered ultrabasic (greenstone terrain)
Tammin Site 118; *n = 5	As-Cr-Cs-Fe-Hf-Rb Eu-La-Sm-Tb-Yb Ce-Na-Sc-Th Eu-Sm	Variable concentration in nodules to 7.1 ppb, host below detection	Deeply weathered feldspathic gneiss
Dumbleyung Site 119; *n = 6	Cr-Fe-Hf-Sc-Th Ce-Eu-La-Sm-Tb	Calcified soil 4.9 ppb Au, Host below detection	Weathered ultrabasic (greenstone terrain)
Lake Magenta Site 122; *n = 4	Fe-Hf Rb-K Cr-Sc Ce-Cs-Th Eu-La-Sm-Tb-Yb Br-Na	Low concentrations up to 3.2 ppb Au in nodules	Gypsiferous dune
Peak Charles Site 127; *n = 6	Cr-Cs-Fe-Rb-Sc As-K Ce-Th Eu-La-Sm-Tb-Yb Na-Ta-U	Variable concentration in nodules to 11.7 ppb, host below detection	Green-brown mottled clay (undifferentiated bedrock)
Salmon Gums N. Site 129; n = 6	Cr-Fe-Rb-Sc-Ta Ce-Eu-La-Sm-Th Eu-La-Sm Br-Na	Concentration in hardpan to 7.1 ppb Au, Upper nodules and lower calcified soil below detection	Undifferentiated calcrete plain

Table 6.3 (cont.)

Site	Element clusters	Calcrete-gold association	Parent Material
Lort River Site 132; *n = 6	As-Cs-K-Sb Br-Ca Cr-Fe-Rb-Sc-Ta Ce-Na-Th-Zr Eu-La-Sm-Tb-Yb	Concentration in nodules to 6.6 ppb Au, host to 2.7 ppb Au	Green-brown mottled clay (undifferentiated bedrock)
Salmon Gums S. Site 134; *n = 4	Cr-Cs-Fe-Rb As-Th Eu-La-Sm-Yb Ba-Br	Nodules up to 7.2 ppb Au, host below detection	Brown mottled clay (undifferentiated bedrock)
Norseman S. Site 136; n = 3	Eu-Fe-Sc Cr-La-Sm-Tb-Yb-Zn As-U Ce-Hf-Th Br-Na Cs-Ca-Ta Ba-Sb	Concentration in incipient nodules up to 39.7 ppb Au	Colluvial siltstone fragments in brown clay.
Broad Arrow Site 137; n = 5	Cr-Sb-Sc As-Ce-Hf-Rb-U Cs-Ta Hf-Th Br-Eu-La-Sm-Yb		Ferruginous duricrust
Ora Banda Site 138; *n = 6	As-Fe-Hf-Sb-Sc-Th Na-Rb-U Ba-Br-Ca-Ce-Eu-La-Sm-Yb	Hardpan up to 1120 ppb Au, ore grade host material	Ferruginous duricrust overlying Au orebody
Kalgoorlie Site 139; n = 6	As-Cr-Fe Ce-Hf-K-Rb-Th-Zn Hf-Th Eu-La-Sm-Tb-Yb Sb-Sc-Ta Br-Na-U	Concentration in calcified soil up to 32.5 ppb Au	Colluvial siltstone fragments in brown clay.
Bardoc Site 145; *n = 5	As-Cr-Fe-Sc Ce-Eu-Sm Ba-La Hf-Ta-Zn Na-Rb-Tb-Th-Yb Br-Ca	Carbonate veins up to 98.2 ppb Au, ore grade host material	Mottled ferruginous clay/saprolite
Menzies Site 148; *n = 5	Fe-Sc-Th Cr-Cs-Na As-U Ce-Hf-Sm-Tb-Yb Ca-Br	nodules and calcified soil to 29.6 ppb, host below detection	Undifferentiated red-brown clay.
Riverina Site 150; *n = 5	As-Fe-Th Cs-K-Rb-Sc-U-Zn Cr-Hf Eu-La-Sm-Tb-Yb Ba-Na Br-Ca	Hardpan up to 48.3 ppb Au, host below detection	Red-brown hardpan
Norseman N. Site 152;*n = 10	Cr-Hf-Rb-Sb-Ta-Zn Cs-Na-Rb-Sc Ce-La-Th Eu-Sm-Yb As-Br-Ca	Calcrete veins up to 18.8 ppb Au, host below detection	Weathered basalt corestone
Fraser Range Site 155; *n = 4	Fe-Sc K-Rb Ba-Cs As-Br-Ca Ce-Eu-Hf-La-Sm-Ta-Tb Cr-Zn	Hardpan up to 8.9 ppb Au, host below detection	Feldspathic gneiss
Balladonia Site 156; n = 4	Fe-Sc Ba-Cs Cr-Th Na-Rb-Ta Ce-Yb Eu-La-Sm-Tb Hf-Zr	Low concentrations up to 3.3 ppb Au in pisoliths	Undifferentiated calcrete plain
Caiguna W. Site 157; *n = 6	Cr-Fe-Sc Cs-Hf-Rb-Th-Ta-Zr Ce-Eu-La-Sm-Yb Br-Ca	Low concentrations up to 4.3 ppb Au in rhizoliths	Neogene Nullarbor Limestone
Wirrulla Site 166; n = 4	Fe-Sb-Sc Hf-Rb-Zr Br-Ta Ce-Cs-La-Sm-Th-U-Yb Ca-As-Cr	Below detection	Undifferentiated red-brown sandy clay
Yarwondutta R. Site 167; *n = 5	Ba-Cs-Eu-Fe-Hf-Sc K-Rb As-Cr Ce-La-Th Sm-Tb-Yb Ta-Na Br-Ca	Hardpan calcrete up to 2.8 ppb Au, host below detection	Weathered granite
Minnippa SW. Site 168; n = 4	As-Cr-Fe-Sc-Th Ba-K Br-Na-Ta Ce-La-Tb Eu-Sm Yb-Zr	Below detection	Undifferentiated alluvial/fluvial brown clay.
Port Lincoln Site 176; *n = 5	Fe-Hf-Th Cs-Sc-Th As-Ce-Cr-La Br-Eu-Na-Sm-U-Yb	Below detection	Feldspathic gneiss

6.4 Element Properties and Associations

The following discussion is a treatment of the statistical results and geochemical properties for the elements analysed in the sampled pedogenic calcrete. The facts concerning the general properties of each individual element are taken from Reimann and de Caritat (1998).

Arsenic maximum and median concentrations in the sampled pedogenic calcrete are 115 and 3.66 ppm, respectively. Minimum concentrations are below the detection limit (0.5 ppm). Rare positive correlation occurs with Br, Ca, Cr, Fe, Sb, Sc and Th; correlation with other elements is rare in the analysed samples. Arsenic is a metalloid element with chalcophile geochemical affinity. Environmental mobility is moderate in acid/alkaline and oxidising conditions and low under reducing conditions. Possible host minerals are feldspars, Fe-oxyhydroxides and adsorbed onto clay particles.

Gold is typically enriched within the pedogenic calcrete and occurs at high concentrations (>1000ppb) in samples overlying gold-bearing host material from Ora Banda gold mine. Gold is a heavy and noble metal with siderophile geochemical association. Environmental mobility is medium to high under oxidising and acid conditions and very low under reducing and alkaline conditions.

Barium maximum and median concentrations in the sampled pedogenic calcrete are 3870 and 163.5 ppm, respectively. Minimum concentrations are below the detection limit (50 ppm). Rare positive correlations occur with Br, Cs, K, La, Na, Rb, Sb, Sm, Tb, Th, U, and Yb in the analysed samples. Barium is a heavy alkaline earth element with a large ion lithophile geochemical affinity. Environmental mobility is low under all conditions and possible host minerals include K-feldspars and micas.

Bromine maximum and median concentrations in the sampled pedogenic calcrete are 157 and 19.35 ppm respectively. Minimum concentration is 0.54 ppm.is a halogen (non-metal) with very high environmental mobility. Bromine is commonly associated with sea-spray and brines and its common positive correlation with Ca and Na suggests concentration of this element through evaporation associated with calcrete precipitation. Bromine shows negative correlation with all other calcrete elements analysed.

Calcium is a light alkaline earth metal with high environmental mobility and is, by definition, the major constituent element within calcrete. Calcium shows negative correlation with all analysed elements except bromine and sodium. Calcium negatively correlates most commonly with Cr, Fe, Hf, Rb, Sc and Th in the analysed samples.

Cerium maximum and median concentrations in the sampled pedogenic calcrete are 96.3 and 14.5 ppm, respectively. Minimum concentrations are below the detection limit (1 ppm). Common positive correlation occurs with La, Sc, Sm, Th and Yb; rare positive correlation occurs with Eu, Tb and Zn in the analysed samples. Cerium is a rare earth element with lithophile geochemical affinity and very low environmental mobility. Possible host materials include feldspar, monazite and zircon.

Cesium maximum and median concentrations in the sampled pedogenic calcrete are 5.3 and 0.69 ppm respectively. Minimum concentrations are below the detection limit (0.2 ppm). Common positive correlations occur with Fe, Rb, and Sc; rare positive associations occur with Ba, Cr, Hf, K, Th, Yb and Zn in the analysed samples. Cesium is a heavy alkali metal with lithophile geochemical affinity and very low environmental mobility. Possible host minerals include micas and K-feldspars.

Chromium maximum and median concentrations in the sampled pedogenic calcrete are 1510 and 21.8 ppm, respectively. Minimum values are below the detection limit (1 ppm). Common positive correlations occur with Cs, Fe, Rb, Sc, Th; rare positive associations occur with As Hf, Sb, Sm, Ta, Yb and Zn in the analysed samples. Strong negative correlation occurs with calcium and bromine in the analysed samples. Chromium is a transition metal with lithophile geochemical association and very low environmental mobility. It is commonly concentrated in residual soils and is unlikely to migrate through vadose and ground waters. Some trees, lichen and moss can accumulate chromium.

Europium maximum and median concentrations are 6.74 and 0.36 ppm respectively. Common positive correlation occurs with La, Sm, Tb, and Yb in the analysed samples. Europium is a rare earth element with lithophile geochemical association and very low environmental mobility. Eu substitutes commonly into feldspars but was excluded from Pearson's value statistical analysis because concentrations are often below the detection level (0.1 ppm).

Iron maximum and median concentrations in the sampled pedogenic calcrete are 15.2 and 0.78 % respectively. Minimum values are below 0.01%. Common correlation occurs with Cr, Cs, Rb, Sc, Th and rare association occurs with Hf, K Sb and Zn in the analysed samples. Strong negative correlation occurs with calcium in the analysed samples. Iron typically occurs in calcrete as oxide hematite and oxyhydroxide goethite.

Hafnium maximum and median concentrations in the sampled pedogenic calcrete are 26.1 and 1.77 ppm, respectively. Minimum concentrations are below the detection limit (0.1 ppm). Common correlation occurs with Cr, Fe, Th, Yb, Zr and rare correlation occurs with Rb, Sc and Ta; Strong negative correlation occurs with

calcium in the analysed samples. Hafnium is a heavy metal with lithophile geochemical affinity and is commonly concentrated in residual soils. Possible host minerals include zircon, biotite and pyroxene.

Potassium maximum and median concentrations in the sampled pedogenic calcrete are 26.1 and 1.77 %, respectively. Minimum concentrations are below the detection limit (0.1 %). Common positive correlations exist with Rb and Th; rare positive correlations exist with Ba, Cs, Fe, Sc, Zn and Zr in the analysed samples. Potassium is an alkali metal (lithophile) with a geochemical affinity for Rb and Ba, an important element in many rock-forming minerals and a major element for plants.

Lanthanum maximum and median concentrations in the sampled pedogenic calcrete are 179 and 8.16 ppm respectively. Minimum concentrations are below the detection limit (0.1 ppm). Common positive correlations occur with Ce, Sm, Tb, Th and Yb; rare positive correlations exist with Cr, Fe, Rb and Sc in the analysed samples. Lanthanum is a rare earth element with lithophile geochemical affinity and very low environmental mobility.

Sodium maximum and median concentrations in the sampled pedogenic calcrete are 3.39 and 0.20 %, respectively. Minimum concentration is 0.06 %. Na has a very high environmental mobility and shows common positive correlation with Br and rare positive correlation with Cr, Rb, Sc, Ta and U in the analysed samples. Sodium is an alkali metal with lithophile geochemical affinity and a major constituent in some rock-forming minerals including alkali feldspar and halite.

Rubidium maximum and median concentrations in the sampled pedogenic calcrete are 140 and 15.9 ppm respectively. Minimum concentrations are below the detection limit (5 ppm). Common positive correlations exist between Rb and Cr, Cs,

Fe, K and Th; rare positive correlations exist with Hf, Na, Sc and Ta in the analysed samples. Rubidium is an alkali metal with lithophile geochemical affinity and low environmental mobility. Possible host minerals include silicates such as feldspar and biotite.

Antimony maximum and median concentrations in the sampled pedogenic calcrete are 3.33 and 0.19 ppm respectively. Minimum concentrations are below the detection limit (0.1 ppm). In the analysed samples Sb shows a rare positive correlation with As, Ba, Cr and Fe. Antimony is a heavy non-metal with chalcophile geochemical affinity and low environmental mobility and is most likely hosted in pedogenic calcrete through adsorption on Fe-oxides and oxyhydroxides.

Scandium maximum and median concentrations in the sampled pedogenic calcrete are 43.2 and 1.54 ppm, respectively. Minimum concentrations are below the detection limit (0.1 ppm). Scandium in the analysed calcrete samples shows common positive correlation with Cr, Fe and Th and rare positive correlation with As, Ce, Cs, Hf and Rb. Scandium is a transition metal with lithophile geochemical affinity. Little is known about its geochemical behaviour except that it is commonly concentrated in residual soils and may be hosted by silicate minerals such as pyroxene, amphibole, biotite and zircon.

Samarium maximum and median concentrations in the sampled pedogenic calcrete are 30.8 and 1.54 ppm, respectively. Minimum concentration is 0.05 ppm. Common positive correlations exist between Sm and Ce, Eu, La, Tb and Yb; rare positive correlation occurs with Th in the analysed calcrete samples. Scandium is a rare earth element with lithophile geochemical affinity and very low environmental mobility. Host minerals include feldspars, zircon, pyroxene and biotite.

Terbium maximum and median concentrations in the sampled pedogenic calcrete are 3.75 and 0.25 ppm, respectively. Minimum concentrations are below the detection limit (0.2 ppm). Common positive correlations occur with Eu, La, Yb, Sm and occasionally with Ba and Ce in the analysed calcrete samples. Terbium is a rare earth element with lithophile geochemical affinity and very low environmental mobility. Typical host minerals include pyroxenes, feldspars and zircon.

Thorium maximum and median concentrations in the sampled pedogenic calcrete are 48.3 and 3.11 ppm, respectively. Minimum concentrations are below the detection limit (0.2 ppm). Common positive correlation occurs with Ce, Cr, Fe, Hf, La, Rb, Sc, Ta and Yb in the analysed calcrete samples. Thorium is a heavy metal (actinide) with lithophile geochemical affininty and very low environmental mobility. It is commonly concentrated in residual soils and can be hosted in zircon and by clay adsorption.

Uranium maximum and median concentrations in the sampled pedogenic calcrete are 8.2 and 0.76 ppm, respectively. Minimum concentrations are below the detection limit (0.5 ppm). Rare positive correlation occurs with As, Ba, Br, Ca and Na in the analysed calcrete samples. Uranium is a heavy metal (actinide) with lithophile geochemical affinity and high environmental mobility except under reducing conditions. It can be hosted in zircon.

Ytterbium maximum and median concentrations in the sampled pedogenic calcrete are 10.8 and 0.76 ppm, respectively. Minimum concentrations are below the detection limit (0.1 ppm). Common positive correlation occurs with Ce, Eu, La, Sm, Tb and Th; rare positive correlations occur with Cr, Hf, Fe, Sc, Th and Zr in the analysed samples. Ytterbium is a rare earth element with lithophile geochemical

affinity and very low environmental mobility. Mineral hosts include feldspars, biotite, pyroxene and zircon.

Zinc maximum and median concentrations in the sampled pedogenic calcrete are 256 and 10.4 ppm, respectively. Minimum concentrations are below the detection limit (10 ppm). Rare positive correlations occur with Ce, Cr, Cs, Fe, K, Rb, Sc and Ta in the analysed samples. Zinc is a heavy metal with chalcophile geochemical affinity with high environmental mobility in acid and oxidising conditions but low mobility under reducing and alkaline conditions. Geochemical barriers include pH and clay/Fe-Mn oxide adsorption.

Zirconium maximum and median concentrations in the sampled pedogenic calcrete are 1130 and 81.7 ppm, respectively. Minimum concentrations are below the detection limit (300 ppm). Common positive correlation occurs with Hf and occasionally with K, Rb, Ta, Th, and Yb. Zirconium is a heavy metal with lithophile geochemical affinity, very low environmental mobility and typically hosted in the mineral zircon.

6.5 Discussion

The associations of the analysed trace elements provided by statistical analysis of the geochemical data set (Tables 6.1, 6.2 and 6.3) indicate that many of the major and trace elements analysed show a negative correlation with calcium. This indicates that they are partitioned within residual phases in the pedogenic calcrete. Several distinct element groupings occur as determined by Pearson's correlation coefficients and element ratios.

The rare earth elements Ce, Eu, La, Sm, Yb, and Tb are associated strongly with one another. These elements have a strong affiliation for feldspars, which are present in most samples. The feldspar varieties identified by both thin section and XRD ranged the whole spectrum from orthoclase and microcline (potassic) to albite (sodic) and anorthite (calcic), commonly occurring as mixtures within the samples. Apart from being derived directly from granitic, gneissic and mafic parent materials, minor amounts occur in profiles developed on aeolian and fluvial parent materials indicating windblown material as a source. Concentrations of Zr also suggest small quantities of windblown zircon grains are present in some samples. Zircon is a possible host for Hf, Th and Yb and there is association of these elements with Zr in the samples.

The broad relationships of the transition metals Cr, Fe, Hf, Sc and alkali metals Cs, K and Rb are complex and combinations of these elements are interrelated in various ways in the analysed samples. The strongest association occurs between Sc, Cr and Fe; these elements are likely to be associated with the iron oxides (hematite) or iron oxyhydroxides (goethite). The elements Ce and Th are variably associated with the above-mentioned elements or with rare earth elements; some of these overlapping correlations may however be coincidental, occurring in profiles with few samples, however, the possibility that two or more phases host these elements is a factor that needs to be taken into consideration. Typically Ce shows a stronger relationship with the rare earth elements whereas Th is commonly correlated with transition metals. Another example of different phases hosting trace elements is the association of Hf with Fe and Cr in profiles where Hf is not associated with Zr.

The alkali metals K, Rb and Cs show a strong interrelation in many samples but are also variably associated with transition metals. Clay minerals are the likely host for these elements, however, considering the limited number of elements analysed in

the dataset and the fact that pedogenic calcrete commonly contains mixtures of clay minerals with a variety of chemical compositions it is difficult to ascertain whether clay minerals are significant hosts for trace elements such as transition metals.

The mobile elements Br and Na show interesting interactions with respect to calcium and their distribution within the pedogenic calcrete profiles investigated. Bromine is the only analysed element to show a common positive correlation with Ca and the cause of this association is considered to be due to the process of evaporation causing congruent distribution of the two soluble elements within the profile. Bromine also shows a common correlation with Na in profiles were it is not correlated to Ca. Correlations between Na and Ca however are uncommon in the analysed samples. Sodium may be hosted as either halite (NaCl) in saline conditions or as a constituent of residual minerals such as alkali feldspar. Whether bromine is chemically incorporated into calcite is uncertain but the fact that there is no three-way association between Ca, Na and Br, as well as the extraction of Br by aqua-regia solution (Figure 6.1) suggests that bromine is present as either mobile or soluble phases and hosted in alkali feldspars.

Uranium does not show any common correlations in the statistical analysis; however, examination of the profile trends of concentration versus depth shows that U concentration is typically increased at the base of a profile, particularly were the base of the profile is dolomitic. This provides possible evidence for the influence of capillary-fringe groundwaters contributing to the precipitation of carbonate at the base of pedogenic calcrete profiles.

The concentrations of some trace elements show no systematic correlation within the sampled pedogenic calcrete profiles. Elements such as As, Ba, Sb and Zn show variable association with each other and various other elements in the geochemical

and statistical analyses. The whole-rock INAA data indicate that the concentration of these elements is highly variable and, with the exception of As, are typically depleted with respect to calcium concentration. The incidental or residual origin of these elements may affect their potential as (exploration) pathfinder elements through their unpredictable behaviour. The association with economically important minerals of these elements, in particular As, Zn and Sb, which are commonly associated with auriferous metal sulfide, vein and hydrothermal deposits and Zn also being associated with volcanic hosted massive sulfide (VMS) and lead-zinc deposits, warrants further investigation into their geochemical and biogeochemical behaviour and use as pathfinder elements.

The current study indicates that gold within pedogenic calcrete is concentrated up to an order of magnitude over the parent material concentration in un-mineralized sites. The cause of the pedogenic calcrete-gold association is yet uncertain but is almost certainly hydromorphic or biogeochemical and associated directly with the formation of pedogenic calcrete rather than being residual or created prior to calcrete formation. The factor that is potentially very important in controlling the distribution of gold and other trace elements within the regolith is the pH contrast that commonly exists between pedogenic calcrete and underlying regolith materials. Pedogenic calcrete is strongly alkaline; the high pH can reduce the chemical mobility and act as a geochemical barrier, thus trapping elements dissolved from underlying neutral to acid regolith and causing their precipitation in the calcrete horizon. Gold and zinc both have medium to high environmental mobility under oxidising and acid conditions but low mobility under alkaline conditions (Reimann and de Caritat 1998).

Chapter 7

Conclusions and Further Work

7.1 Research Outcomes

Research on the micro-morphological properties of pedogenic calcrete has shown a biogenic origin for many of the samples analysed. Some of the important points resulting from this work are:

- Typical pedogenic calcrete nodules, pisoliths and hardpan contain abundant calcified filaments that are readily visible using thin sections stained with combined potassium ferricyanide and Alizarin red solution.
- Organic matter associated with the calcified filaments is common in many samples. These samples are viable for growth and reproduction in the laboratory, however, further research by biologists is necessary to purify and identify the organisms responsible for calcite precipitation.
- Pedogenic calcrete with petrographic features indicating rhizogenic origin occur in a number of forms: rhizomorphic taproot fragments, platy hardpan with fenestral pores, root-like sheets and channels containing needle-fibre calcite or other textures, and nodules with channels and alveolar-like fabrics.
- Cathodoluminesence petrography allows visual recognition of different cement phases within the pedogenic calcrete. Evidence for neomorphism or replacive and displacive growth was not seen in the samples examined with CL and further research is needed to illuminate this area of investigation.

7.2 Isotopic Disequilibrium

The results of multiple aliquot carbon and oxygen isotope analyses show significant within-sample variability and co-variation in $\delta^{13}C$ and $\delta^{18}O$ for many samples, indicating that two or more factors can contemporaneously affect the isotopic composition of pedogenic calcrete. Therefore, in order to make valid conclusions about within-profile and regional isotopic trends and their meaning, we need to consider all the possible causes of internal isotopic variation.

Samples containing abundant calcified filaments, typically the laminar coatings in nodules and hardpan, invariably have $\delta^{13}C$ values higher than –6 ‰ and show an increase in the upper 0.2 – 0.5m of the profile suggesting that they are a possible cause of $\delta^{13}C$ enrichment. The organic matter present in most of the samples was found to be associated with the calcified filaments; however, soil organic matter $\delta^{13}C$ values show no systematic relationship to the carbonate $\delta^{13}C$ value and there is commonly greater than 17‰ differences in carbonate and coexisting organic matter $\delta^{13}C$. That the soil organic matter $\delta^{13}C$ shows minimal variation over the large geographical area sampled suggests that the organism responsible for the formation of calcified filaments only one of several possible factors contributing to the carbon isotopic composition of pedogenic calcrete.

Rhizogenic influence is a significant contributing factor to the $\delta^{13}C$ composition of pedogenic calcrete. Samples with rhizogenic micro-morphology such as in-filled root channels, needle-fibre calcite, alveolar and fenestral fabrics typically have $\delta^{13}C$ values significantly lower than –6 ‰.

In-mixing and diffusion of atmospheric carbon (dioxide) is the cause of pedogenic carbonate $\delta^{13}C$ values averaging –6 ‰, possibly diluting the effects of C3/C4 vegetation contributing to $\delta^{13}C$ within a pedogenic calcrete profile. That $\delta^{18}O$ values are commonly covariant with $\delta^{13}C$ within samples suggests that evaporation and carbon dioxide degassing occur concurrently and are strong contributing factors in pedogenic carbonate precipitation. Within pedogenic calcrete profiles $\delta^{13}C$ and $\delta^{18}O$ values show varying upward trends that cannot always be explained by atmospheric carbon in-mixing and evaporation and carbon dioxide degassing effects. The amount and type of the various biogenic and micritic cements must therefore contribute to variations in isotopic composition causing disequilibrium between soil organic matter and precipitated pedogenic carbonate.

Data from South Australia and Western Australia show different regional trends with respect to climate and distance inland. Pedogenic calcrete samples from arid inland regions of the Yilgarn Craton have depleted $\delta^{13}C$ values giving evidence for C3-dominated vegetation, the regional trend contradicting the current climate and vegetation and the high $\delta^{13}C$ values from pedogenic calcrete sampled from inland regions of the South Australian Gawler Craton and Murray Basin. Too little is known about the photosynthetic pathways of the indigenous flora, soil respiration rates and organic matter decomposition at the sites to relate carbon isotopic composition to climate in a meaningful way. Furthermore, the question of temporal relationships of pedogenic calcrete formation and whether changes in the dominant vegetation have occurred during or since the formation of the sampled pedogenic calcrete is uncertain.

The current research was carried out over a very wide geographical area and, as such, is limited to some extent in detail for individual profiles. Further research on the rhizogenic and microbiological properties of pedogenic calcrete is needed using

detailed studies on a few carefully selected profiles with attention to the following factors:

- Microscopic and geochemical analysis of plant root systems and the rhizogenic carbonate associated with them.
- Biological precipitation of the samples and purification of the organisms responsible for carbonate precipitation along with isotopic analysis of laboratory-produced organic matter and biogenic carbonate.
- Microscopic carbon (and oxygen) isotope analysis of the various components with the aim of understanding the end-member values of biogenic (calcified filaments) and inorganically precipitated carbonate.
- Geochemical modelling on the effect of carbon dioxide degassing on carbon isotopic composition within a profile.
- Age determination of the pedogenic calcrete.

7.3 Age Determination of Pedogenic Calcrete

The use of calcrete development stages such as developed by Machette (1985) and others provides a means to compare regional differences and gross estimates of the elapsed time interval involved in the formation of the sampled pedogenic calcrete; these range in age from newly formed (stage 1 and 2) powder calcrete in recent aeolian dunes, to early stage nodular calcretes in the areas of the Yilgarn Craton, to mature (stage 5 and 6) hardpan and boulder calcrete formed as calcrete plains on stable land surfaces of southeastern South Australia. Absolute age determination can, however, only be determined on pedogenic calcrete by radiogenic methods. While such age measurement was not attempted in the present study, a discussion of the techniques useful for dating pedogenic calcrete and the suitability of the

pedogenic calcrete sampled for such techniques is useful in the context of possible further research.

There are many pitfalls for researchers wanting to accurately measure the age of a particular pedogenic calcrete, not least of which is the propensity of pedogenic calcrete to form over long time spans; typically thousands to hundreds of thousands of years. Furthermore, problems arise from the open-system behaviour and the dissolution/reprecipitation reactions commonly encountered in attempts to date pedogenic calcrete using radiometric methods (Branca *et al.*, 2004). Until relatively recently dating of pedogenic calcrete using uranium series dating, in particular the U-Th isotopic system which has a range of up to 350 ka, was considered impractical because of the detrital impurities contained within the samples, in particular aluminosilicate clays, contaminating samples with extraneous uranium and thorium. Significant and unpredictable transfer of radionuclides occurs from the detritus to the leachate in commonly used selective leaching procedures (Ku and Liang, 1984; Schwarcz and Latham, 1989). However, total sample dissolution (TSD) techniques to correct for such contamination have been shown by Bischoff and Fitzpatrick (1991) and Luo and Ku (1991) to yield precise ages provided certain conditions are met. In summary, this technique corrects for initial ^{230}Th using an isochron approach to graphically display the multiple coeval data points and calculate the initial isotopic disequilibrium for the $^{230}Th/^{234}U$ clock. A plot of $^{230}Th/^{232}Th$ versus $^{234}U/^{232}Th$ derives the initial condition assuming a common initial $^{230}Th/^{232}Th$ in the coeval sample aliquots. Deviation from linearity of the plot reflects open system behaviour in the sample.

Some calcrete researchers have used luminescence methods to date quartz grains within the host pedogenic calcrete (Singhvi *et al.*, 1996; Budd *et al.*, 2002). The principles of luminescence dating are complex in detail; put simply however, it

involves the optical bleaching of exposed sediment (usually quartz grains) to a residual value, then upon burial, a fresh acquisition of luminescence through irradiation caused by the decay of uranium (238), thorium (323) and potassium (40). This method (Singhvi *et al.*, 1996) is considered less susceptible to post-depositional changes associated with the open-system behaviour of pedogenic calcrete and deals with the difference between age of sediment deposition and actual age of pedogenic calcrete by measuring the luminescence signals from both the carbonated and un-carbonated mineral separates.

Both these techniques are potentially useful in determining the age and duration of formation of the sampled pedogenic calcrete provided the sampling regime is rigorous enough to ensure that the analysed samples contain cement generations that span the entire range of ages of formation. Such research will be invaluable in constraining the age and temporal patterns of pedogenic calcrete formation in the southern regions of the Australian continent. Another useful avenue for further research is carbon-14 dating of the soil organic matter fraction. Possible questions can be raised in regard to whether or not the soil organic matter commonly found in the sampled pedogenic calcrete is in fact preserved from the time of formation or whether it is perpetually renewed by biological activity.

7.3 The Use of Pedogenic Calcrete as a Geochemical Sample Medium

While the usefulness of pedogenic calcrete as a geochemical sample medium for gold exploration has been demonstrated in numerous studies over buried ore systems, other potentially useful pathfinder elements have, in large part, been neglected in this type of research. The correlation between gold and calcium within pedogenic calcrete is supported by the results of the present study in that, even in seemingly un-mineralised areas, there is a significant increase of the Au content in

the pedogenic calcrete over that in the host material. Statistical analysis on other major and trace element co-variations and ratios within individual profiles show that many major and trace elements are strongly correlated with residual phases and negatively correlated with calcium in pedogenic calcrete profiles. Some economically important ore elements, in particular arsenic and zinc show variability and correlation with calcium in some profiles. The potential of these elements as pathfinder elements is also suggested by their geochemical properties in that they are insoluble and precipitate out of solution in alkaline conditions; making them potential elements of interest in future geochemical exploration research.

Strontium isotopic analyses on selected profiles shows a distinct contrast between South Australian and Western Australian samples in that the former show a strong marine signature, even in samples collected in inland arid regions, whereas the Western Australian samples show significantly greater calcium input from host material sources. Many theories exist on the origins of calcrete-gold phase relationships in geochemical exploration. The fact that the carbonate in pedogenic calcrete in some regions appears to be derived (almost) wholly by atmospheric contribution while retaining increased gold concentrations relative to host material suggests that the phase relationship between gold and pedogenic calcrete is secondary (Lintern *et al*. submitted). That is, being a consequence of the precipitation of carbonate within a soil profile rather than a residual association caused by surface gold accumulation prior to calcrete formation. Determining the actual mechanism of gold accumulation in pedogenic calcrete will require further research into the form or type of gold present and calcrete morphological association of that microscopic gold.

References

Alderman A.R. and Skinner H.C.W 1957. Dolomite sedimentation in the southeast of South Australia. *American Journal of Science*. **255;8**, 561-567.

Alonzo-Zarsa A.M., Silva P.G., Goy J.L., and Zazo C. 1998. Fan-surface dynamics and biogenic calcrete development: interactions during ultimate phases of fan evolution in the semiarid SE Spain (Murcia). *Geomorphology*, **24**, 147-167.

Amundson R.G., Chadwick O.A., Sowers J.M. and Doner H.E. 1988. Relationship between climate and vegetation and the stable carbon isotope chemistry of soils in the eastern Mojave, Nevada. *Quaternary Research*, **29**, 245-254.

Amundson R.G., Chadwick O.A., Sowers J.M. and Doner H.E. 1989. The stable isotope chemistry of pedogenic carbonates at Kyle Canyon, Nevada. *Soil Science Society of America Journal*, **53**, 201-210.

An Zhisheng, Bowler J.M., Opdyke N.D., Macumber P.G and Firman J.B. 1986. Palaeomagnetic stratigraphy of Lake Bungunnia: Plio-Pleistocene precursor of aridity in the Murray Basin, Southeastern Australia. In: A.R. Chivas, T. Torgersen and J.M. Bowler (eds), *Palaeo-environments of salt lakes. Paleaogeography, Palaeoclimatology, Palaeoecology*, **54**, 219-239.

Anand R.R., Phang C., Wildman J.E. and Lintern M.J. 1997 Genesis of some calcretes in the southern Yilgarn Craton, Western Australia: implications for mineral exploration. *Australian Journal of Earth Sciences* **44,** 877-103**.**

Anand R.R., Phang C., Wildman J.E. and Lintern M.J 1998. Reply: Genesis of some calcretes in the southern Yilgarn Craton, Western Australia: implications for mineral exploration. *Australian Journal of Earth Sciences* **45,** 181-182.

Anand R.R. and Paine M. 2002. Regolith Geology of the Yilgarn Craton, Western Australia: implications for exploration. *Australian Journal of Earth Sciences*, **49**, 3-163.

Arakel A.V. 1982. Genesis of calcrete in Quaternary soil profiles, Hutt and Leeman Lagoons, Western Australia. *Journal of Sedimentary Petrology*, **52**, 109-125.

Arakel A.V. 1986. Evolution of Calcrete in palaeodrainages of the Lake Napperby area, central Australia. *Palaeogeography, Palaeoclimatology, Palaeoecology*, **54**, 283-303.

Beier J.A. 1987. Petrographic and geochemical analysis of caliche profiles in a Bahamian Pleistocene Dune. *Sedimentology*, **34**, 991-998.

Bischoff J.A. and Fitzpatrick J.A. 1991. U-series dating of impure carbonates: an isochron technique using total-sample dissolution. *Geochimica et Cosmochimica Acta*. **55**, 543-554.

Boquet E., Boronat A. and Ramos-Cormenzana A. 1973. Production of calcite (calcium carbonate) crystals by soil bacteria is a general phenomenon. *Nature*, **246**, 527-528.

Boutakoff N. 1963. The geology and geomorphology of the Portland area. *Geological Survey of Victoria Memoir*, **22**.

Bowler J.M. 1976. Aridity in Australia: Age, origin and expression in aeolian landforms and sediments. *Earth-Science Rreviews*, **12**, 279.

Bowler J.M. and Polach H.A, 1971. Radiocarbon analysis of soil carbonates: an evaluation from palaeosols in southeastern Australia. In *Palaeopedology- Origin, Nature and Dating of Palaeosols*. D. Yaalon (ed), pp 97-108. Jerusalem: Israel University Press.

Braithwaite C. J. R. 1983. Calcrete and other soils in Quaternary limestones: structures, processes and applications. *Journal of the Geological Society of London*, **140**, 351-363.

Branca M., Masi U. and Voltaggio M. 2004. An unsuccessful attempt at U/Th dating of soil calcretes from the Doukkali area (western Morocco) and environmental applications. *Chemie der Erde*. In press.

Brewer R. and Sleeman J.R 1988. *Soil Structure and Fabric*. CSIRO Division of Soils: Adelaide.

Buczynski C.and Chafetz H.S. 1987. Siliclastic grain breakage and displacement due to carbonate crystal growth: an example from the Lueders Formation (Permian) of north-central Texas, U.S.A. *Sedimentology*, **34**, 837-843.

Budd D.A., Pack S.M. and Fogel M.L. 2002. The destruction of paleoclimatic isotopic signals in Pleistocene carbonate soil nodules of Western Australia. *Palaeogeography, Palaeoclimatology, Palaeoecology*, **188**, 249-273.

Butt C.R.M., Horwitz R.C. and Mann A.W. 1977. Uranium occurrences in calcrete and associated sediments in Western Australia, CSIRO Mineral Research Laboratories, Division of Mineralogy Report FP. **16**, 67.

Cailleau G., Braissant O., Dupraz C., Aragno M., Verrecchia E. P., 2005. Biologically induced accumulations of $CaCO_3$ in Orthox soils of Biga, Ivory Coast. *Catena*, **59**, 1-17.

Callot G., Guyen A. and Mousain D. 1985. Inter-relations entre aiguilles de calcite et hyphes myceliens. *Agronomie*, **5**, 209-216.

Capo R. C., and Chadwick O. A. 1999. Sources of strontium and calcium in desert soil and calcrete. Earth and Planetary Science Letters. **170**, 61-72.

Capo R. C., Stewart B. W. and Chadwick O. A. 1998. Strontium isotopes as tracers of ecosystem processes; theory and methods. In: Biogeochemistry of isotopes in soil environments; theory and application. Nordt L. C., Kelly E. F., Boutton T. W. and Chadwick O. A. (eds). *Geoderma*. **82**, 197-225.

Calvet F. 1982. Constructive micrite envelopes developed in vadose continental environments in Pleistocene eolianites of Mallorca (Spain). *Acta Geologica Hispanola*, **17**, 169-178.

Calvet F. and Julia R. 1983. Pisiods in the calcite profiles of Tarragona, north-east Spain. In *Coated Grains* Peryt T.M (ed), pp 456-473. Springer-Verlag, Berlin, Heidelberg, New York.

Carlisle D. 1980. Possible variation in the calcrete-gypcrete uranium model. *U.S Dept. Energy Open File Report GJBX*-53(80), pp 38.

Carlisle D., Merifield P., Orme A. and Kolker O. 1978. The distribution of calcretes and gypcretes in southwestern United States and their uranium favourability, based on a study of deposits in Western Australia and Southwest Africa (Namibia). *U.S Dept. Energy Open File Report GJBX*-29 (78). pp 274.

Cerling T.E. 1984. The stable isotopic composition of modern soil carbonate and its relationship to climate. *Earth and Planetary Science Letters*, **71**, 229-240.

Cerling T.E., Quade J., Yang W. and Bowman J.R. 1989. Carbon isotopes in soils and paleaosols as ecology and palaeoecology indicators. *Nature*, **341**, 138-139.

Chadwick O.A. and Nettleton W.D. 1990. Micromorphological evidence of adhesive and cohesive forces in soil cementation. In: *Soil Micromorphology: A Basic and Applied Science.* L.A. Douglas (ed), pp 207-212. Developments in Soil Science No. 19. Elsevier, Amsterdam.

Chadwick O.A., Sowers J.M. and Amundson R.G. 1987. Morphology of calcic crystals in clast coatings from four soils in the Mojave Desert region. *Soil Science Society of America Journal*, **53**, 211-219.

Chafetz H. and Buczynski C. 1992. Bacterially induced lithification of microbial mats. *Palaios*, **7,** 277-293.

Chen X.Y., Lintern M.J. and Roach I.C. 2002. *Calcrete: Characteristics, Distribution and Use in Mineral Exploration*. CSIRO Exploration and Mining. Kensington, Western Australia.

Chiquet A., Michard A., Nahon D. and Hamelin B. (1999). Atmospheric input vs in situ weathering in the genesis of calcretes; an Sr isotope study at Galvez (central Spain). *Geochimica et Cosmochimica Acta*, **63**, 311-323.

Crawford H.M. 1965. The geology of Yorke Peninsula. *Geological Survey of South Australia. Bulletin*, **39**. 96pp.

Crocker R.L. 1946. Post-Miocene climatic and geologic history and its significance in relation to the major soil types of South Australia. CSIRO Bulletin No. 39.

Dixon J.A.D. 1965. A modified staining technique for carbonates in thin section. *Nature*, pp 587.

Durand R. 1980. L'evolution d'une rendzina encroutee sur la craie de Champagne: Association Francaise d'Etude des sols, Bulletin, *Science du Sol*, **3**, 201-216.

Emrich K.D., Ehalt H. and Vogel J.C. 1970. Carbon isotope fractionation during the precipitation of calcium carbonate. *Earth and Planetary Science Letters*, **8**, 363-371.

Esteban M. 1974. Caliche textures and *Microcodium*. *Bulletin Society of Geology Italy*, **92**, 105-125.

Esteban. C M. 1976. Vadose pisolite and caliche. *American Association Petroleum Geologists Bulletin*, **60**, 2048-2057.

Esteban M. and Klappa C.F. 1983. Subaerial exposure environment. *Memoirs American Association Petroleum Geologists*, **33**, 1-54.

Firman J.B. 1963. Quaterary geological events near Swan Reach in the Murray Basin, South Australia. *Geological Survey of South Australia Quarterly Geological Notes*, **5**, 6-7.

Firman J.B. 1964. The Bakara soil and other stratigraphic units of Late Cainozoic age in the Murray Basin, South Australia. *Geological Survey of South Australia Quarterly Geological Notes,* **10**, 2-5.

Firman J.B. 1966. Stratigraphy of the Chowilla area in the Murray Basin. *Geological Survey of South Australia Quarterly Geological Notes*, **20**, 3-7.

Firman J.B. 1967a. Late Cainozioc stratigraphic units in South Australia. *Geological Survey of South Australia Quarterly Geological Notes*, **22**, 4-7.

Firman J.B. 1967b. Stratigraphy of Late Cainozoic deposits in South Australia. *Proceedings of the Royal Society of South Australia*, **91**, 166-178.

Folk R.L. 1974. The natural history of crystalline calcium carbonate: effect of magnesium content and salinity. *Journal of Sedimentary Petrology*, **44**, 40-53.

Garnett D.l., Rea W.J. and Fuge R. 1982. Geochemical exploration techniques applicable to calcrete-covered areas. In H.W. Glenn (Ed.) Proceedings of the 12th Commonwealth Mining and Metallurgical Congress, Geological Society of South Africa, Johannesburg, pp 945-955.

Gile L.H., Peterson F.F. and Grossman R.B. 1966. Morphological and genetic sequences of carbonate accumulations in desert soils. *Soil Science*, **100**, 347-360.

Given K.R. and Wilkinson B.H. 1985. Kinetic control of morphology, composition and mineralogy of abiotic sedimentary carbonates. *Journal of Sedimentary Petrology*, **55**, 109-119.

Goldsmith J.R., Graf D.L. and Heard H.C 1961. Lattice constants of the calcium-magnesium carbonates. *American Mineralogist*, **46**, 453-457.

Goudie A.S. 1973. *Duricrusts in Tropical and Subtropical Landscapes*. Clarendon Press, Oxford.

Goudie A.S. 1983. Calcrete. In: *Chemical Sediments and Geomorphology* (Eds. A.S Goudie and K. Pye), pp 93-131. Academic Press, London, New York.

Graf D. Goldsmith J. R. 1956. Some hydrothermal syntheses of dolomite and protodolomite. *Journal of Geology*, **64**, 173-186.

Gregory J.W. 1914. The lake system of Westralia. *Geographical Journal*, **80**, 656-664.

Hamidi E. M., Colin F., Michard A., Boulange B. and Nahon D. 2001 Isotopic tracers of the origin of Ca in a carbonate crust from the Middle Atlas, Morocco. *Chemical Geology*, **176**, 93-104.

Hardy R. and Tucker M. 1988. X-ray powder diffraction of sediments. In: *Techniques in Sedimentology.* Tucker M. (ed). Blackwell Scientific Publications, Oxford.

Harrison R.S. 1977. Caliche profiles: indicators of near surface subaerial diagenesis, Barbados, West Indies. *Bulletin of Canadian Petrology and Geology*, **25**, 123-173.

Hattersley, P.W., 1983. The distribution of C_3 and C_4 grasses in Australia in relation to climate. *Oecologia*, **57**, 113-128.

Hay R.L. and Reeder R.J. 1978. Calcretes of Olduvai Gorge and Ndolanya Beds of Northern Tanzania. *Sedimentology*, **25**, 649-673.

Hay R.L. and Wiggins B. 1980. Pellets, ooids, sepiolite and silica in three calcretes of south-western United States. *Sedimentology*, **27**, 559-576.

Hesse P.P. 1994. The record of continental dust from Australia in Tasman Sea Sediments. *Quaternary Science Reveiws*, **13**, 257-272.

Hill, S.M., Taylor, G., and McQueen, K.G. 1998. Discussion. Genesis of some calcretes in the southern Yilgarn Craton, Western Australia: implications for mineral exploration. *Australian Journal of Earth Sciences*, **45**, 177-179.

Hinston F.J. and Gailitis V. 1976. The geographic variation of salt precipitated over Western Australia. *Australian Journal of Soil Research*, **14**, 319-335.

Hutton J.T. 1982. Calcium carbonate in rain. In: R.J. Wasson (ed.) *Quaternary Dust Mantles of China, New Zealand and Australia*. Proceedings of a workshop, ANU, Canberra, pp 149-152.

Hutton, J.T. and Dixon, J.C. 1981. The chemistry and mineralogy of some South Australian calcretes and associated soft carbonates and their dolomitisation. *Australian Journal of Earth Sciences*, **28**, 71-79.

James N.P. 1972. Holocene and Pleistocene calcareous crust (caliche profiles: criteria for subaerial exposure. *Journal of Sedimentary Petrology*, **42**, 817-836.

Kahle, C.F. 1977. Origin of subaerial Holocene calcareous crusts: role of algae, fungi and sparmicritisation. *Sedimentology*, **24**, 413-435.

Keywood M.D., Chivas A.R., Fifield L.K., Cresswel R.G. and Ayers G.P. 1997. The accession of chloride to the western half of the continent. *Australian Journal of Soil Research*, **35**, 1177-1189.

Khadkikar A.S., Chamyal A.S. and Ramesh R. 2000. The character and genesis of calcretes in Late Quaternary alluvial deposits, Gujarat, western India, and its bearing on the interpretation of ancient climates. *Palaeogeography, Palaeoclimatology, Palaeoecology*, **162**, 239-261.

Klappa C.F. 1978. Biolithogenesis of *Microcodium*: elucidation. *Sedimentology*, **25**, 489-522.

Klappa C.F. 1979a. Lichen stromatolites: criterion for subaerial exposure and a mechanism for the formation of laminar calcrete (caliche). *Journal of Sedimentary Petrology*, **49**, 387-400.

Klappa C.F. 1979b. Calcified filaments in Quaternary calcretes: organo-mineral interactions in the subaerial vadose environment. *Journal of Sedimentary Petrology*, **49**, 955-968.

Klappa C.F. 1980. Rhizoliths in terrestrial carbonates: classification, recognition, genesis and significance. *Sedimentology*, **27**, 613-629.

Knox G.F. 1977. Caliche profile formation, Saldahna Bay (South Africa). *Sedimentology*, **24**, 657-674.

Krumbein W.E. 1968. Geomicrobiology and geochemistry of the 'Nari-Lime-Crust' (Israel). In: *Recent Developments in Carbonate Sedimentology in Central Europe*. Friedman G.M. (ed), pp 138-147.

Krumbein W.E. and Giele C. 1979. Calcification in a coccoid – cyanobacterium associated with the formation of desert stromatolites. *Sedimentology*, **26**, 593-604.

Ku T.L and Liang Z.C. 1984. The dating of impure carbonates with decay-series isotopes. *Nuclear Instrumental Methods*. **223**, 563-571.

Langmuir D. 1968. Stability of calcite based on aqueous solubility measurements. *Geochimica et Cosmochimica Acta*. **32**, 835-851.
Lamplugh G.W. 1902. Calcrete. *Geological Magazine*, **39**, 575.

Lawrence C.R. 1966. Cainozoic stratigraphy and structure of the Mallee region, Victoria. *Proceedings of the Royal Society of Victoria*, **79**, 517-553.

Lintern M.J. 1989. Study of the distribution of gold in soils at Mt Hope. *CRC LEME Open File Report* 65, Perth.

Lintern M.J. 2002. Calcrete sampling for mineral exploration. In Chen X.Y., Lintern M.J. and Roach I.C. 2002. Calcrete: characteristics, distribution and use in mineral exploration. CRC LEME Kensington, WA.

Lintern M.J. and Butt C.R.M. 1993. Pedogenic carbonate: an important sample medium for gold exploration in semiarid areas. *Exploration Research News*, **7**, 7-11.

Lintern M.J., Sheard M.J. and Chivas A.R. 2006. The origin of pedogenic calcrete associated with gold in the western Gawler Craton, South Australia. *Chemical Geology* (In press).

Lippman F. 1973. *Sedimentary Carbonate Minerals*. Springer, New York.

Loisy C., Verrechia E.P. and Dufour P. 1999. Microbial origin for pedogenic micrite associated with a carbonate palaeosol (Champagne, France). *Sedimentary Geology*, **126**, 193-204.

Ludwig K.R. and Paces J.B. 2002. Uranium series dating of pedogenic silica and carbonate, Crater Flat, Nevada. *Geochimicha et Cosmochimica Acta*, **66**, 487-506.

Luo S. and Ku T.L. 1991. U-series isochron dating: a generalised method employing total-sample dissolution. *Geochimica et Cosmochimica Acta*. **55**, 555-564.

Machette M.N. 1985. Calcic soils of the southwestern United States. *Geological Society of America Special Paper* No 203, pp 1-21.

Mann A.W. and Horwitz R.C. 1979. Groundwater calcrete deposits in Australia. Some observations from Western Australia. *Journal of the Geological Society of Australia*, **26**, 293-303.

Margaritz M. and Amiel A.J. 1980. Calcium carbonate in calcareous soil from the Jordan Valley, Israel; its origin revealed by the stable carbon isotope method. *Soil Science Society of America Journal*, **44**, 1059-1062.

Mazzucheli R.H. 1972. Secondary geochemical dispersion patterns associated with nickel sulphide deposits at Kambalda, Western Australia. *Journal of Geochemical Exploration*. **1**, 103-116

Miller J. 1988. Cathodoluminescence microscopy. In: *Techniques in Sedimentology.* Tucker M. (ed). Blackwell Scientific Publications, Oxford.

Milnes A.R. 1992. Calcrete. In.Martini I.D. and Chesworth W. (Eds.): *Developments in earth surface processes, weathering, soils and palaeosols*. Elsevier, Amsterdam. pp309-347.

Milnes A.R. and Hutton J.T. 1983. Calcretes in Australia. In: *Soils: an Australian Viewpoint*, pp 119-162. CSIRO. Academic Press, London, New York.

Monger H.C., Daugherty L.A., Linderman W.C. and Liddell C.M. 1991. Microbial precipitation of pedogenic calcite. *Geology*, **19**, 997-1000.

Naiman Z., Quade J. and Patchett P. J. 2000 Isotopic evidence for eolian recycling of pedogenic carbonate and variations in carbonate dust sources throughout the Southwest United States. *Geochimica et Cosmochimica Acta*. **64**, 3099-3109.

Nakata P.A. 2003. Advances in our understanding of calcium oxalate crystal formation and function in plants. *Plant Science*. **164**, 901-909.

Nash D.J. and Mclaren S.J. 2003. Kalahari valley calcretes; their nature, origins, and environmental significance. Thomas D.S.G. (ed.) In: Late Quaternary environmental change in African drylands. *Quaternary International*. **111**, 3-22. 2003.

Netterberg F. 1967. Some road making properties of South African calcretes. *Proceedings of the 4th Regional Conference of African Soil Mechanical Foundations and Engineering, Cape Town*, **1**, 77-81.

Netterberg F. 1980. Geology of southern African calcretes. I. Terminology, description, macrofeatures and classification. *Transactions of the Geological Society of South Africa*, **83**, 255-283.

Northrop J. I. 1890 Notes on the geology of the Bahamas. *Transactions of the New York Academy of Sciences*. pp 4-22.

Ollier C.D. 1978. Early landform evolution. In Jeans D.N. (ed.): *The Natural Environment*. Sydney University Press, Sydney. pp 97-116.

Ollier C.D., Chan R.A., Craig M.A. and Gibson D.L. 1988. Aspects of landscape history and regolith in the Kalgoorlie region, Western Australia. *BMR Journal of Australian Geology and Goephysics*, **10**, 309-321.

Pendall E.G., Harden J.W., Trumbore S.E. and Chadwick O.A. 1994. Isotopic approach to soil carbonate dynamics and implications for paleaoclimatic interpretations. *Quaternary Research*, **42**, 60-71.

Phillips S.E. and Milnes A.R. 1988. The Pleistocene terrestrial carbonate mantle on the south-eastern margin of the St Vincent Basin, South Australia. *Australian Journal of Earth Sciences*, **35**, 463-481.

Phillips S.E., Milnes A.R. and Foster R.C. 1987. Calcified Filaments: an example of biological influences in the formation of calcrete in South Australia. *Australian Journal of Soil Research*, **25**, 405-428.

Phillips S.E. and Self P.G. 1987. Morphology, crystallography and origin of needle-fibre calcite in Quaternary pedogenic carbonates of South Australia. *Australian Journal of Soil Research*, **25**, 429-444.

Quade J., Cerling T.E. and Bowman J.R. 1989. Systematic variations in the carbon and oxygen isotopic composition of pedogenic carbonate along elevation transects in the southern Great Basin, United States. *Geological Society of America Bulletin*, **101**, 464-475.

Quade J., Chivas A.R. and McCulloch M.T. 1995. Strontium and carbon isotope tracers and the origins of soil carbonate in South Australia and Victoria. *Palaeogeography, Palaeoclimatology and Palaeoecology*, **113**, 103-117.

Raven P.H., Evert R.F. and Eichhorn S.F. 1986. *The Biology of Plants*. Worth Publishers. New York.

Read J.F. 1974. Calcrete deposits and Quaternary sediments, Edel Province, Shark Bay, Western Australia. *American Association of Petroleum Geology Memoirs*, **22**, 250-282.

Reeves C.C. 1976. *Caliche: Origin, Classification, Morphology and Uses*. Estacado Books, Texas.

Reimann C. and de Caritat P. 1998. Chemical elements in the environment: factsheets for the geochemist and environmental scientist. Springer-Verlag, Berlin.

Robie R.A., Hemingway B.S., and Fisher J.R. 1978. Thermodynamic properties of minerals and related substances at 298.15K and 1 bar (10^5 pascals) pressure and higher temperaratures. *Bulletin of the United States Geological Survey*. 1259.

Ruellan A. 1971. Les Sols a Profil Calcaire Differencie Des Plaines de la Basse Moulouya (Maroc Oriental). *Memoire ORSTOM*, **54**.

Schwarcz H.P. and Latham A.G. 1989. Dirty calcites 1. Uranium-series dating of contaminated calcite using leachates alone. *Chemical Geology*. **80**, 35-43.

Sehgal J.L. and Stoops G. 1972. Pedogenic calcite accumulations in arid and semi-arid regions of the Indo-Gangetic alluvial plain of Erstwhile Punjab (India). *Geoderma*, **8**, 59-72.

Semeniuk V. and Meagher T.D. 1981. Calcrete in Quaternary coastal dunes in south western Australia: a capillary-rise phenomenon associated with plants. *Journal of Sedimentary Petrology*, **51**, 47-68.

Siesser W. G. 1973. Diagenetically formed ooids and intraclasts in South African calcretes. *Sedimentology*, **20**, 539-551.

Sharp W.D., Ludwig K.R., Chadwick O.A., Amendson R. and Glaser L.L. 2003. Dating fluvial terraces by ^{230}Th/U on pedogenic carbonate, Wind River Basin, Wyoming. *Quaternary Research*, **59**, 139-150.

Singhvi A.K., Banerjee D., Ramesh R., Rajaguru S.N. and Gogte V. 1996. A luminescence method for dating 'dirty' pedogenic carbonates for paleoenvironmental reconstruction. *Earth and Planetary Science Letters*. **139**, 321-332.

Solomon S.T. and Walkden G.M. 1985. The application of cathodoluminescence to interpreting the diagenesis of an ancient calcrete profile. *Sedimentology*, **32**, 877-896.

Tandon S.K. and Friend P.F. 1989. Near-surface shrinkage and carbonate replacement processes, Arran Cornstone Formation, Scotland. *Sedimentology*, **36**, 1113-1126.

Tandon S.K. and Narayan D. 1981. Calcrete conglomerate, a case-hardened conglomerate and cornstone-a comparative account of pedogenic and non-pedogenic carbonates from the continental Siwalik Group, Punjab, India. *Sedimentology*, **28**, 353-367.

Thompson W.W. 1975. The structure and function of salt glands. In: Poljakoff A. and Gale J. (eds). *Plants in saline environments*. Springer-Verlag New York. pp 119-146.

Tribble J. S., Arvidson R. S.,Lane M. and Mackenzie F. T. 1995. Crystal chemistry, and thermodynamic and kinetic properties of calcite, dolomite, apatite, and biogenic silica; applications to petrologic problems. *Sedimentary Geology*. **95**, 11-37.

van de Graaf W.J.E., Crowe R.W.A., Bunting J.A. and Jackson M.J. 1977. Relict Early Cainozoic drainages in arid Western Australia. *Zeitschrift fur Geomorphologie*, **21**, 379-400.

Verrecchia E.P. and Verrecchia K.E. 1994. Needle-fibre calcite: a critical review and a proposed classification. *Journal of Sedimentary Research A*. **64**, 650-664.

Warren J. 2000. Dolomite: occurrence, evolution and economically important associations. *Earth-Science Reviews*, **52**, 1-81.

Watts N.L. 1978. Displacive calcite: evidence from recent and ancient calcretes. *Geology*, **6**, 699-703.

Watts N.L. 1980. Quaternary pedogenic calcretes from the Kalahari (southern Africa): mineralogy, genesis and diagenesis. *Sedimentology*, **27**, 661-686.

Wieder M. and Yaalon D.H. 1974. Effect of matrix composition on carbonate nodule crystallization. *Geoderma*, **11**, 95-121.

Wieder M. and Yaalon D.H. 1982. Micromorphological fabrics and developemental stages of carbonate nodular forms related to soil characteristics. *Geoderma*, **28**, 203-220.

Williams G.E. 1973. Late Quaternary Piedmont sedimentation, soil formation and palaeo-climates in arid South Australia. *Zeitschrift Fur Geomorphologie*, **17**, 102-125.

Williams G.E and Polach H.A. 1971. Radiocarbon dating of arid zone calcareous palaeosols. *Bulletin of the Geological Society of America*, **82**, 3069-3086.

Williams M.A.J., Dunkerley D., De Decker P., Kershaw P. and Chappel J. 1998. *Quaternary Environments*, Arnold Publishers, London New York Sydney Auckland.

Wright V.P. 1986. The role of fungal biomineralisation in the formation of Early Carboniferous soil fabrics. *Sedimentology*, **33**, 831-838.

Wright V.P. 1989. Terrestrial stromatalites and laminar calcretes: a review. *Sedimentary Geology*, **65**, 1-13.

Wright V.P. 1990. Estimating rates of calcrete formation and sediment accretion in ancient alluvial deposits. *Geological Magazine*, **127**, 273-276.

Wright V.P. and Tucker M.E. 1991. *Calcretes: An introduction*. pp 1-22. Blackwell, Boston, Massachussetts,.

Wright V.P., Platt N.H. and Wimbledon W.A. 1988. Biogenic laminar calcretes: evidence of calcified root-mat horizons in palaeosols. *Sedimentology*, **35**, 603-620.

Yaalon D.H. 1988. Calcic horizon and calcrete in aridic soils and palaeosols: progress in the last twenty-two years. *Soil Science Society of America Agronomy Abstract*.

Appendix I: Pedogenic Calcrete Logs

This section illustrates and describes the pedogenic calcrete sites examined in the thesis. Sites with good exposure were logged and photographed before sampling. Most of the detailed petrographic and geochemical analysis was carried out on these samples and detailed logs are given on the following pages. At sites where pedogenic calcrete outcrop was restricted, either as surface exposure of the highly indurated hardpan layer or as profiles with shallow depth, grab samples were collected. Description of these is given in the section succeeding the logs.

The text box on the right of the page gives information on the location, flora and host material as well as a description of the micro-morphology of the sampled pedogenic calcrete. On the left a diagrammatic log shows the morphology of the collected samples and a graph shows carbonate content as determined gravimetrically as total carbonate remaining after acetic acid digestion, and by whole-rock instrumental neutron activation analysis (INAA) for calcium. Ca concentration is normalised to the molecular weight of calcium carbonate to represent the relative amount of calcite in the sample. The difference in the gravimetric and INAA $CaCO_3$ % is therefore indicative of the amount of magnesium and iron in the carbonate fraction.

Stable carbon and oxygen isotopic composition and carbonate mineralogy in corresponding samples are plotted against depth below the log and description in order to show down-profile trends. The residual minerals as determined by whole-rock XRD are listed at the base of the page.

Key to logs:

 Nodular calcrete

 Pisoliths

 Hardpan calcrete

 Laminar or platy calcrete

 Calcified soil calcrete and powder calcrete

 Rhizoliths

 Mottled calcrete

 Unconsolidated sand or wacke

 Limestone

 Claystone or siltstone

 Crystalline rocks

 Volcanic rocks

 Lithified sandstone

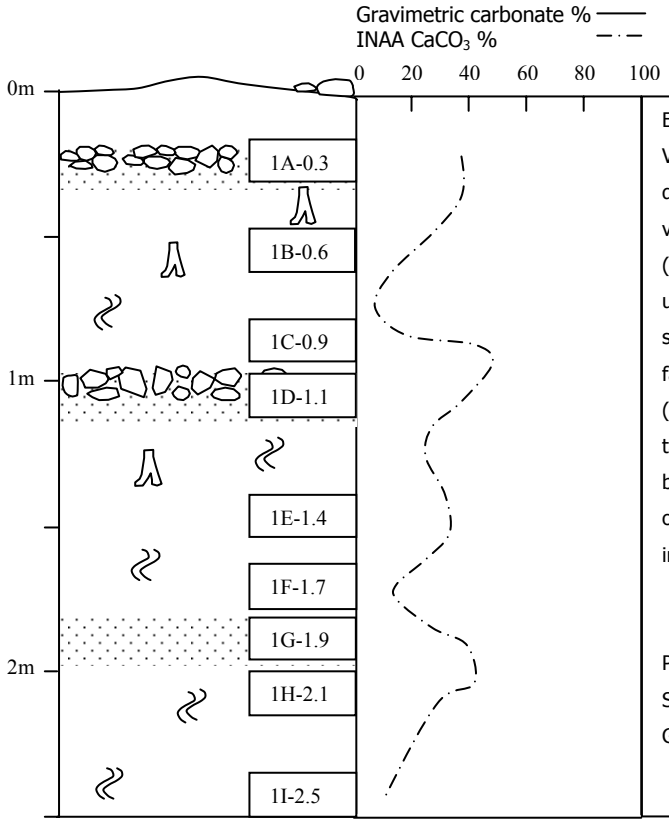

Nyah West Site 1

Exposed at the railway cutting at Nyah West, NW Victoria, are three calcareous soils (paleaosols) developed in red sands of dunefield. The vegetation, now cleared, consisted of Mallee (*Eucalypt sp.*) and spinifex (*Triodia sp.*) understorey. The calcrete samples are massive semi-indurated to friable with a grain-supported fabric composed of subangular to rounded quartz (< 0.7 mm) in a porous micritic matrix. Vertical taproot fragments and calcareous mottles occur between the layers of calcrete. Calcified filaments occur occasionally and no organic matter is visible in thin section.

Polished sections: 1A-0.3, 1B-0.6, 1D-1.1

SEM: PG1D-1.1

Geographic co-ordinates: 35° 11' 22.77" S
143° 21' 01.36" E

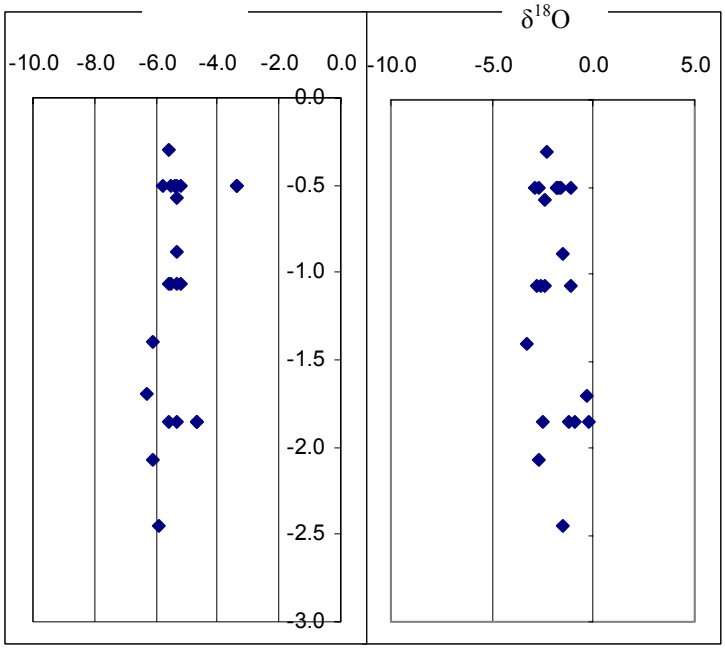

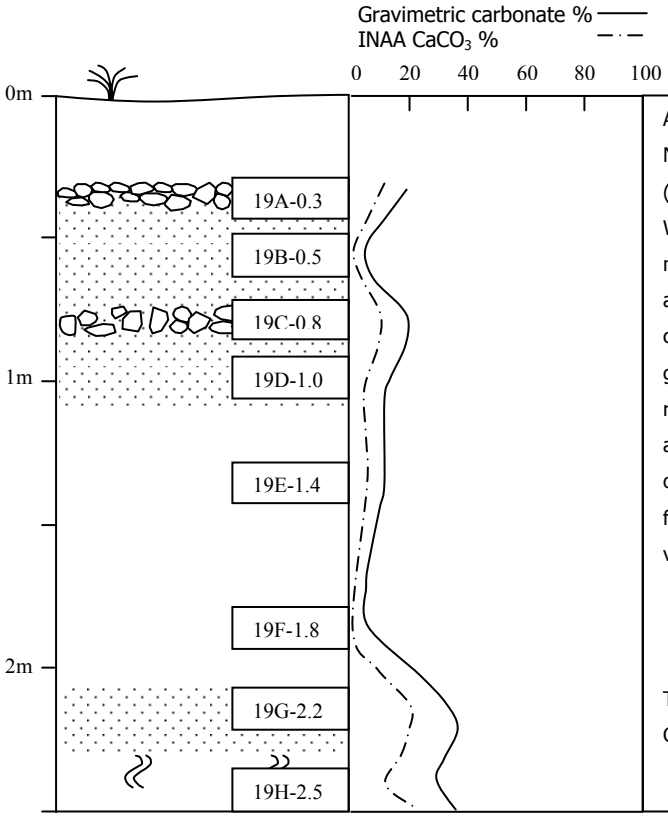

Carwarp Site 19

A road cutting on the east side of Calder Highway, NW Victoria, exposes three calcareous soils (paleaosols) developed in red sand of the aeolian Woorinen Formation. The dominant vegetation, now cleared, consisted of Mallee (*Eucalypt sp.*) and spinifex (*Triodia sp.*) understorey. The calcrete samples are massive and friable with a grain-supported fabric composed of subangular to rounded quartz (< 0.7 mm) in a porous micritic and clay matrix. Powdery calcareous mottles occur at the base of the section. Calcified filaments are sparse and no organic matter is visible in thin section.

Thin sections: 19C-0.8, 19D-1.0, 19E-1.4, 19H2.5
Geographic co-ordinates: 34° 24' 13.76" S
142° 11' 12.43" E

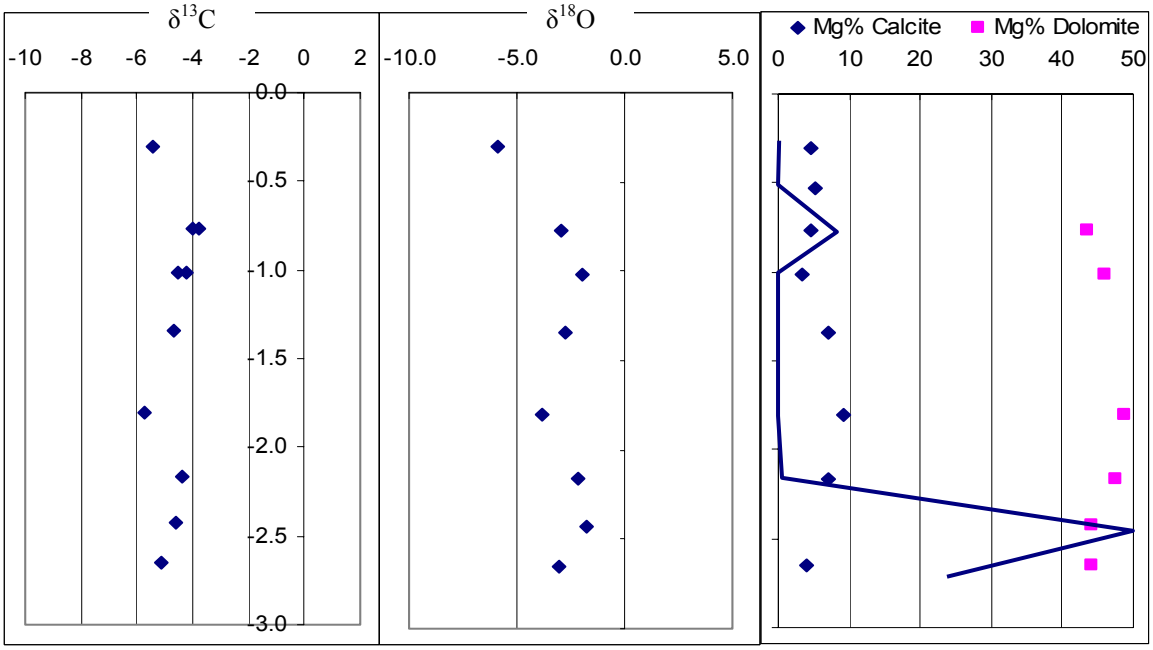

Residual minerals
Minor (<25%): quartz feldspar
Trace (<5%): illite geothite hematite

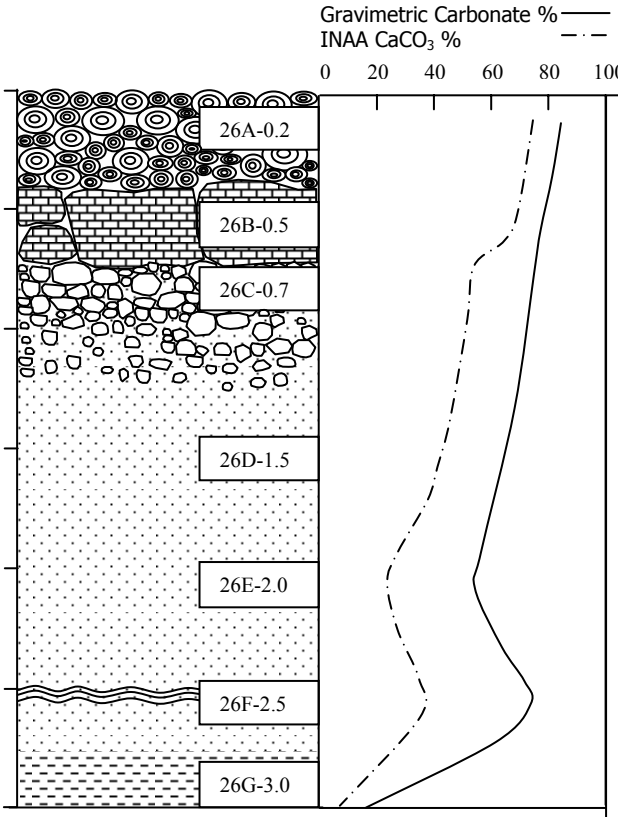

Renmark Site 26

Exposed on the cliffs of the Murray River 7 km east of Renmark, Murray Basin, S.A., is a reworked pisolitic/boulder/nodular calcrete developed on green dolomitic Blanchetown Clay. Pisoliths and nodules contain core of fragmented dolomitic mudstone with sparitic calcite penetrating in fractures and around round quartz grains (< 1 mm). Surrounding the core, thick (< 30 mm) concentric laminea are composed of calcified filaments and undulose layers of microspar displacing fine quartz (< 0.4 mm). Dissolution features occur crosscutting concentric laminea and contain pore-filling microspar with an undulose laminated micrite. Large boulders are composed of cemented pisoliths and clotted micrite as pisolith cores and interstitial cement. Organic matter is abundant. At 2.5 m a thin (< 60 mm) dolomitic laminar calcrete (lacustrine in origin) is composed of undulose and botryiodal laminations and ooids.
Thin sections: 26A-0.2, 26B-0.5, 26C-0.7, 26F-2.5
Geographic co-ordinates: 34° 17' 35.58" S
140° 51' 31.61" E

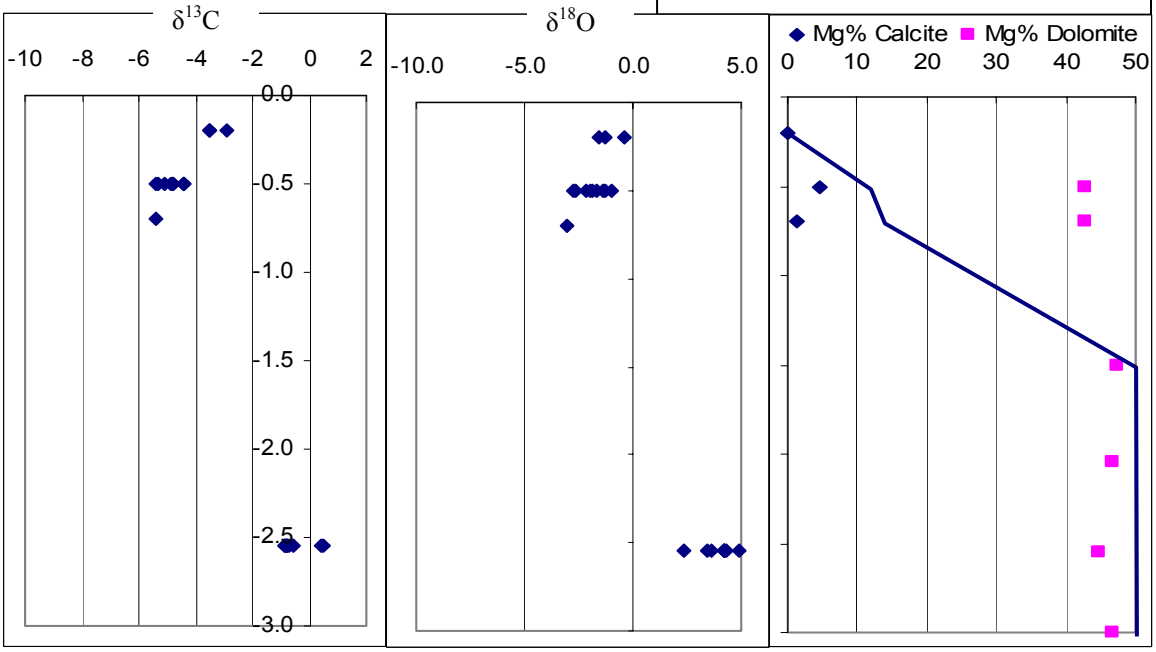

Residual Minerals
Minor (<25%): quartz illite
Trace (<5%): kaolinite palygorskite hematite

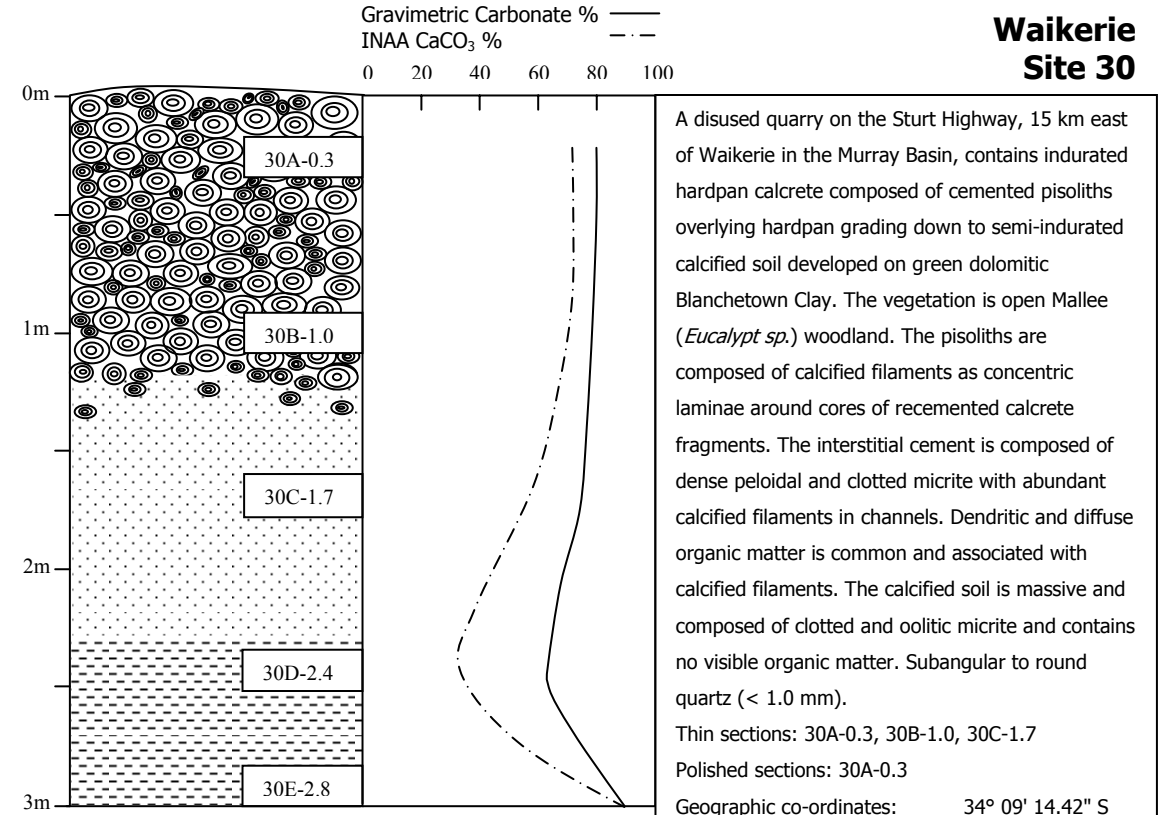

Waikerie Site 30

A disused quarry on the Sturt Highway, 15 km east of Waikerie in the Murray Basin, contains indurated hardpan calcrete composed of cemented pisoliths overlying hardpan grading down to semi-indurated calcified soil developed on green dolomitic Blanchetown Clay. The vegetation is open Mallee (*Eucalypt sp.*) woodland. The pisoliths are composed of calcified filaments as concentric laminae around cores of recemented calcrete fragments. The interstitial cement is composed of dense peloidal and clotted micrite with abundant calcified filaments in channels. Dendritic and diffuse organic matter is common and associated with calcified filaments. The calcified soil is massive and composed of clotted and oolitic micrite and contains no visible organic matter. Subangular to round quartz (< 1.0 mm).

Thin sections: 30A-0.3, 30B-1.0, 30C-1.7

Polished sections: 30A-0.3

Geographic co-ordinates: 34° 09' 14.42" S
140° 11' 20.87" E

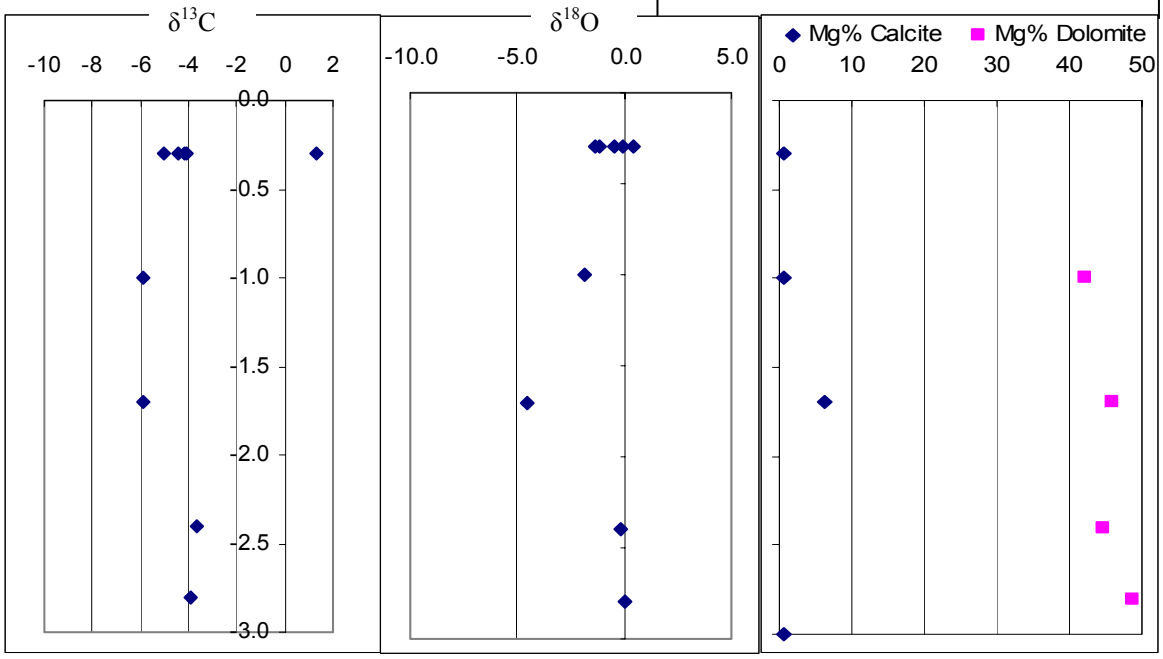

Residual Minerals
Minor (<25%): illite quartz
Trace (<5%): kaolinite palygorskite montmorillonite sepiolite hematite geothite

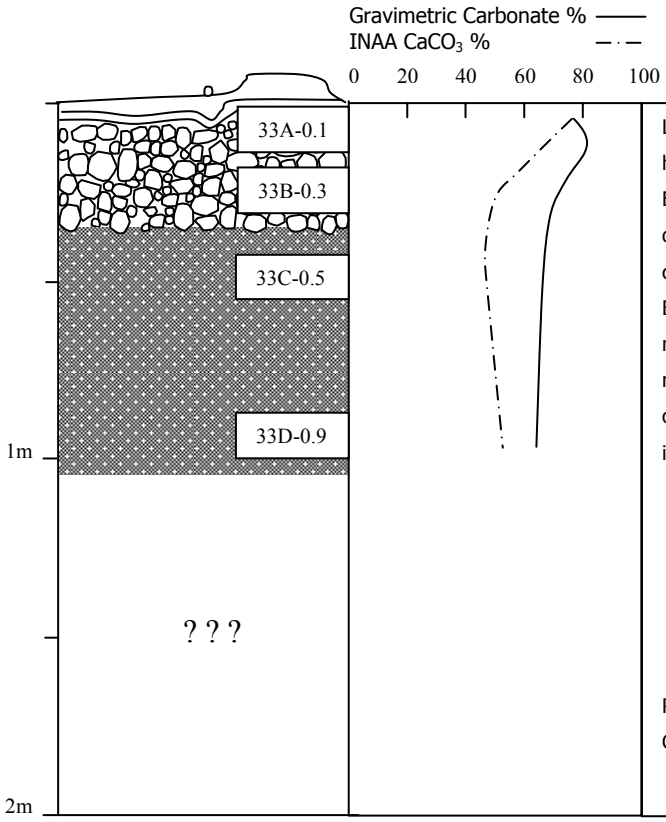

Gandy Range Homestead
Site 33

Located on a small mesa at 'Gandy Range' homestead 7 km north of the Sturt Highway on the Bungunnia Homestead Road is a profile containing dense micritic nodules with thick external laminar coatings. The host material is massive dolomitic Bungunnia Limestone. Channels containing organic matter and calcified roots penetrate the internal massive cement. Occasional fine quartz (<0.2mm) occurs in the dense micritic cement. The vegetation is chenopod shrub (*Atriplex sp.*).

Polished sections: 33A-0.1

Geographic co-ordinates: 33° 54' 50.11"
139° 44' 09.17"

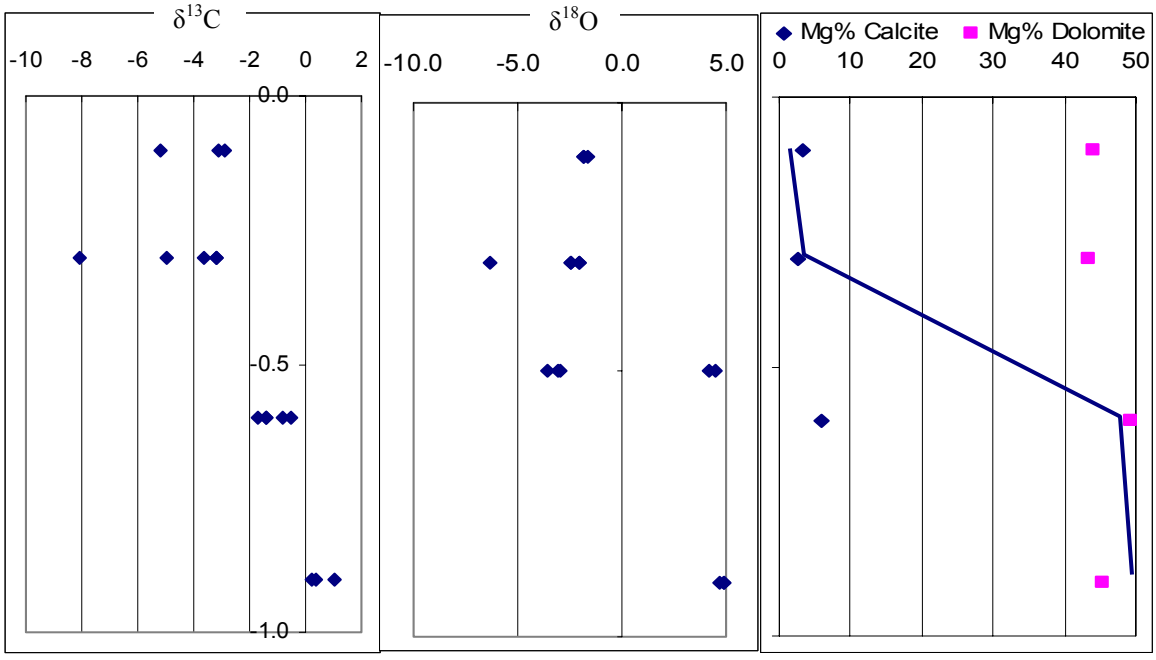

Residual Minerals
Minor (<25%): illite quartz
Trace (<5%): palygorskite montmorillonite feldspar sepiolite

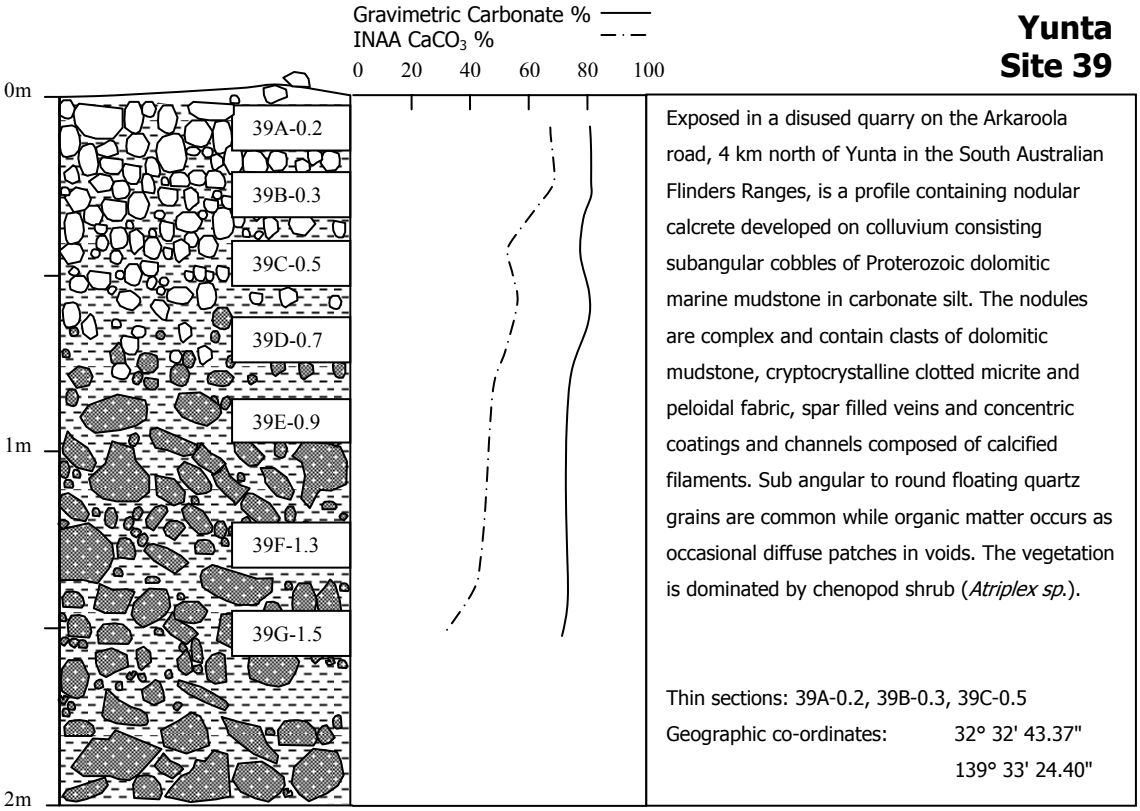

Yunta Site 39

Exposed in a disused quarry on the Arkaroola road, 4 km north of Yunta in the South Australian Flinders Ranges, is a profile containing nodular calcrete developed on colluvium consisting subangular cobbles of Proterozoic dolomitic marine mudstone in carbonate silt. The nodules are complex and contain clasts of dolomitic mudstone, cryptocrystalline clotted micrite and peloidal fabric, spar filled veins and concentric coatings and channels composed of calcified filaments. Sub angular to round floating quartz grains are common while organic matter occurs as occasional diffuse patches in voids. The vegetation is dominated by chenopod shrub (*Atriplex sp.*).

Thin sections: 39A-0.2, 39B-0.3, 39C-0.5

Geographic co-ordinates: 32° 32' 43.37"
139° 33' 24.40"

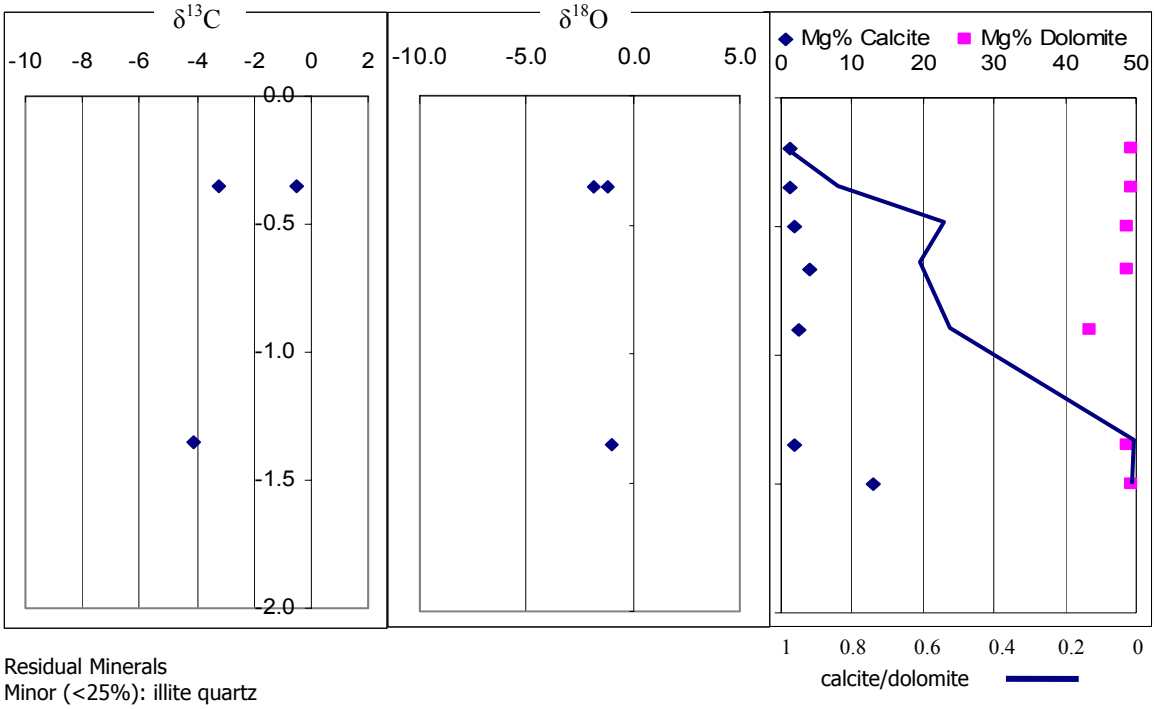

Residual Minerals
Minor (<25%): illite quartz
Trace (<5%): feldspar montmorillonite palygorskite sepiolite

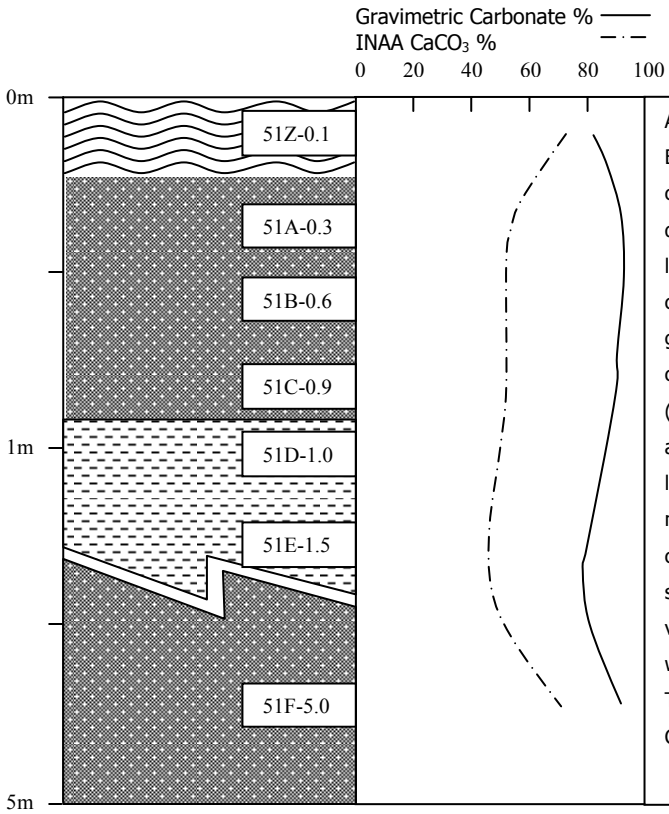

Blanchetown South Site 51

A small borrow pit located 5 km south of Blanchetown in the South Australian Murray Basin contains a thin (~ 0.2 m) laminar calcrete crust developed on weathered Eocene-Miocene marine limestone. The laminations are composed of calcified filaments displacing fine subround quartz grains (< 0.5 mm), and dense clotted micrite containing (relatively) densely packed quartz grains (<1.0 mm). Filamentous organic matter is common and associated with calcified filaments. The limestone immediately below the calcrete horizon is massive, grey and dolomitic with channels containing diffuse organic matter. Vegetation is sparse and heavily grazed. Pre-settlement vegetation probably open Mallee (*Eucalypt* sp.) woodland.

Thin sections: 51Z-0.1, 51A-0.3

Geographic co-ordinates: 34° 23' 53.35" S
139° 36' 15.09" E

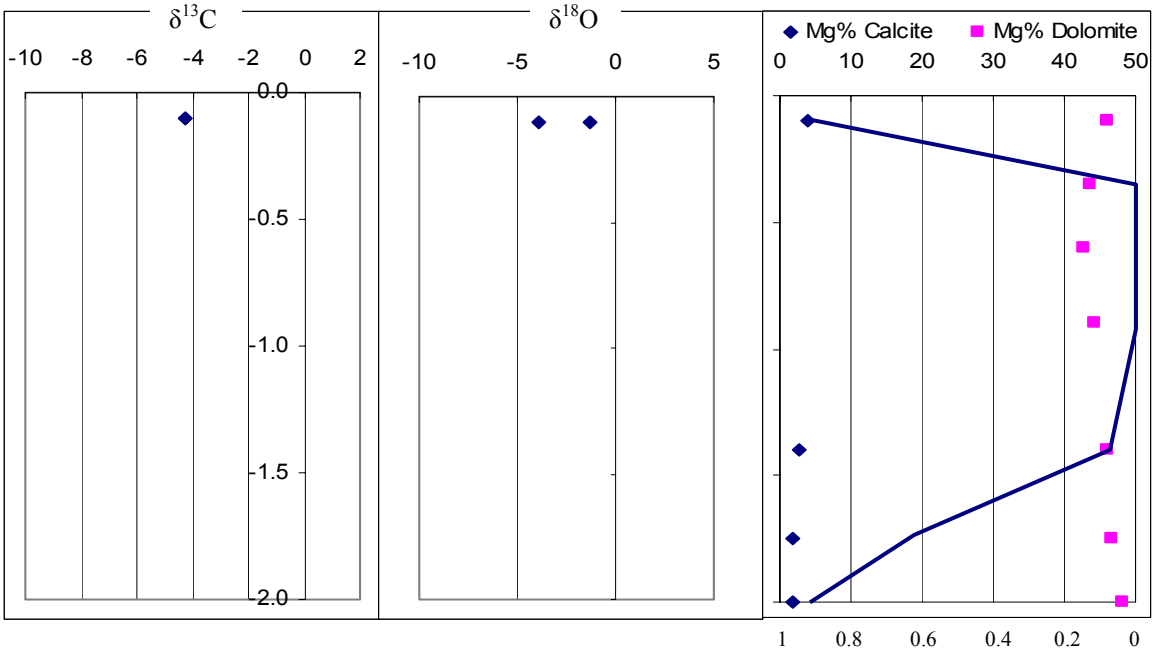

Residual Minerals
Minor (<25%): illite quartz
Trace (<5%): palygorskite montmorillonite feldspar sepiolite goethite hematite

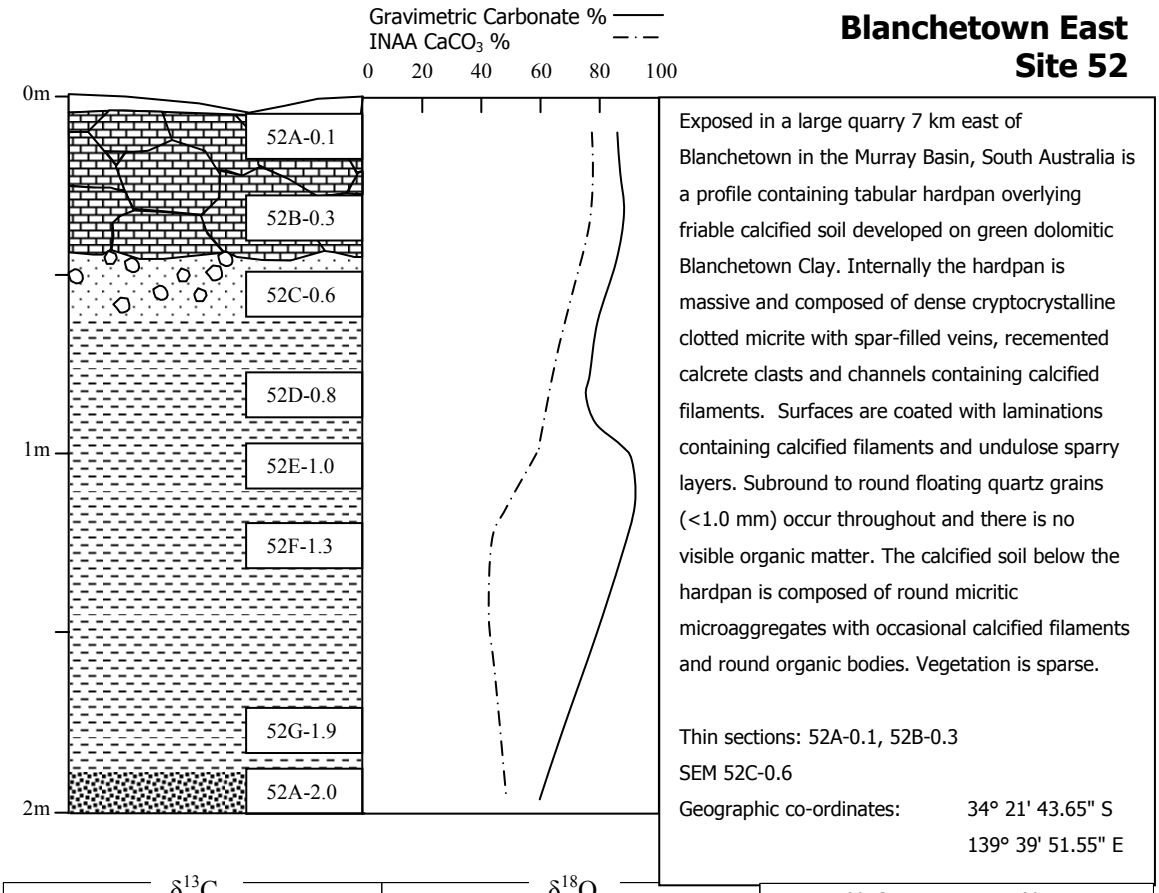

Blanchetown East
Site 52

Exposed in a large quarry 7 km east of Blanchetown in the Murray Basin, South Australia is a profile containing tabular hardpan overlying friable calcified soil developed on green dolomitic Blanchetown Clay. Internally the hardpan is massive and composed of dense cryptocrystalline clotted micrite with spar-filled veins, recemented calcrete clasts and channels containing calcified filaments. Surfaces are coated with laminations containing calcified filaments and undulose sparry layers. Subround to round floating quartz grains (<1.0 mm) occur throughout and there is no visible organic matter. The calcified soil below the hardpan is composed of round micritic microaggregates with occasional calcified filaments and round organic bodies. Vegetation is sparse.

Thin sections: 52A-0.1, 52B-0.3
SEM 52C-0.6
Geographic co-ordinates: 34° 21' 43.65" S
139° 39' 51.55" E

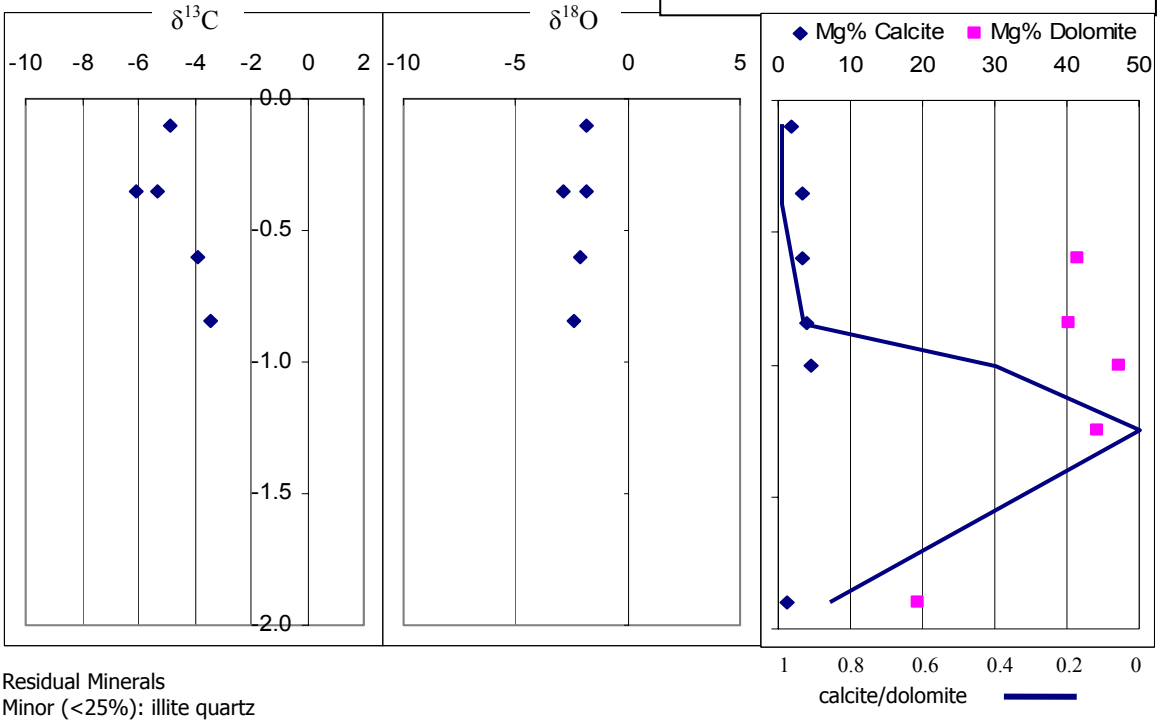

Residual Minerals
Minor (<25%): illite quartz
Trace (<5%): feldspar palygorskite montmorillonite kaolinite sepiolite hematite

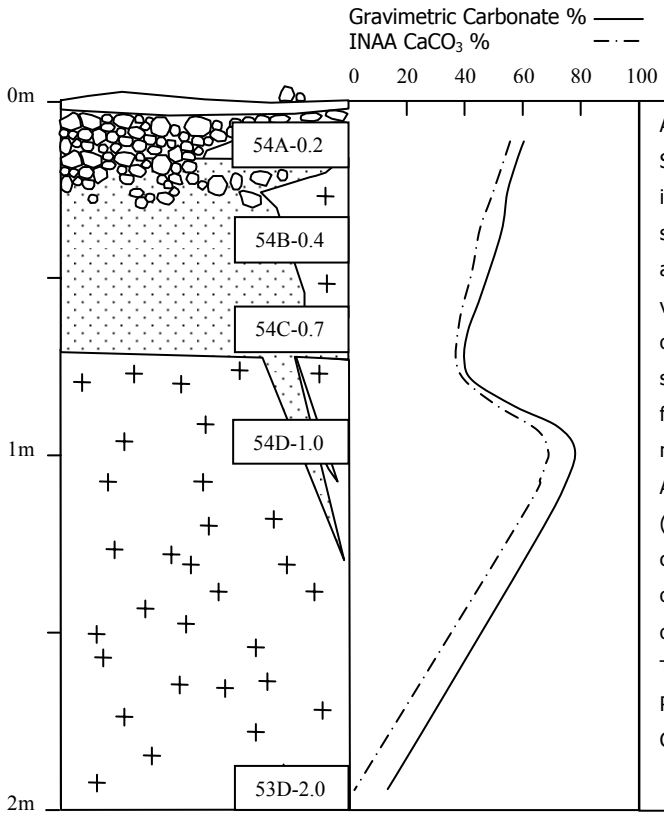

Long Ridge Site 54

A large granite quarry 13km NE of Sedan in SE South Australia exposes a profile containing semi-indurated calcrete nodules developed in calcareous soil. The nodules are intensely veined or channeled and contain fragmented massive micritic fabric and veins/channels composed of calcified filaments and occasional alveolar septal structure and calcified spheres. Angular to subround quartz and minor feldspar and muscovite occur as floating grains (< 2 mm). Organic matter is not visible in thin section. Approximately 200 m downslope from the quarry (site 53) is a recemented boulder calcrete containing clasts of varying sizes composed variably of clotted micrite and laminated coatings composed of calcified filaments.

Thin Sections: 54A-0.2, 53B-0.5, 53C-0.9

Polished sections: 53C-0.9

Geographic co-ordinates: 34° 29' 07.96" S
139° 21' 36.62" E

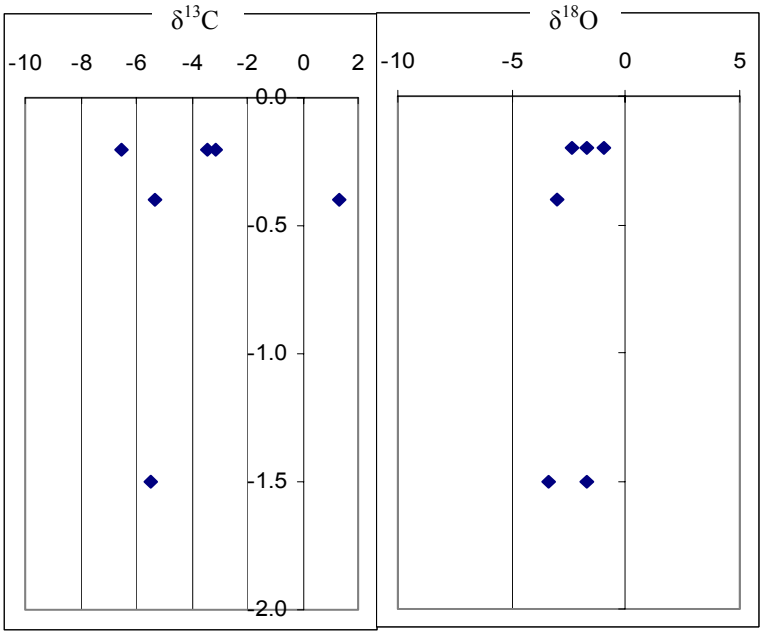

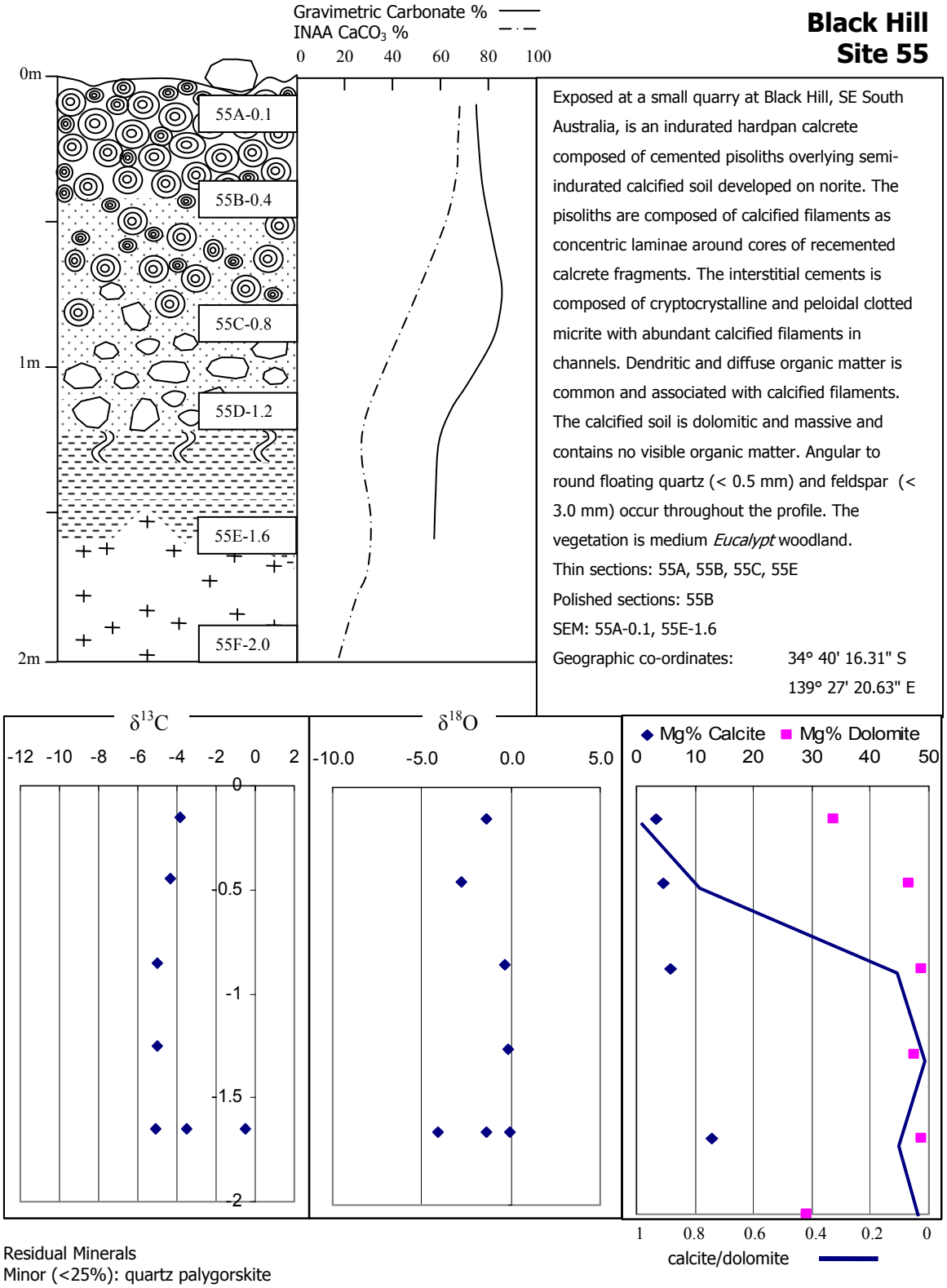

Black Hill
Site 55

Exposed at a small quarry at Black Hill, SE South Australia, is an indurated hardpan calcrete composed of cemented pisoliths overlying semi-indurated calcified soil developed on norite. The pisoliths are composed of calcified filaments as concentric laminae around cores of recemented calcrete fragments. The interstitial cements is composed of cryptocrystalline and peloidal clotted micrite with abundant calcified filaments in channels. Dendritic and diffuse organic matter is common and associated with calcified filaments. The calcified soil is dolomitic and massive and contains no visible organic matter. Angular to round floating quartz (< 0.5 mm) and feldspar (< 3.0 mm) occur throughout the profile. The vegetation is medium *Eucalypt* woodland.

Thin sections: 55A, 55B, 55C, 55E

Polished sections: 55B

SEM: 55A-0.1, 55E-1.6

Geographic co-ordinates: 34° 40' 16.31" S
139° 27' 20.63" E

Residual Minerals
Minor (<25%): quartz palygorskite
Trace (<5%): feldspar hypersthene enstatite grunerite

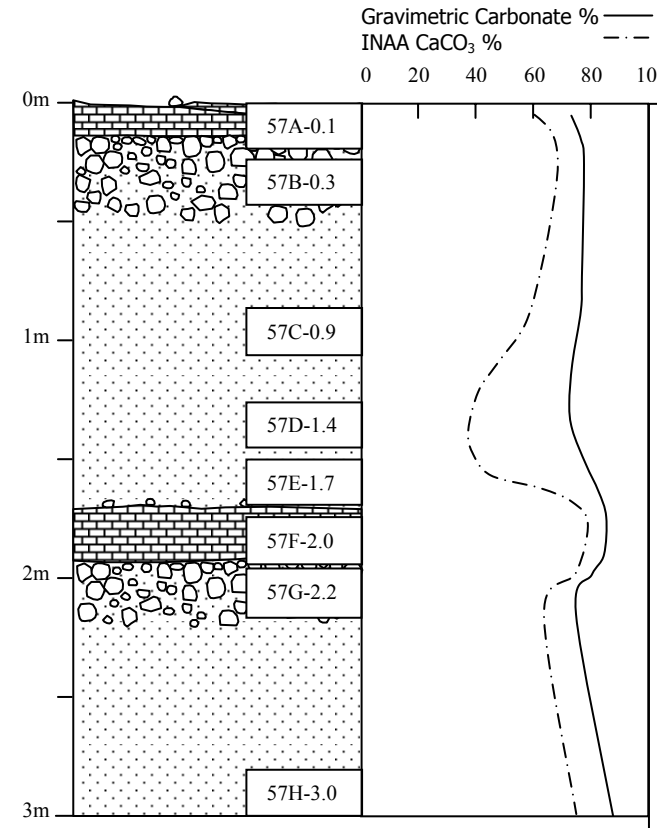

Tailem Bend
Site 57

Exposed on the bank of the Murray River, 3 km south of Tailem Bend SE South Australia is a profile containing two indurated tabular hardpan calcretes overlying nodules and friable yellow calcified soil (or carbonate silt). The upper hardpan and nodules are dark brown in colour, massive and composed of cryptocrystalline clotted micrite, recemented clasts and black pebbles and a thin (< 10 mm) cream coloured micritic coating. The calcified soil is composed of massive microcrystalline dolomite. The lower hardpan is brecciated and composed of fragmented microcrystalline dolomite clasts up to 30 mm with coatings and veins composed of calcified filaments. Floating subround quartz (< 0.5 mm) throughout and filamentous organic matter associated with calcified filaments occurs occasionally in hardpans.

Thin sections: 57A-0.1, 57C-0.9, 57F-2.0

SEM: 57A-0.1, 57C-0.9, 57D-1.4

Geographic co-ordinates: 35° 16' 07.30" S
139° 27' 29.77" E

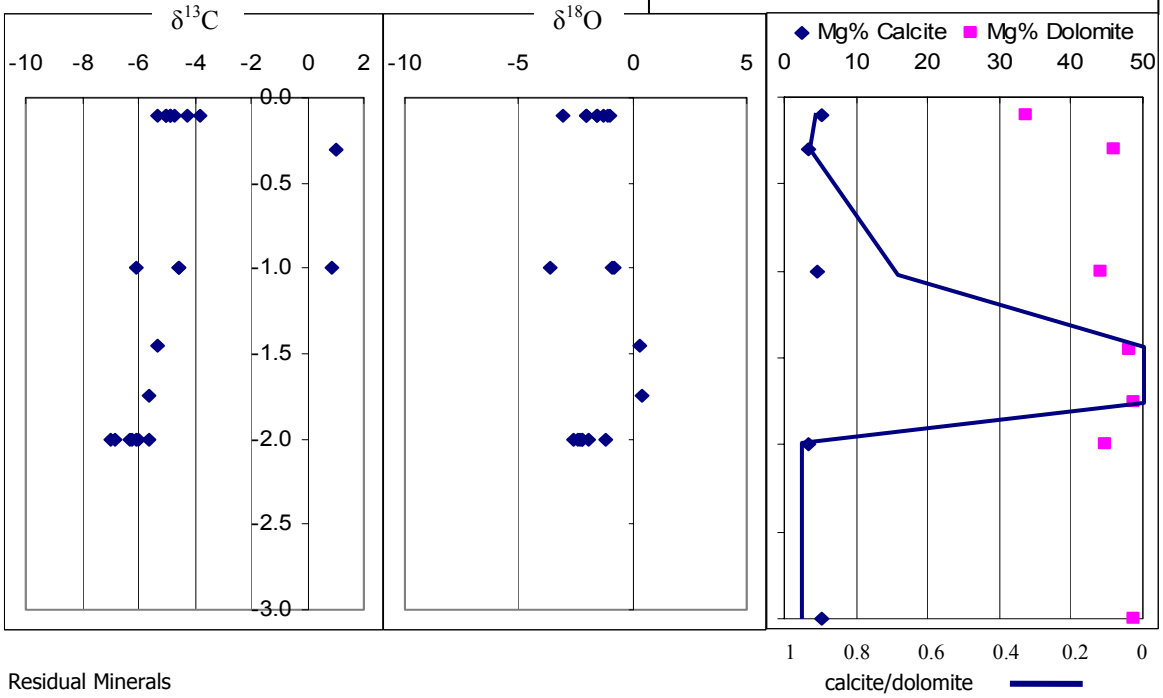

Residual Minerals
Minor (<25%): illite quartz palygorskite montmorillonite
Trace (<5%): feldspar sepiolite goethite

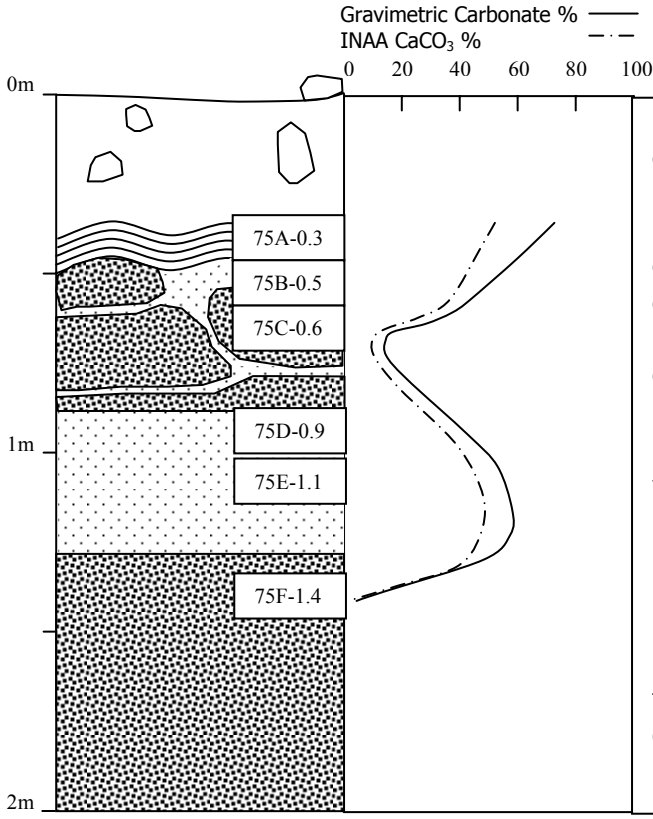

Wirramana Site 75

Exposed in a borrow pit 69 km NW of Pimba, central South Australia, is a semi-indurated platy hardpan calcrete with veins penetrating Mesozoic lithified red-brown sandstone. The calcrete is composed of horizontal and subhorizontal veins composed of peloidal and cryptocrystalline clotted micrite often with fenestral fabric, needle-fibre calcite and alveolar-like textures. Massive organic matter colonies occur within voids. Residual minerals are absent in calcrete veins. The vegetation is mulga (*Acacia sp.*) woodland.

Thin sections: 75C-0.6, 75E-1.1

Geographic co-ordinates: 31° 10' 08.0" S
136° 07' 07.2" E

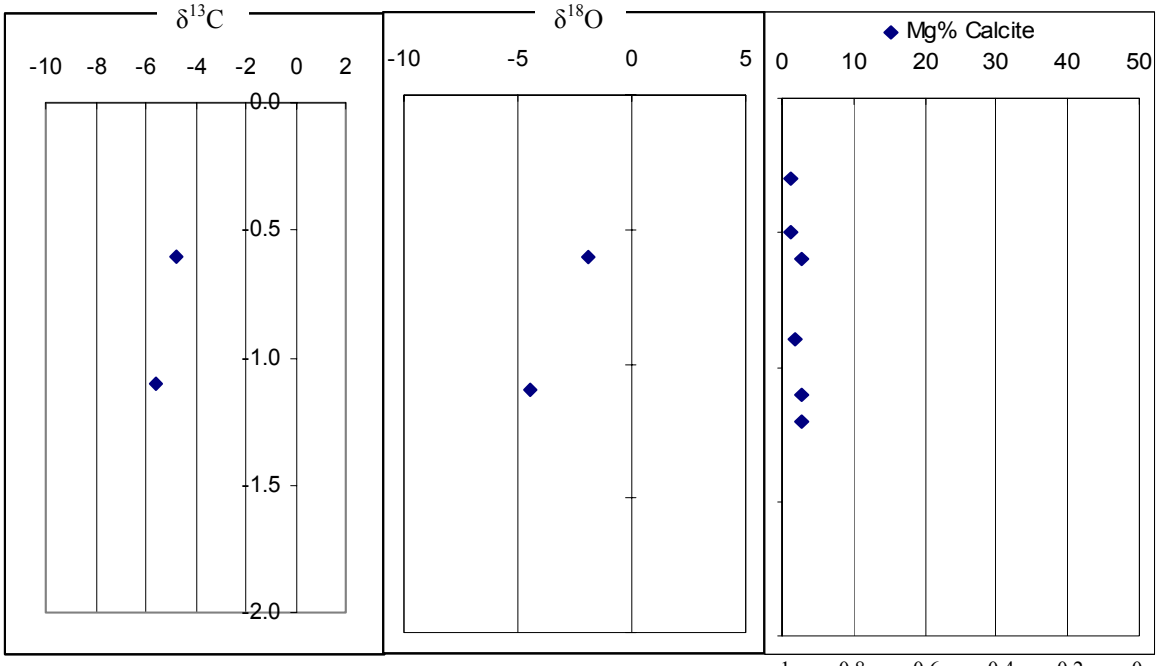

Residual Minerals
Minor (<25%): quartz illite montmorillonite
Trace (<5%): palygorskite kaolinite feldspar sepiolite hematite goethite

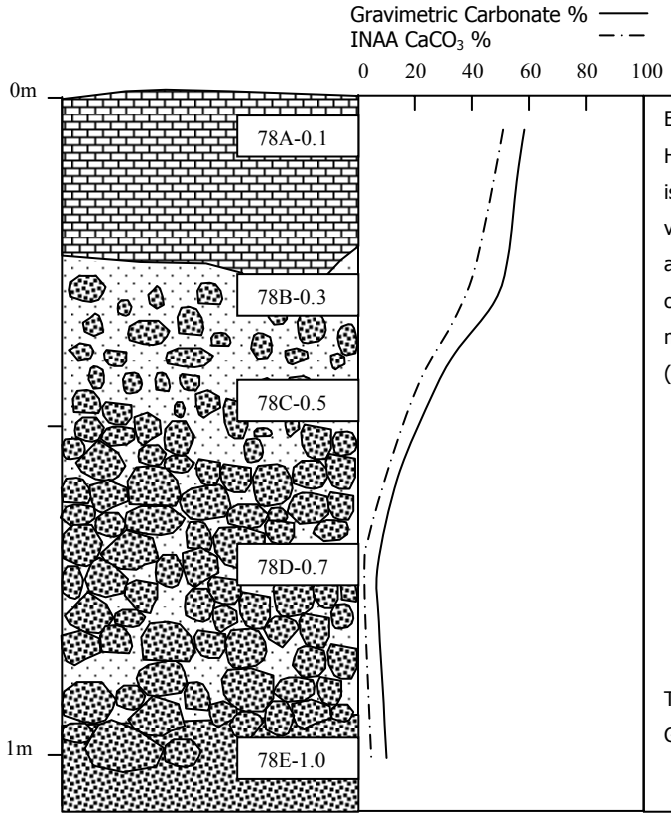

Glendambo North Site 78

Exposed in a borrow pit 5.3 km south of the Stuart Highway turnoff located 51 km north of Glendambo is a massive semi-indurated hardpan overlying veins displacing red-brown hardpan. The hardpan and veins are massive and composed of cryptocrystalline clotted micrite. The vegetation is mixed mulga (*Acacia sp.*) and chenopod shrub (*Atriplex sp.*).

Thin sections: 78A-0.1

Geographic co-ordinates: 30° 52' 40.4" S
135° 07' 23.8" E

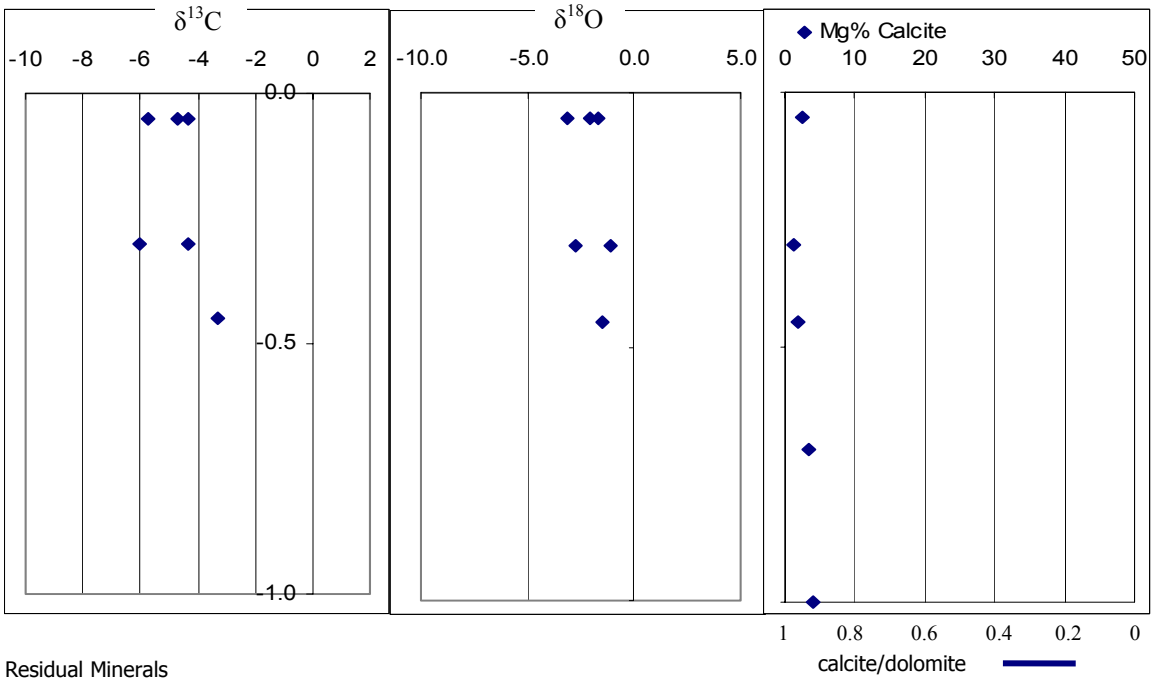

Residual Minerals
Minor (<25%): quartz illite montmorillonite
Trace (<5%): palygorskite kaolinite feldspar

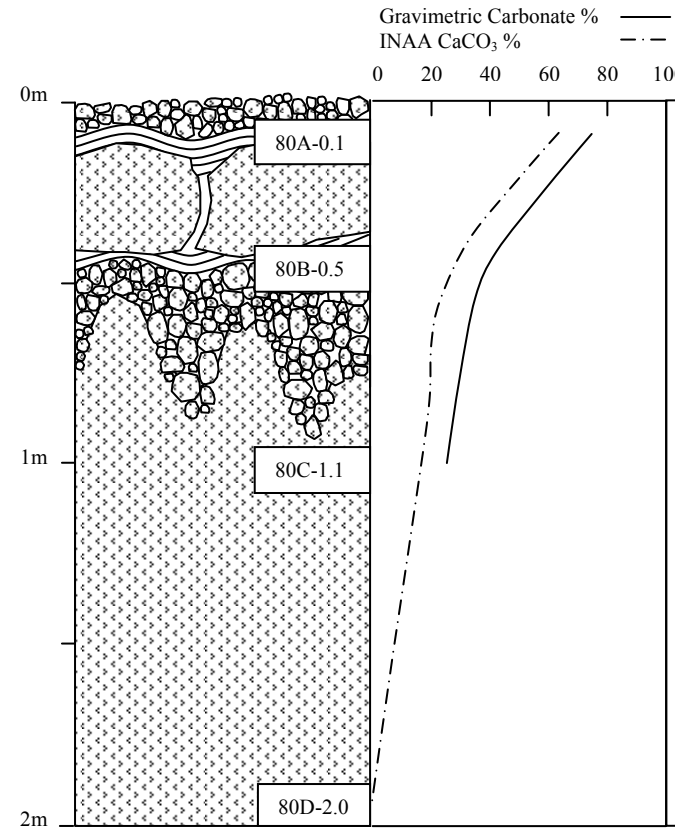

Kingoonya West Site 80

Exposed at a railway cutting through a bare low rise 42.1 km west of Kingoonya, central South Australia is a calcified soil developed in weathered volcanics of the Archaean Mulgathing Complex, Gawler Craton. Thin (~2 cm) laminar calcrete occurs at a bare surface and is composed of sub-millimetre layers of dense micrite and calcified filaments. Immediately below the laminations is porous fabric containing microrods. Semi-indurated and porous calcified soil occurs to 1.2 m depth below large boulders of weathered host material. Thin section examination shows it is composed of peloidal micrite aggregates with an open framework porosity and sub round clasts of host material and iron oxides with in-filled channels with a central pore or root mould and occasional needle fibre calcite.

Thin sections: 80A-0.1, 80B-0.5, 80C1.1, 80D-2.0
SEM: 80A-0.1
Geographic co-ordinates: 30° 50' 55.8" S
134° 54' 20.4" E

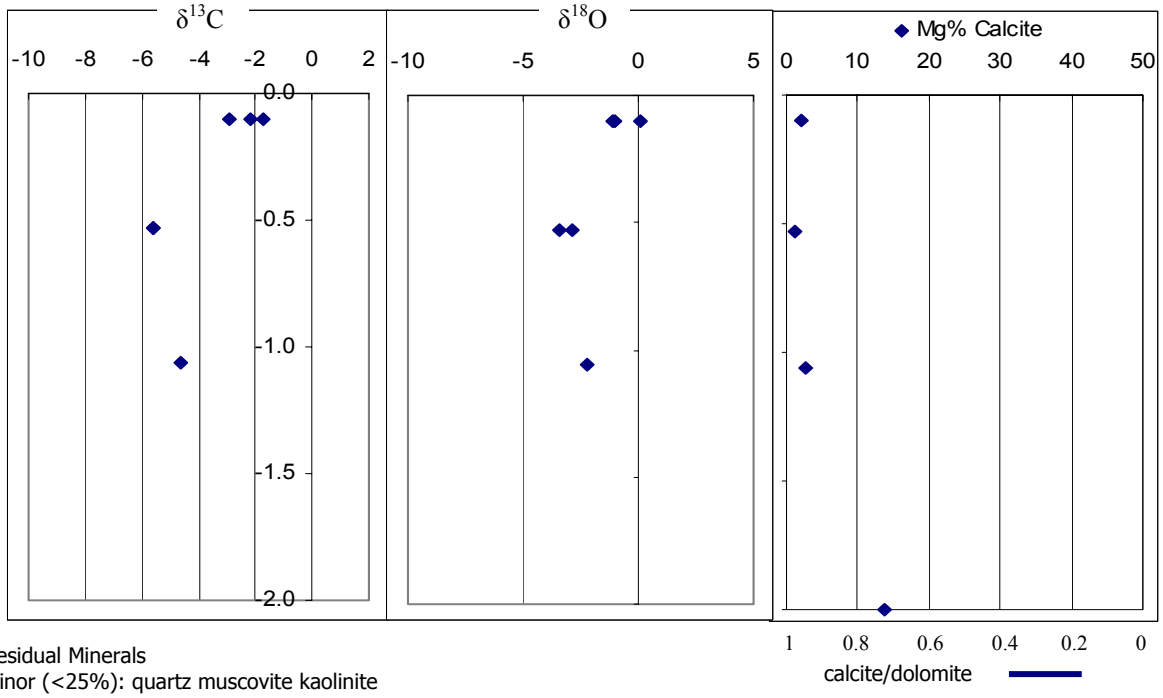

Residual Minerals
Minor (<25%): quartz muscovite kaolinite
Trace (<5%): feldspar

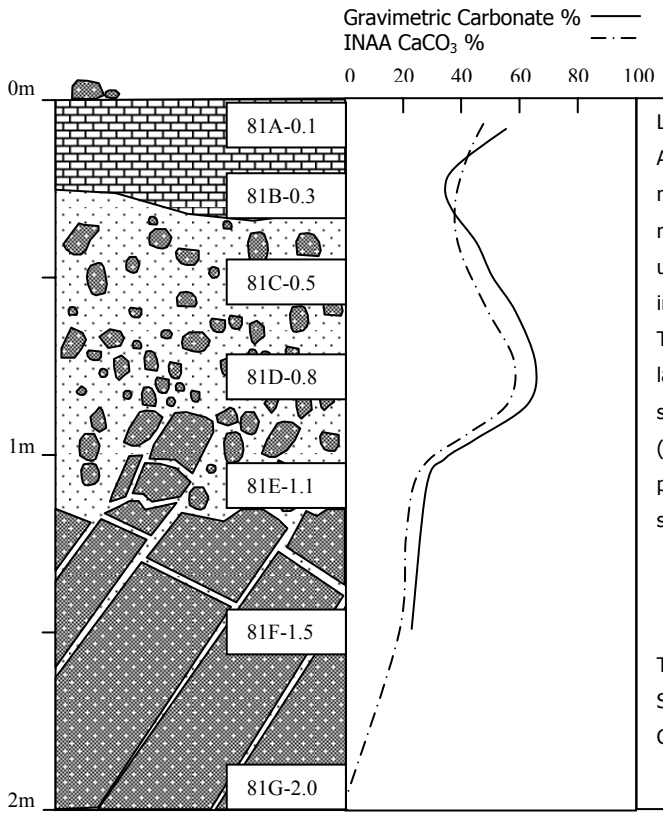

Tarcoola Railway Quarry Site 81

Located 7 km west of Tarcoola, central South Australia, in a railway quarry in siliceous metasediment. This calcrete profile has platy morphology at 0 to 0.5 m depth and a bare surface, underlain by brecciated bedrock clasts with semi-indurated calcrete solutional veins down to 1.5 m. The indurated platy hardpan samples are crudely laminated. Microscopically the veins and indurated samples are composed of round clasts of iron oxide (hematite) and host material in micritic matrix with porous micritic peloidal fabrics. Vegetation is sparse.

Thin sections: 81B-0.3, 81E-1.1

SEM: 81A-0.1, 81B-0.3, 81E1.1

Geographic co-ordinates: 30° 43' 08.6" S
134° 29' 54.7" E

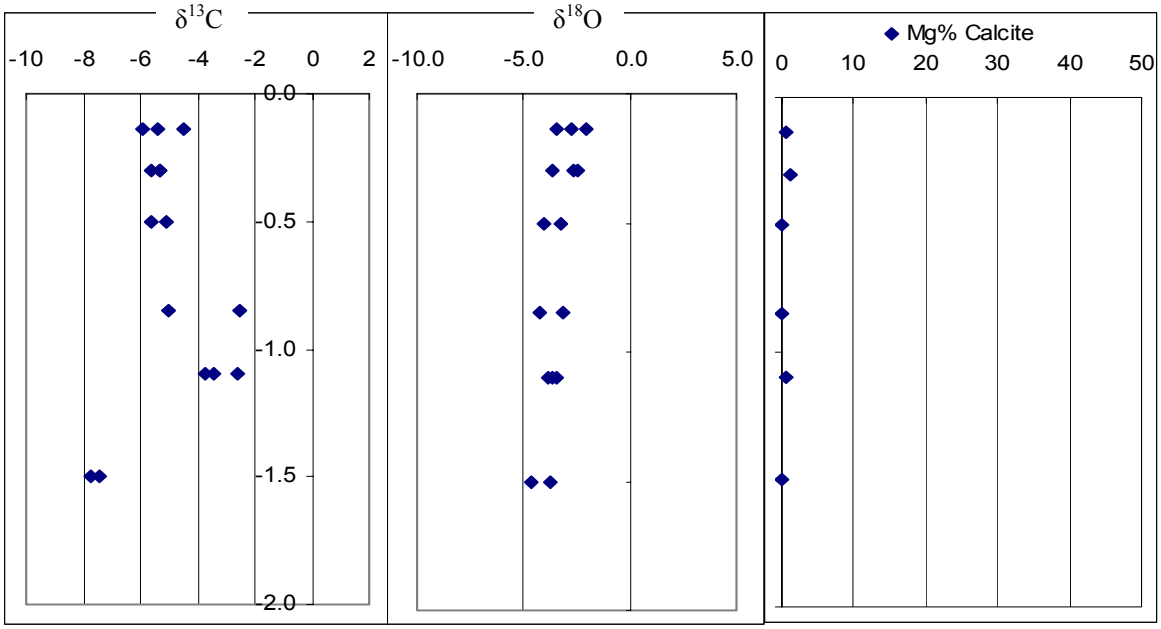

Residual Minerals
Minor (<25%): illite quartz montmorillonite kaolinite feldspar
Trace (<5%): palygorskite goethite hematite sepiolite

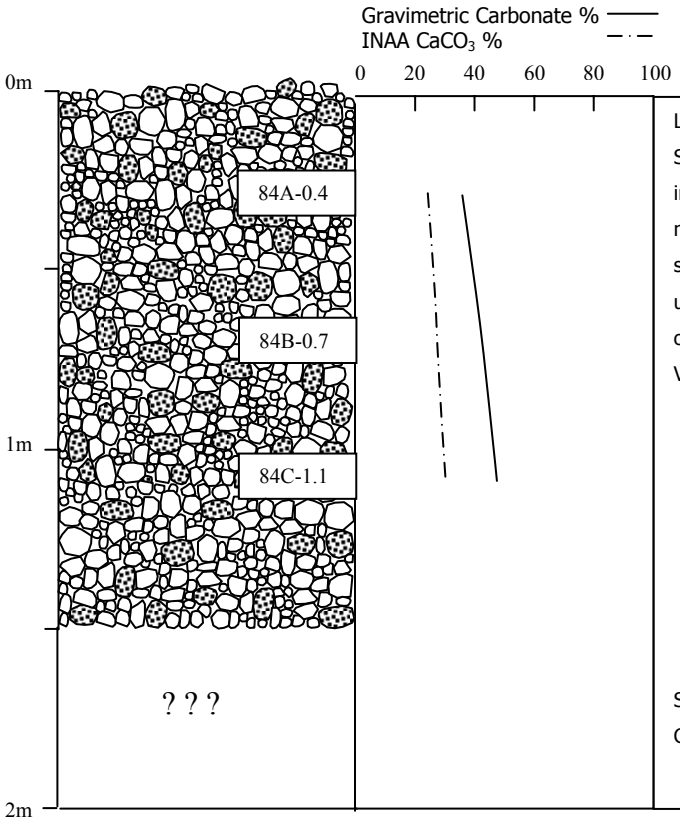

Kingoonya South Site 84

Located in a borrow pit 7km south of Kingoonya, South Australia, and 200m west of the road, is an indurated calcrete composed of massive micritic nodules mixed with clasts of lithified red-brown sandstone. Scanning electron microscopy shows unusually textured micrite, very fine needle-fibres of uncertain origin and gel-like substances. Vegetation is sparse.

SEM: 84A-0.4, 84C-1.1

Geographic co-ordinates: 30° 57' 42.5" S
135° 21' 17.0" E

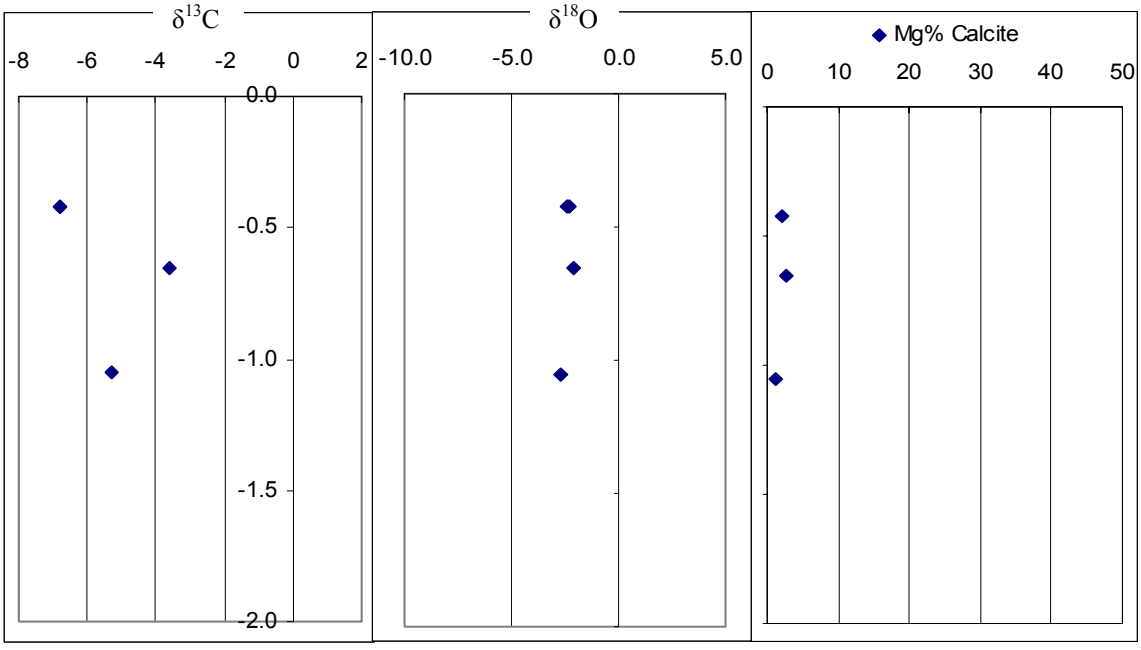

Residual minerals
Minor (<25%): illite quartz montmorillonite palygorskite
Trace (<5%): kaolinite feldspar goethite hematite

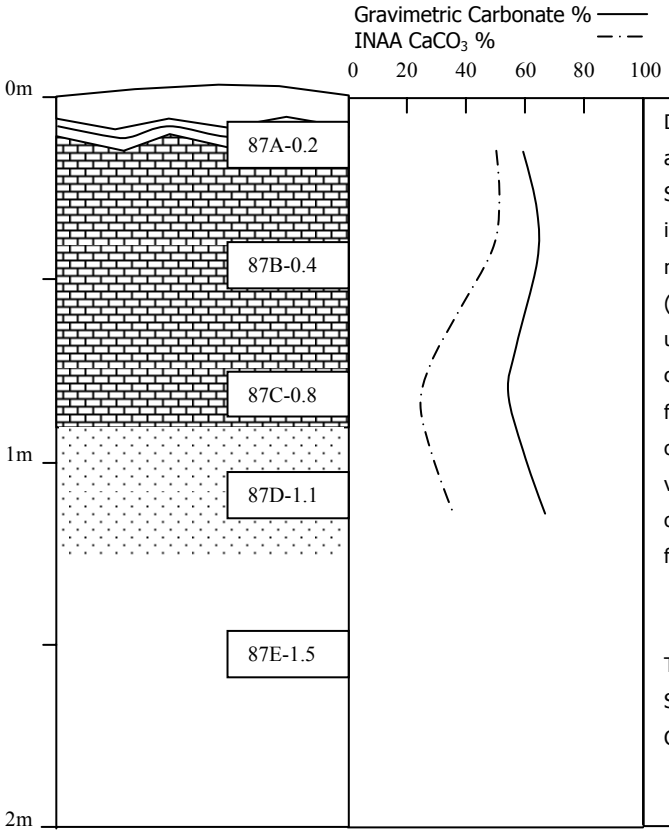

Kokatha Site 87

Developed in unconsolidated red sandy clay of an aeolian dune 74 km south of Kingoonya, central S.A., is a massive hardpan grading down to semi indurated calcified soil below 0.8 m. Vegetation is mixed open mulga (*Acacia sp.*) and Belah (*Casuarina sp.*) woodland with chenopod shrub under storey. Indurated calcrete composed of cryptocrystalline and peloidal clotted micrite with floating subround quartz (< 0.8 mm) and occasional calcified filaments and microsparitic veins and channels. Occasional filamentous organic matter is associated with calcified filaments.

Thin sections: 87A-0.2, 87B-0.4
SEM: 87A0.2, 87B-0.4
Geographic co-ordinates: 31° 27' 37.6" S
135° 22' 12.2" E

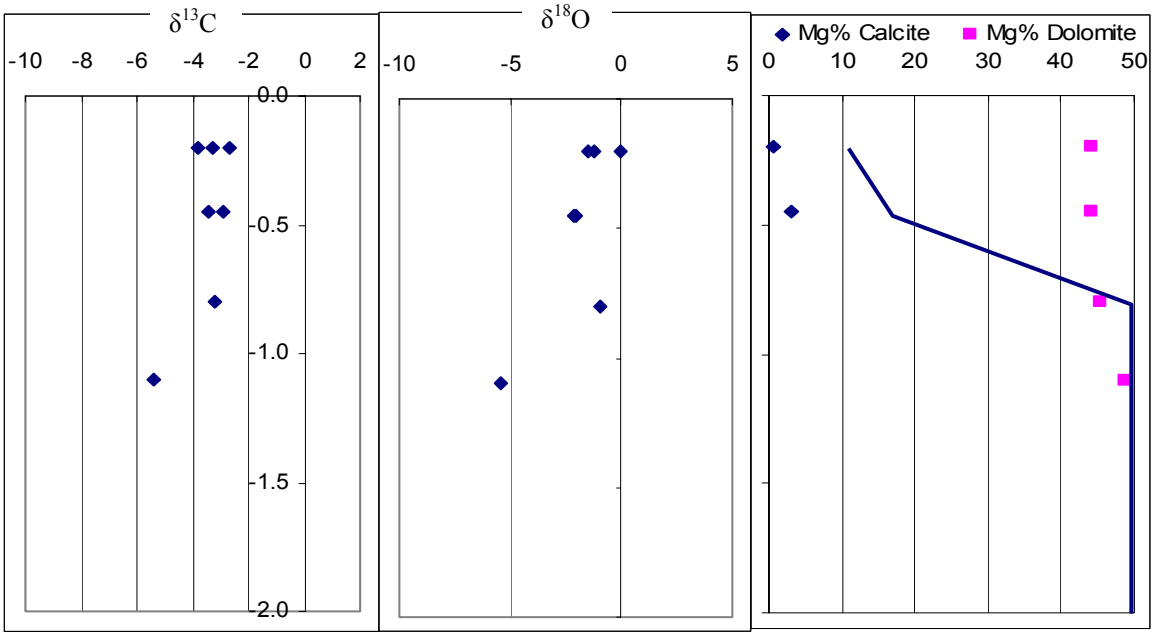

Residual Minerals
Minor (<25%): quartz illite palygorskite montmorillonite
Trace (<5%): feldspar sepiolite goethite

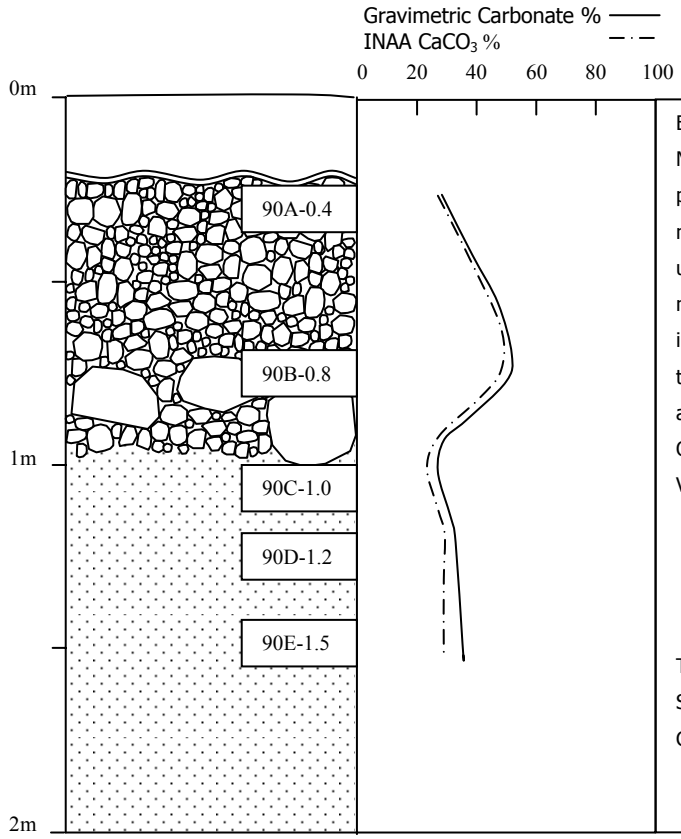

Lake Everard Site 90

Exposed in a creek bank 68 km south of Moonaree homestead, central South Australia, is a profile containing densely packed and cemented nodules overlying powdery calcrete developed in unconsolidated red clayey sand. Internally the nodules are massive with clotted fabric, intergranular sparitic veins and floating subround to round quartz (< 0.7 mm). The nodule coatings and cement are composed of calcified filaments. Organic matter was not visible in thin section. Vegetation is Mulga (*Acacia sp.*) woodland.

Thin section: 90B-0.8

SEM: 90B-0.8

Geographic co-ordinates: 32° 00' 02.0" S
135° 52' 13.7" E

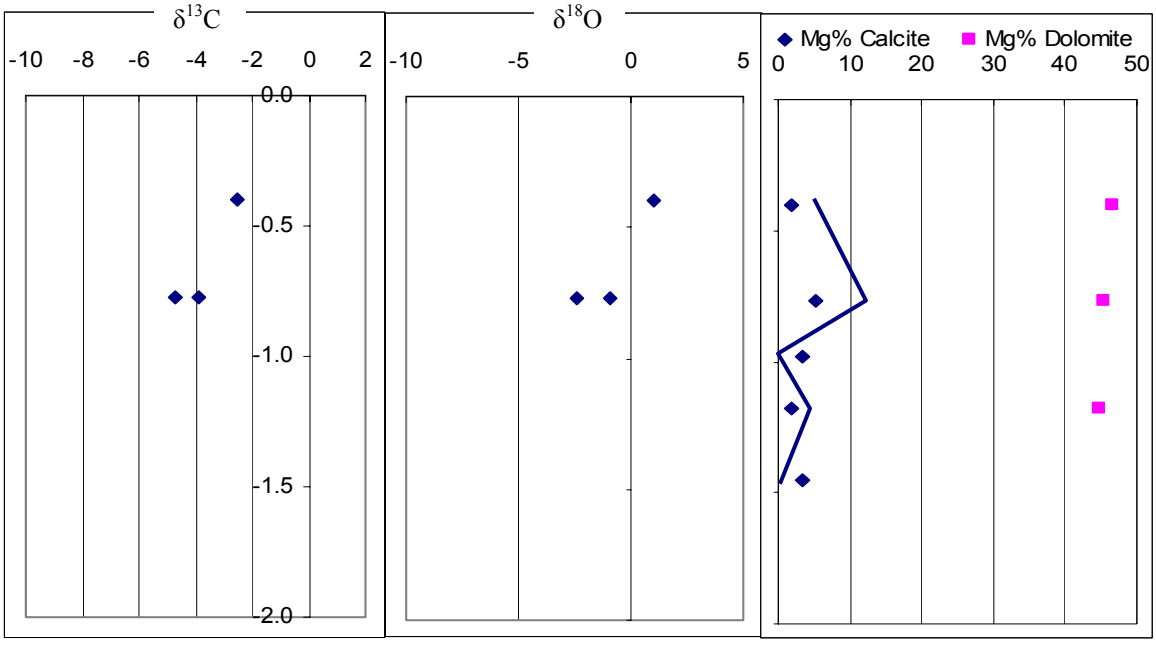

Residual Minerals
Minor (<25%): quartz illite feldspar
Trace (<5%): montmorillonite palygorskite kaolinite hematite

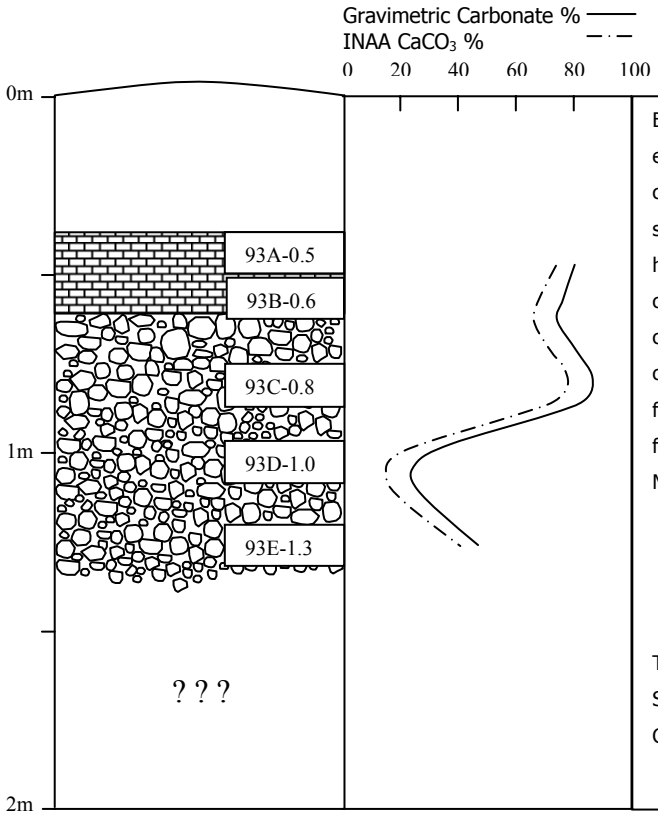

Kimba East
Site 93

Exposed in a cutting on the Eyre Highway 64 km east of Kimba, Eyre peninsula S.A. is an indurated calcrete developed in unconsolidated red clayey sand. The internal microstructure of the nodules and hardpan is massive and composed of cryptocrystalline clotted micrite and occasional calcified filaments as coatings on recemented calcrete clasts. The samples contain abundant floating quartz (< 0.8 mm) and occasional filamentous organic matter. Vegetation is open Mallee (*Eucalypt sp.*) woodland.

Thin sections: 93A-0.5, 93D-1.0

SEM: 93D-1.0

Geographic co-ordinates: 32° 52' 34.3" S
136° 59' 22.5"

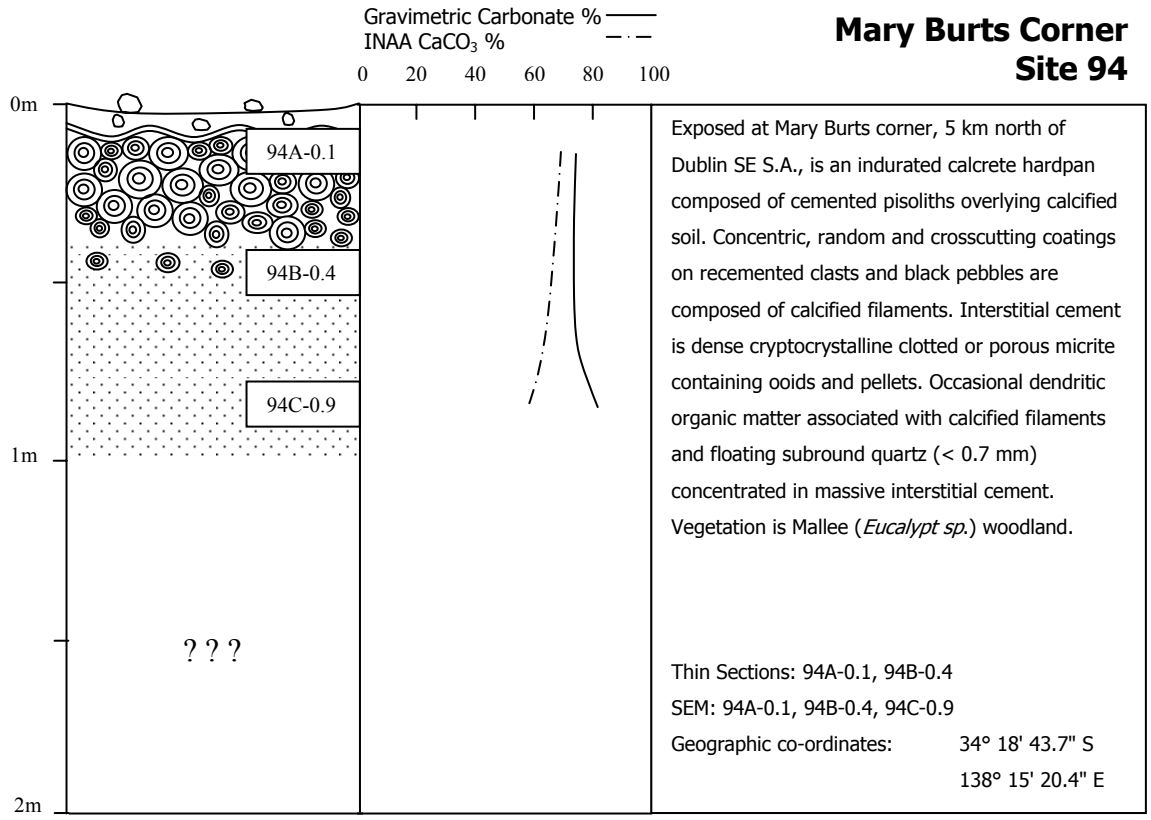

Mary Burts Corner
Site 94

Exposed at Mary Burts corner, 5 km north of Dublin SE S.A., is an indurated calcrete hardpan composed of cemented pisoliths overlying calcified soil. Concentric, random and crosscutting coatings on recemented clasts and black pebbles are composed of calcified filaments. Interstitial cement is dense cryptocrystalline clotted or porous micrite containing ooids and pellets. Occasional dendritic organic matter associated with calcified filaments and floating subround quartz (< 0.7 mm) concentrated in massive interstitial cement. Vegetation is Mallee (*Eucalypt sp.*) woodland.

Thin Sections: 94A-0.1, 94B-0.4
SEM: 94A-0.1, 94B-0.4, 94C-0.9
Geographic co-ordinates: 34° 18' 43.7" S
138° 15' 20.4" E

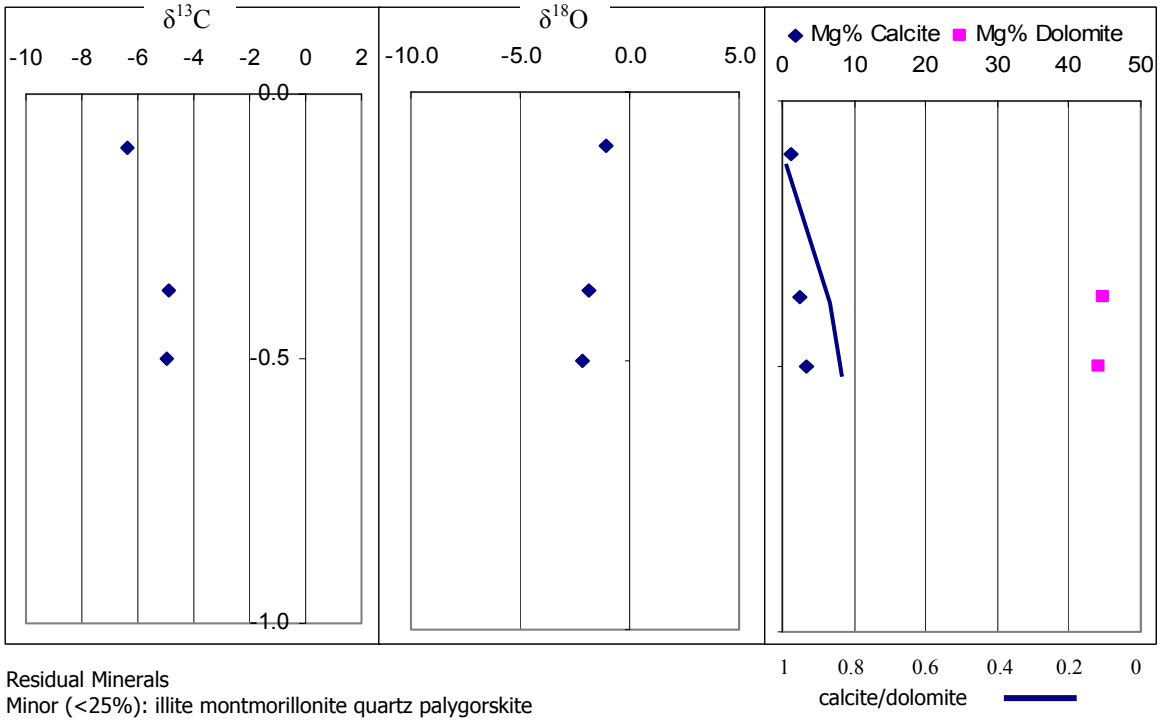

Residual Minerals
Minor (<25%): illite montmorillonite quartz palygorskite
Trace (<5%): feldspar kaolinite sepiolite goethite

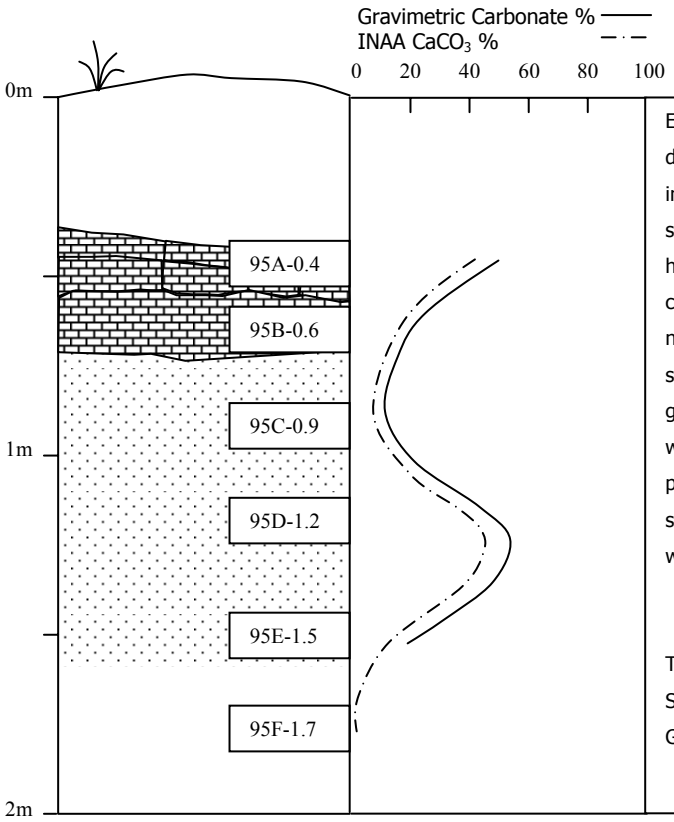

Killora
Site 95

Exposed in a railway cutting through an aeolian dune at Killora, SE S.A., is a tabular semi-indurated hardpan overlying powdery calcareous soil developed in unconsolidated red sand. The hardpan is composed of infilled horizontal channels consisting calcified filaments and rare needle-fibre calcite within semi indurated grain-supported quartz sand (subangular to round with grain size < 0.8 mm). Calcareous soil is porous with channel and vughy porosity with densely packed quartz grains. No visible organic matter in samples. Vegetation is Mallee (*Eucalypt sp.*) woodland.

Thin sections: 95A-0.4, 95D-1.2

SEM: 95D-1.2

Geographic co-ordinates: 34° 14' 07.0" S
138° 17' 38.5" E

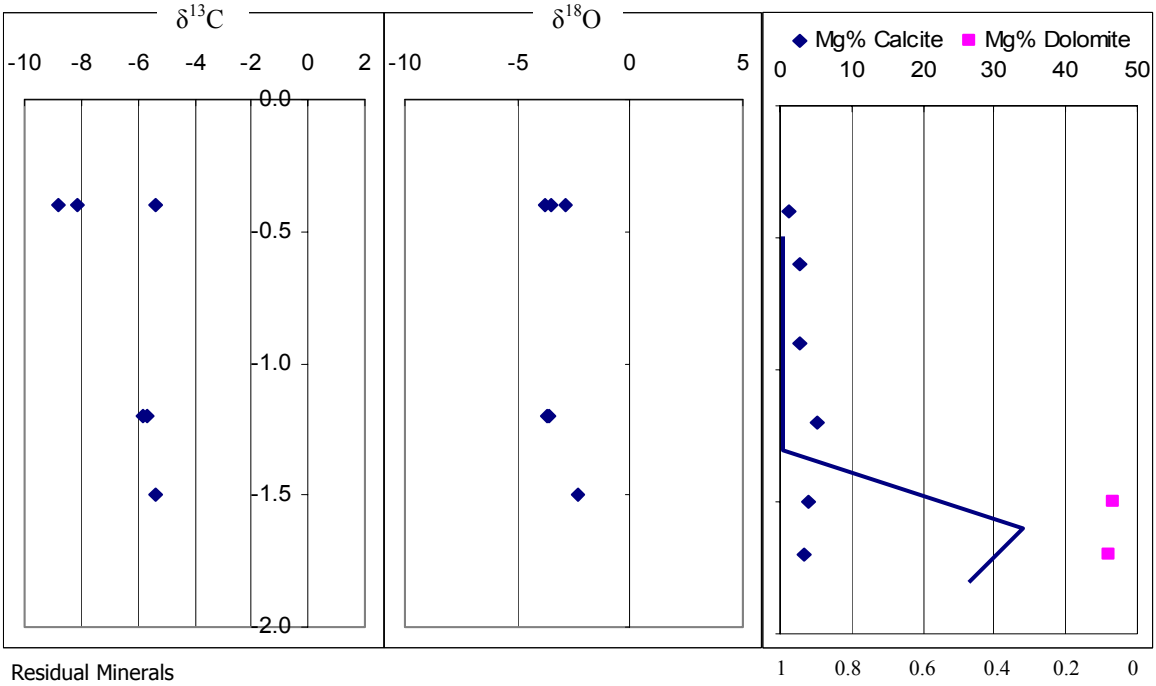

Residual Minerals
Minor (<25%): quartz illite montmorillonite feldspar
Trace (<5%): palygorskite hematite kaolinite sepiolite goethite

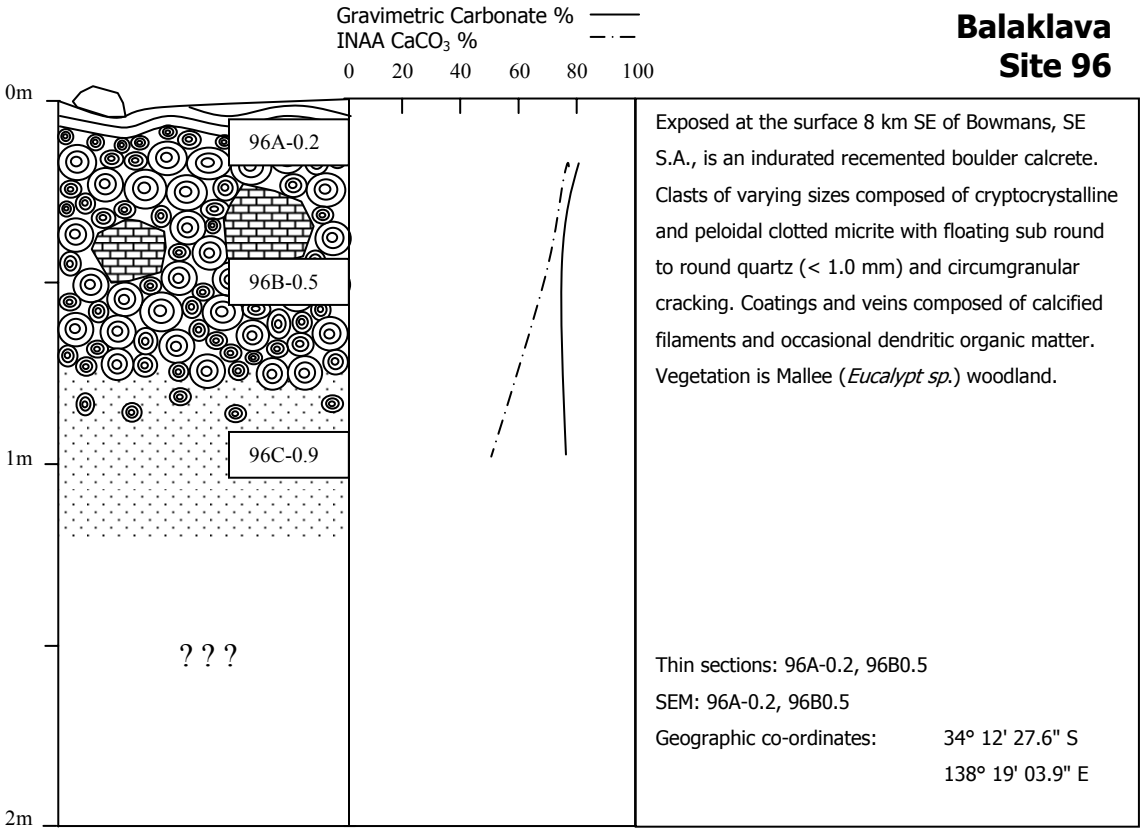

Balaklava
Site 96

Exposed at the surface 8 km SE of Bowmans, SE S.A., is an indurated recemented boulder calcrete. Clasts of varying sizes composed of cryptocrystalline and peloidal clotted micrite with floating sub round to round quartz (< 1.0 mm) and circumgranular cracking. Coatings and veins composed of calcified filaments and occasional dendritic organic matter. Vegetation is Mallee (*Eucalypt sp.*) woodland.

Thin sections: 96A-0.2, 96B0.5
SEM: 96A-0.2, 96B0.5
Geographic co-ordinates: 34° 12' 27.6" S
138° 19' 03.9" E

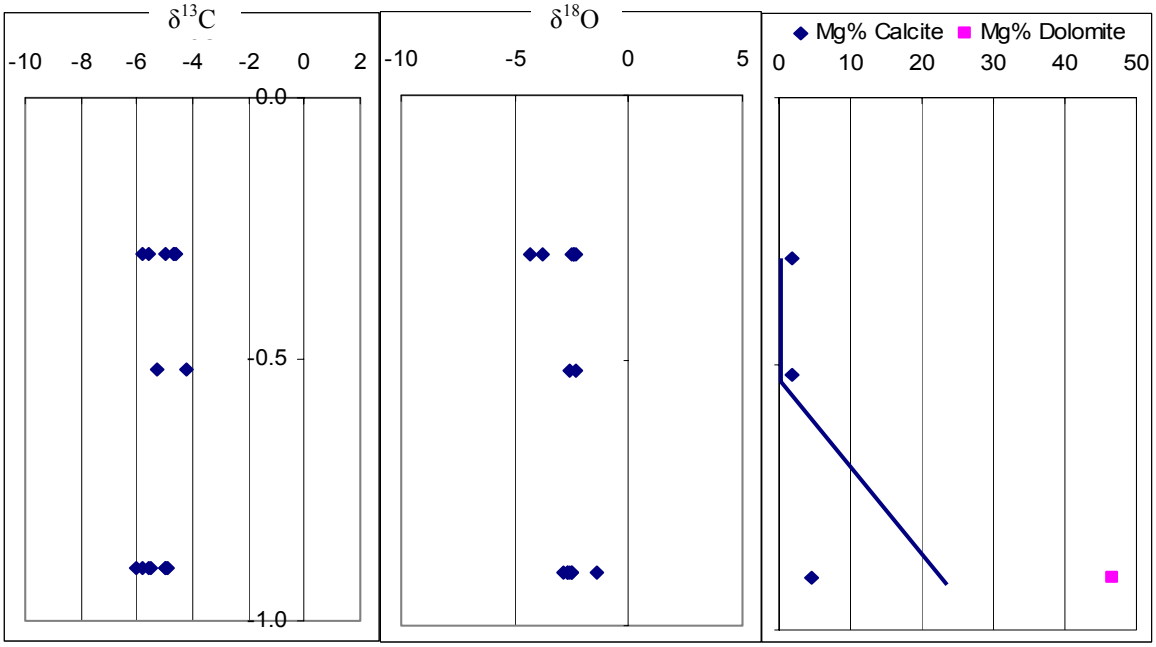

Residual Minerals
Minor (<25%): illite quartz feldspar
Trace (<5%): palygorskite montmorillonite sepiolite goethite hematite

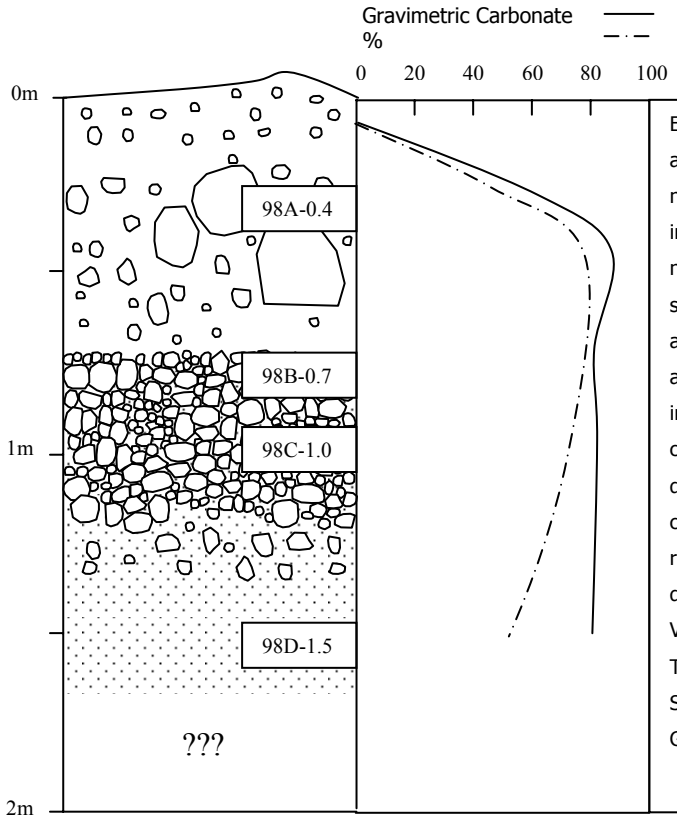

Bute
Site 98

Exposed in a cutting 4 km north of Bute, SE S.A. is a profile containing indurated loose reworked nodules and boulders in brown clay overlying semi-indurated nodules in calcified soil. The loose nodules and boulders have a brecciated internal structure composed of clotted micrite with floating angular to subround quartz (< 0.6 mm) and veins and coatings composed of calcified filaments. Semi-indurated nodules are massive containing abundant calcified filaments, floating angular to subround quartz (< 0.5 mm) and occasional recemented clasts. No organic matter is visible in samples. A recent powder calcrete is developed in an aeolian dune 200 m north of exposure (sample 98X). Vegetation is Mallee (*Eucalypt sp.*) woodland.

Thin sections: 98B-0.7

SEM: 98B-0.7

Geographic co-ordinates: 33° 50' 03.0" S
138° 01' 06.2" E

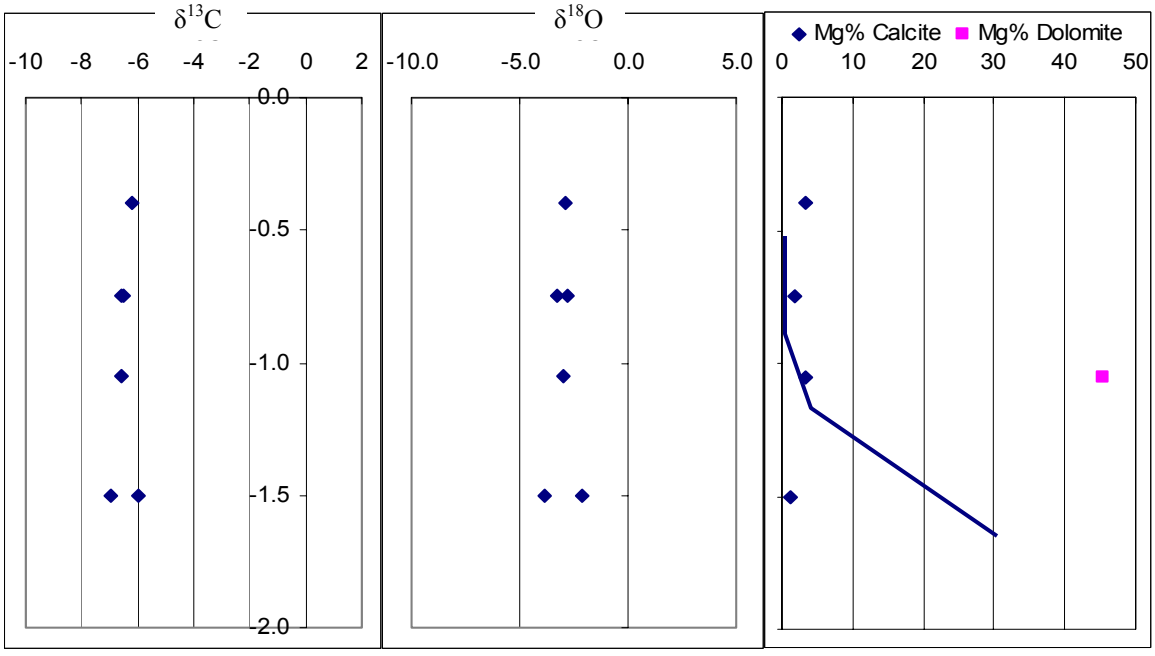

Residual Minerals
Minor (<25%): illite montmorillonite palygorskite quartz
Trace (<5%): kaolinite feldspar sepiolite hematite

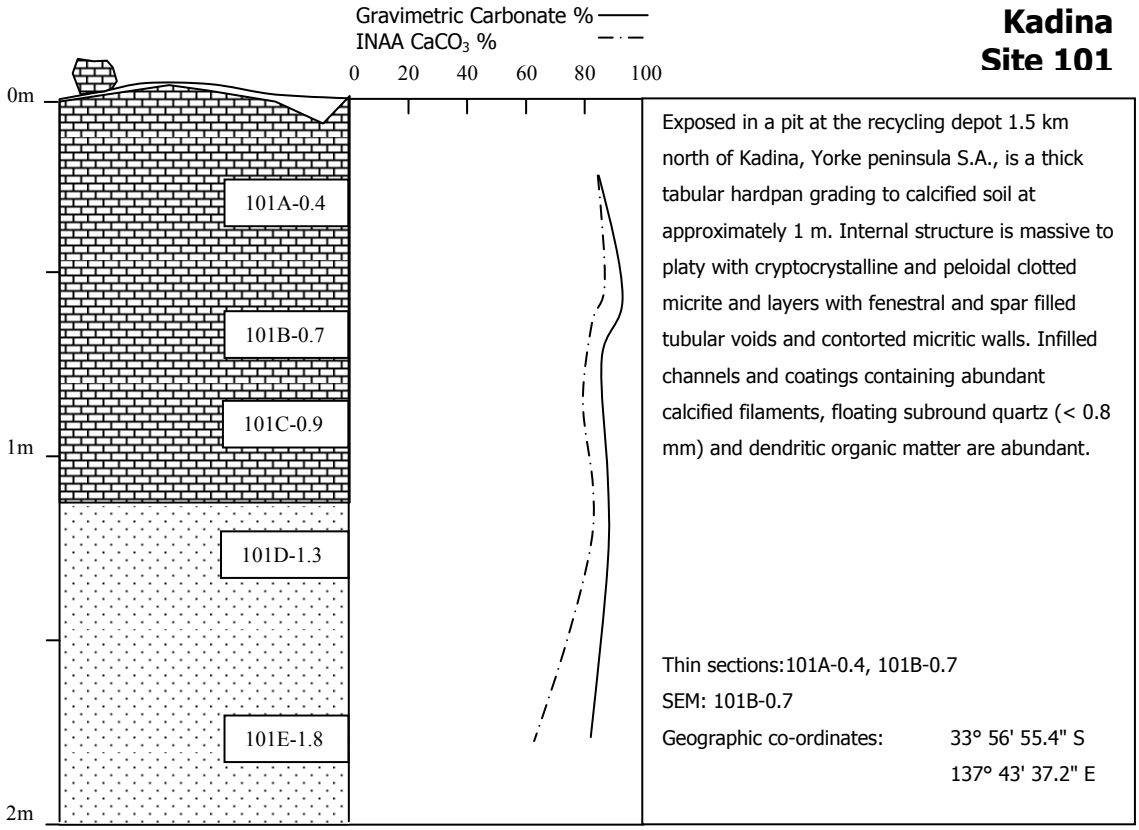

Kadina
Site 101

Exposed in a pit at the recycling depot 1.5 km north of Kadina, Yorke peninsula S.A., is a thick tabular hardpan grading to calcified soil at approximately 1 m. Internal structure is massive to platy with cryptocrystalline and peloidal clotted micrite and layers with fenestral and spar filled tubular voids and contorted micritic walls. Infilled channels and coatings containing abundant calcified filaments, floating subround quartz (< 0.8 mm) and dendritic organic matter are abundant.

Thin sections:101A-0.4, 101B-0.7

SEM: 101B-0.7

Geographic co-ordinates: 33° 56' 55.4" S
137° 43' 37.2" E

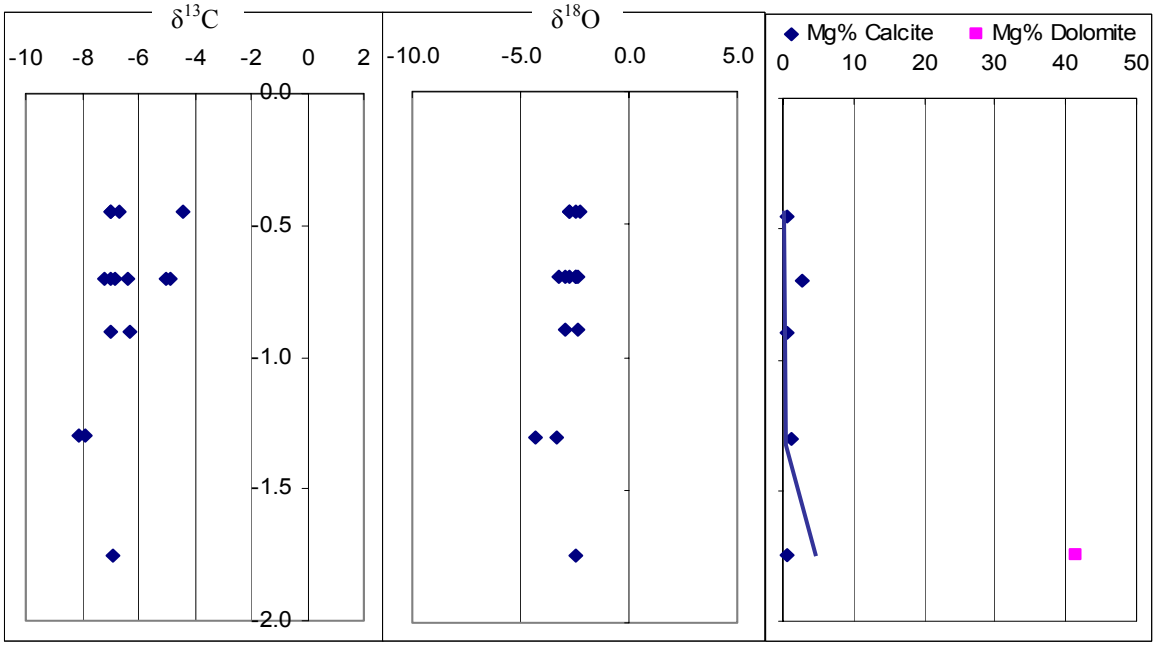

Residual Minerals
Minor (<25%): illite montmorillonite palygorskite
Trace (<5%): quartz kaolinite feldspar sepiolite hematite

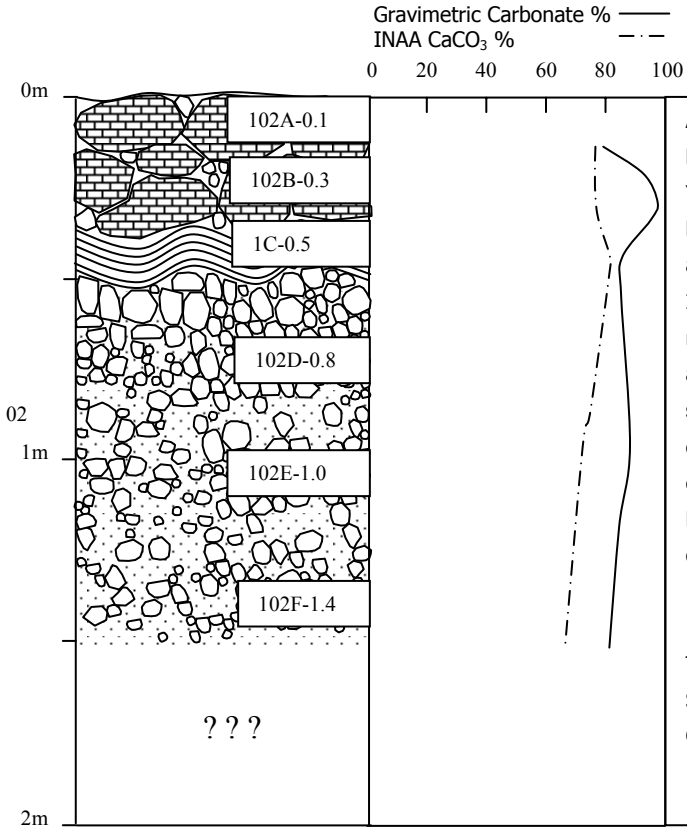

Moonta Site 102

A thick indurated calcrete profile exposed in a borrow pit at 'Cunliffe' 13 km east of Moonta, Yorke Peninsula S.A., contains a laminar or platy layer at 0.4 - 0.5 m with spar filled tubular voids and contorted micritic walls (fenestral fabric). Internal structure of the boulders and upper nodules is brecciated containing cryptocrystalline and peloidal secondary crystic fabric with floating sub round quartz (< 1.0 mm), and infilled channels and fissures containing abundant calcified filaments and dendritic organic matter. Lower nodules are micritic and massive grading down to calcified soil with porous micritic fabric.

Thin sections: 102A-0.1, 102D-0.8

SEM: 102B-0.3

Geographic co-ordinates: 34° 05' 00.6" S
137° 43' 52.4" E

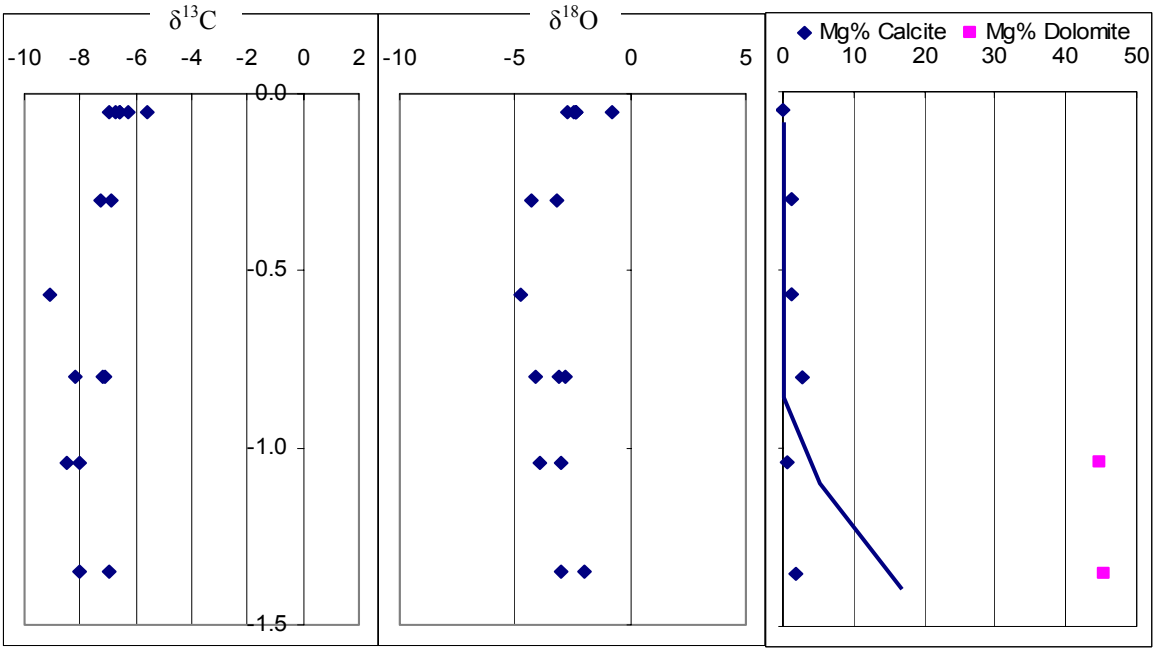

Residual Minerals
Minor (<25%): illite montmorillonite palygorskite
Trace (<5%): quartz kaolinite feldspar sepiolite hematite

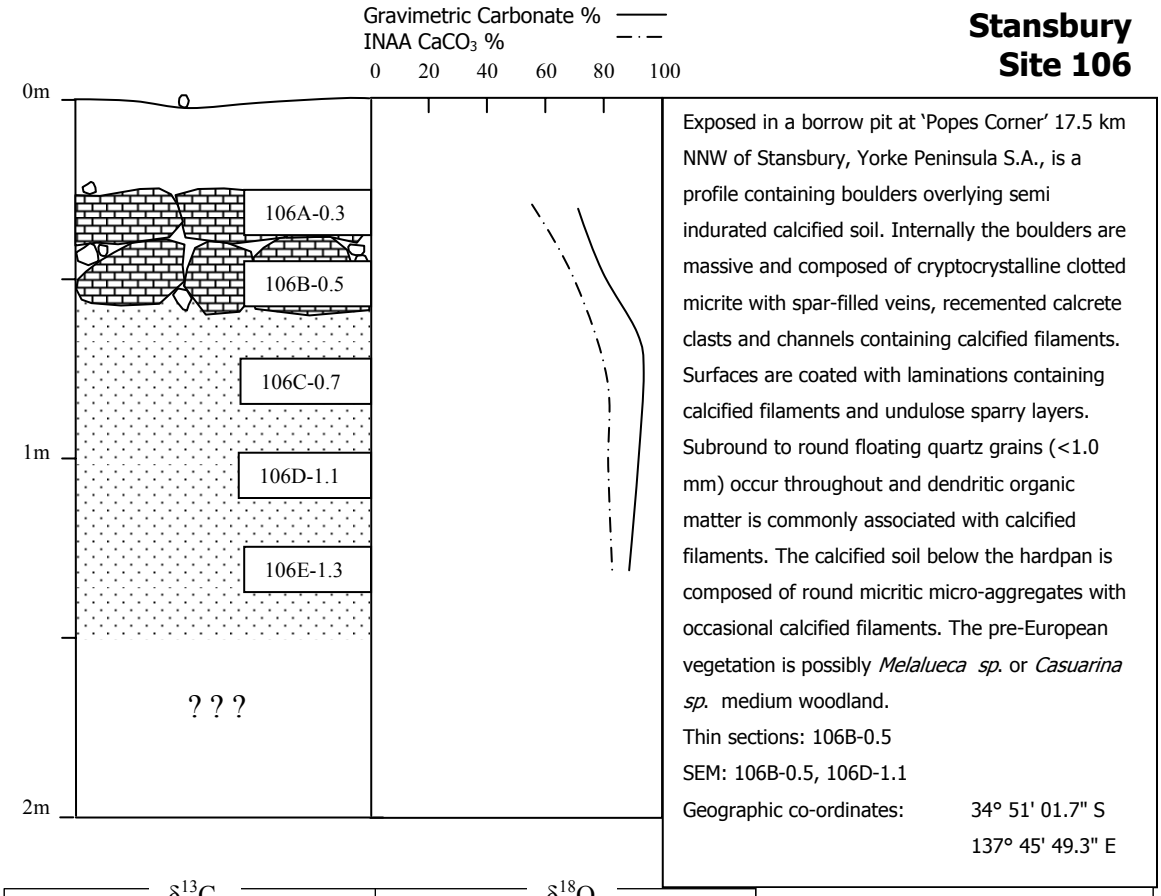

Stansbury Site 106

Exposed in a borrow pit at 'Popes Corner' 17.5 km NNW of Stansbury, Yorke Peninsula S.A., is a profile containing boulders overlying semi indurated calcified soil. Internally the boulders are massive and composed of cryptocrystalline clotted micrite with spar-filled veins, recemented calcrete clasts and channels containing calcified filaments. Surfaces are coated with laminations containing calcified filaments and undulose sparry layers. Subround to round floating quartz grains (<1.0 mm) occur throughout and dendritic organic matter is commonly associated with calcified filaments. The calcified soil below the hardpan is composed of round micritic micro-aggregates with occasional calcified filaments. The pre-European vegetation is possibly *Melalueca sp.* or *Casuarina sp.* medium woodland.

Thin sections: 106B-0.5

SEM: 106B-0.5, 106D-1.1

Geographic co-ordinates: 34° 51' 01.7" S
137° 45' 49.3" E

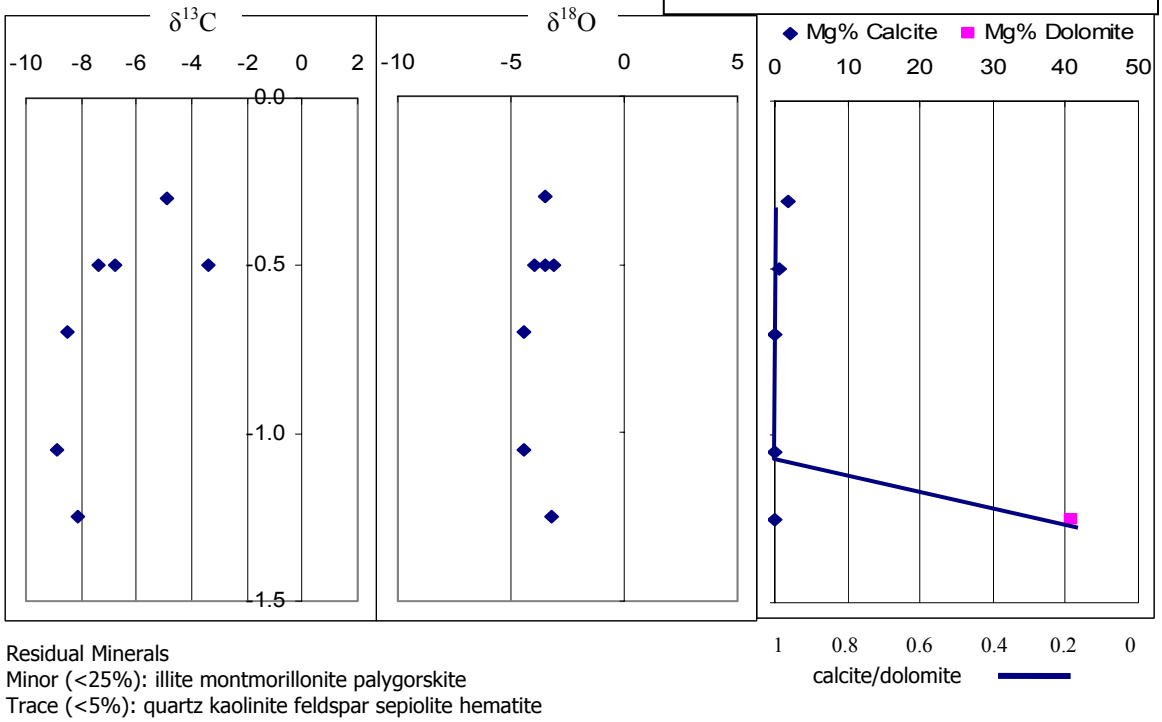

Residual Minerals
Minor (<25%): illite montmorillonite palygorskite
Trace (<5%): quartz kaolinite feldspar sepiolite hematite

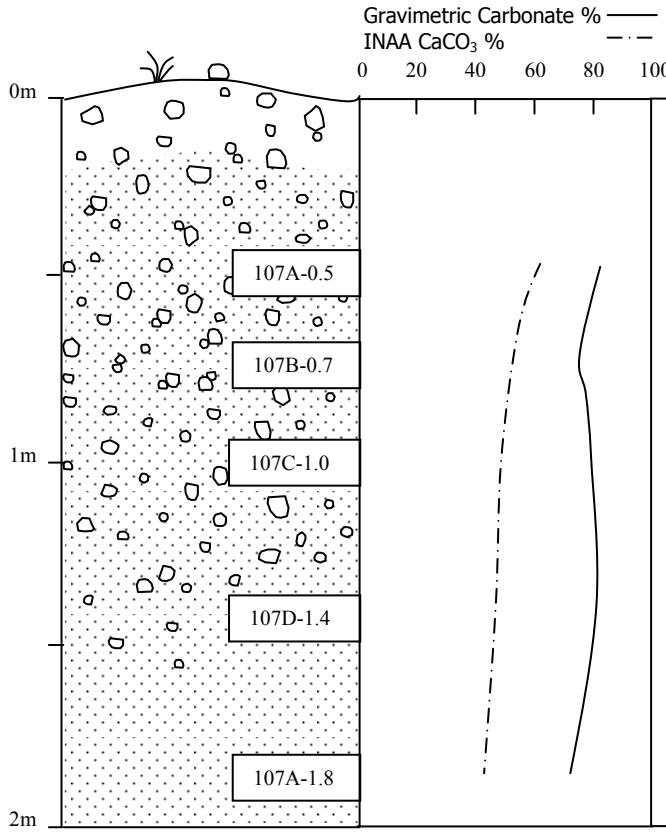

Yorketown Site 107

Exposed in a road cut 10 km NW of Yorketown, Yorke Peninsula S.A. is a recent calcareous aeolian dune with weak nodular calcrete development. The calcrete samples are massive semi-indurated to friable with matrix-supported fabric composed of subangular to rounded quartz (< 0.7 mm) in a porous micritic matrix. Calcified filaments occur rarely and no organic matter is visible in thin section. The pre-European vegetation is possibly *Melalueca sp.* or *Casuarina sp.* medium woodland.

Thin sections: 107C-1.0

Geographic co-ordinates: 34° 59' 02.0" S
137° 30' 45.8" E

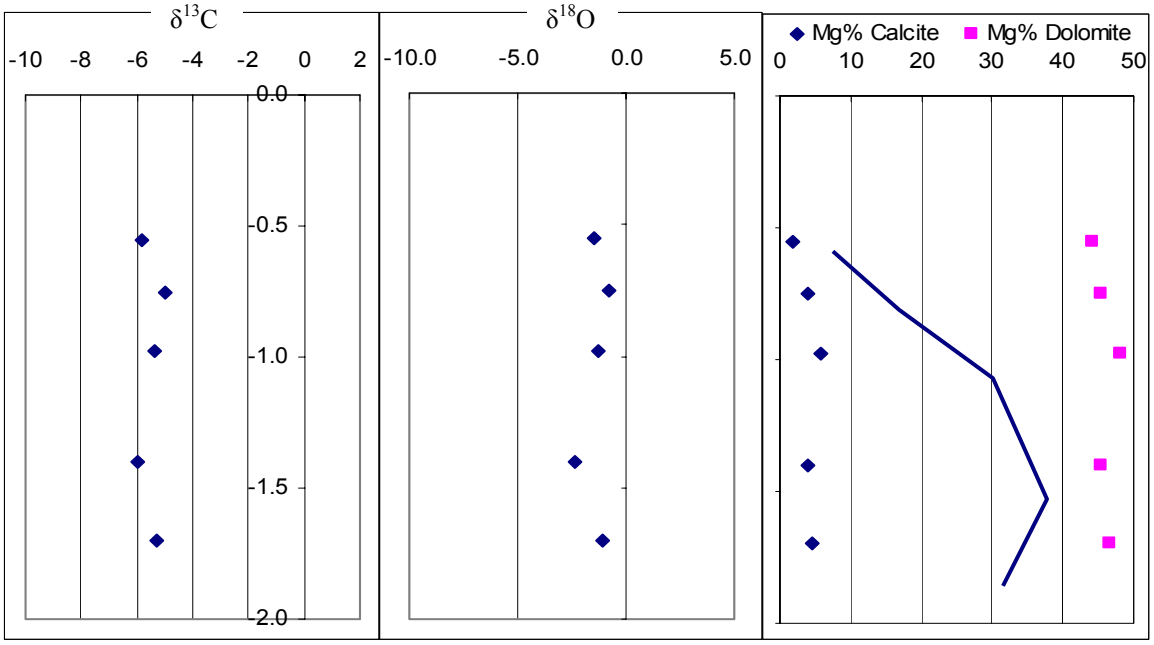

Residual Minerals
Minor (<25%): illite montmorillonite
Trace (<5%): quartz feldspar sepiolite palygorskite

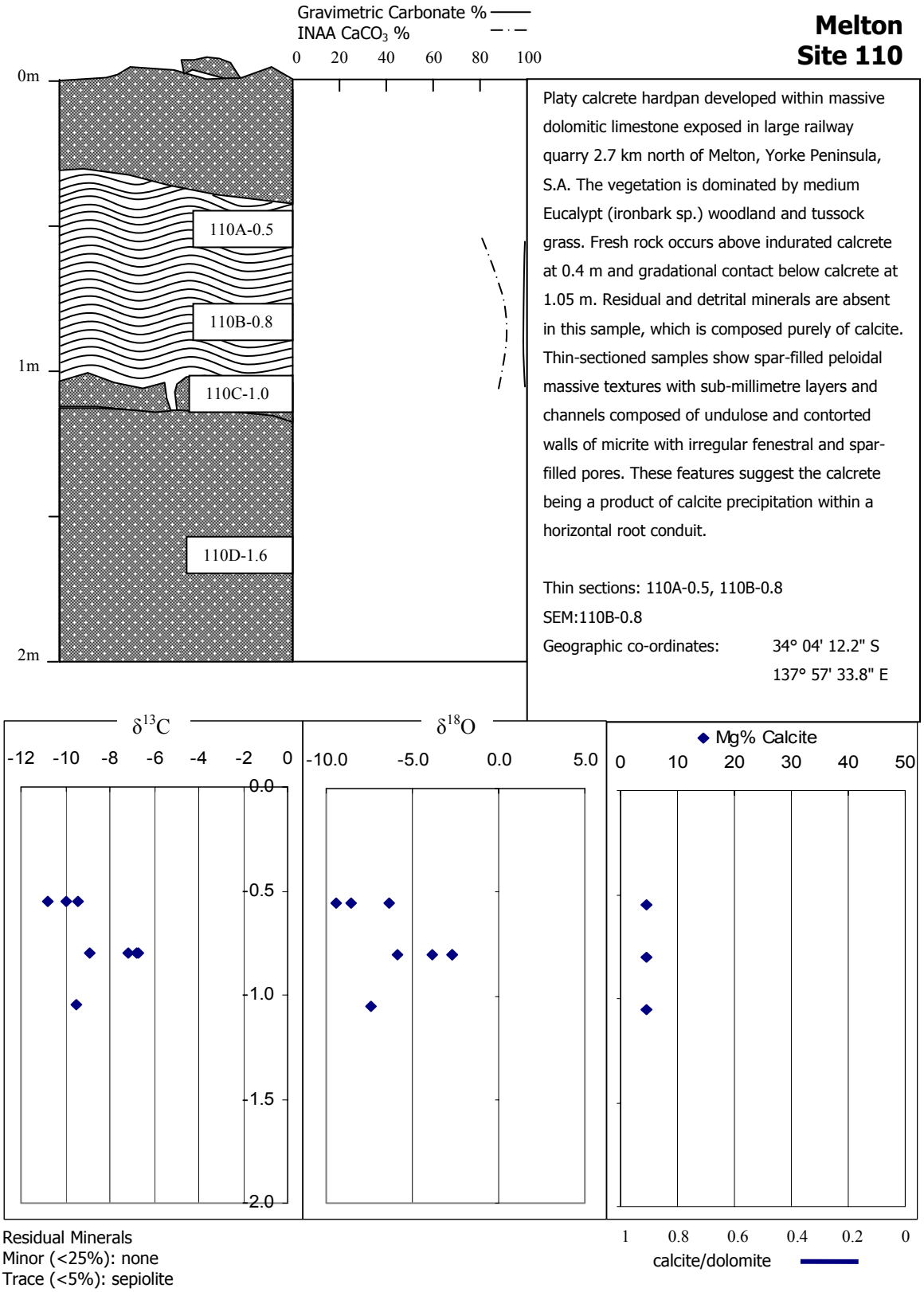

Melton Site 110

Platy calcrete hardpan developed within massive dolomitic limestone exposed in large railway quarry 2.7 km north of Melton, Yorke Peninsula, S.A. The vegetation is dominated by medium Eucalypt (ironbark sp.) woodland and tussock grass. Fresh rock occurs above indurated calcrete at 0.4 m and gradational contact below calcrete at 1.05 m. Residual and detrital minerals are absent in this sample, which is composed purely of calcite. Thin-sectioned samples show spar-filled peloidal massive textures with sub-millimetre layers and channels composed of undulose and contorted walls of micrite with irregular fenestral and spar-filled pores. These features suggest the calcrete being a product of calcite precipitation within a horizontal root conduit.

Thin sections: 110A-0.5, 110B-0.8

SEM:110B-0.8

Geographic co-ordinates: 34° 04' 12.2" S
137° 57' 33.8" E

Residual Minerals
Minor (<25%): none
Trace (<5%): sepiolite

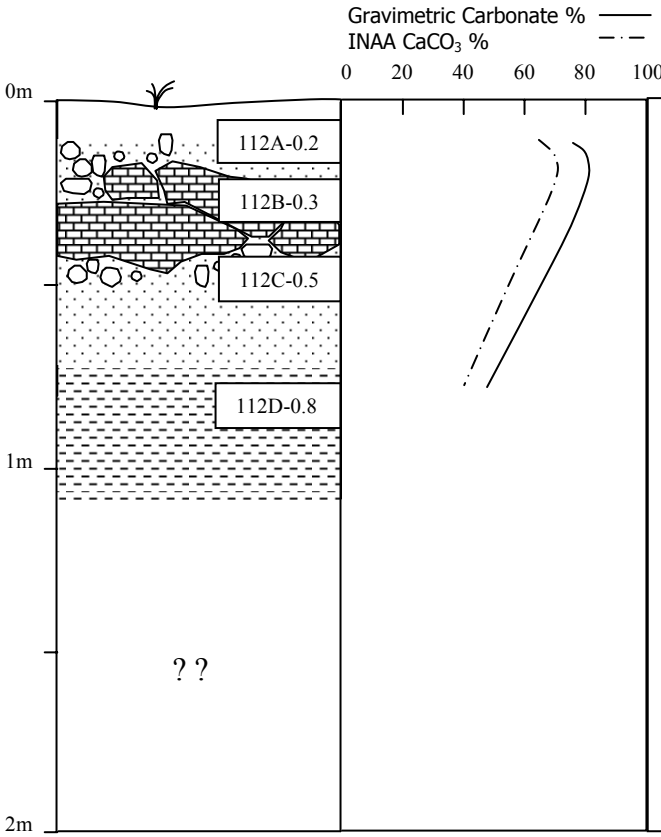

Whyte-Yarcowie Site 112

A borrow pit at 'Wuapunya', 25 km NE of Hallet in the Mt Lofty Ranges, SE South Australia, exposes a profile containing tabular hardpan overlying calcified soil developed on red sandy clay. Internally the hardpan is massive with occasional recemented calcrete clasts and microscopically composed of cryptocrystalline and clotted micrite with floating sub round quartz (< 0.5 mm) and occasional calcified filaments and dendritic organic matter. The vegetation is Mallee (*Eucalypt sp.*) woodland.

Thin Sections: 112B-0.3

Geographic co-ordinates: 33° 11.418' S
139° 00.217' E

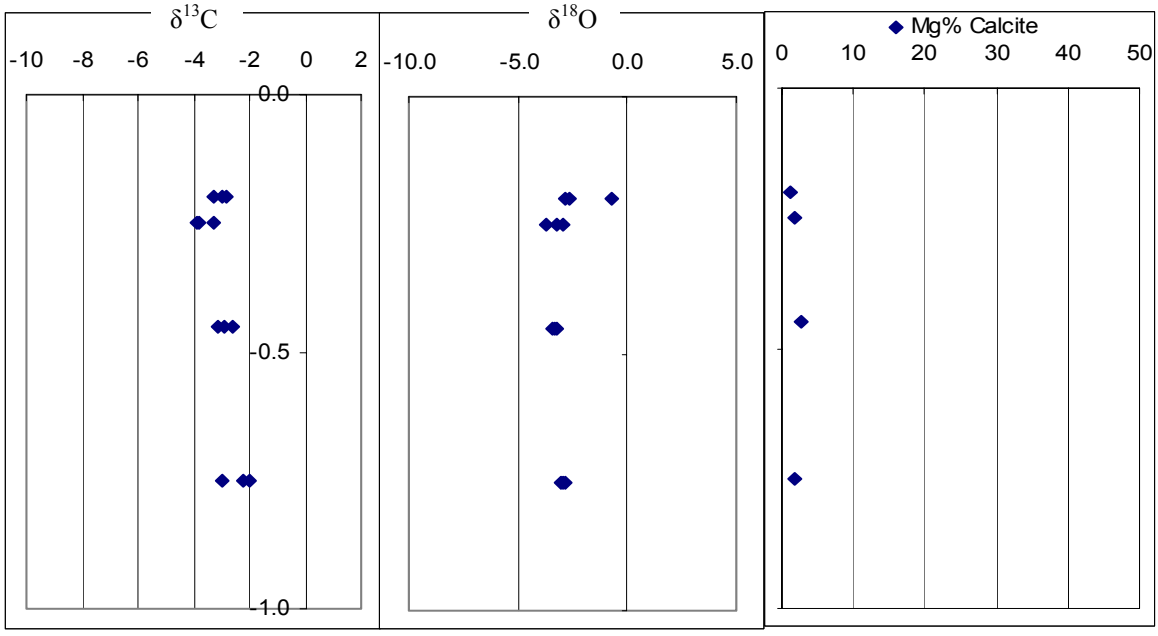

Residual Minerals
Minor (<25%): illite quartz
Trace (<5%): feldspar kaolinite palygorskite goethite

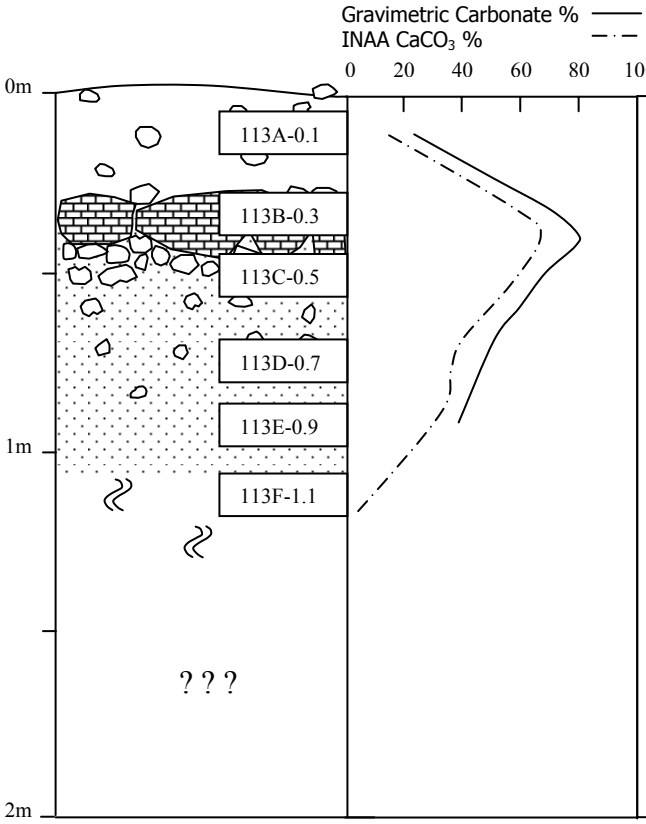

Kimba North West
Site 113

A borrow pit 14 km N of Kimba, Eyre Peninsula S.A. exposes a profile containing tabular hardpan overlying calcified soil developed on red sandy clay. Internally the hardpan is massive with occasional recemented calcrete clasts and composed of cryptocrystalline and peloidal clotted micrite with floating sub round quartz (< 0.5 mm) and calcified filaments and in thin coatings and channels. No organic matter is visible in thin section. The calcified soil below 0.5 m is massive semi-indurated and composed of micrite and occasional calcified filaments with porous fabric. The vegetation is Mallee (*Eucalypt sp.*) woodland.

Thin sections: 113B-0.3, 113D-0.7

Geographic co-ordinates: 33° 03.241' S
136°19.528' E

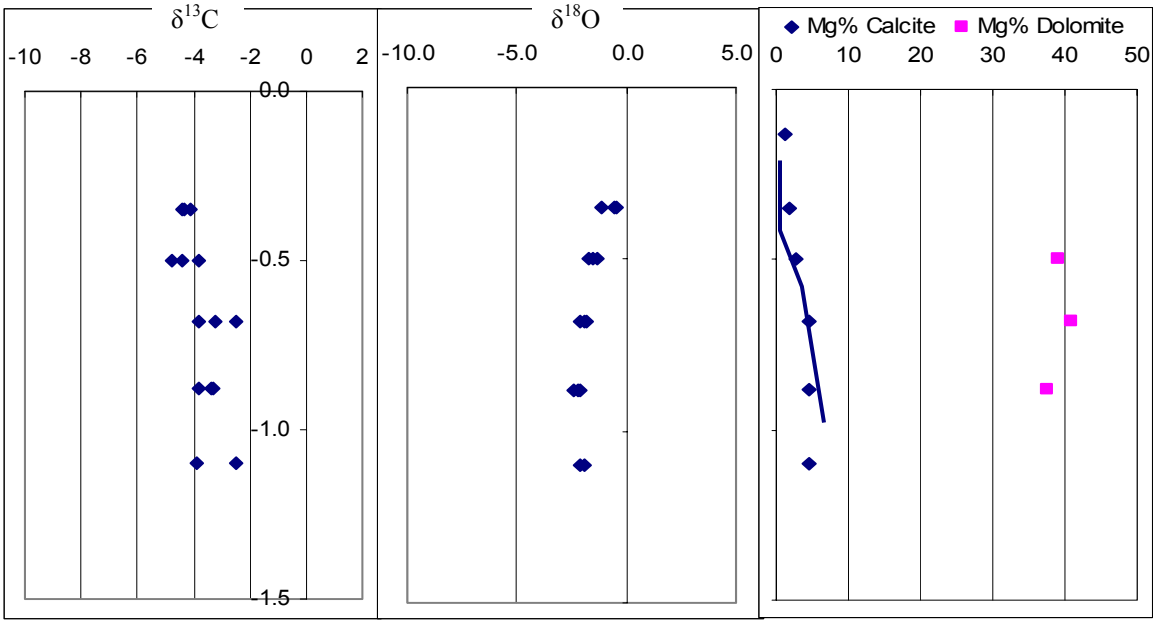

Residual Minerals
Minor (<25%): illite quartz kaolinite
Trace (<25%): feldspar palygorskite goethite hematite

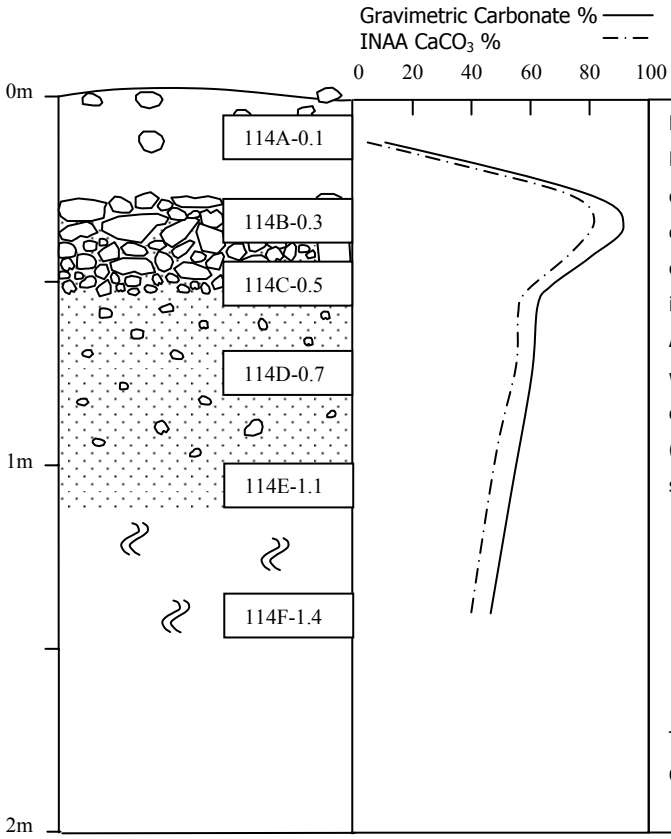

Buckleboo-Kyancutta Site 114

Exposed in a borrow pit 20 km south of Buckleboo, Eyre peninsula SA, is a profile containing nodules in calcified soil overlying calcrete mottles developed in unconsolidated red clayey sand. Upper nodules have a brecciated internal structure while lower nodules are massive. All composed of cryptocrystalline clotted micrite with abundant calcified filaments in channels and coatings and floating subangular to round quartz (< 1.0 mm). No organic matter was visible in thin section.

Thin sections: 114B-0.3, 114C-0.5

Geographic co-ordinates: 33° 00.955' S
136° 03.386' E

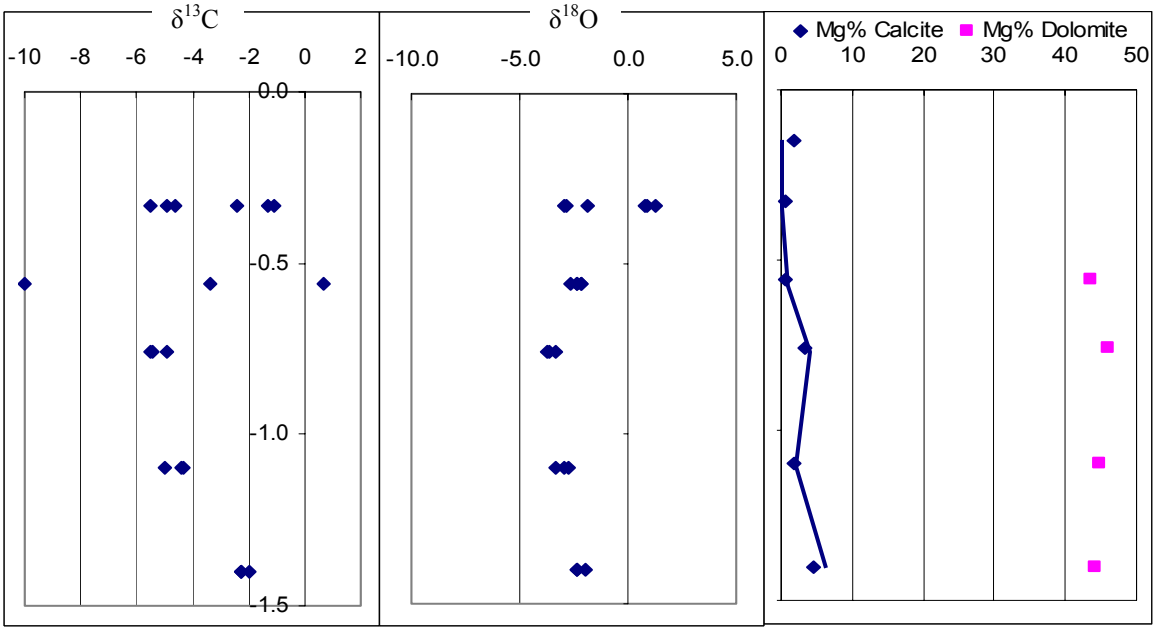

Residual Minerals
Minor (25%): illite quartz
Trace (<5%): montmorillonite palygorskite sepiolite goethite kaolinite

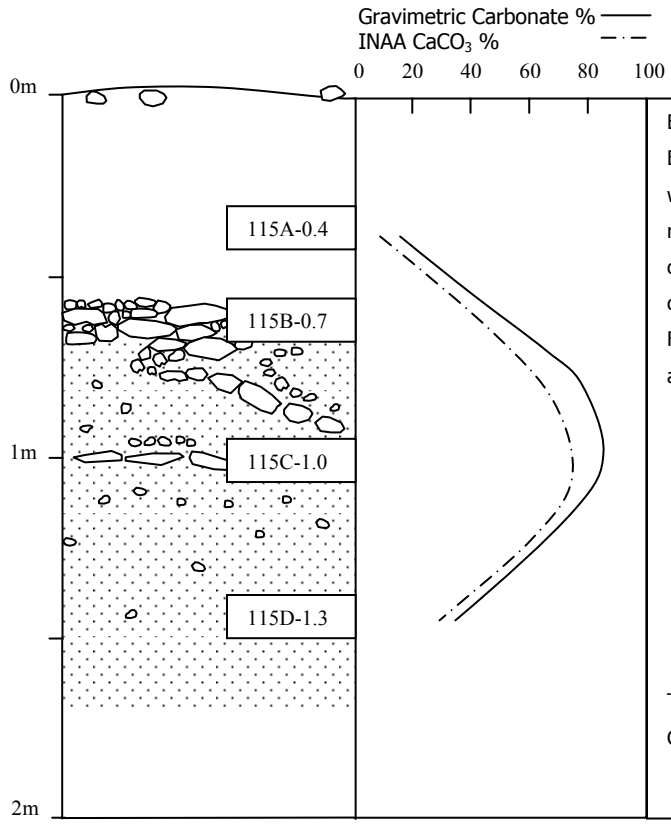

Pinkawillinie Site 115

Exposed in a borrow pit 30 km south of Buckleboo, Eyre peninsula S.A., is a profile containing nodules within calcified soil developed in unconsolidated red sand. Nodules are massive and composed of cryptocrystalline clotted micrite with abundant calcified filaments in channels and coatings. Floating subangular to round quartz (< 1.0 mm) and no visible organic matter.

Thin sections: 115B-0.7, 115C-1.0

Geographic co-ordinates: 33° 08.348' S
136° 00.100' E

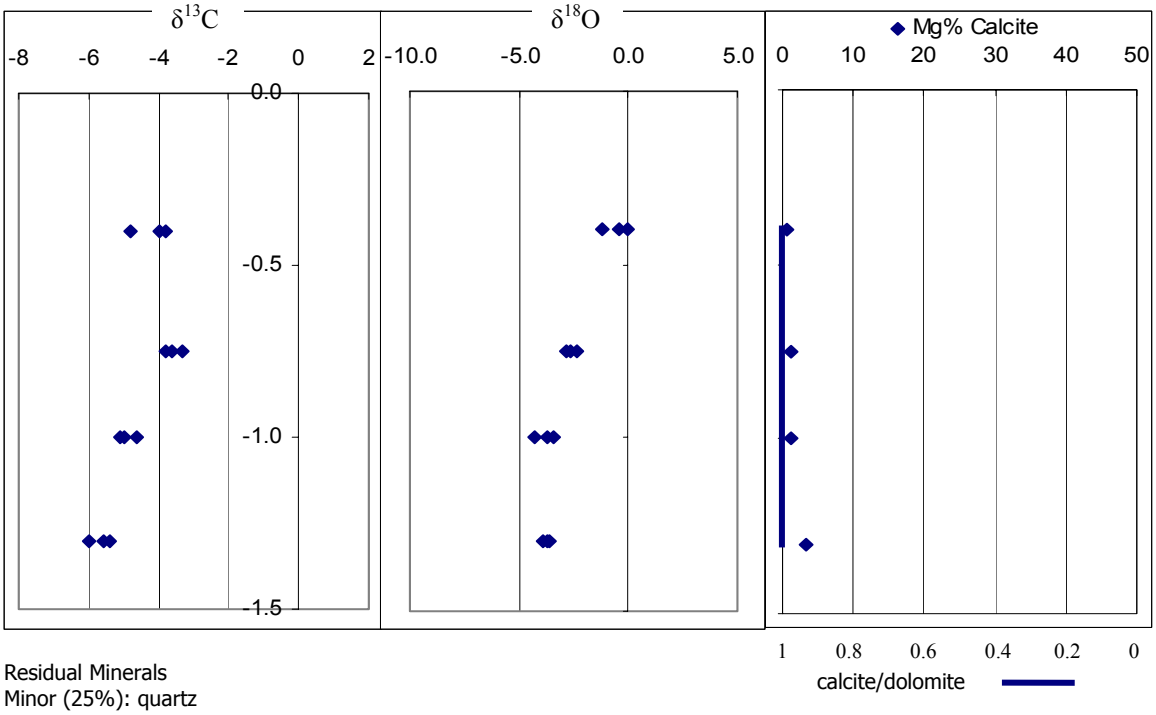

Residual Minerals
Minor (25%): quartz
Trace (<5%): illite feldspar kaolinite palygorskite sepiolite goethite

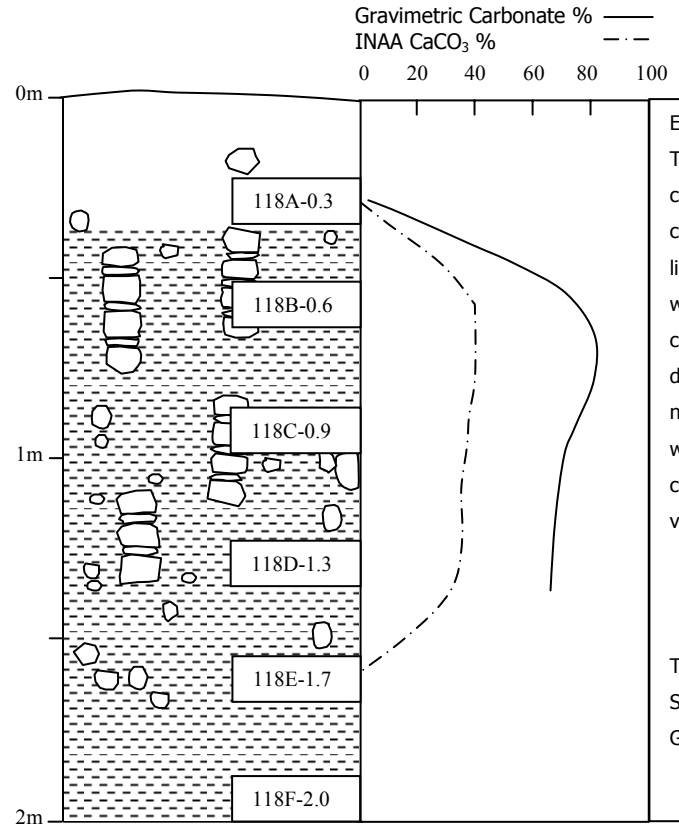

Tammin
Site 118

Exposed at a the railway cutting 6.1 km west of Tammin, W.A., is a profile containing massive pink coloured nodules and plates stacked in vertical columns from 0.4 to 1.7 m. The host material is light brown clayey soil developed on deeply weathered feldspathic gneiss. The vegetation now cleared probably consisted medium woodland dominated by *Eucalyptu. sp.* The plates and nodules are composed of microcrystalline dolomite with an alveolar-like fabric (resembling replaced cells) with micrite walls and void-filling microspar visible in thin section.

Thin sections: 118B-0.6
SEM: 118B-0.6
Geographic co-ordinates: 31° 37.956' S
117° 32.832' E

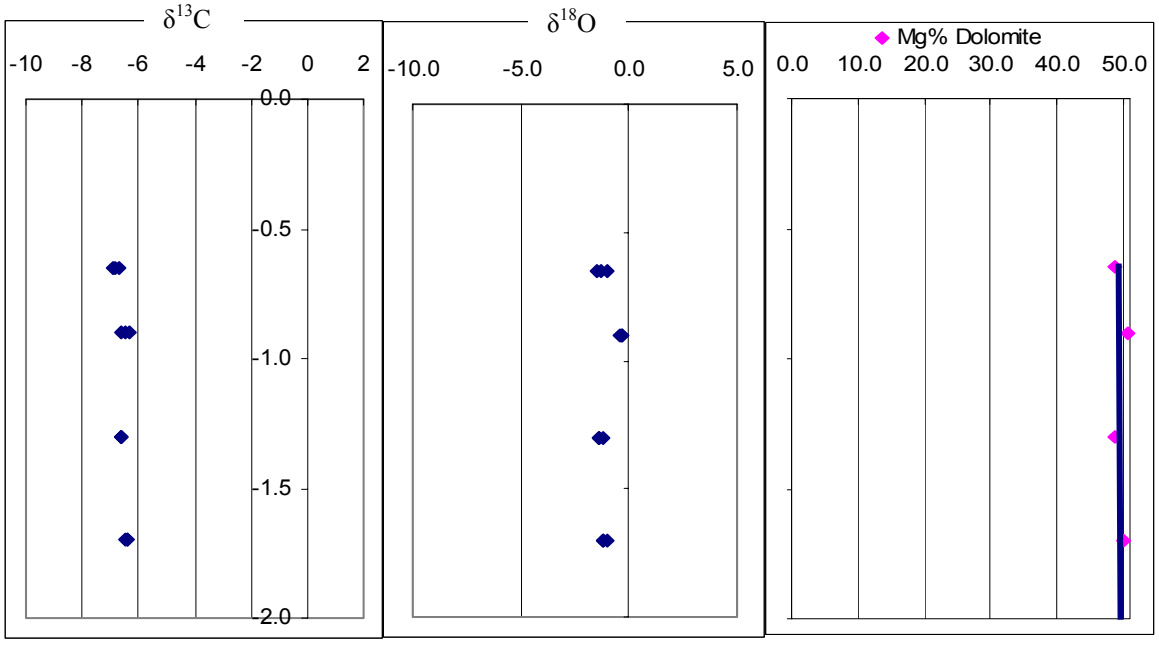

Residual Minerals
Minor (<25%): illite quartz kaolinite
Trace (<%5): feldspar montmorillonite palygorskite sepiolite goethite hematite

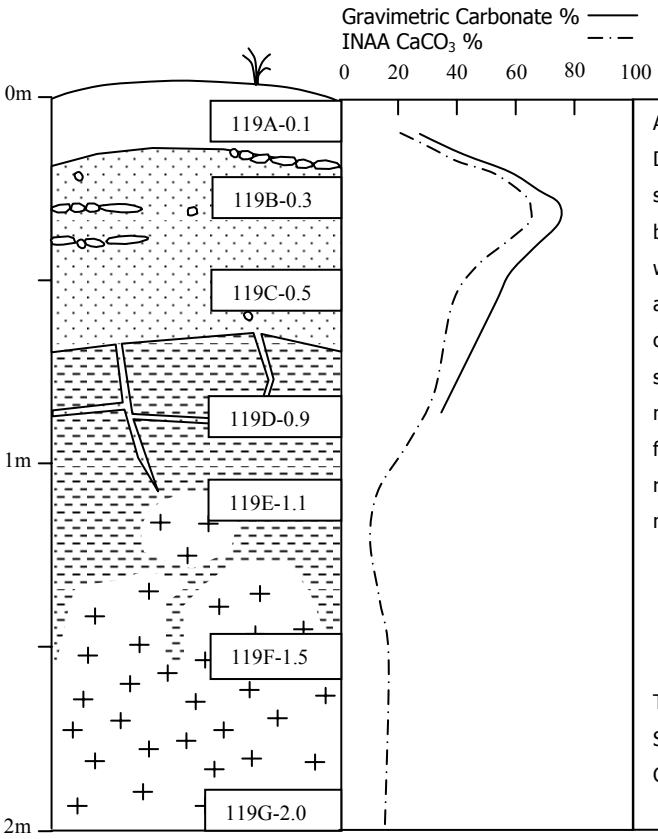

Dumbleyung Site 119

A road cutting through a low rise 11.9 km west of Dumbleyung, W.A. exposes a friable white calcified soil with a platy structure at 0.2 to 0.6m overlain by organic-rich black soil. Stringers penetrate into weathered ultramafic igneous rock down to approximately 1 m. The vegetation, now cleared, consisted medium woodland dominated by *Eucalypt* sp. The samples are friable to semi-indurated, massive and composed almost wholly of needle fibre calcite with micritic overgrowths forming a random mesh micro-texture. Occasional fine (< 0.2 mm) quartz occurs down to 0.5m.

Thin sections: 119C-0.5

SEM: 119C-0.5

Geographic co-ordinates: 33° 17.236' S
117° 37.270' E

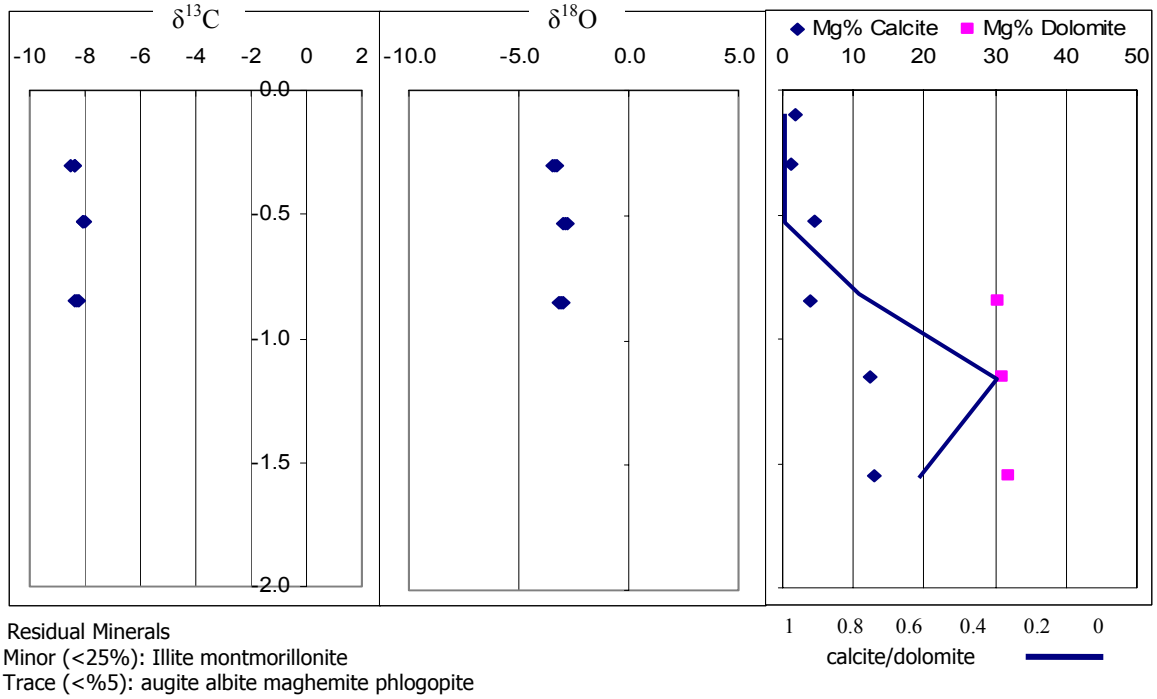

Residual Minerals
Minor (<25%): Illite montmorillonite
Trace (<%5): augite albite maghemite phlogopite

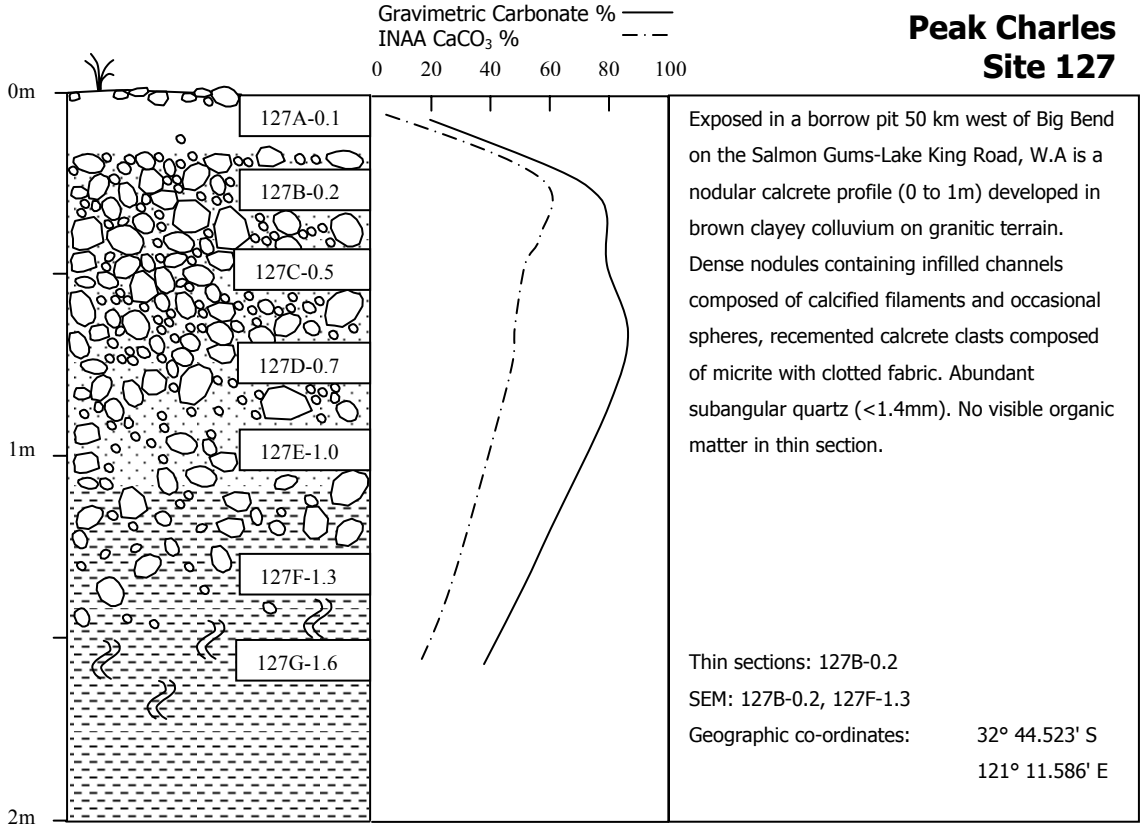

Peak Charles Site 127

Exposed in a borrow pit 50 km west of Big Bend on the Salmon Gums-Lake King Road, W.A is a nodular calcrete profile (0 to 1m) developed in brown clayey colluvium on granitic terrain. Dense nodules containing infilled channels composed of calcified filaments and occasional spheres, recemented calcrete clasts composed of micrite with clotted fabric. Abundant subangular quartz (<1.4mm). No visible organic matter in thin section.

Thin sections: 127B-0.2
SEM: 127B-0.2, 127F-1.3
Geographic co-ordinates: 32° 44.523' S
121° 11.586' E

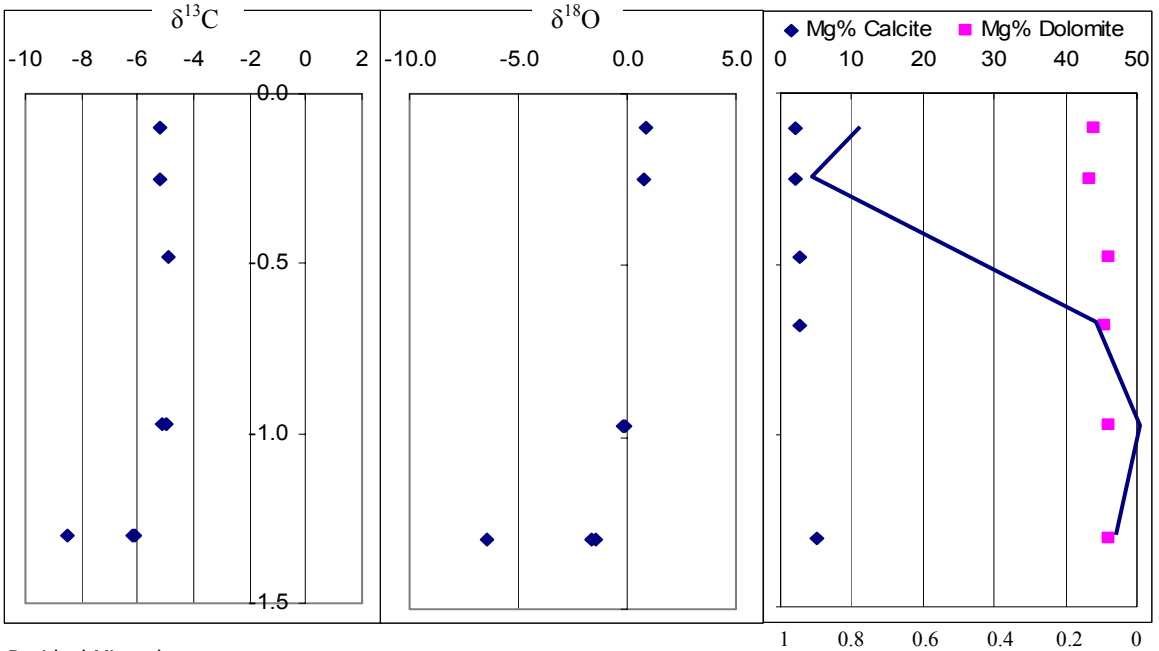

Residual Minerals
Minor (<25%): illite quartz kaolinite
Trace (<5%): goethite hematite illite sepiolite

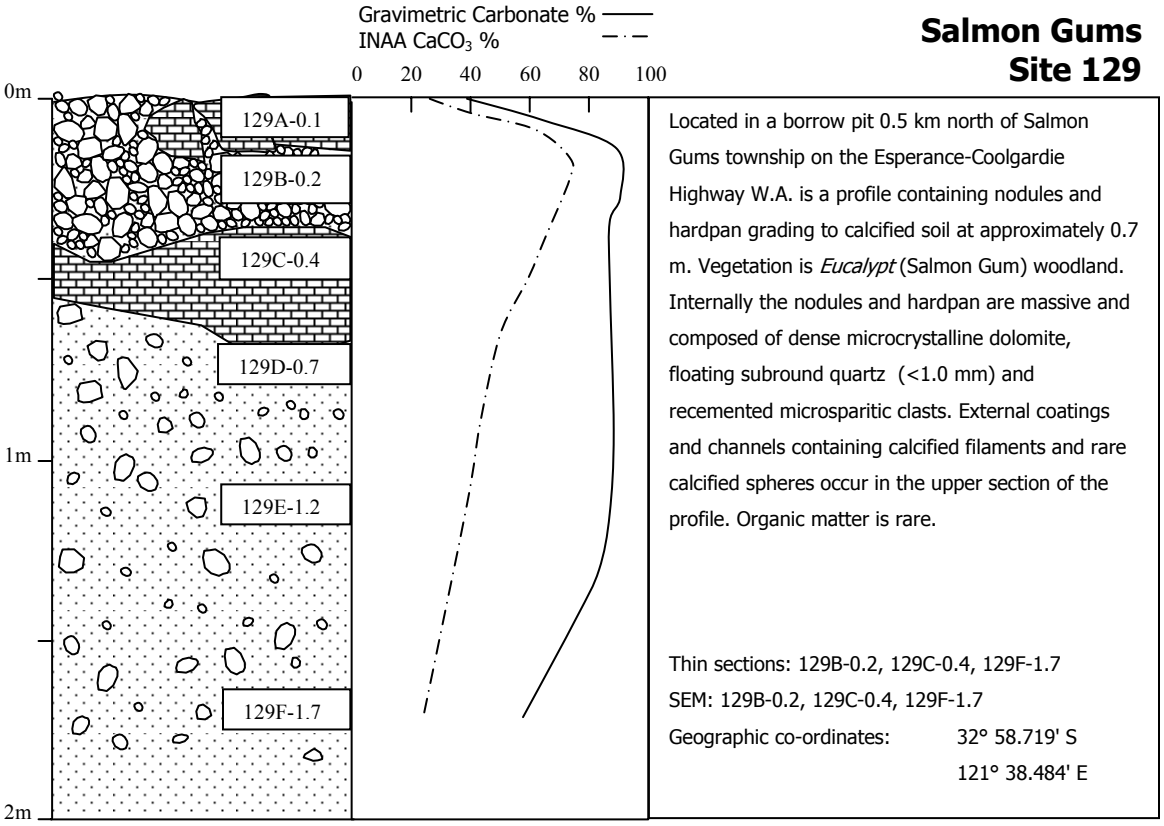

Salmon Gums
Site 129

Located in a borrow pit 0.5 km north of Salmon Gums township on the Esperance-Coolgardie Highway W.A. is a profile containing nodules and hardpan grading to calcified soil at approximately 0.7 m. Vegetation is *Eucalypt* (Salmon Gum) woodland. Internally the nodules and hardpan are massive and composed of dense microcrystalline dolomite, floating subround quartz (<1.0 mm) and recemented microsparitic clasts. External coatings and channels containing calcified filaments and rare calcified spheres occur in the upper section of the profile. Organic matter is rare.

Thin sections: 129B-0.2, 129C-0.4, 129F-1.7
SEM: 129B-0.2, 129C-0.4, 129F-1.7
Geographic co-ordinates: 32° 58.719' S
121° 38.484' E

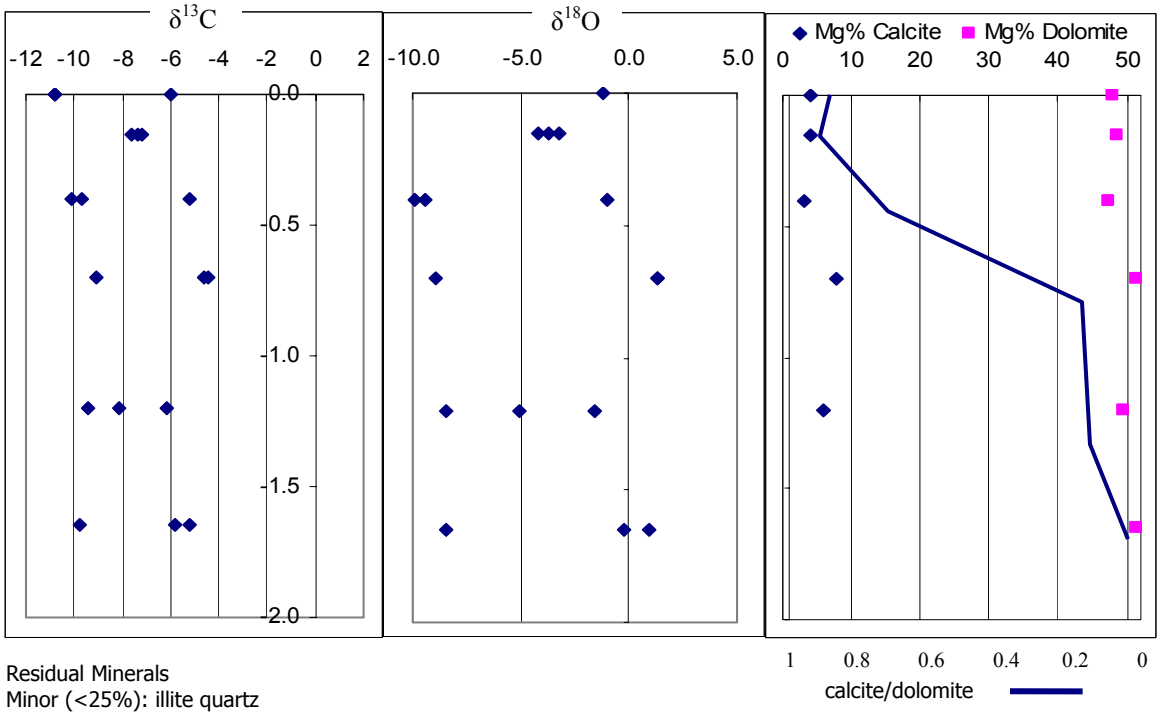

Residual Minerals
Minor (<25%): illite quartz
Trace (<5%): hematite goethite sepiolite

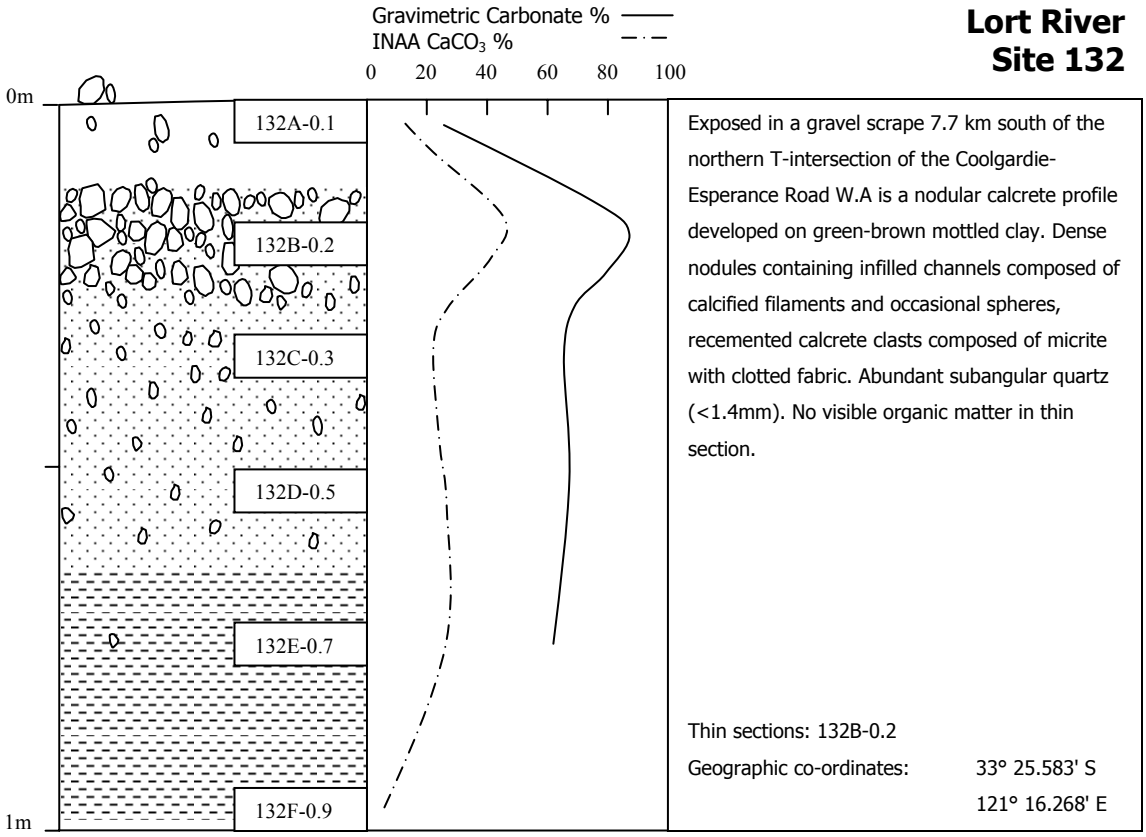

Lort River Site 132

Exposed in a gravel scrape 7.7 km south of the northern T-intersection of the Coolgardie-Esperance Road W.A is a nodular calcrete profile developed on green-brown mottled clay. Dense nodules containing infilled channels composed of calcified filaments and occasional spheres, recemented calcrete clasts composed of micrite with clotted fabric. Abundant subangular quartz (<1.4mm). No visible organic matter in thin section.

Thin sections: 132B-0.2

Geographic co-ordinates: 33° 25.583' S
121° 16.268' E

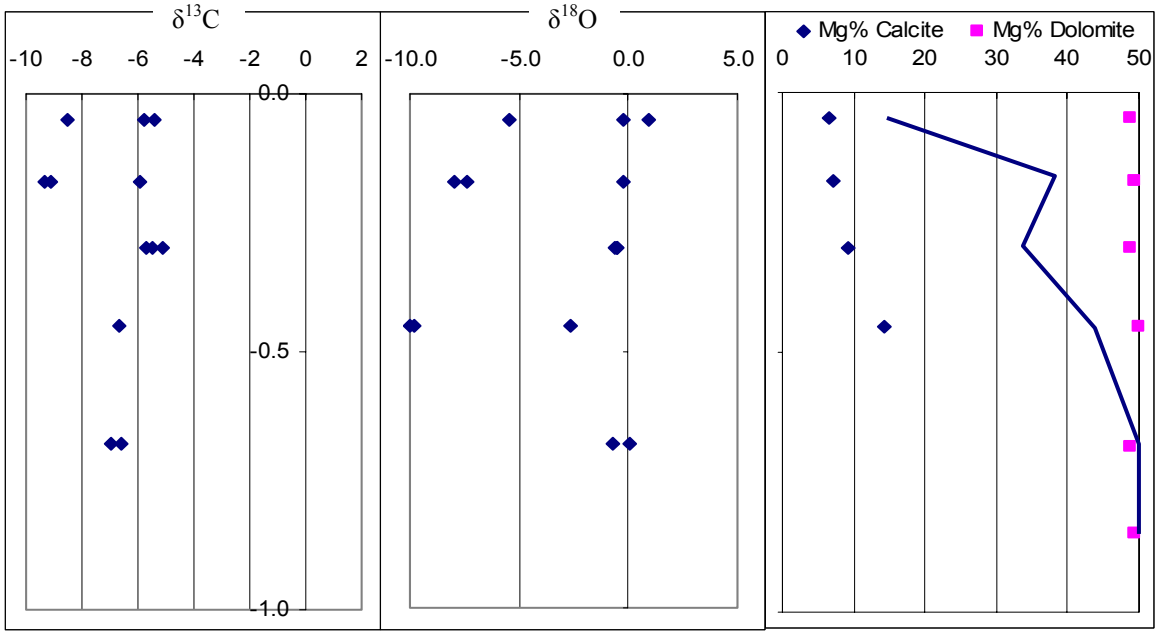

Residual Minerals
Minor (<25%): quartz illite
Trace (<5%): kaolinite feldspar goethite sepiolite

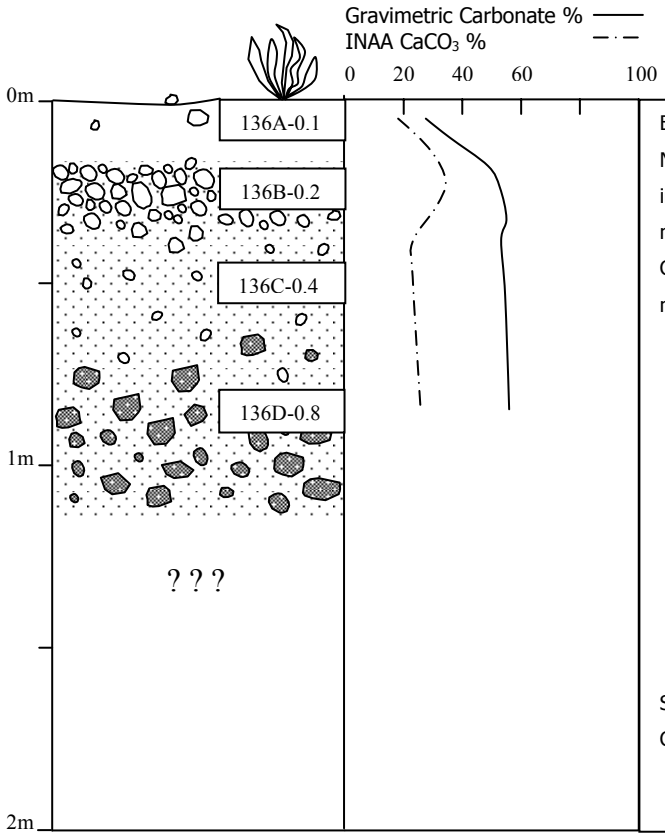

Norseman South
Site 136

Exposed in a dug channel 100 m south of the Norseman town sign W.A. is a profile composed of incipient nodules developed on brown sandy soil and mixed colluvial fragments. Vegetation is medium Salm Gum (*Eucalypt sp.*) woodland. No thin sections made.

SEM: 136C-0.4

Geographic co-ordinates: 32° 12.882' S
121° 46.680' E

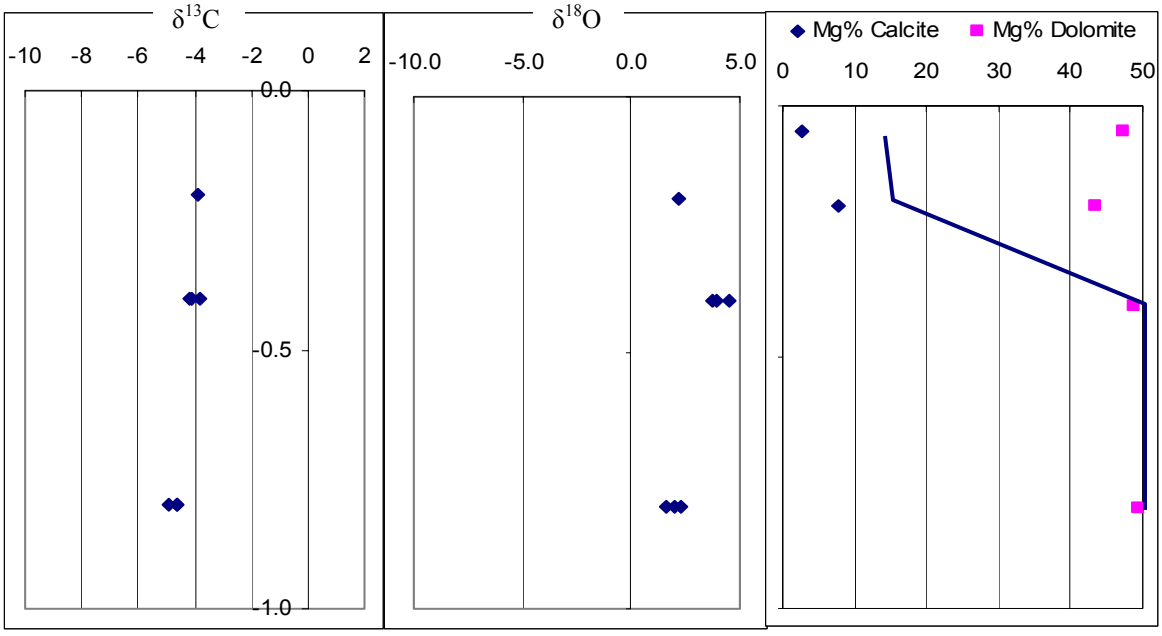

Residual Minerals
Minor (<25%): quartz illite hornblende feldspar
Trace (<5%): kaolinite hematite goethite

Ora Banda
Site 138

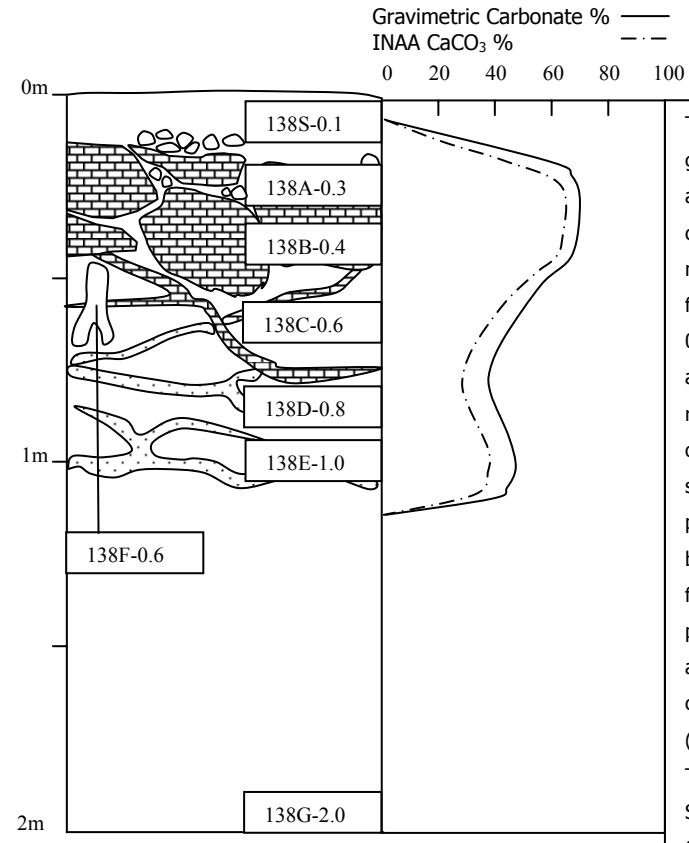

Two kilometres north of Ora Banda, in the W.A. goldfields region and exposed on the north face of an open pit mined for supergene gold, this calcrete profile is developed in clay with hematite nodules, weathered from and underlying thick ferruginous duricrust. The morphology between 0.2 and 0.5 m is massive semi-indurated nodules and boulders. Veins and stringers and occasional rhizoliths occur down to 1.1 m. SEM examination of massive nodules shows birds-nest and root-like structures and (P-type) needle-fibre calcite polycrystals. In thin section the nodules and boulders contain round clasts of hematite and floating quartz and the matrix is micritic and peloidal with open framework porosity. The veins and stringers are composed of strange sparitic crazed fabric. The vegetation is open Mulga (*Acacia* sp.) shrubland.

Thin sections: 138A-0.3, 138B-0.4, 138D-0.8

SEM: 138A-0.3, 138D-0.8

Geographic co-ordinates: 30° 21.548' S
121° 03.325' E

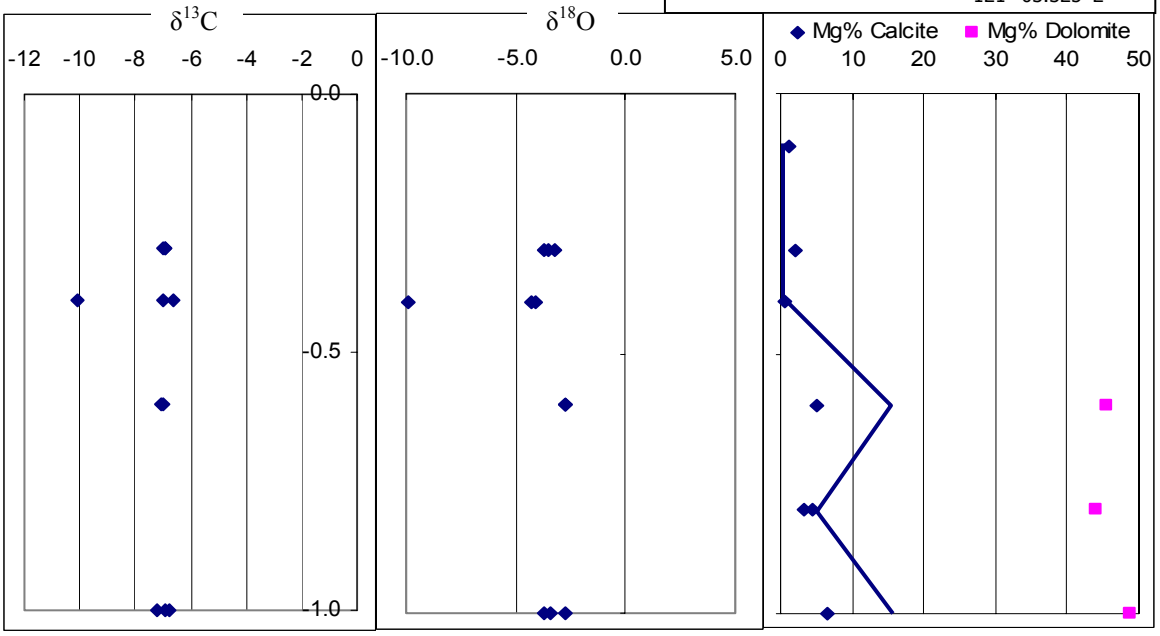

Residual Minerals
Minor (<25%): kaolinite hornblende quartz hematite
Trace (<5%): goethite

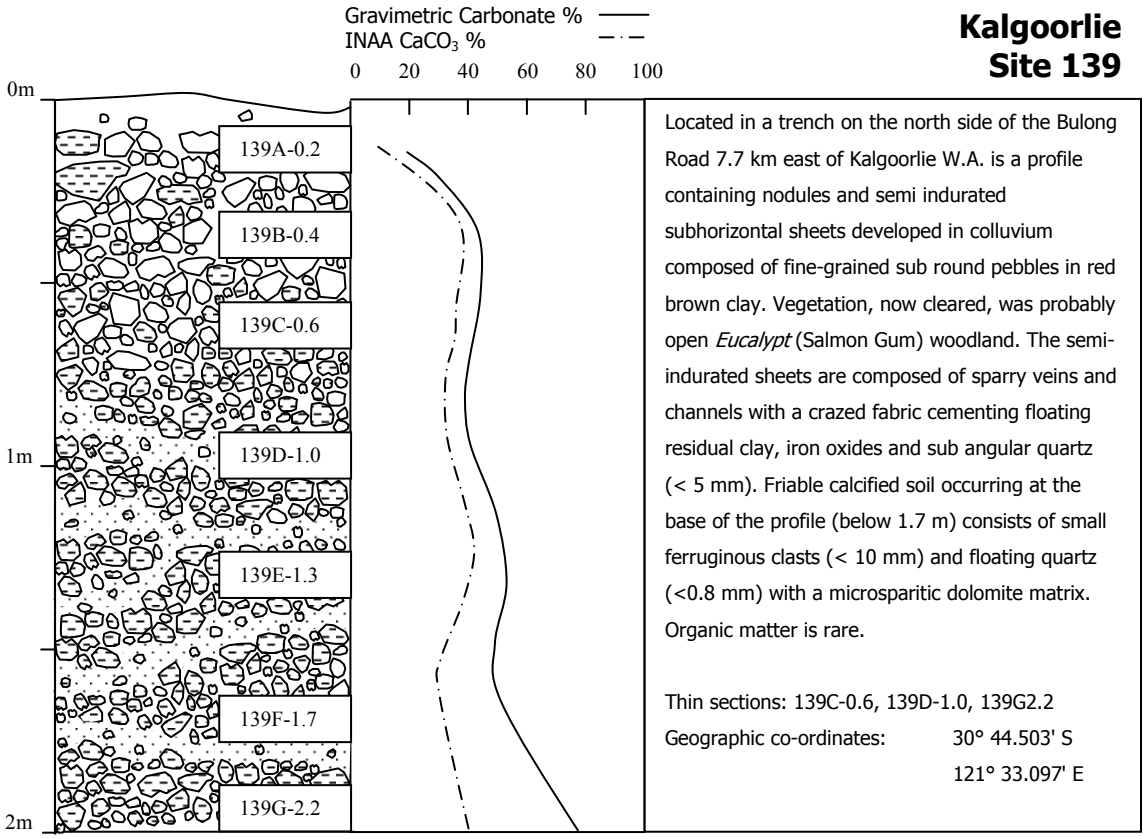

Kalgoorlie Site 139

Located in a trench on the north side of the Bulong Road 7.7 km east of Kalgoorlie W.A. is a profile containing nodules and semi indurated subhorizontal sheets developed in colluvium composed of fine-grained sub round pebbles in red brown clay. Vegetation, now cleared, was probably open *Eucalypt* (Salmon Gum) woodland. The semi-indurated sheets are composed of sparry veins and channels with a crazed fabric cementing floating residual clay, iron oxides and sub angular quartz (< 5 mm). Friable calcified soil occurring at the base of the profile (below 1.7 m) consists of small ferruginous clasts (< 10 mm) and floating quartz (<0.8 mm) with a microsparitic dolomite matrix. Organic matter is rare.

Thin sections: 139C-0.6, 139D-1.0, 139G2.2

Geographic co-ordinates: 30° 44.503' S
121° 33.097' E

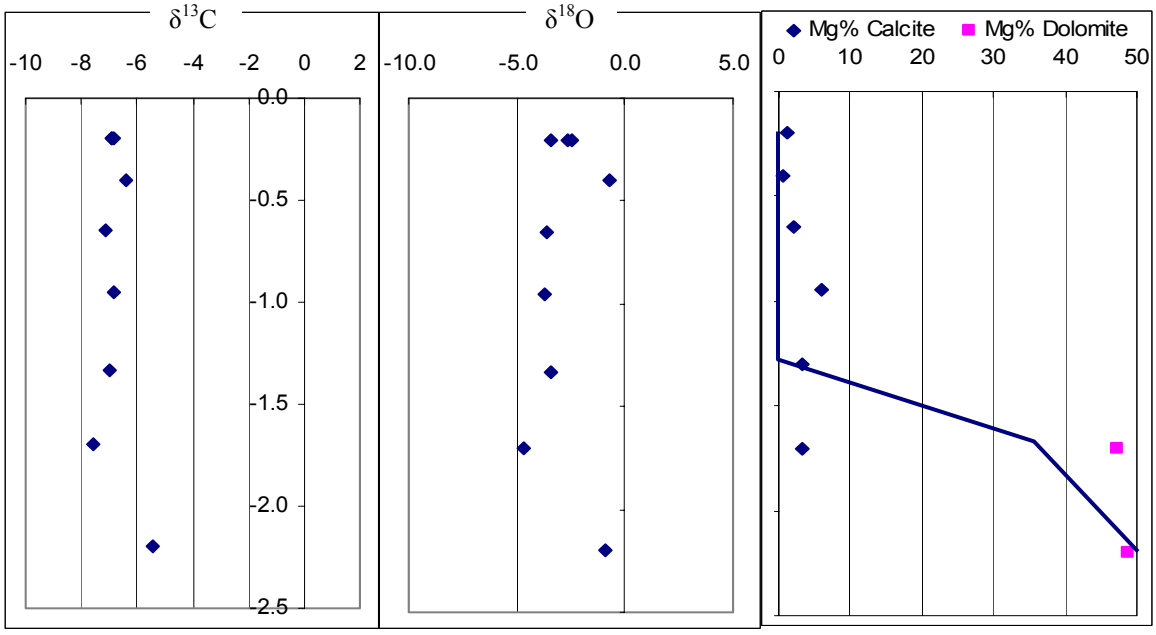

Residual Minerals
Minor (<25%): quartz illite kaolinite
Trace (<5%): hematite goethite palygorskite

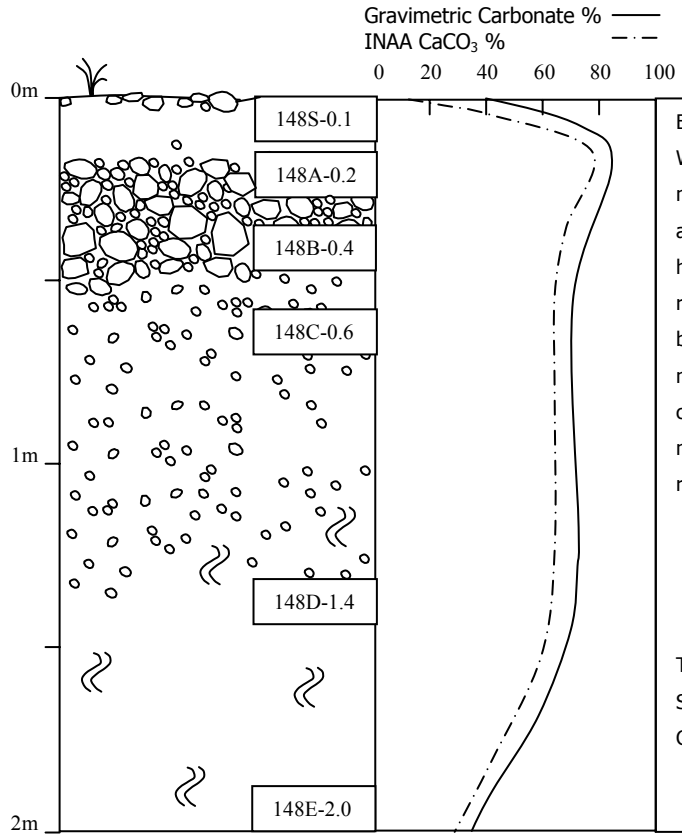

Menzies

Site 148

Exposed in a borrow pit 9.3 km west of Menzies, W.A., is a profile containing packed massive nodules down to 0.5 m overlying mottled powder and incipient nodules down to one metre. The host material is undifferentiated alluvial/fluvial red-brown clay and the vegetation is dominated by Mulga (*Acacia* sp.) shrubland. The upper nodules contain calcified filaments and dense clotted micrite with floating quartz. The incipient nodules contain remnants of plant intracellular replacement by calcite.

Thin sections: 148B-0.46

SEM: 148C-0.6

Geographic co-ordinates: 29° 42.429' S
120° 56.070' E

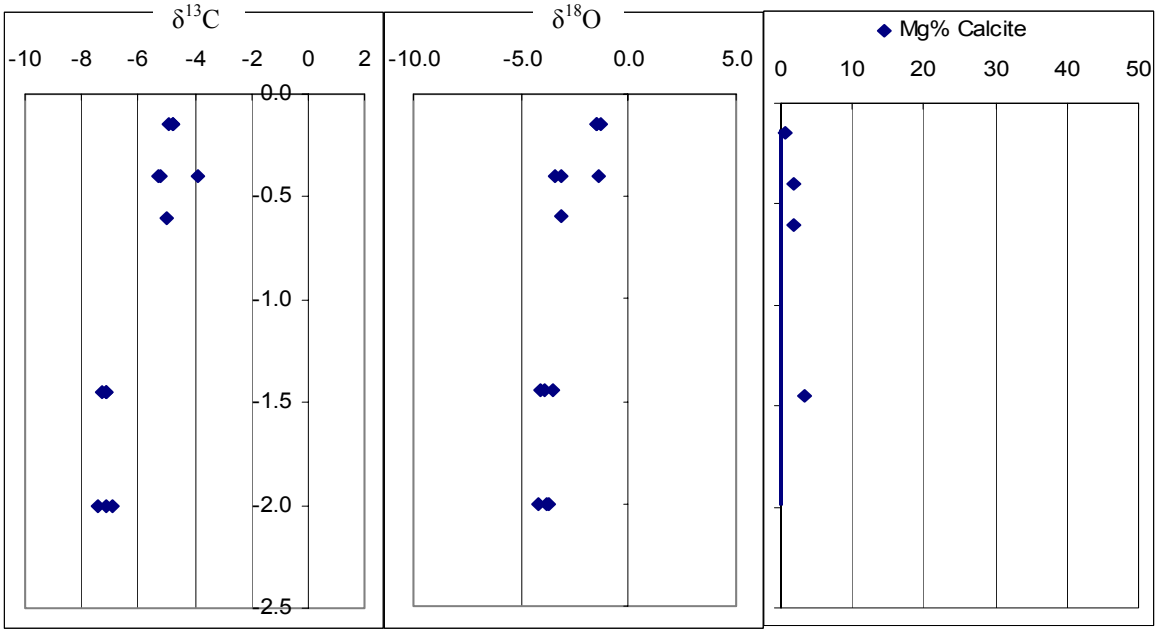

Residual Minerals
Minor (<25%): illite kaolinite quartz
Trace (<5%): palygorskite hematite feldspar

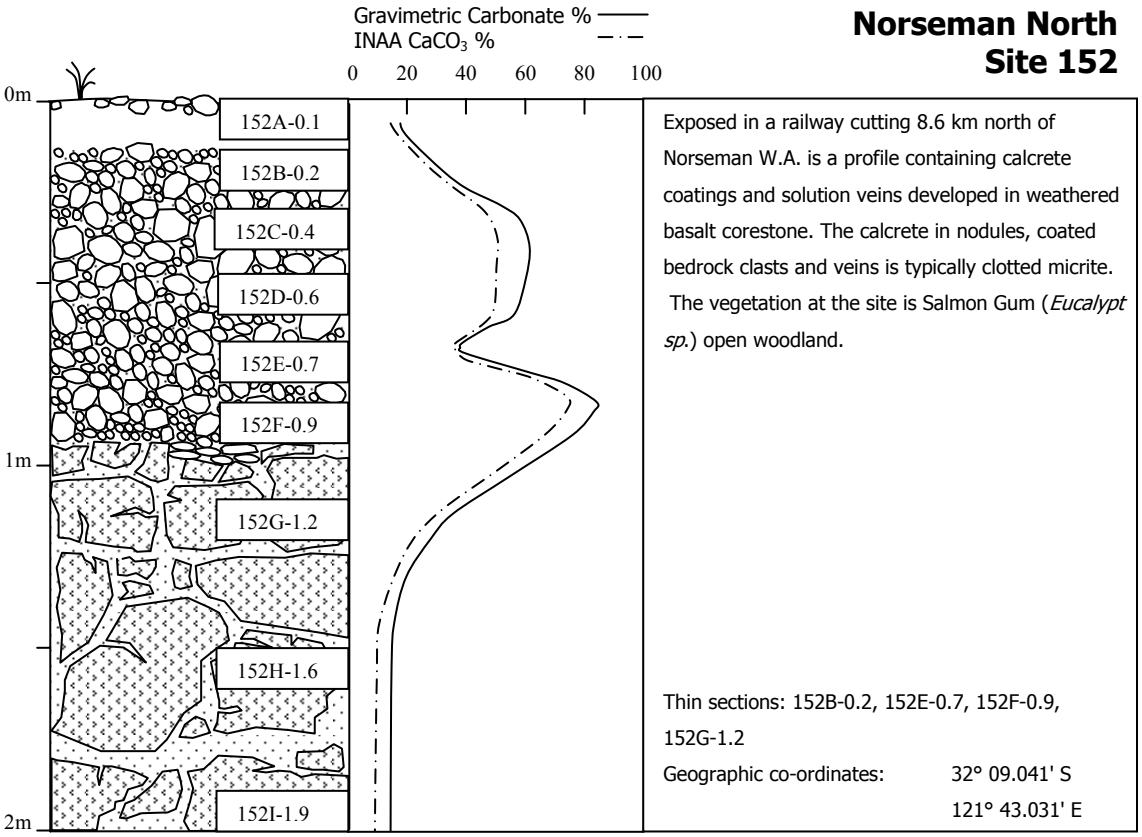

Norseman North Site 152

Exposed in a railway cutting 8.6 km north of Norseman W.A. is a profile containing calcrete coatings and solution veins developed in weathered basalt corestone. The calcrete in nodules, coated bedrock clasts and veins is typically clotted micrite. The vegetation at the site is Salmon Gum (*Eucalypt sp.*) open woodland.

Thin sections: 152B-0.2, 152E-0.7, 152F-0.9, 152G-1.2

Geographic co-ordinates: 32° 09.041' S
121° 43.031' E

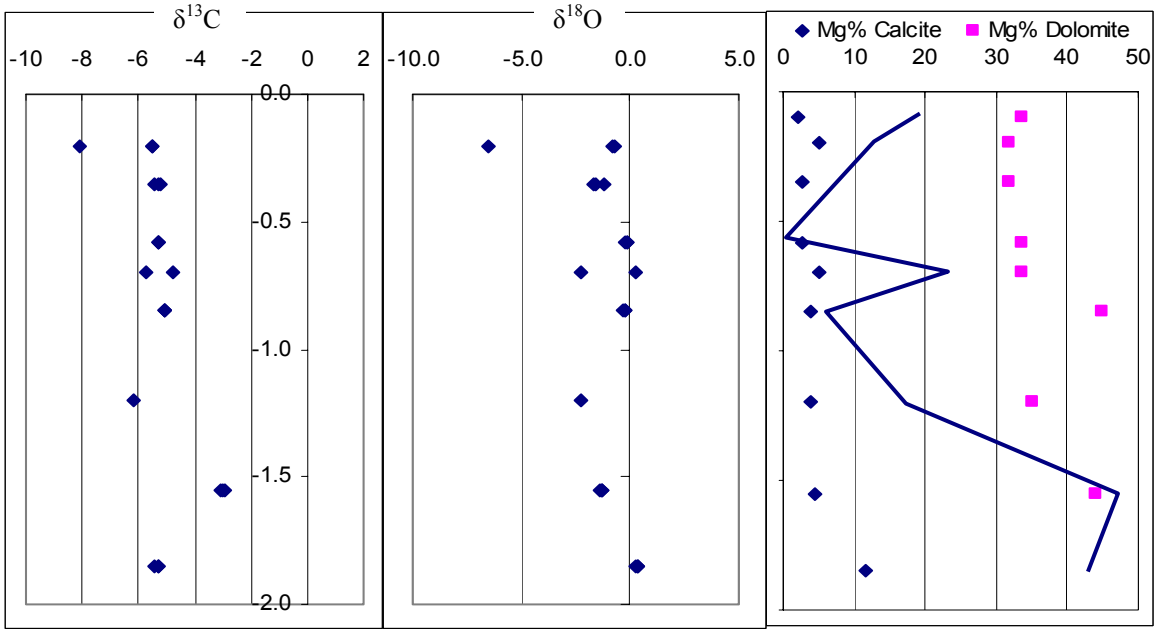

Residual Minerals
Minor (<25%): feldspar hornblende amphibole illite kaolinite
Trace (<5%): quartz palygorskite pyrophyllite goethite

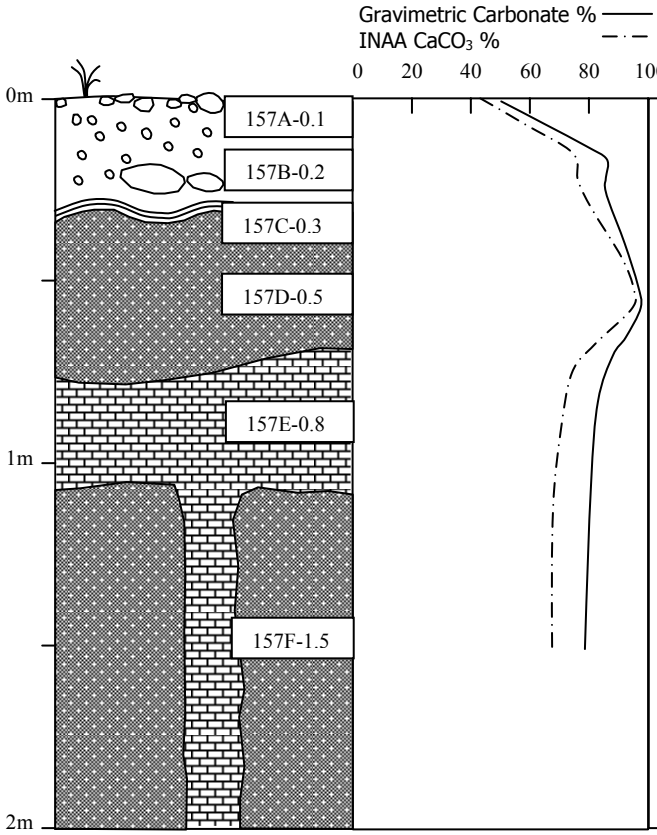

Caiguna West Site 157

Exposed in a quarry 140 km east of Balladonia on the Western Australian Nullarbor Plain is a profile containing pisoliths and a laminar layer developed on massive Nullarbor Limestone. Within the limestone dissolution has caused a horizontal layer (0.7 - 1 m) and vertical tube (0.3 - 1 m) infilled with indurated calcrete composed of massive cryptocrystalline and mottled clotted micrite with occasional calcified filaments, recemented clasts and floating subangular quartz (< 0.2 mm). Occasional organic matter is associated with voids and channels. The pisoliths and laminar calcrete is composed of micritzed calcified filaments, floating subangular quartz (< 0.2 mm) and dendritic organic matter. The vegetation is low chenopod shrub.

Thin sections: 157C-0.3, 157F-1.5

Geographic co-ordinates: 32° 19.347' S
125° 02.922' E

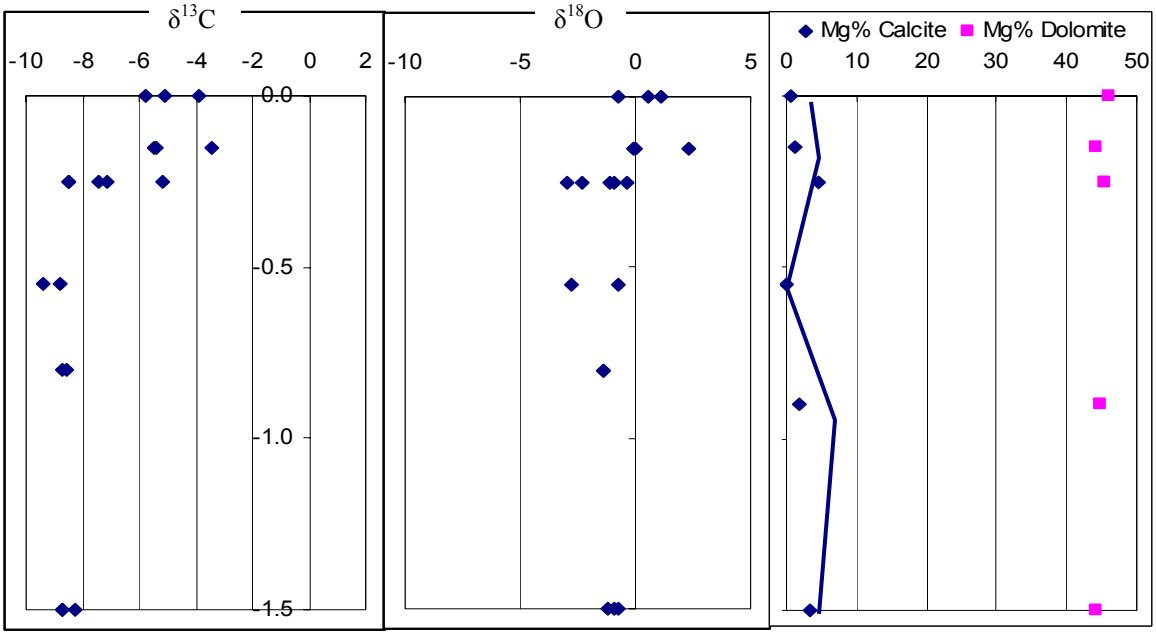

Residual Minerals
Minor (<25%): illite
Trace (<5%): quartz feldspar kaolinite sepiolite hematite

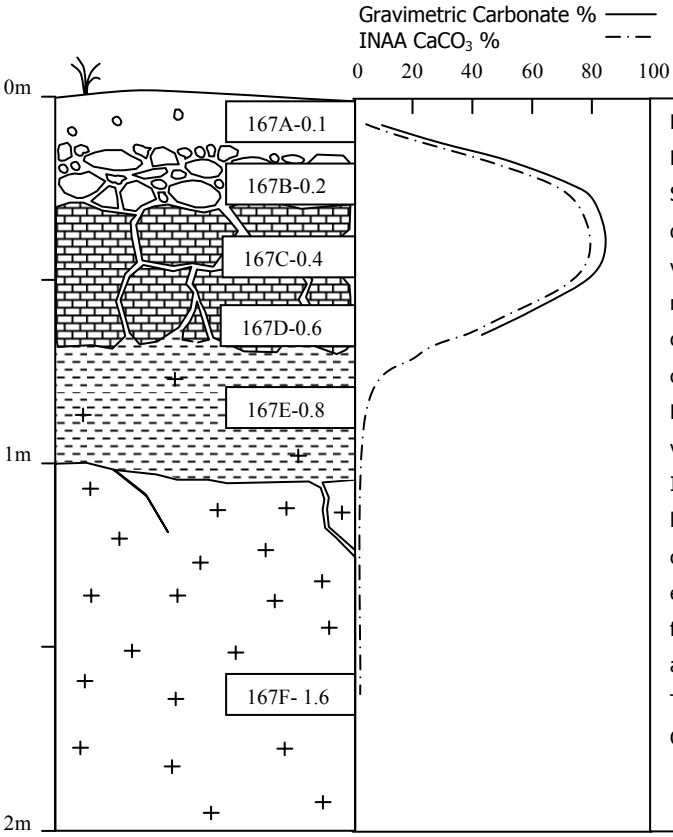

Yarwondutta Rocks
Site 167

Exposed in a granite quarry at Yarwondutta Rocks, 4 km north of Minnipa, Eyre Peninsula S.A., is a nodular and hardpan calcrete profile developed in coarse soil (weathered granite). The vegetation is *Eucalypt* (Mallee) woodland. The nodules are massive and composed of cryptocrystalline clotted micrite with abundant calcified filaments in channels and thin coatings. Floating sub round quartz (< 0.5 mm) and no visible organic matter occur in thin section. Internally the hardpan is composed of displaced large granitic quartz grains (< 10 mm) in a matrix composed of calcified filaments with a thick exterior coating also composed of calcified filaments. Occasional diffuse organic matter is associated with vughs and channels.

Thin sections: 167B-0.2, 167C-0.4

Geographic co-ordinates: 32° 48.944' S
135° 09.543' E

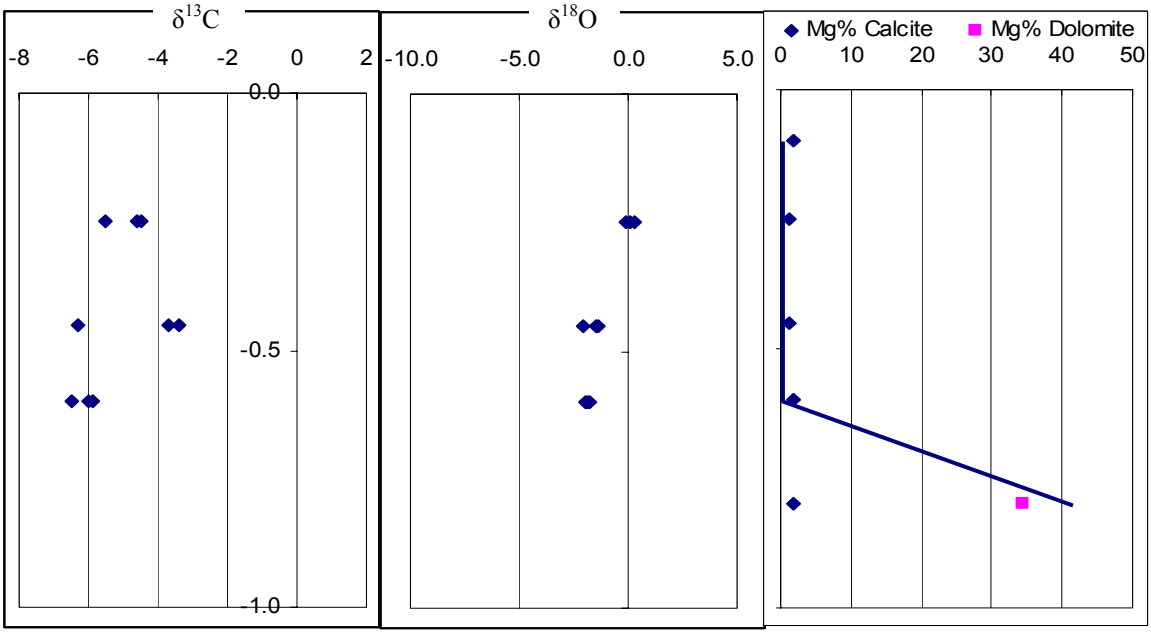

Residual Minerals
Minor (<25%): quartz feldspar illite
Trace (<5%): aragonite sepiolite kaolinite biotite

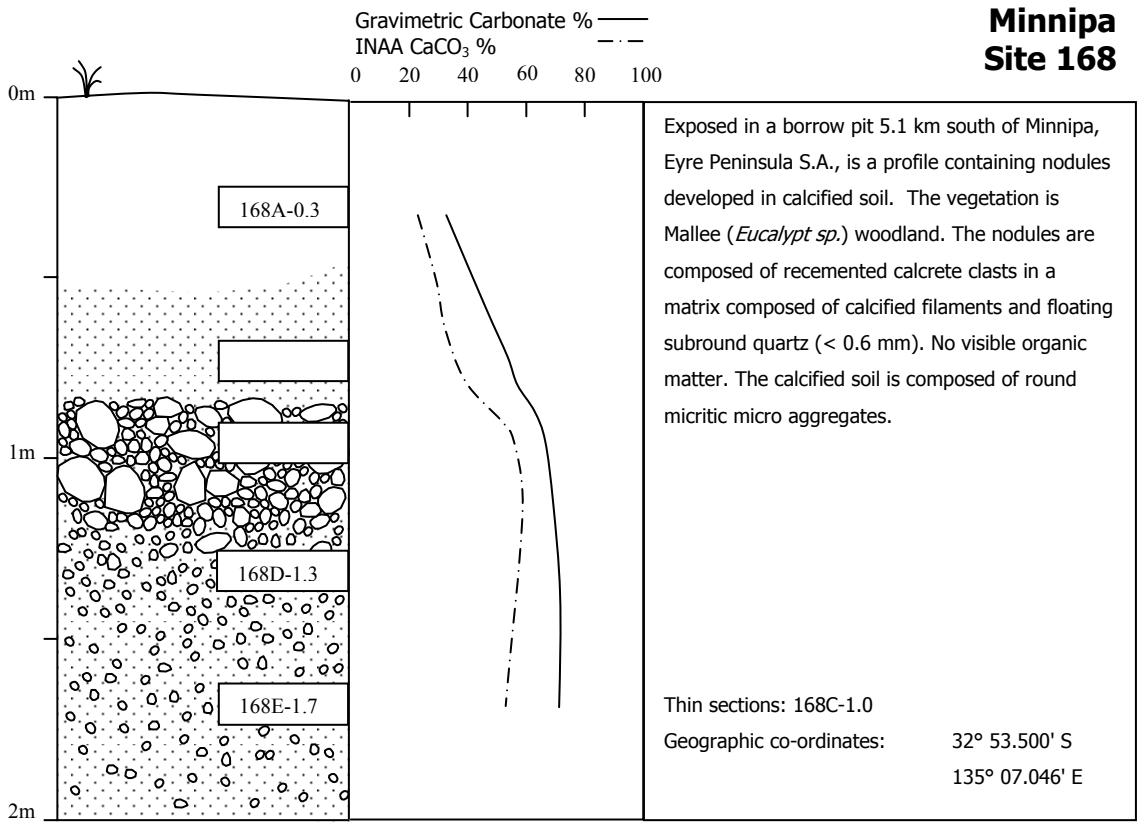

Minnipa
Site 168

Exposed in a borrow pit 5.1 km south of Minnipa, Eyre Peninsula S.A., is a profile containing nodules developed in calcified soil. The vegetation is Mallee (*Eucalypt sp.*) woodland. The nodules are composed of recemented calcrete clasts in a matrix composed of calcified filaments and floating subround quartz (< 0.6 mm). No visible organic matter. The calcified soil is composed of round micritic micro aggregates.

Thin sections: 168C-1.0

Geographic co-ordinates: 32° 53.500' S
135° 07.046' E

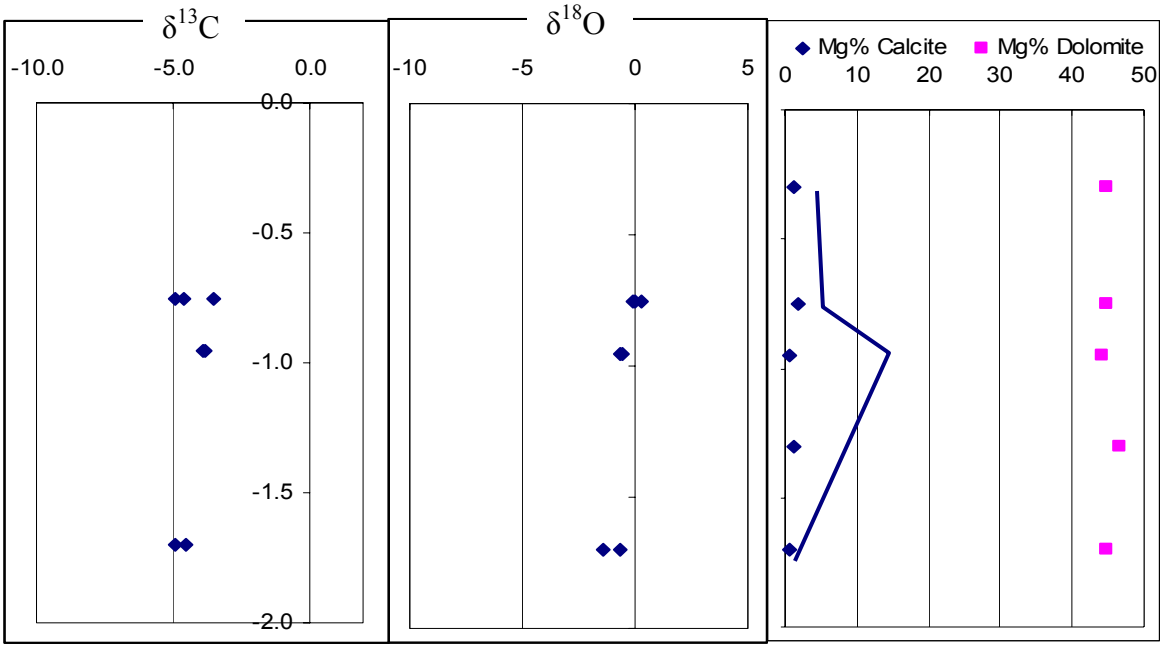

Residual Minerals
Minor (<25%): quartz feldspar
Trace (<5%): illite aragonite palygorskite sepiolite kaolinite goethite

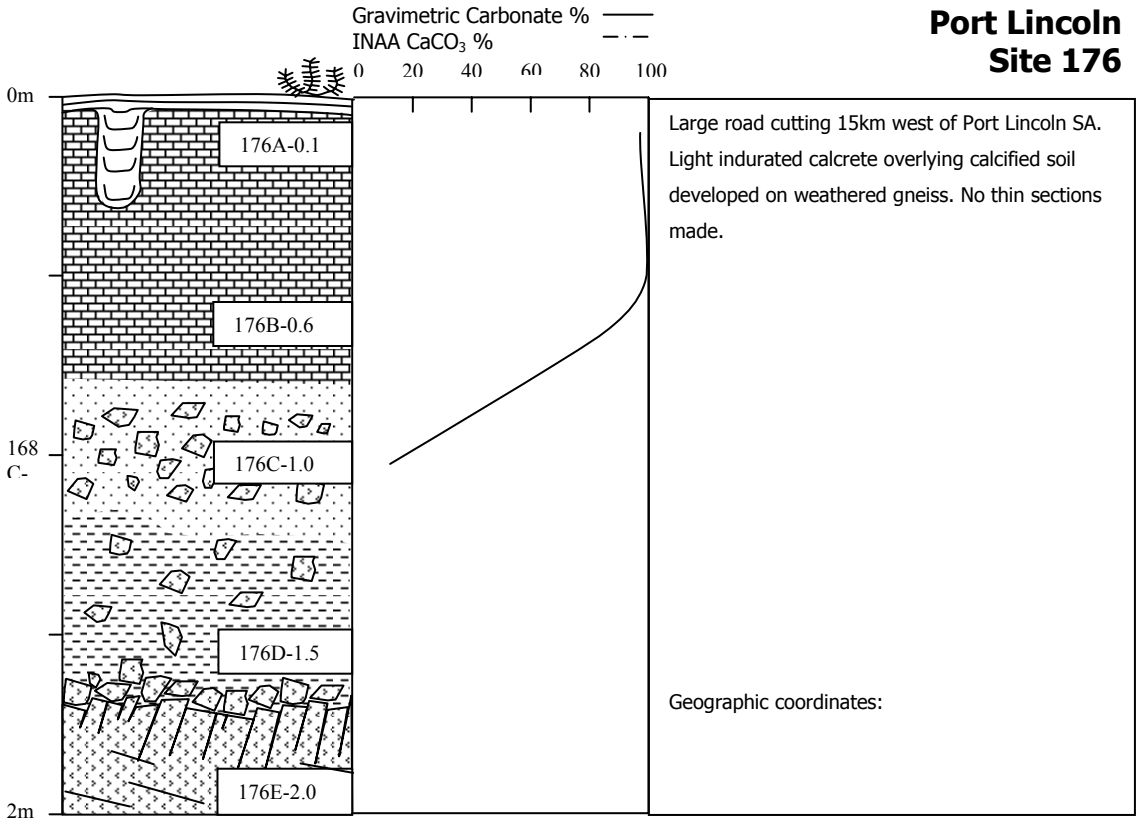

Port Lincoln
Site 176

Large road cutting 15km west of Port Lincoln SA. Light indurated calcrete overlying calcified soil developed on weathered gneiss. No thin sections made.

Geographic coordinates:

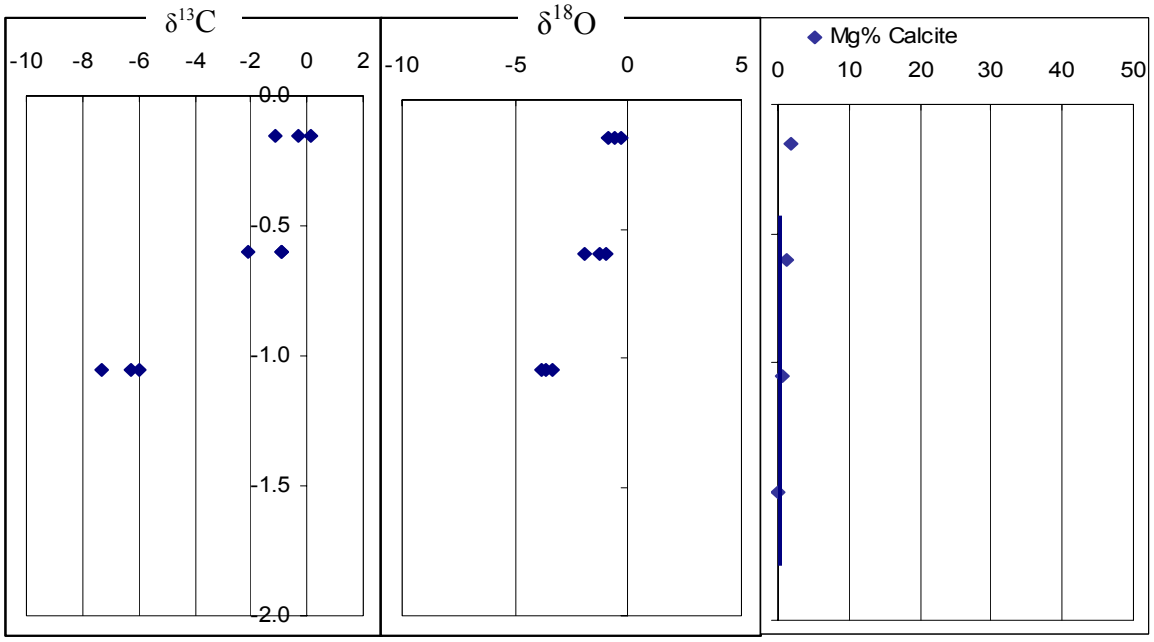

Residual Minerals
Minor (<25%): illite feldspar quartz
Trace (<5%):

Grab Samples

Fletchers Lake

Site 20

Geographic co-ordinates: 33° 49' 42.93" S
142° 04' 38.31" E

Exposed in a borrow pit on the east side of Wentworth-Pooncarrie road, NSW, 16km north of the Fletchers Lake intersection. Sample 20A-0.05 is a massive loose nodule; samples 20B-0.3 and 20C-0.6 are massive semi-indurated calcified soil; sample 20D-0.0 is a surficial lag nodule. No micro-morphological analysis made on these samples.

Pooncarrie South

Site 22

Geographic co-ordinates: 33° 39' 44.93" S
142° 26' 05.69" E

Exposed in a cutting on the west side of Wentworth-Pooncarrie road, NSW, 36km south of Pooncarrie. Massive hardpan calcrete overlying lithified sandstone, sample 22A-0.0 taken at surface. Sample analysed by thin section and SEM. At the base the sample is composed of grey micritic cement with spar-filled fractures, residual floating quartz grains (<0.5mm) and secondary goethite. A sharp horizontal boundary is overlain by brecciated packstone composed of clotted micrite and coated basal clasts. Calcified filaments are abundant in channels and coatings along with occasional calcified spheres and dendritic organic matter.

Cullulleraine

Site 24

Geographic co-ordinates: 34° 16' 35.95" S
141° 38' 58.46" E

Sampled on the north side of Sturt Highway 5km east of Lake Cullulleraine, Victoria are two soft powdery calcrete layers (sample 24A-0.2 and 24B-0.5) in sandy dune. No micro-morphological analysis made on these samples.

Monash

Site 28

Geographic co-ordinates: 34° 17' 35.58" S
140° 51' 31.61" E

10km north of Monash, SA, powder calcrete (sample 28A-0.5) developed in aeolian dune. No micro-morphological analysis made on this sample.

Tiverton Homestead

Site 38

Geographic co-ordinates: 32° 43' 22.01" S
139° 42' 48.05" E

Massive calcrete sampled from gully on the west side of the road heading south from Yunta, SA, 0.7km north of turnoff to Tiverton Homestead. Thin section 38B-0.4 of hardpan sampled at 0.4 to 0.5m is a massive packstone composed of calcite spar with granularic fabric and sub-angular to sub-round quartz (<0.7mm) and contains channel porosity and rare organic matter as diffuse and massive patches.

Manna Hill

Site 40

Geographic co-ordinates: 32° 31' 01.37" S
140° 03' 25.45" E

Sampled in a deep gutter on the NE side of track 0.75km SE of Oulnina Homestead toward Dlorah Downs is a semi-indurated calcified soil with small incipient nodules developed on steeply dipping (~45°) dolomitic siltstone. Thin section 40A-0.2 is small massive nodule composed of clotted micrite with sub-angular to sub-round quartz (<1.0mm).

Dlorah Downs Homestead

Site 43

Geographic co-ordinates: 32° 40' 13.34" S
140° 10' 23.83" E

Hardpan calcrete sampled in road gutter 5km north of Dlorah Downs Homestead (now abandoned), SA, in granitic terrain. Thin section 43D-0.2 is a massive packstone composed of clotted micrite with circumgranular cracking and occasional calcified filaments in channels, large clasts of recemented calcrete, granitic quartz grains (<10mm) and fine subround quartz (<0.25mm). No visible organic matter. Sample 44A-0.1 is a surficial laminar calcrete developed as sheets on granitic terrain 1.0km south of Dlorah Downs Homestead. No micro-morphological analysis made on these samples.

Canegrass Dam

Site 47

Geographic co-ordinates: 32° 36' 14.24" S
140° 23' 20.21" E

Exposed in gutter on the east side of road 13.4km north-east of Canegrass Dam. Proterozoic sediments cemented and veined with laminar calcrete rinds (sample 47A-0.1). No micro-morphological analysis made on this sample.

Burra

Site 50

Geographic co-ordinates: 33° 41' 22.26" S
138° 55' 43.23" E

Exposed on an eroded embankment in a colluvial slope 1.2kms south of Burra, SA, is a massive indurated (eroded?) calcrete Thin section and SEM of sample 50A-0.5 is a massive packstone composed of calcite spar with granularic fabric and sub-angular to sub-round quartz (<0.7mm) and contains channel porosity and rare organic matter as diffuse and massive patches.

Mannum

Site 56

Geographic co-ordinates: 32° 40' 13.34" S
140° 10' 23.83" E

Exposed in a road cutting 3.2km east of Murray River Bridge at Mannum, SA, is a thin hardpan (56A-0.1) calcrete overlying yellow calcareous soils (ex limestone?). No micro-morphological analysis was made on these samples.

Morgan

Site 63

Geographic co-ordinates: 33° 57' 47.0" S
139° 34' 49.7" E

Exposed in a road cut 12.3km west of Morgan, SA, on road to Burra, is a profile containing incipient nodules and powdery mottles (samples 63A-0.1, 63B-0.3 63C-0.55 and 63D0.85) in red-brown sandy clay with iron nodules. No micro-morphological analysis was made on these samples.

Wirrealpa South

Site 70

Geographic co-ordinates: 31° 20' 12.1" S
138° 58' 05.9" E

Exposed in a small scrape on the east side of road, south of Wirrealpa, SA, is a nodular calcrete (samples 70A-0.2, 70B0.4 and 70C-0.65) developed in alluvial sheets in a large flat alluvial area. No micro-morphological analysis was made on these samples.

Wirrealpa North

Site 71

Geographic co-ordinates: 31° 09' 17.5" S
138° 56' 33.3" E

Sampled from gravel pits located southwest of Wirrealpa, SA, on track south of homestead is a hardpan calcrete (sample 71-A0.1) developed in alluvial sheets in a large flat alluvial area. No micro-morphological analysis was made on this sample.

Kingoonya Dacite Quarry

Site 82

Geographic co-ordinates: 30° 55' 53.8" S
135° 31' 37.8" E

Exposed at the surface of a large quarry 21.4km west of Glendambo Highway turnoff toward Kingoonya, SA, then due north for 0.9km. Sample analysed by thin section and SEM. Surficial carbonate (sample 82A-0.1) composed of channels and colloform/undulose layers of spar and calcified filaments cementing carbonate clasts (< 0.15mm) of microspar with granularic and clotted fabrics. Sub-round to sub-angular quartz (<0.5mm) and occasional dendritic and filamentous organic matter.

Kambalda Turnoff

Site 116

Geographic co-ordinates: 31° 18.324' S
121° 30.325' E

Exposed in a small pit 2.2km north of Kambalda turnoff from the Norseman-Coolgardie road, WA. Boulders (sample 116A-0.2), nodules (samples 116B-0.2 and 116C-0.55) and taproot fragments (sample 116D-0.0) developed in soil on greenstone bedrock terrain. No micro-morphological analysis was made on these samples.

Lake Cobham

Site122

Geographic co-ordinates: 33° 27.246' S
119° 16.774' E

Located in a shallow pit 100m west of mine entry at gypsum mine at Lake Cobham, WA. Nodular calcrete (sample 122B-0.25) overlying calcified soil (samples 122C-0.7 and 122D-0.9) developed in gypsiferous dune. No micro-morphological analysis was made on this sample.

Salmon Gums South

Site134

Geographic co-ordinates: 33° 08.815' S
121° 42.336' E

Located in large gravel pit 100m from the west side of Esperance Highway, WA, 19.5 km south of Salmon Gums. Massive nodules (samples 134B-0.45 and 134C-0.8) developed in kaolinitic clay saprolite. Internally the nodules are composed of fenestral-like fabric (resembling replaced cells) composed of a micritic framework with void-filling microspar. Common floating sub-round to sub-angular quartz (<1.5mm) and in-filled channels containing of calcified filaments. No visible organic matter.

Broad Arrow

Site 137

Geographic co-ordinates: 30° 25.981' S
121° 17.170' E

Exposed in a road cutting 4.6km west of the Kalgoorlie-Menzies Highway along Ora Banda Road, WA, are platy and nodular surficial calcrete and thick indurated veins penetrating ferruginous duricrust down to 1.0m. Calcrete nodule (sample 137A-0.2) composed of grey micrite and microspar with normalic fabric cementing corroded hematite clasts (<3.0mm) and sub-round quartz (<0.3mm). No visible organic matter. Calcareous veins (samples 137C-0.9) composed of massive carbonate with peloidal fabric with occasional calcified filaments and fenestral-like micrite and micospar present as infilled channels. Sub-round hematite clasts (<15mm) and fine sub-angular quartz (<0.35mm) and diffuse organic matter present in channels and fissures. Laminated surficial crust (sample 137E-0.2) composed of irregular and discontinuous horizontal channels containing peloidal micrite and calcified filaments

and sub-round hematite clasts (<15mm) and fine sub-angular quartz (<0.35mm) and dendritic organic matter inter-layered with ferruginous duricrust.

Kanowna

Site 144

Geographic co-ordinates:

Calcretized saprock/saprolite. Platy structure with abundant fragments of weathered host rock and ferruginous clasts. Random mesh fabric ith preserved/calcified roots and infilled channels containing filaments, sub-round quartz (<1.0mm) and dendritic and filamentous organic matter in channels and vughs.

Bardoc

Site 145

Geographic co-ordinates:

Bardoc disused mine 15km north of Ora Banda turnoff along Kalgoorlie-Menzies Highway. Carbonate veins in mottled ferruginous red and green mottled clay on greenstone bedrock terrain. Calcretized saprock/saprolite with platy structure (sample 145B) containing abundant fragments of weathered host rock and ferruginous clasts. Internal fabric is a porous peloidal and random mesh with preserved/calcified roots and infilled channels containing filaments, sub-round quartz (<1.0mm) and dendritic and filamentous organic matter in channels and vughs.

Riverina

Site 150

Geographic co-ordinates: 29° 43.475' S

120° 49.976' E

Exposed in borrow pits on the northern side of the road heading 19.6km west of Menzies, WA, is a nodular and hardpan calcrete overlying semi-indurated stringers penetrating into red-brown hardpan. Internally the hardpan and nodules (samples 150A-0.4 and 150E-0.1) are complex and composed of recemented pisoliths and interstitial cement with dense clotted micrite and floating sub-round to sub-angular quartz (<1.0mm). Calcified filaments are abundant in pisoliths and channels whereas organic matter and calcified spheres occur rarely.

Fraser Range

Site 155

Geographic co-ordinates: 32° 02.154' S

122° 45.508' E

Exposed on the south side of the Eyre Highway, 98.5km east of Norseman, WA, are sheetlike calcrete hardpan developed directly on slightly weathered gneiss (sample 155B-0.1). No micro-morphological analysis was made on this sample.

Balladonia

Site 156

Geographic co-ordinates: 32° 21.233' S

123° 36.983' E

Exposed in a gravel scrape directly opposite the Balladonia motel/service station, WA, is a profile composed of loose calcrete pisoliths developed in red-brown sand (samples 156A-0.1, 156B-0.28, 156C-0.58 and 156D-0.9). No micro-morphological analysis was made on these samples.

Madura

Site 159

Geographic co-ordinates: 31° 53.861' S
127° 01.033' E

Exposed on a steep slope on the north side of the Eyre Highway, 70m west of the Madura Hotel, WA, is a thick calcrete developed on Nullarbor limestone. The calcrete (sample 159A-0.5 and 159B-1.25) consists of cemented boulders and laminated/platy crusts internally consisting massive, dense micritic calcrete with peloids and abundant calcified filaments and occasional sub-angular quartz (<0.4mm). Organic matter was not visible in thin section. The limestone below a sharp contact at 1.25m is composed of micritised allochems.

Nundroo

Site 163

Geographic co-ordinates: 31° 48.471' S
132° 14.278' E

Small cutting on the south side of Eyre Hwy, SA, 2.2km east of Nundroo Roadhouse. Dense pisolitic calcrete composed of calcified filaments and dense micritic cement.

Wirrulla

Site 166

Geographic co-ordinates: 32° 24.303' S
134° 30.919' E

South side of Eyre Hwy, SA, 1.1km west of Wirrulla. No micro-morphological analysis was made on this sample.

Appendix II: Stable Carbon and Oxygen Isotope Results

Site	Depth (m)	SOM $\delta^{13}C$	Carbonate $\delta^{13}C$	Carbonate $\delta^{18}O$	Calcrete Description ? = possible inaccurate isotope results
Nyah West (Site1)					
A	0.3m	-24.3	-5.6	-2.3	massive nodules, loose, semi indurated
B	0.57m	-23.46	-5.3	-2.4	mottled powder
C	0.88m	-24.1	-5.3	-1.5	mottled powder
D	1.07m	-23.4	-5.2	-1.1	massive nodules, loose, semi indurated
			-5.3	-2.8	massive nodules, loose, semi indurated
			-5.5	-2.4	massive nodules, loose, semi indurated
			-5.6	-2.6	massive nodules, loose, semi indurated
E	1.4m		-6.1	-3.3	mottled powder
F	1.7m		-6.3	-0.3	mottled powder
G	1.85m		-5.6	-0.2	mottled powder
			-4.7	-0.9	mottled powder
			-5.3	-2.5	mottled powder
			-4.7	-1.2	mottled powder
H	2.07m		-6.1	-2.7	mottled powder
I	2.45m		-5.9	-1.5	mottled powder
K	0.5m		-5.8	-1.1	rhizolith, taproot fragment 2cm diameter
			-5.2	-1.7	rhizolith, taproot fragment 2cm diameter
			-5.4	-1.6	rhizolith, taproot fragment 2cm diameter
			-5.3	-1.8	rhizolith, taproot fragment 2cm diameter
			-3.4	-2.7	rhizolith, taproot fragment 2cm diameter
			-3.4	-2.9	rhizolith, taproot fragment 2cm diameter
			-5.5	-1.8	rhizolith, taproot fragment 2cm diameter
Carwarp (Site19)					
A	0.3m	-24	-5.4	-5.9	massive nodules, loose, semi indurated
B	0.53m	-25			mottled fine carbonate
C	0.77m	-24.5	-3.8	-2.9	massive nodule, loose, semi indurated
			-4	-3.2	massive nodule, loose, semi indurated
D	1.02m		-4.2	-2	mottled fine powder
			-4.5	-4.2	mottled fine powder
E	1.34m		-4.7	-2.7	mottled fine powder
F	1.8m		-5.7	-3.8	mottled fine powder
G	2.16m		-4.4	-2.2	massive nodule, loose, semi indurated
H	2.43m		-4.6	-1.8	mottled fine powder
I	2.65m		-5.1	-3	mottled fine powder
Fletchers Lake (Site20)					
A	0.05m	-22	-3	-2.1	massive loose nodule
B	0.3m		-3.3	-2.7	massive, semi-indurated calcified soil
C	0.6m		-4.1	-0.9	massive, semi-indurated calcified soil
D	0m		-3.5	-2.7	surface lag nodule
Pooncarrie South (Site22)					
	0.1m		-1.3	-1.8	laminar rind in hardpan
			-2.9	-3.1	laminar rind in hardpan
			-2.9	-2.6	spar clast
			-4.9	-2.6	spar clast
			-3.1	-3	laminar rind in hardpan
			-4.4	-3.3	laminar rind in hardpan
			-4.7	-3.5	laminar rind in hardpan

Site	Depth (m)	SOM	Carbonate		Calcrete Description
		$\delta^{13}C$	$\delta^{13}C$	$\delta^{18}O$	
Cullulleraine (Site 24)					
	0.5m	-23.2	-4.5	-3.6	fine powder
			-4.2	-3.1	fine powder
Renmark (Site26)					
A	0.2m	-22.4	-3.5	-1.3	laminar rind on pisolith
			-3.5	-1.6	laminar rind on pisolith
			-2.9	-0.4	pisolith core
B	0.5m	-23	-5.3	-2.2	interstitial micrite between pisos
			-5.1	-2.6	laminar rind in boulder
			-5.4	-2.7	nodule core in pisolith
			-4.8	-2	laminar rind on pisolith
			-4.8	-1.7	laminar rind on pisolith
			-4.9	-1.9	laminar rind on pisolith
			-4.4	-1.3	laminar rind on pisolith
			-4.4	-1.4	laminar rind on pisolith
			-4.4	-1	laminar rind on pisolith
C	0.7m		-5.4	-3	laminar rind on nodule
F	2.55m		-0.6	4.9	laminar dolomitic carbonate
			0.5	3.6	laminar dolomitic carbonate
			0.4	3.4	laminar dolomitic carbonate
			-0.7	2.4	laminar dolomitic carbonate
			-0.8	4.3	laminar dolomitic carbonate
			-0.9	4.2	laminar dolomitic carbonate
Monash (Site28)					
		-22.9	-4.9	-4.3	fine powder
Waikerie (Site 30)					
A	0.3m	-21.9	-4.1	-1.2	laminar rind on cemented pisolith
			-5	0.4	black intraclast
			1.3	-0.1	laminar rind on cemented pisolith
			-4.4	-0.5	laminar rind on cemented pisolith
			-4.2	-1.4	laminar rind on cemented pisolith
B	1m	-22	-5.9	-1.9	laminar rind on cemented pisolith
C	1.7m		-5.9	-4.5	massive dense hardpan
D	2.4m		-3.7	-0.2	pink carbonate in cavity of green claystone
E	2.8m > OM		-3.9	0	pink carbonate in cavity of green claystone
Gandy Range Homestead (Site 33)					
A	0.1m > OM		-2.9	-1.8	laminar rind on nodule
			-5.2	-1.6	laminar rind on nodule
			-3.1	-1.8	laminar rind on nodule
B	0.3m > OM		-5	-2.4	massive dense micrite in nodule
			-3.2	-2	massive dense micrite in nodule
			-3.6	-2.5	massive dense micrite in nodule
			-3.2	-2	massive dense micrite in nodule
			-8.1	-6.3	massive dense micrite in nodule
C	0.9m		-0.5	4.5	dolomitic limestone
			-0.8	4.2	dolomitic limestone
			-1.4	-3.1	dolomitic limestone
			-1.7	-3.6	dolomitic limestone
			-1.4	-3	dolomitic limestone

Site	Depth (m)	SOM	Carbonate		Calcrete Description
		$\delta^{13}C$	$\delta^{13}C$	$\delta^{18}O$	
D	2.5m		1	4.9	dolomitic limestone
			0.2	4.9	dolomitic limestone
			0.4	4.7	dolomitic limestone
E	3.0m		-0.3	3.7	dolomitic limestone
			-0.4	3.6	dolomitic limestone
			-0.4	3.5	dolomitic limestone
Triverton Homestead (Site 38)					
	0.4m		-7.4	-5	massive cement
			-7.5	-5.2	massive cement
Yunta (Site 39)					
A	0.2m				
B	0.35m		-3.2	-1.2	massive dense micrite in nodule
			-0.5	-1.8	massive dense micrite in nodule
C	0.5m	-21			
F	1.35m		-4.1	-1	massive dense micrite in nodule
G	1.5m	-7.1			
Manna Hill (Site 40)					
A	0.2m		-3.6	-0.5	massive nodule, loose, semi indurated
B	0.5m				
Dlorah Downs Homestead (Site 43)					
B	0.2m		-2.3	0.9	fine powder
D		-21.7	-4	-1.2	dense micrite in massive hardpan
E			-2.6	-4.1	dense micrite in massive hardpan
	0.1m	-21.1	-4.1	-2.6	laminar rind
	0.1m	-30.19	-3.7	0.4	laminar rind
			-4.3	-2.7	dense micrite in massive hardpan
	0.3m	-24.7	-5.4	-1.7	laminar rind
Burra (Site 50)			-6.8	-3.9	massive columnar hardpan
	0.5m		-0.9	-3	massive hardpan
Blanchetown South (Site 51)					
Z	0.1m	-22.7	-4.3	-3.9	laminar rind in sheetlike hardpan
			-4.3	-1.3	laminar rind in sheetlike hardpan
Blanchetown East (Site 52)					
A	0.1m		-4.9	-1.8	laminar rind on nodule
B	0.35m	-22.2	-6.1	-2.9	laminar rind on nodule
			-5.3	-1.8	nodule core
C	0.6m	-22.4	-3.9	-2.1	massive, semi-indurated calcified soil
D	0.84m		-3.4	-2.4	massive, semi-indurated calcified soil
Long Ridge (Site 53)					
A	0.1m		-6.9	-2.3	
			-7.4	-2.6	
B	0.5m		-6.5	-2.2	
			-6.4	-3	
C	0.9m		-7.1	-2.6	laminar rind in hardpan
			-7.6	-2.3	laminar rind in hardpan
			-3.4	-0.5	soft micrite
			-1.8	-1.8	hard micrite

Site	Depth (m)	SOM	Carbonate		Calcrete Description
		$\delta^{13}C$	$\delta^{13}C$	$\delta^{18}O$	
Long Ridge (Site 54)					
A	0.2m	-23.4	-6.5	-1	laminar rind on nodule
			-3.4	-1.7	veined nodule interior
			-3.1	-2.4	veined nodule interior
B	0.4m	-22.7	-5.3	-3	massive, semi-indurated calcified soil
			-4.8	-2.9	
C	0.7m	-22.9			
D	1m	-21.8	-5.5	-3.4	fine powder
			-5.3	-1.7	fine powder
E	1.5m	-23.2			
Black Hill (Site 55)					
A	0.15m	-20.1	-3.8	-1.4	hardpan, cemented pisoliths
B	0.45m	-22.1	-4.3	-2.8	hardpan, cemented pisoliths
C	0.85m		-5	-0.3	nodules in powder
D	1.25m		-5	-0.2	powder
E	1.65m	-26.9	-0.5	4.1	dolomite clast
			-3.5	-1.4	micrite
			-5.1	-0.1	soft dolomite
Mannum (Site 56)					
A	0.1m	-21.6	-5	-2	hardpan, cemented nodules
			-4.4	-1.7	
B	0.33m		-5.2	-2.5	massive nodules
C	0.5m		-4.8	-1.3	powder and small nodules
D	0.9m		-4.7	-1.2	yellow lime soil
E	1.25m				yellow lime soil
Tailem Bend (Site 57)					
A	0.1m	-22.5	-5	-1.3	oolitic outer coating on surface of hardpan
			-5.3	-2	laminar rind on surface of hardpan
			-3.8	-1	dark brown dense micrite in hardpan
			-4.3	-1.1	dark brown dense micrite in hardpan
			-4.9	-1.6	dark brown dense micrite in hardpan
			-4.7	-1.6	dark brown dense micrite in hardpan
			-4.9	-2	dark brown dense micrite in hardpan
			-5	-3.1	black intraclast
B	0.3m		-5.4	-1.2	nodules
C	1m	-23.2	-6.1	-3.6	massive, semi-indurated calcified soil
			-4.6	-0.9	massive, semi-indurated calcified soil
			-4.6	-0.8	massive, semi-indurated calcified soil
			-4.8	-1.2	massive, semi-indurated calcified soil
D	1.45m		-5.3	0.3	massive, semi-indurated calcified soil
E	1.75m		-5.6	0.4	massive, semi-indurated calcified soil
F	2m		-6.8	-1.2	dolomite clast in hardpan
			-5.6	-1.9	dense micrite in hardpan
			-7	-2.6	laminar rind
			-6.2	-2.3	spar vein
			-6	-2.2	dense micrite in hardpan
			-6.3	-2.4	dense micrite in hardpan
			-6.1	-2.2	dense micrite in hardpan
G	3m	-24.43			Nodules
H	5m	-21.65			Lime soil

FIELD TRIP 2: South Australia (Flinders Ranges, Gawler Craton and southeast plains)

Site	Depth (m)	SOM	Carbonate		Calcrete Description
		$\delta^{13}C$	$\delta^{13}C$	$\delta^{18}O$	
Morgan (Siite 63)					
A	0.1m		-1.5	1.6	loose powdery nodules
B	0.3m		-4	1.2	loose powdery nodules
			-4	0.8	loose powdery nodules
			-3.9	0.6	loose powdery nodules
C	0.55m				Mottled powder and R-B clay
D	0.85m				R-B clay and Fe-nodules
E	1.3m		-3.8	1.4	mottled fine powder
			-3.1	0.9	mottled fine powder
Wirrealpa South (Site 70)					
A	0.2m		-1.1	-2.8	massive dense micrite in loose nodule
B	0.4m		-1.6	-1.9	massive dense micrite in loose nodule
C	0.65m		-1.4	-2.4	massive dense micrite in loose nodule
Wirrealpa North (Site 71)					
	0.2m		-2.4	-1.6	massive dense micrite in hardpan
	0.2m	-21.7	-2.7	-0.6	laminar rind in hardpan
Wirramina (Site 75)					
A	0.3m				hardpan, sheetlike
B	0.5m	-21.9			
C	0.6m	-23.1	-4.8	-1.9	platy or sheetlike hardpan
D	0.9m				
E	1.1m		-5.6	-4.5	massive, semi-indurated calcified soil
Glendambo North (Site 78)					
A	0.05m	-20.7	-5.7	-1.7	hardpan, cemented nodules
			-4.3	-2.1	?
			-4.7	-3.1	?
B	0.3m	-21.7	-4.3	-1.1	?semi-indurated veins
			-6	-2.7	?
C	0.45m	-21.2	-3.3	-1.5	?semi-indurated veins
D	0.7m				semi-indurated veins
E	1m				lthified R-B sandstone
Kingoonya West (Site 80)					
A	0.1m		-2.2	-1	laminar
			-2.9	-1.1	massive
			-1.7	0.1	?hardpan, sheetlike
B	0.53m	-21.9	-5.6	-3.4	massive semi-indurated veins
			-5.6	-2.9	?
C	1.06m	-22.2	-4.6	-2.2	?semi-indurated veins
D	2m				fresh volcanics
Tarcoola Railway Quarry (Site 81)					
A	0.14m	-22.5	-5.9	-3.4	massive hardpan, sheetlike
			-4.5	-2.1	?
			-5.4	-2.7	?
B	0.3m	-22.6	-5.3	-3.6	massive hardpan, sheetlike
			-5.6	-2.5	?
			-5.3	-2.6	?
C	0.5m	-22.1	-5.6	-4	?massive cement/ semi-indurated veins
			-5.1	-3.2	?massive cement/ semi-indurated veins
D	0.85m	-21.3	-5	-4.2	?massive cement/ semi-indurated veins

Site	Depth (m)	SOM	Carbonate		Calcrete Description
		$\delta^{13}C$	$\delta^{13}C$	$\delta^{18}O$	
Tarcoola Railway Quarry (Site 81) cont.					
			-2.5	-3.1	?massive cement/ semi-indurated veins
E	1.1m	-22.9	-3.7	-3.8	massive cement/ semi-indurated veins
			-2.6	-3.6	?massive cement/ semi-indurated veins
			-3.4	-3.4	?massive cement/ semi-indurated veins
F	1.5m		-7.7	-4.6	weathered bedrock
			-7.4	-3.7	weathered bedrock
G	3m				fresh bedrock
Kingoonya Dacite Quarry (Site 82)					
	0.1m	-30.64			surficial calcrete
Kingoonya South (Site 84)					
A	0.42m	-21.7	-6.8	-2.4	massive hardpan, cemented nodules
			-6.8	-2.3	?massive hardpan, cemented nodules
B	0.65m	-22	-3.6	-2.1	?massive hardpan, cemented nodules
C	1.05m	-23.6	-5.3	-2.7	massive hardpan, cemented nodules
			-7	-4.2	?massive hardpan, cemented nodules
Kokatha (Site 87)					
A	0.2m	-21.8	-3.8	-1.5	?massive hardpan, cemented nodules
			-3.3	-1.2	?
			-2.7	0	?
B	0.45m	-22.1	-3.4	-2	massive hardpan, cemented nodules
			-2.9	-2.1	?
C	0.8m		-3.2	-0.9	?nodules and semi-indurated cement
D	1.1m		-5.4	-5.4	?nodules and semi-indurated cement
Lake Everard (Site 90)					
A	0.4m	-20.8	-2.5	1	?coated dacite clasts
B	0.77m	-22.6	-4.7	-2.4	coated dacite clasts
			-3.9	-0.9	massive internal cement
C	0.98m	-23.2			fine sand and powder
D	1.18m	-23.3			fine sand
E	1.45m				fine sand
Kimba East (Site 93)					
A	0.5m	-20.9			hardpan, cemented nodules
B	0.64m	-21.3			hardpan, cemented nodules
C	0.83m	-22.5			nodules
D	1.02m	-22			nodules
E	1.25m	-23.2			nodules
Mary Burts Corner (Siite 94)					
A	0.1m	-21.2	-6.4	-1.1	massive hardpan, cemented nodules
B	0.37m		-4.9	-1.9	massive hardpan, cemented nodules
C	0.5m		-5	-2.2	massive hardpan, cemented nodules
Kallora (Site 95)					
A	0.4m	-20.7	-5.4	-3.8	massive semi-indurated
			-8.8	-3.5	massive semi-indurated
			-8.1	-2.9	massive semi-indurated
B	0.6m	-22.2			massive semi-indurated
C	0.9m				powder
D	1.2m	-20.5	-5.7	-3.6	powder
			-5.8	-3.7	powder
E	1.5m		-5.4	-2.3	powder

Site	Depth (m)	SOM	Carbonate		Calcrete Description
		$\delta^{13}C$	$\delta^{13}C$	$\delta^{18}O$	
Balaklava (Site 96)					
A	0.3m	-21.6	-4.6	-2.3	laminar rind on cemented pisolith
			-4.7	-4.3	laminar rind on cemented pisolith
			-5	-3.8	laminar rind on cemented pisolith
			-5.8	-2.5	laminar rind on cemented pisolith
			-5.6	-2.4	massive interstitial cement
			-4.7	-2.4	massive interstitial cement
B	0.52m		-5.3	-2.6	laminar rind on cemented pisolith
			-4.2	-2.3	massive interstitial cement
C	0.9m		-5.6	-2.7	laminar rind on cemented pisolith
			-5.5	-2.7	laminar rind on cemented pisolith
			-4.9	-2.5	laminar rind on cemented pisolith
			-5	-1.4	massive interstitial cement
			-5	-2.5	massive interstitial cement
			-6	-2.9	massive interstitial cement
			-5.8	-2.6	massive interstitial cement
Bute (Site 98)					
A	0.4m	-22.8	-6.2	-2.9	laminar rind on nodule
B	0.75m	-23	-6.5	-2.8	massive dense micrite in nodule
			-6.6	-3.3	laminar rind on nodule
C	1.05m		-6.6	-3	massive semi-indurated calcified soil
D	1.5m		-6	-2.1	massive semi-indurated calcified soil
E			-7	-3.8	massive semi-indurated calcified soil
X		-22.1			powder in aeolian dune (nearby)
Kadina (Site 101)					
A	0.45m	-22.1	-7	-2.5	massive dense micrite in hardpan
			-7	-2.7	massive dense micrite in hardpan
			-6.7	-2.3	massive dense micrite in hardpan
			-4.4	-2.7	laminar rind in hardpan
B	0.7m		-6.4	-2.4	laminar rind in hardpan
			-5	-2.5	laminar rind in hardpan
			-4.9	-2.5	laminar rind in hardpan
			-6.8	-2.7	massive dense micrite in hardpan
			-7	-2.9	laminar rind in hardpan
			-7.2	-3.2	laminar rind in hardpan
C	0.9m		-6.3	-2.4	massive dense micrite in hardpan
			-7	-2.9	massive dense micrite in hardpan
D	1.3m	-21.3	-8	-4.3	massive semi-indurated calcified soil
			-7.9	-3.3	massive semi-indurated calcified soil
E	1.75m		-6.9	-2.5	massive semi-indurated calcified soil
Moonta (Site102)					
AA	0.05m		-7	-2.5	laminar rind in hardpan
			-6.6	-2.4	massive interstitial cement
			-6.7	-2.4	laminar rind in hardpan
			-6.3	-2.4	laminar rind in hardpan
			-6.6	-2.7	massive interstitial cement
			-5.6	-0.8	laminar infill cavity or channel
A	0.3m		-6.9	-4.3	laminar rind in hardpan
			-7.3	-3.2	massive dense micrite in hardpan
B	0.57m		-9.1	-4.8	massive dense micrite in hardpan

Site	Depth (m)	SOM	Carbonate		Calcrete Description
		$\delta^{13}C$	$\delta^{13}C$	$\delta^{18}O$	
Moonta (Site102) cont.					
C	0.8m		-7.2	-2.8	massive dense micrite in hardpan
			-8.2	-4.1	laminar rind in hardpan
			-7.1	-3.1	massive dense micritic nodule
D	1.04m		-8	-3.9	laminar rind in hardpan
			-8.5	-3	massive dense micritic nodule
E	1.35m		-7	-2	massive dense micritic nodule
			-8	-3	massive dense micritic nodule
Stansbury (Site 106)					
A	0.3m		-4.9	-3.5	massive dense micrite in hardpan
B	0.5m		-6.8	-3.5	laminar rind in hardpan
			-3.4	-3.1	laminar rind in hardpan
			-7.4	-4	massive dense micrite in hardpan
C	0.7m		-8.5	-4.4	massive semi-indurated calcified soil
D	1.05m		-8.9	-4.4	massive semi-indurated calcified soil
E	1.25m		-8.1	-3.2	massive semi-indurated calcified soil
Yorketown (Site 107)					
A	0.55m		-5.8	-1.5	massive semi-indurated calcified soil
B	0.75m		-5	-0.8	massive semi-indurated calcified soil
C	0.98m		-5.4	-1.3	massive semi-indurated calcified soil
D	1.4m		-6	-2.4	massive semi-indurated calcified soil
E	1.7m		-5.3	-1.1	massive semi-indurated calcified soil
Melton (Site 110)					
A	0.55m		-9.4	-6.3	platy, undulose thick (1 - 2 cm) laminations
			-10.8	-9.4	platy, undulose thick (1 - 2 cm) laminations
			-10	-8.6	platy, undulose thick (1 - 2 cm) laminations
B	0.8m		-7.2	-3.8	platy, undulose thick (1 - 2 cm) laminations
			-6.7	-2.7	platy, undulose thick (1 - 2 cm) laminations
			-6.8	-2.7	platy, undulose thick (1 - 2 cm) laminations
			-8.9	-5.9	platy, undulose thick (1 - 2 cm) laminations
C	1.05m		-9.5	-7.4	platy, undulose thick (1 - 2 cm) laminations
D	1.6m				massive limestone
Field Trip 3: South Australia and Western Australia (Gawler Craton and Yilgarn Craton)					
Whyte-Yarcowie (Site 112)					
AA	0.2m		-3	-2.8	massive dense micrite in hardpan
			-2.8	-2.6	massive dense micrite in hardpan
			-3.3	-0.7	massive dense micrite in hardpan
A	0.25m		-3.3	-2.9	massive dense micrite in hardpan
			-3.8	-3.2	massive dense micrite in hardpan
			-3.9	-3.7	massive dense micrite in hardpan
B	0.45m		-2.6	-3.4	massive dense micrite in hardpan
			-3.1	-3.3	massive dense micrite in hardpan
			-2.9	-3.2	massive dense micrite in hardpan
C	0.75m		-3	-3	massive semi-indurated calcified soil
			-2	-2.9	massive semi-indurated calcified soil
			-2.2	-2.8	massive semi-indurated calcified soil
Kimba North-West (Site 113)					
B	0.35m		-4.1	-1.1	massive dense micrite in nodule
			-4.3	-0.5	massive dense micrite in nodule

Site	Depth (m)	SOM	Carbonate		Calcrete Description
		$\delta^{13}C$	$\delta^{13}C$	$\delta^{18}O$	
Kimba North-West (Site 113) cont.					
			-4.4	-0.6	massive dense micrite in nodule
C	0.5m		-4.8	-1.3	massive dense micrite in nodule
			-3.8	-1.7	massive dense micrite in nodule
			-4.4	-1.5	massive dense micrite in nodule
D	0.68m		-3.2	-1.8	massive semi-indurated calcified soil
			-2.5	-1.9	massive semi-indurated calcified soil
			-3.8	-2.1	massive semi-indurated calcified soil
E	0.88m		-3.4	-2.1	massive semi-indurated calcified soil
			-3.8	-2.2	massive semi-indurated calcified soil
			-3.3	-2.4	massive semi-indurated calcified soil
F	1.1m		-3.9	-1.9	mottled fine powder
			-2.5	-2.1	mottled fine powder
Buckleboo-Kyancutta (Site 114)					
B	0.33m		-5.5	-2.8	massive dense micrite in nodule
			-4.9	-1.9	massive dense micrite in nodule
			-4.6	-2.9	massive dense micrite in nodule
			-2.4	1.3	laminar coating on nodule
			-1.1	0.8	laminar coating on nodule
			-1.3	0.9	laminar coating on nodule
C	0.56m		-3.4	-2.6	massive dense micrite in nodule
			0.7	-2.2	massive dense micrite in nodule
D	0.76m		-5.5	-3.7	massive dense micrite in nodule
			-5.4	-3.6	massive dense micrite in nodule
			-4.9	-3.3	massive dense micrite in nodule
E	1.1m		-4.4	-2.9	massive semi-indurated calcified soil
			-4.3	-2.7	massive semi-indurated calcified soil
			-5	-3.3	massive semi-indurated calcified soil
F	1.4m		-2	-2.4	mottled fine powder
			-2.3	-2	mottled fine powder
			-2.3	-2.4	mottled fine powder
Pinkawillinie (Site 115)					
A	0.4m	-23	-4.8	-1.2	red-brown sandy loam with fine powder
			-3.8	0	red-brown sandy loam with fine powder
			-4	-0.4	red-brown sandy loam with fine powder
B	0.75m	-20.5	-3.3	-2.8	massive semi-indurated nodules
			-3.8	-2.6	massive semi-indurated nodules
			-3.6	-2.4	massive semi-indurated nodules
C	1m	-17.7	-5.1	-4.3	massive semi-indurated nodules
			-4.6	-3.4	massive semi-indurated nodules
			-5	-3.7	massive semi-indurated nodules
D	1.3m	-23.2	-5.4	-3.6	fine powder
			-6	-3.9	fine powder
			-5.6	-3.7	fine powder
Kambalda Turnoff (Site 116)					
A	0.2m	-21.3	-6	-2.1	massive dense micrite in boulder
			-5.9	-1.7	massive dense micrite in boulder
			-6.1	-2.2	massive dense micrite in boulder
B	0.2m	-21.6	-5.8	-0.2	massive dense micrite in nodule
			-5.9	-0.3	massive dense micrite in nodule

Site	Depth (m)	SOM	Carbonate		Calcrete Description
		$\delta^{13}C$	$\delta^{13}C$	$\delta^{18}O$	
Kambalda Turnoff (Site 116) cont.					
			-6.2	-0.7	massive dense micrite in nodule
C	0.55m		-4.6	-0.1	massive semi-indurated nodules
			-4.6	0	massive semi-indurated nodules
			-4.7	-0.2	massive semi-indurated nodules
D	0m		-4.8	-0.5	rhizolith, taproot fragment (5cm diameter)
			-4.9	-0.7	rhizolith, taproot fragment (5cm diameter)
			-4.7	-0.4	rhizolith, taproot fragment (5cm diameter)
Tammin (Site 118)					
B	0.65m		-6.7	-1	massive dense dolomitic nodules
			-6.9	-1.5	massive dense dolomitic nodules
			-6.8	-1.3	massive dense dolomitic nodules
C	0.9m		-6.5	-0.4	massive dense dolomitic nodules
			-6.3	-0.3	massive dense dolomitic nodules
			-6.6	-0.3	massive dense dolomitic nodules
D	1.3m		-6.6	-1.4	massive dense dolomitic nodules
			-6.6	-1.4	massive dense dolomitic nodules
			-6.6	-1.2	massive dense dolomitic nodules
E	1.7m		-6.4	-1.2	massive dense dolomitic nodules
			-6.5	-1.2	massive dense dolomitic nodules
			-6.4	-1	massive dense dolomitic nodules
Dumbleyung (Site 119)					
A	0.1m	-25.5			
B	0.3m	-23.6	-8.5	-3.5	massive semi-indurated calcified soil
			-8.4	-3.3	massive semi-indurated calcified soil
			-8.4	-3.4	massive semi-indurated calcified soil
C	0.53m	-23	-8	-2.8	massive semi-indurated calcified soil
			-8.1	-2.9	massive semi-indurated calcified soil
			-8.1	-3	massive semi-indurated calcified soil
D	0.85m	-23.1	-8.2	-3.1	massive semi-indurated stringers
			-8.3	-3.2	massive semi-indurated stringers
			-8.4	-3	massive semi-indurated stringers
Lake Magenta (Site 122)					
A	0.15m	-23.9			
B	0.25m	-22.5	-7.1	-2.9	massive dense micrite in nodules
			-7	-2.8	massive dense micrite in nodules
			-7	-2.7	massive dense micrite in nodules
C	0.7m		-6.9	-2.6	massive dense micrite in nodules
			-7	-2.6	massive dense micrite in nodules
			-6.9	-2.7	massive dense micrite in nodules
D	0.9m		-6.7	0	massive semi-indurated calcified soil
			-6.4	0.1	massive semi-indurated calcified soil
			-5.6	1.1	massive semi-indurated calcified soil
Peak Charles (Site 127)					
B	0.25m	-21.6	-5.2	0.9	massive dense micrite in nodules
			-5.2	0.8	massive dense micrite in nodules
			-4.9	0.6	massive dense micrite in nodules
C	0.48m				
D	0.68m				
E	0.97m		-5	-0.1	massive dense micrite in nodules

Site	Depth (m)	SOM	Carbonate		Calcrete Description
		$\delta^{13}C$	$\delta^{13}C$	$\delta^{18}O$	
Peak Charles (Site 127) cont.					
			-5.1	-0.2	massive dense micrite in nodules
F	1.3m		-8.5	-6.4	massive dense micrite in nodules
			-6.2	-1.6	massive dense micrite in nodules
			-6.1	-1.4	massive dense micrite in nodules
Salmon Gums North (Site 129)					
A	0m		-6	-1.2	massive semi-indurated nodules
			-10.8	-11.2	massive semi-indurated nodules
			-10.8	-11.1	massive semi-indurated nodules
B	0.15m		-7.6	-4.2	laminar rind on nodule
			-7.4	-3.7	massive dense micrite in nodules
			-7.2	-3.2	massive dense micrite in nodules
C	0.4m		-10.1	-9.9	massive dense micrite in hardpan
			-9.7	-9.4	massive dense micrite in hardpan
			-5.2	-1	massive dense micrite in hardpan
D	0.7m		-4.4	1.3	massive dense micrite in nodules
			-4.6	1.3	massive dense micrite in nodules
			-9.1	-8.9	massive dense micrite in nodules
E	1.2m		-9.4	-8.5	massive dense micrite in nodules
			-8.1	-5.1	massive dense micrite in nodules
			-6.2	-1.6	massive dense micrite in nodules
F	1.65m		-5.8	-0.2	massive semi-indurated calcified soil
			-5.2	0.9	massive semi-indurated calcified soil
			-9.8	-8.5	massive semi-indurated calcified soil
Lort River (Site 132)					
A	0.05m		-8.5	-5.5	light grey sandy loam with fine powder
			-5.8	-0.2	light grey sandy loam with fine powder
			-5.4	0.9	light grey sandy loam with fine powder
B	0.17m		-5.9	-0.2	massive dense micrite in nodules
			-9.3	-8	massive dense micrite in nodules
			-9.1	-7.4	massive dense micrite in nodules
C	0.3m		-5.7	-0.5	massive semi-indurated calcified soil
			-5.1	-0.5	massive semi-indurated calcified soil
			-5.5	-0.6	massive semi-indurated calcified soil
D	0.45m		-10.2	-9.8	small massive dense nodules
			-10.3	-10	small massive dense nodules
			-6.7	-2.6	massive semi-indurated calcified soil
E	0.68m		-6.6	0.1	mottled fine powder
			-7	-0.7	mottled fine powder
			-12.5	-12.2	mottled fine powder
Salmon Gums South (Site 134)					
A	0.1m	-23.5			soil
B	0.45m	-24.4			nodules
C	0.8m				nodules
D	1.05m				colluvium
Norseman South (Site 136)					
A	0.05m				
B	0.2m		-3.9	2.2	small dense massive nodules
C	0.4m		-4.1	3.9	massive semi-indurated calcified soil
			-4.2	3.7	massive semi-indurated calcified soil

Site	Depth (m)	SOM	Carbonate		Calcrete Description
		$\delta^{13}C$	$\delta^{13}C$	$\delta^{18}O$	
Norseman South (Site 136) cont.					
			-3.8	4.5	massive semi-indurated calcified soil
D	0.8m		-4.6	2	massive semi-indurated calcified soil
			-4.6	2.3	massive semi-indurated calcified soil
			-4.9	1.6	massive semi-indurated calcified soil
Broad Arrow (Site 137)					
A	0.2m		-7.2	-3.5	massive dense indurated vein
			-7.4	-4.5	massive dense indurated vein
B	0.4m		-6.7	-2	massive dense indurated vein
			-6.7	-1.7	massive dense indurated vein
C	0.9m		-7	-3.1	massive dense indurated vein
			-6.9	-3.4	massive dense indurated vein
			-7.3	-3.3	massive dense indurated vein
D	0.9m		-6.4	-0.9	massive dense indurated vein
			-6.5	-1.3	massive dense indurated vein
			-6.4	-1.3	massive dense indurated vein
E	0.2m		-6.9	-3.4	massive dense platy calcrete
			-6.1	-2.7	massive dense platy calcrete
			-6.1	0	massive dense platy calcrete
Ora Banda (Site 138)					
A	0.3m		-6.9	-3.2	massive dense nodule
			-7	-3.7	massive dense nodule
			-6.9	-3.5	massive dense nodule
B	0.4m	-22.2	-6.6	-4.3	massive dense hardpan
			-7	-4.1	massive dense hardpan
			-10.1	-9.9	massive dense hardpan
C	0.6m		-7.1	-2.7	massive semi-indurated stringers
			-7	-2.7	massive semi-indurated stringers
E	1m		-6.9	-3.4	massive semi-indurated stringers
			-6.8	-2.7	massive semi-indurated stringers
			-7.2	-3.7	massive semi-indurated stringers
F	0.6m		-7.5	-4	rhizolith, taproot fragment 5cm diameter
			-6.6	-3	rhizolith, taproot fragment 5cm diameter
			-7.3	-3.9	rhizolith, taproot fragment 5cm diameter
Kalgoorlie (Site 139)					
A	0.2m		-6.9	-2.6	massive dense micrite in nodules
			-6.9	-2.5	massive dense micrite in nodules
			-6.8	-3.4	massive dense micrite in nodules
B	0.4m	-22.2	-6.4	-0.7	massive dense micrite in nodules
C	0.65m	-22.5	-7.1	-3.6	massive dense micrite in nodules
D	0.95m	-23.3	-6.8	-3.7	massive semi-indurated stringers
E	1.33m	-23.1	-7	-3.4	massive semi-indurated stringers
F	1.7m		-7.6	-4.7	massive semi-indurated stringers
G	2.2m		-5.4	-0.9	massive semi-indurated stringers
Bardoc (Site 145)					
A	0.15m	-23.5	-8.3	-4.3	massive sheetlike hardpan
			-7.4	-3.4	massive sheetlike hardpan
			-7.9	-4.2	massive sheetlike hardpan
B	0.4m	-22.5	-6.6	-1.6	massive sheetlike hardpan
			-7.5	-4.4	massive sheetlike hardpan

Site	Depth (m)	SOM	Carbonate		Calcrete Description
		$\delta^{13}C$	$\delta^{13}C$	$\delta^{18}O$	
Bardoc (Site 145) cont.					
			-7.2	-3.4	massive sheetlike hardpan
			-6.9	-2.8	massive sheetlike hardpan
C	0.6m		-6.9	-3.1	massive semi indurated stringers
			-8	-5.2	massive semi indurated stringers
			-8.3	-5.8	massive semi indurated stringers
D	1.45m		-6.4	-1.8	massive semi indurated stringers
			-5.9	-0.5	massive semi indurated stringers
Menzies (Site 148)					
A	0.15m	-22	-4.8	-1.5	massive dense nodules
			-4.8	-1.5	massive dense nodules
			-4.9	-1.3	massive dense nodules
B	0.4m	-22.4	-3.9	-1.4	massive dense nodules
			-5.2	-3.4	massive dense nodules
			-5.3	-3.1	massive dense nodules
C	0.6m	-22.6	-5	-3.1	massive dense incipient nodules
D	1.45m		-7.3	-4.1	massive dense incipient nodules
			-7.1	-3.5	massive dense incipient nodules
			-7.1	-3.9	massive dense incipient nodules
E	2m		-6.9	-4.2	mottled fine powder
			-7.1	-3.7	mottled fine powder
			-7.4	-3.8	mottled fine powder
Riverina (Site 150)					
A	0.4m	-21	-3.4	-1	laminar rind on cemented pisolith
			-3.3	-1	laminar rind on cemented pisolith
			-2.9	-1.6	massive interstitial cement
B	0.7m	-22.7	-4.4	-3	massive dense micritic hardpan
			-5.6	-3.1	massive dense micritic hardpan
			-6.7	-3.4	massive dense micritic hardpan
C	1m		-5.8	-2.6	massive semi indurated stringers
			-6	-3.1	massive semi indurated stringers
			-5.6	-2.9	massive semi indurated stringers
E	0.2m		-4	-0.6	laminar rind on cemented pisolith
			-4.4	-1.2	laminar rind on cemented pisolith
			-3.3	-1.9	massive interstitial cement
Norseman North (Site 152)					
B	0.2m	-23.4	-5.5	-0.8	massive semi-indurated nodules
			-8.1	-6.5	massive semi-indurated nodules
			-5.5	-0.7	massive semi-indurated nodules
C	0.35m	-23	-5.4	-1.2	sheetlike massive hardpan
			-5.3	-1.7	sheetlike massive hardpan
			-5.2	-1.6	sheetlike massive hardpan
D	0.58m	-22.5	-5.3	-0.1	sheetlike massive hardpan
			-5.3	-0.1	sheetlike massive hardpan
			-5.3	-0.2	sheetlike massive hardpan
E	0.7m	-22.6	-4.8	0.3	sheetlike massive veins
			-5.7	-2.3	sheetlike massive veins
F	0.85m		-5.1	-0.2	sheetlike massive veins
			-5.1	-0.3	sheetlike massive veins
			-5.1	-0.2	sheetlike massive veins

Site	Depth (m)	SOM	Carbonate		Calcrete Description
		$\delta^{13}C$	$\delta^{13}C$	$\delta^{18}O$	
Norseman North (Site 152) cont.					
G	1.2m		-6.2	-2.3	sheetlike massive veins
H	1.55m		-3.1	-1.3	sheetlike massive veins
			-3	-1.3	sheetlike massive veins
			-2.9	-1.4	laminar rind on basalt clast
I	1.85m		-5.3	0.4	laminar rind on basalt clast
			-5.4	0.3	laminar rind on basalt clast
			-5.3	0.4	laminar rind on basalt clast
Fraser Range (Site 155)					
B		-18.5	-1.5	-2.1	massive semi-indurated surficial cement
			-1.6	-2.1	massive semi-indurated surficial cement
			-1.3	-2	massive semi-indurated surficial cement
C			-1.8	-2.1	massive semi-indurated surficial cement
			-1.8	-2.1	massive semi-indurated surficial cement
			-1.7	-2.1	massive semi-indurated surficial cement
Balladonia (Site 156)					
A	0.1m		-3.8	0.3	laminar rind on small loose pisolith
			-2.9	0.1	laminar rind on small loose pisolith
			-2.7	0.8	laminar rind on small loose pisolith
B	0.28m		-3.6	1.8	pisolith core
			-3.5	1.2	pisolith core
			-4.6	1.2	laminar rind on pisolith
C	0.58m	-22.5	-4.8	-0.6	laminar rind on pisolith
			-4.9	-0.1	laminar rind on pisolith
			-4.9	-0.1	laminar rind on pisolith
D	0.9m		-5.1	-0.4	laminar rind on pisolith
			-4.9	-0.3	laminar rind on pisolith
			-5.1	-0.5	laminar rind on pisolith
Caiguna West (Site 157)					
A	0m		-5.8	0.6	nodules as surface lag
			-5.1	-0.7	nodules as surface lag
			-3.9	1.1	nodules as surface lag
B	0.15m		-3.4	2.3	laminar rind on pisolith
			-5.5	0	pisolith core
			-5.4	-0.1	pisolith core
C	0.25m		-7.4	-1.1	laminar calcrete directly on limestone
			-5.2	-0.9	laminar calcrete directly on limestone
			-7.1	-2.3	laminar calcrete directly on limestone
			-8.5	-3	coating on limestone
			-8.5	-0.4	coating on limestone
D	0.55m		-8.8	-0.7	coating on limestone
			-9.4	-2.8	limestone
E	0.7m		-8.7	-1.4	massive dense horizontal layer
			-8.6	-1.4	massive dense horizontal layer
F	1.1m		-8.7	-0.9	massive dense tube filling(large rhizolith)
			-8.3	-0.7	massive dense tube filling(large rhizolith)
			-8.7	-1.2	massive dense tube filling(large rhizolith)

Site	Depth (m)	SOM	Carbonate		Calcrete Description
		$\delta^{13}C$	$\delta^{13}C$	$\delta^{18}O$	
Madura (Site 159)					
A	0.5m		-8.1	-3.5	laminar rind in hardpan
			-8	-3.5	laminar rind in hardpan
			-8	-3.7	laminar rind in hardpan
B	1.25m		-7.1	-2.8	sheet-like dense massive hardpan
			-7.1	-2.7	sheet-like dense massive hardpan
			-7.1	-3	sheet-like dense massive hardpan
C	2.4m		-2	-3	limestone, micritised
			-2	-3.2	limestone, micritised
			-2.1	-3.2	limestone, micritised
Nundroo (Site 163)					
A	0m		-6.1	-1.6	laminar rind in hardpan
			-6.3	-2.6	laminar rind in hardpan
			-6.2	-2.6	laminar rind in hardpan
			-6.7	-1.7	black pebble
			-6	-1.3	black pebble
B	0m		-8.5	-4.2	limestone
			-8.4	-4.1	limestone
			-8.5	-4.2	limestone
Wirrulla (Site 166)					
S	0m		1.2	2.4	loose fine powder
			1	1.4	loose fine powder
			1.6	1.3	loose fine powder
A	0.2m	-22.6	-5.6	-1.9	interstitial cement
			-5.9	-1.9	interstitial cement
			-5.6	-2.6	laminar rind in hardpan
			-5.6	-2.5	laminar rind in hardpan
B	0.6m		-8.3	-3.2	massive dense hardpan
			-5.7	-2.2	massive dense hardpan
			-8.2	-2.5	massive dense hardpan
C	0.9m		-7.3	-2.8	massive semi-indurated calcified soil
			-6.9	-2.9	massive semi-indurated calcified soil
			-7.1	-3	massive semi-indurated calcified soil
D	1.2m		-6.6	-1.4	massive semi-indurated calcified soil
			-6.4	-1.2	massive semi-indurated calcified soil
Yarwondutta Rocks (Site 167)					
B	0.25m		-5.5	0.1	massive dense nodules
			-4.6	-0.1	massive dense nodules
			-4.5	0.3	massive dense nodules
C	0.45m	-22.3	-6.3	-2.1	massive dense hardpan
			-3.4	-1.4	massive dense hardpan
			-3.7	-1.5	massive dense hardpan
D	0.6m	-23.7	-5.9	-2	massive dense hardpan
			-6	-1.9	massive dense hardpan
			-6.5	-1.8	massive dense hardpan
Minnippa South West (Site 168)					
B	0.75m		-3.5	0	massive semi-indurated calcified soil
			-4.9	0.3	massive semi-indurated calcified soil
			-4.6	-0.1	massive semi-indurated calcified soil
C	0.95m		-3.8	-0.7	massive dense nodules

Site	Depth (m)	SOM	Carbonate		Calcrete Description
		$\delta^{13}C$	$\delta^{13}C$	$\delta^{18}O$	
Minnippa South West (Site 168), cont.					
			-3.9	-0.6	massive dense nodules
E	1.7m		-4.5	-0.7	massive semi-indurated calcified soil
			-4.9	-1.4	massive semi-indurated calcified soil
Warnambool West (Site 174)					
A	0.15m		-7.5	-3.1	surficial laminar calcrete
			-7.8	-3.5	surficial laminar calcrete
			-8	-3.5	surficial laminar calcrete
B	0.2m		-7.7	-3.9	massive dense micritic hardpan
			-0.9	0.3	massive dense micritic hardpan
			-5.5	-1.4	massive dense micritic hardpan
C	0.65m		-7.9	-3.3	large rhizolith
			-7.2	-2.8	large rhizolith
			-7.5	-3.2	large rhizolith
Port Lincoln (Site 176)					
A	0.15m		-0.3	-0.6	massive dense micritic hardpan
			0.1	-0.3	massive dense micritic hardpan
			-1.1	-0.9	massive dense micritic hardpan
B	0.6m		-0.9	-1	massive dense micritic hardpan
			-0.9	-1.3	massive dense micritic hardpan
			-2.1	-1.9	massive dense micritic hardpan
C	1.05m		-6.3	-3.4	loose fine powder
			-7.3	-3.8	loose fine powder
			-6	-3.6	loose fine powder